# Metal phosphate and precious metal catalysts for selective oxidation

2012

Gareth Thomas Whiting

Prof. G. J. Hutchings
Dr. S. H. Taylor

# Declaration

This work has not been submitted in substance for any other degree or award at this or any other university or place of learning, nor is being submitted concurrently in candidature for any degree or other award.

Signed …… (candidate) Date ……

**STATEMENT 1**

This thesis is being submitted in partial fulfillment of the requirements for the degree of ……(insert MCh, MD, MPhil, PhD etc, as appropriate)

Signed …… (candidate) Date ……

**STATEMENT 2**

This thesis is the result of my own independent work/investigation, except where otherwise stated.
Other sources are acknowledged by explicit references. The views expressed are my own.

Signed …… (candidate) Date ……

**STATEMENT 3**

I hereby give consent for my thesis, if accepted, to be available for photocopying and for inter-library loan, and for the title and summary to be made available to outside organisations.

Signed …… (candidate) Date ……

# Acknowledgements

Upon the completion of this PhD, I would like to express my gratitude to a number of people, as this thesis has only proved possible with their help and support.

Firstly, I would like to thank my supervisor Prof. Graham Hutchings and my co-supervisor Dr. Stuart Taylor, for giving me the opportunity to study this project at Cardiff University, and also for their invaluable support and guidance throughout my three year study.

I would also like to extend my gratitude to other members of the group, in particular, Dr. Jonathan Bartley, Dr. Nicholas Dummer, Dr. Nikolaos Dimitratos and Dr. Tom Davies, as their knowledge, input and advice has helped me vastly during this period.

For their patience and guidance, I would again like to thank Dr. Jonathan Bartley and Dr. Stuart Taylor, for taking the time to read and correct this thesis.

Of course, without funding, this research would not have been possible, and so I am incredibly grateful to both the EPSRC and Cardiff University.

Finally, I would like to thank my parents for their constant support and encouragement to complete this PhD, and to my friends in Cardiff for making my time there so enjoyable.

# Abstract

The main objective researched in this thesis involves the selective oxidation of methanol to formaldehyde, using metal phosphate based catalysts. Molybdenum and vanadium phosphate based catalysts have been prepared, thoroughly characterised and tested as active catalysts for the selective oxidation of methanol to formaldehyde. Initial investigations highlighted the relatively low activity of both metal phosphate catalysts, however, significant enhancements in the catalytic activity and formaldehyde selectivity of both materials have been achieved in this research, primarily by supporting molybdenum phosphate catalysts using a range of supports, and also promoting both molybdenum and vanadium pyrophosphates with transition metals. It was discovered that a catalyst of 10 wt% $(MoO_2)_2P_2O_7$ supported on $SiO_2$ containing 1 mol% vanadium (as a promoter) achieved significantly higher formaldehyde per pass yields (>20 %) than $MoO_3$ supported on $SiO_2$ (reported in the literature) and comparable activity to that of the commercial iron molybdate catalyst. Due to the promotional effect of vanadium, and the known activity of $V_2O_5$ catalysts for the oxidation of methanol to formaldehyde, molybdenum promoted $(VO_2)_2P_2O_7$ catalysts were tested for this reaction and reported for the first time. Catalytic studies revealed that there is a direct correlation between molybdenum content and catalytic activity, indicating a synergistic effect of the two transition metals.

The penultimate chapter of this thesis involves the use of supported mono- and bi-metallic gold(palladium) catalysts and their use in both CO oxidation and selective methanol oxidation. A novel method of maintaining considerably small Au(Pd) nanoparticle size (unlike the standard thermal treatment method) has been discovered by the Hutchings group at Cardiff Catalysis Institute, involving the removal of stabilising

ligands with a solvent extraction method. Using high resolution microscopy and a range of characterization techniques, the nanoparticle size was attributed to the surprisingly high activity achieved for both CO oxidation and methanol oxidation to methyl formate, at low temperatures which, particularly in the case of methanol oxidation, is a remarkable discovery.

# Glossary

| | |
|---|---|
| a.u. | Arbitrary units |
| BET | Brunauer, Emmet and Teller |
| DMM | Dimethoxy methane |
| DME | Dimethyl ether |
| $cm^{-1}$ | Reciprocal centimeters |
| CO | Carbon monoxide |
| $CO_2$ | Carbon dioxide |
| EDX | Energy-dispersive X-ray spectroscopy |
| eV | Electron volts |
| FID | Flame ionisation detector |
| FA | Formaldehyde |
| g | Gram |
| GC | Gas Chromatography |
| GHSV | Gas hourly space velocity |
| h | Hours |
| HAADF | High annular angle dark field |
| He | Helium |
| *i.d.* | Inner diameter |
| m | Meter |
| MeOH | Methanol |
| min | Minutes |
| mol | Moles |
| mol% | Mole percent |
| nm | Nanometer |
| $O_2$ | Oxygen |
| PVA | Poly vinyl alcohol |
| RF | Response factor |
| s | Seconds |
| SEM | Scanning electron microscopy |
| STEM | Scanning transmission electron microscopy |
| TCD | Thermal conductivity detector |
| TEM | Transmission electron microscopy |
| TGA | Thermogravimetric analysis |
| UHV | Ultra high vacuum |
| vol% | Volume percent |
| wt% | Weight percent |
| XPS | X-ray photoelectron spectroscopy |
| XRD | X-ray diffraction |

# Contents

# 1

# *Chapter 1 – Introduction*

## 1.1 – Catalysis

### *1.1.1 – History and principles of catalysis*

The first reported use of a 'catalyst' was in 1552 by Cordus[1] when sulphuric acid was used to catalyse the conversion of alcohol to ether. Although at this time the word 'catalyst' had not been heard, it was not until 1835 that Berzelius[2] used the word 'catalysis' to describe the effect of sulphuric acid on ethanol to the decomposition of hydrogen peroxide, and drawing analogies with the conversion of starch into sugar. In between the work of Cordus and Berzalius, in 1794 Fulhame[3] presented the first principles of catalysis when she suggested that small amounts of water were needed for the oxidation of carbon monoxide, and observed that water was unaffected by the chemical reaction. Two later discoveries were reported in 1813 by Thenard,[4,5] who discovered that metals were capable of decomposing ammonia, and in 1823 by Dobereiner,[6] who observed that manganese oxide could affect the rate of decomposition of potassium chlorate. However, the major advance in understanding catalysis was reported by Lemoine[7] who showed that a catalyst could change the rate at which a chemical equilibrium was reached, and that the position of the equilibrium remains unaltered.

A catalyst is defined as a substance which increases the rate at which a chemical reaction approaches equilibrium, by providing an alternative route for the reaction with a lower activation energy (compared to the uncatalysed reaction), without the catalyst itself undergoing a chemical change, or being consumed in the process. It can be observed simply, using a potential energy profile for a catalysed and an uncatalysed reaction (Figure 1.1).

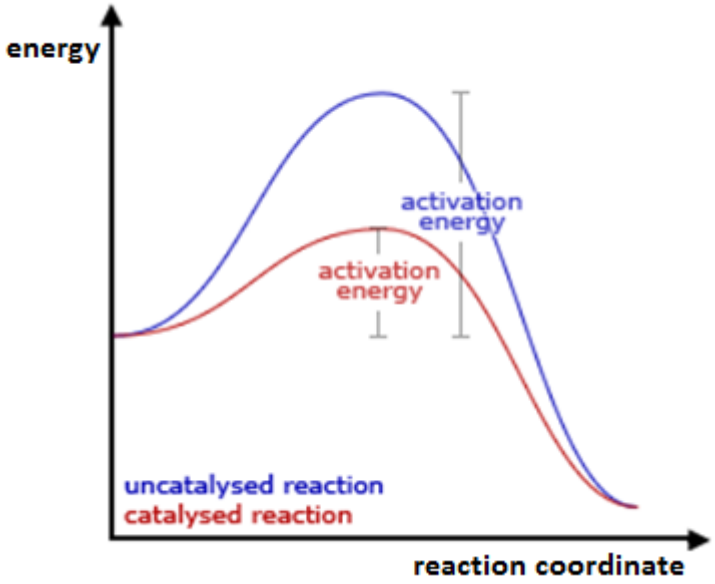


**Figure 1.1** – Potential energy profile for an exothermic reaction, showing lower activation energy of the catalysed reaction.

There are three types of catalysts; Homogeneous, Heterogeneous and Biocatalysts. Homogeneous catalysts operate in the same phase as the reagents *i.e.* a liquid-liquid phase, such as dissolved metal complexes in solution. The reaction temperatures of homogeneous catalytic reactions are generally lower than 250 °C. Heterogeneous catalysts operate in a separate phase to the reagents *i.e.* solid catalyst with a gaseous reagent. Heterogeneous catalysis has several advantages over homogeneous catalysts such as; the easy separation of catalyst from products, avoiding formation of inorganic salts and, catalysts are recyclable which if not, can be expensive and problematic. The

advantages of homogeneous catalysis are; higher contact areas, the rate of catalysis is often much higher and, reaction temperatures are generally lower than the heterogeneous catalysis temperatures (250-600 °C). Biocatalysts involve the chemical transformation of organic compounds using mainly enzymes, and is the least reported out of the three classes of catalysts.

### *1.1.2 – Heterogeneous catalysis*

In general terms, heterogeneous catalysis involves a catalyst which provides a surface, on which the reactants temporarily become adsorbed. Bonds in the reactant molecules become weakened, and new bonds are created between the adsorbed species on the surface of the catalyst. After undergoing a reaction with other participating molecules, adsorbed products are formed, and due to the weak bond with the surface, desorb, and hence release the product.

An early observation of heterogeneous catalysis was noted by Paul Sabatier,[8] who observed that nickel hydrogenated ethene giving ethane in 1987, and since this time, heterogeneous catalysis has been, and continues to be, carried out in a vast nuumber of industrial processes, such as the Haber process[9] for production of ammonia using an iron catalyst, and the Contact process[10] for the production of sulphuric acid using a platinum (or vanadium oxide) catalyst. Other well studied examples can be seen in Table 1.1.

**Table 1.1:** Examples of uses of heterogeneous catalysis in industrial processes.

| **Reaction** | **Heterogeneous catalyst** |
|---|---|
| Polymerisation of alkenes | Phosphoric acid |
| Hydrogen peroxide decomposition | Gold |
| Water gas shift reaction | Magnetite ($Fe_3O_4$) |
| Hydrogenation of alkenes to alkanes | Platinum, Nickel or Palladium |

## 1.2– Methanol oxidation

### *1.2.1 – Uses and properties of methanol and formaldehyde*

#### *1.2.1.1 – Methanol*

Methanol is a volatile, toxic, flammable liquid with a density of 0.791 g $cm^{-3}$ and a boiling point of 64.7 °C. It is the simplest alcohol and is also referred to as methyl alcohol with the chemical formula, $CH_3OH$. It can be produced in nature by a variety of bacteria using their anaerobic metabolism, and is mainly made from common fossil fuels such as natural gas and coal, but also from renewable resources like biomass, landfill gas and even power plant emissions. Methanol was first isolated by Boyle in 1661, where he used the distillation of boxwood, later to be known as 'pyroxyilc spirit'. BASF were the first industrial company to produce methanol via the conversion of synthesis gas (Patent no. 1,569,775 filed 12 January 1926), but modern day production of methanol uses copper based catalysts, unlike the chromium and manganese oxide catalysts used by Mittash and Pier,[11] where 'harsh' reaction conditions were needed (50–220atm, 450 °C). The use of a copper zinc oxide and alumina catalyst which was developed by ICI in the 1960s, allowed the conversion of synthesis gas at lower pressures (50–100 atm, 250 °C).[12]

Three processes are currently used commercially to produce synthesis gas from the methane component of natural gas;

1. The endothermic steam-methane reforming process (SMR), which uses a nickel catalyst at moderate pressures (40 atm) and high temperatures (850 °C), where

methane reacts with steam in the following reaction process to produce syngas:

$$CH_4 + H_2O \rightarrow CO + 3H_2$$

2. The exothermic partial oxidation of methane with molecular oxygen:

$$2CH_4 + O_2 \rightarrow 2CO + 4H_2$$

3. The combination of the two above processes, since the SMR reaction has heat transfer limitations which can be solved by combing both reactions, referred to as autothermal reforming.

By using the copper based catalyst developed by ICI under 50–100atm and 250 °C, a high selectivity of methanol can be produced from CO and $H_2$:

$$CO + 2H_2 \rightarrow CH_3OH$$

Methanol has many uses, the major one being as a feedstock for other chemicals such as formaldehyde,[13-15] which uses about 40 % of methanol (Figure 1.2). Another major use of methanol is in the petrochemical industry in the United States, large amounts of methanol are used to produce the gasoline additive methyl *tert*-butyl ether (MTBE).[16] A recent application is in Direct Methanol Fuel Cells (DMFC), as methanol allows fuel cells to operate at lower temperatures and pressures, which can decrease the size of the cell dramatically.

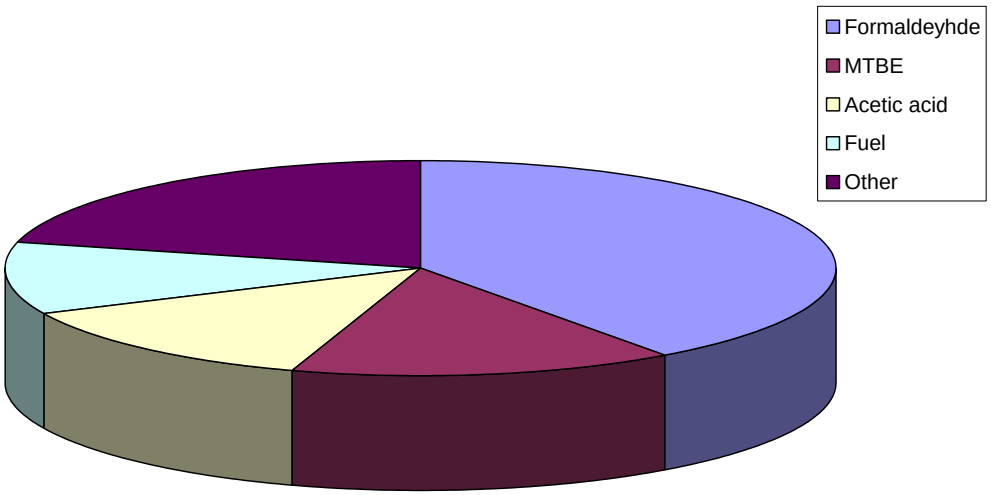


**Figure 1.2 –** Industrial uses of methanol.

### *1.2.1.2 – Formaldehyde*

Formaldehyde is the simplest aldehyde with the formula $CH_2O$, and can be referred to as methanal. It is a colourless gas which has a characteristic odour, and has high toxicity. Pure anhydrous formaldehyde is a gas at room temperature with a boiling point of -19 °C and a melting point of -92 °C, but readily converts to various derivatives often used by industry instead of the gaseous form.[17] Formaldehyde occurs in nature from photochemical processes which contribute to 90 % of the total formaldehyde in the environment, and also incomplete combustion of organic materials. Formaldehyde is highly reactive and has many uses in industries, such as the synthetics resins industry and in the textiles industry. Formaldehyde is used to generate urea-formaldehyde resin, melamine resin and phenol formaldehyde resin among others (Figure 1.3), where most tend to be thermosetting resins, oil soluble resins and adhesives. In the textiles industry these resins are used as finishers to make crease resistant fabrics. It is also used to make a

range of other materials such as plywood, carpeting, paper, fertilizers, disinfectants, embalming agents and other chemicals[14]

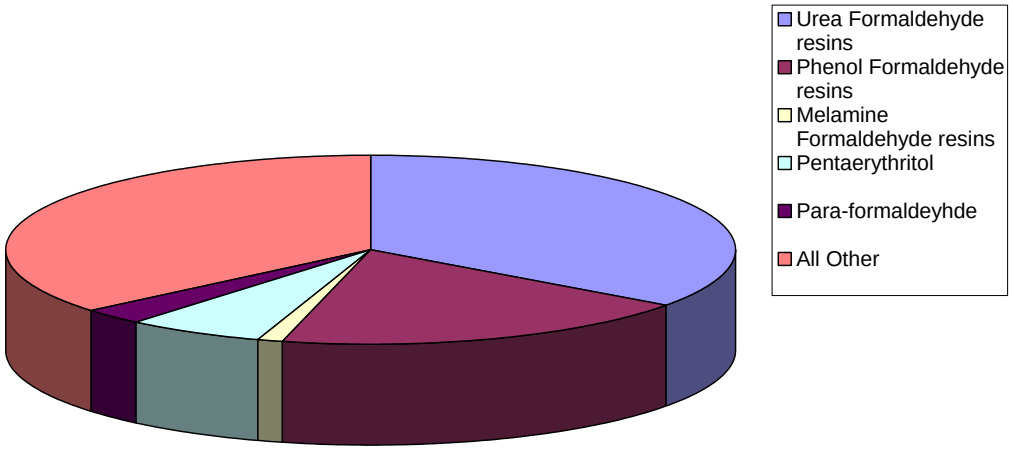


**Figure 1.3 –** Industrial uses of formaldehyde.

The first recorded production of formaldehyde is said to be carried out by Butlerov[18] in 1859 when he hydrolised methylene acetate and, in 1868 von Hofmann performed the synthesis using heated platinum spirals to oxidise methanol vapours using air.[19] The first industrial catalyst to be used for formaldehyde production was a copper gauze catalyst developed by Loew (1886) and Trillat (1889). Blank (1910) was first to use a silver catalyst, which replaced copper due to higher yields and higher resistance to poisoning.[20] In 1931, the main catalyst used industrially today was developed by Adkins and Peterson,[21] who used an iron molybdenum oxide catalyst in the selective oxidation of methanol to formaldehyde.

### *1.2.2 – Thermodynamics of methanol oxidation*

The most thermodynamically favourable reaction (at 250 °C) of methanol oxidation, is the combustion reaction (eq. 1 and 2 in Table 1.2) to $CO_x$ products (Figure 1.4). It is then

clear that the choice of catalyst will play a massive role in determining which reaction pathway is taken, either by oxidative dehydrogenation (eq. 3), dehydrogenation (eq. 4 and 5) or by dehydration of methanol (eq. 6).

**Table 1.2:** Methanol oxidation pathways with corresponding enthalpies of reaction.

| | | |
|---|---|---|
| $CH_3OH + O_2 \rightarrow CO + 2H_2O$ | ($\Delta H$ = -400 kJ $mol^{-1}$) | (eq.1) |
| $CH_3OH + 1½\ O_2 \rightarrow CO_2 + 2H_2O$ | ($\Delta H$ = -707 kJ $mol^{-1}$) | (eq.2) |
| $CH_3OH + ½\ O_2 \rightarrow H_2CO + H_2O$ | ($\Delta H$ = -164 kJ $mol^{-1}$) | (eq.3) |
| $CH_3OH \rightarrow H_2CO + H_2$ | ($\Delta H$ = +80 kJ $mol^{-1}$) | (eq.4) |
| $CH_3OH \rightarrow CO + 2H_2$ | ($\Delta H$ = +88 kJ $mol^{-1}$) | (eq.5) |
| $2CH_3OH \rightarrow CH_3OCH_3 + H_2O$ | ($\Delta H$ = -27 kJ $mol^{-1}$) | (eq.6) |

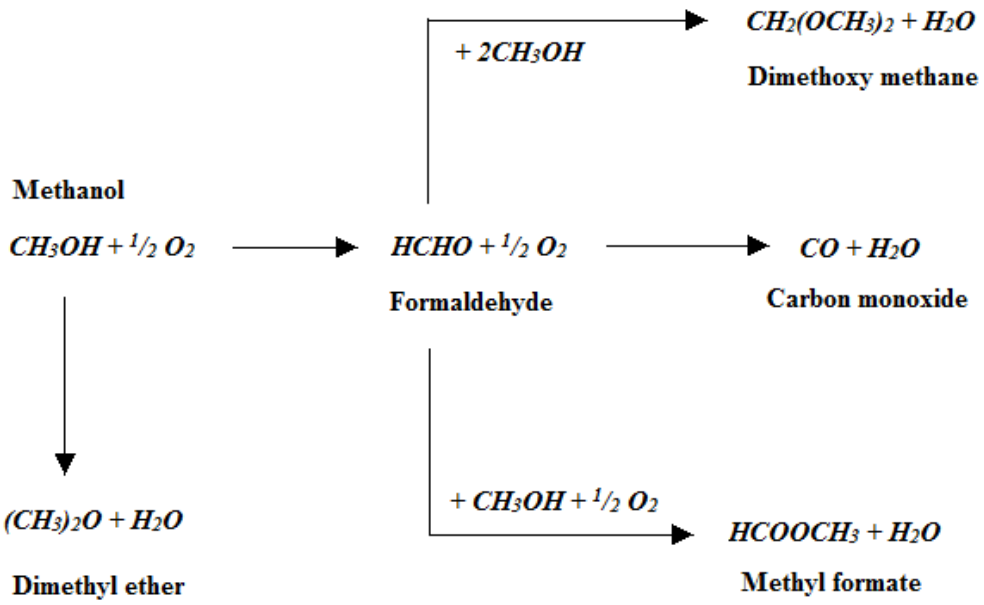


**Figure 1.4:** Possible reaction pathways of methanol oxidation using a heterogeneous catalyst.[22]

### *1.2.3– Industrial Catalysts*

There are many heterogeneous catalysts that have been used for the oxidation of methanol to formaldehyde, but the two most widely utilised catalysts are silver and/or iron molybdate.[13,14,17,23,24]

#### *1.2.3.1 – Silver process*

The production of formaldehyde using silver catalysts operates using methanol oxidation (eq. 3) and methanol dehydrogenation (eq. 4). There are two main silver catalysed processes[25] used commercially:

1. Methanol ballast process, where only pure methanol and air are passed, which is used by ICI and Degussa. (Incomplete conversion of methanol)
2. Water ballast process, which uses excess water with the reactant mixture, and is used by BASF. (Complete conversion of methanol)

The water ballast process has the advantage of enhanced catalyst lifetime, since the water vapour burns away the coke which would deactivate the catalyst. In general, the process is carried out at atmospheric pressure by passing methanol vapour, in the presence of steam and air, through a thin bed of electrolytic silver catalyst operating at temperatures between 650 °C and 680 °C.[26,27] By using an excess of methanol relative to oxygen, and adding water, near complete conversion is achieved with around 90 % selectivity towards formaldehyde,[28] and approximately 8 - 10 % of the methanol oxidised to $CO_2$ and $H_2O$, or $CO_2$ and $H_2$.[26]

Waterhouse *et al.*[26] provide equations frequently used in the literature for the oxidation of methanol on silver surfaces using industrial conditions (Table 1.3):

**Table 1.3:** Reaction pathways for methanol oxidation on a silver catalyst. the $O_{(a)}$ denotes some form of chemisorbed atomic oxygen on silver.

| | |
|---|---|
| $CH_3OH_{(g)} \rightarrow CH_2O_{(g)} + H_{2(g)}$ | (eq.7) |
| $CH_3OH_{(g)} + O_{(a)} \rightarrow CH_2O_{(g)} + H_2O_{(g)}$ | (eq.8) |
| $2CH_3OH_{(g)} + O_{(a)} \rightarrow 2CH_2O_{(g)} + H_2O_{(g)} + H_{2(g)}$ | (eq.9) |
| $CH_3OH_{(g)} + 3O_{(a)} \rightarrow CO_{2(g)} + 2H_2O_{(g)}$ | (eq.10) |
| $CH_2O_{(g)} + 2O_{(a)} \rightarrow CO_{2(g)} + H_2O_{(g)}$ | (eq.11) |
| $CH_2O_{(g)} + O_{(a)} \rightarrow CO_{2(g)} + H_{2(g)}$ | (eq.12) |
| $H_{2(g)} + O_{(a)} \rightarrow H_2O_{(g)}$ | (eq.13) |
| $CH_2O_{(g)} \rightarrow CO_{(g)} + H_{2(g)}$ | (eq.14) |

In 1986, Lefferts *et al.*[28] suggested a theory of the interaction between oxygen and silver. At this time, there was limited literature reporting the mechanism of the reaction, however, Lefferts and co-workers proposed a theory that there are two types of oxygen sites involved in the reaction, and that only the layer near the surface of the silver catalyst bed is active for methanol oxidation, where oxygen is present. The literature during this period[29-31] put forward the idea that selective oxidation and dehydrogenation reactions of methanol take place at sites associated with the strongly bound surface oxygen, whereas the total oxidation reaction proceeds with the weakly bound surface oxygen. More recently, Qian and co-workers[25] proposed a theory similar to the one proposed by Lefferts *et al.*[28] but with some new suggestions. Qian *et al.* observes that there are three different oxygen species ($O_\alpha$, $O_\beta$, $O_\gamma$) involved in the methanol oxidation reaction. Molecular oxygen dissociates on the silver surface and forms the weakly bound atomic surface

oxygen species, $O_\alpha$, (Ag-O-Ag bridging) which enhances the formation of formaldehyde and the complete oxidation to form $CO_2$ and $H_2O$ (in agreement with Lefferts *et al.*). Since silver and oxygen have similar atomic dimensions, ($^{ø}$Ag = 60 Å, $^{ø}$O = 62 Å), the oxygen may dissolve into the silver lattice now called $O_\beta$. These oxygen species are not involved in the reaction directly, but only when they diffuse to the surface and become $O_\gamma$ (Ag=O), which are strongly bound and tend to only catalyse the dehydrogenation of methanol.

### *1.2.3.2 – Iron molybdate process*

There are many catalysts that have been tested for methanol oxidation to formaldehyde (*i.e.* supported ruthenium oxide clusters (<25 % formaldehyde selectivity),[32] evaporated sodium catalysts (45 % methanol conversion, 40 % formaldehyde selectivity),[33] and Ag-$SiO_2$-MgO-$Al_2O_3$ (10 % methanol conversion, 99 % formaldehyde selectivity),[34] but few are as successful as iron molybdate in giving the high selectivity of formaldehyde (>95 %) with high conversion (98 – 99 %) at a moderate temperature (<400 °C).

The iron molybdate catalyst has advantages to the silver catalyst, as the process operates at a much lower temperature of ~350 °C, and this has obvious economic positives. The other advantages are that the silver catalyst operates using a methanol/air ratio above the upper explosion limit, whereas the iron molybdate process uses a methanol/air ratio below it, so there is less danger involved, and also, iron molybdate is less sensitive to contamination by normal methanol impurities.[35] Iron molybdate catalysts in the literature are usually prepared using co-precipitation from solutions of sodium molybdate and iron (III) chloride,[36] or from iron (III) nitrate and ammonium heptamolybdate, which avoids the contamination with sodium and chlorine.[37-46]

Industrially, iron molybdate catalysts are prepared using ammonium heptamolybdate and iron (III) chloride solutions.[47,48]

There is a contradiction in the literature as to whether the catalytic behaviour of iron molybdates is mainly dependant on the Mo/Fe atomic ratio, and if there is indeed an optimum ratio.[37,38] It is generally accepted that the best industrial catalysts for iron molybdates consists of a mixed phase of iron molybdate [$Fe_2(MoO_4)_3$] and molybdena [$MoO_3$].[35,49-51] There is a synergistic effect between the two, as the $MoO_3$ exhibits high selectivity with poor activity, whereas the $Fe_2O_3$ has poor selectivity for formaldehyde, but leads to an increase in activity.[38,39,52] As well as this reason, Bowker *et al.*[53] also suggest that although it seems that molybdena could be used on its own, a high surface area is difficult to obtain, plus the iron content may play a part in maintaining a higher oxidation state of the surface molybdenum than would otherwise be the case if iron was not present. Many researchers have proposed theories on the role of iron in the iron molybdate catalyst; Sun-Kou *et al.*[54] and Novakova *et al.*[55] propose that Fe favours the transfer of $O_2$ and $H_2O$ between the surface and the gas phase, which helps to re-oxidise the reduced molybdenum. Fagherazzi and Pernicone[51] postulated that the presence of Fe (III) ions increases the concentration of methanol adsorption sites, which consist of an anion vacancy (acidic site) and an $O^{2-}$ (basic site).

Catalyst deactivation occurs when molybdenum is lost from the surface to give an iron-rich phase which, as previously stated, is less selective than a molybdenum-rich phase. To prevent deactivation, the catalysts contain excess molybdenum and industrial catalysts usually have a Mo/ Fe atomic ratio of 2.3-5.[24] Another side effect of Mo leaving the bulk catalyst, is that it crystallizes in a fibrous material in the reactor, which leads to a pressure drop through the catalyst bed.[56]

The mechanism of formaldehyde production using iron-molybdate catalysts is thought to follow a Mars Van Krevelen type reaction, but not identical,[57] since the Mars Van Krevelen mechanism usually only takes into account reactions with surface oxygen. The reason it is not identical, is that there are theories from various literature that suggest that at 300 °C there is a reduction of the bulk of the catalysts and considerable mobility of oxygen in the lattice.[53] The surface lattice oxygen in the catalyst is able to react with methanol selectively without the need for gas phase oxygen. The presence of two terminal oxygen atoms ($O_t$) double bonded to molybdenum, means that methanol molecules can be bonded simultaneously at two points on the surface, where hydrogen abstraction from the hydroxyl group produces a methoxy species, which goes on to produce formaldehyde with the bridging oxygen species ($O_b$) [52] shown in the equations in Table 1.4.

High oxidation states of the surface metals ($Mo^{6+}$) are required so that the surface oxide is reduced to hydroxide,[58] while the Mo is converted to a lower oxidation state ($Mo^{5+}$).

**Table 1.4:** Methanol oxidation reaction over an iron molybdate catalyst

| | |
|---|---|
| $Fe_2(MoO_4)_3 + CH_3OH \rightarrow 2FeMoO_4 + MoO_3 + H_2CO + H_2O$ | (eq.15) |
| $CH_3OH + O_t \rightarrow CH_3O + OH$ | (eq.16) |
| $CH_3O + O_b \rightarrow H_2CO + H_2O$ | (eq.17) |
| $CH_3OH + Mo^{6+}O^{2-} \rightarrow Mo\text{-}OCH_3^{5+} + OH^-$ | (eq.18) |

### *1.2.4 – Literature review of alternative catalysts*

#### *1.2.4.1 – Vanadium oxide based catalysts*

Vanadium pentoxide ($V_2O_5$) has been studied by several authors for methanol oxidation with extremely high selectivity to formaldehyde. Tatibouet and Germain[59] discovered that at low methanol conversion, 97 % selectivity to formaldehyde is achieved, and it is postulated that this is dependent on the exposed face of $V_2O_5$, with authors suggesting that the (010) face is important for formaldehyde formation.[60,61] Supported vanadium oxide catalysts are widely reported in the literature for a range of other partial oxidation reactions such as ethane, propane and o-xylene oxidation. Vanadium supported on a range of metal oxide supports ($TiO_2$,[62] $ZrO_2$,[63] $CeO_2$,[64, 65] $Al_2O_3$,[66] $Fe_2O_3$ and $Co_3O_4$[67]) have been reported as catalysis for methanol oxidation to formaldehyde, and is thought that the activity of the vanadia catalyst is strongly dependent on the support used.[68,69]

The metal oxide supports frequently reported in the literature to have high activity are titania and zirconia. Wang and Madix[62] studied vanadia adlayers with varying coverages on $TiO_2$ (110), prepared by codosing $VOCl_3$ and water. By varying the coverage of vanadia on the support from sub-monolayer to multilayer, the optimum coverage was achieved in terms of activity and selectivity to formaldehyde. Wang *et al*. found that a monolayer of vanadia produces the highest activity for oxy-dehydrogenation of the methoxide intermediate, which supports their hypothesis that as multilayer coverage is reached, the active V-O-Ti bonds are increasingly difficult to access, and hence the formation of formaldehyde is reduced. As well as the accessibility of the V-O-Ti bonds, the oxidation state of the vanadium cation plays an important role in the activity, with the $V^{5+}$ oxidation state producing the highest activity, and this state can be found in the highly active monolayer coverage. A recent report has seen the use of zirconia as a

support[63] where the amount of vanadium was varied on the zirconia support, ranging from sub-monolayer to above-monolayer, with similar results to Wang and Madix.[62] The addition of vanadium increased the production of formaldehyde up to monolayer coverage, and the mechanism of the reaction was thought to occur on both the Zr-O-Zr and the V-O-Zr species, to form Zr-$OCH_3$/Zr-OH and V-$OCH_3$/Zr-OH pairs respectively. The $ZrO_2$ support on its own forms only methoxide and hydroxyl species[70] which when heated, produce $H_2$ and CO as the only products.

A non-metal oxide support which has only become prominent in the past few years is the use of gold. Strum *et al.*[71] report the use of well-ordered thin $V_2O_5$ (001) films supported on Au (111)[72,73] for the use of partial methanol oxidation to formaldehyde. As bulk terminated surfaces are inactive, reduced surfaces are used, formed by electron irradiation, which removes mainly the vanadyl oxygen atoms, and so on this reduced surface, methanol forms methoxy groups which react to produce only formaldehyde and water as products, whereas the methanol adsorbs in a molecular form on non-reduced surfaces, which leads to no formaldehyde production.

Another vanadium based catalyst for the use in methanol oxidation to formaldehyde is V-Mg-O. Isaguliants *et al.*[74] has shown that in the temperature range of 450 °C, excellent selectivity to formaldehyde (97 %) can be reached with high methanol conversion even after 60 hours of reaction.

#### *1.2.4.2 – Molybdenum oxide based catalysts*

Molybdenum based materials have proved to be good catalysts for selective methanol oxidation, in particular, the main industrial catalyst iron molybdate. Molybdenum is present in this catalyst in the form of $MoO_3$, and this alone has been reported in the

literature to be an effective catalyst for the oxidation of methanol to formaldehyde. Bulk $MoO_3$ as a catalyst for this reaction is rarely studied, however, Cheng[75] reported an active $MoO_3$ catalyst where 95 % selectivity to formaldehyde is reached with around 50 % conversion of methanol. It is suggested that the high formaldehyde selectivity of unsupported $MoO_3$ is due to water, which is coproduced with formaldehyde in the methanol oxidation reaction and, corresponding with results found with formaldehyde oxidation on this catalyst, (where formaldehyde conversion decreases when water is added to the feed) it retards the further oxidation of formaldehyde, and hence high selectivity.

The majority of reports of unsupported $MoO_3$ as a catalyst for methanol oxidation are related to single crystal studies, where single crystals of orthorhombic $MoO_3$ are obtained via the sublimation of $MoO_3$ powder at 800 °C under an oxygen atmosphere.[76,77] Extensive studies discuss the relevant planes of $\alpha$-$MoO_3$, and how these relate to product formation. It is observed that there is a strong dependence between selectivity and the crystallographic exposed faces, *i.e.* products such as formaldehyde, methyl formate and dimethyl ether are produced on different faces with the rate depending on the nature of the given face.[60,61,78] Sleight *et al.*[79-81] came to the conclusion that during methanol oxidation on $MoO_3$, the (100) face oxidised methanol to formaldehyde, whereas the (010) face produced fully oxidised products, and does not have Lewis acid sites which are known to be able to adsorb methanol dissociatively, and so this face is inactive.

The most extensively reported molybdenum based catalyst for methanol oxidation apart from iron molybdate is however, supported molybdenum trioxide, most commonly on silica,[82-86] alumina[87] and titania.[88] The use of alumina as a support for $MoO_3$ is limited as it contains acidic sites, which can react with methanol at a moderate temperature to

produce dimethyl ether with 100 % selectivity. Generally, supported $MoO_3$ catalysts have a lower selectivity to formaldehyde than bulk $MoO_3$, but higher conversion. The explanation of the lower formaldehyde selectivity is due to excess $CO_x$ production, but this is not related to the further oxidation of formaldehyde alone.[75] The main product produced during the reaction of methanol with $MoO_3/SiO_2$ is formaldehyde, with other side products including methyl formate and $CO_x$. The formation of methyl formate reaches a maximum selectivity at 200 °C (generally higher selectivity with higher loading of molybdenum oxide)[89] and is converted to $CO_x$ above 200 °C, due to the further decomposition of formate ions.[90] Methanol oxidation studies by Kim *et al.*[91] revealed that the most active support is titania, which has turn over frequencies (TOFs) that are at least 1-2 orders of magnitude higher than the alumina or silica supported catalysts. This demonstrates that the metal oxide support plays a specific role in the reactivity of the molybdenum oxide phase, which has led to extensive studies on the surface structure of the molybdenum oxide species present. As stated previously, the support which has received the most interest is silica, as this is also an active catalyst for methane oxidation to methanol and formaldehyde. Unlike the titania and alumina supports where the molybdenum oxide species possess a highly distorted octahedrally coordinated surface molybdenum oxide species, (known as mono-oxomolybdate, with one short Mo=O bond regardless of the molybdenum loading) the molybdenum species present on the silica support are controversially reported by many authors.[90- 95] Activity and structure of $MoO_3/SiO_2$ catalysts are thought to vary with the preparation technique used to disperse molybdenum oxide on the support. Rodrigo *et al.* studied catalysts prepared by both $Mo(\eta 3\text{-}C_3H_5)_4$ and ammonium heptamolybdate tetrahydrate $(NH_4)_6Mo_7O_{24}\cdot 4H_2O$, and following characterization deduced that the ammonium heptamolybdate tetrahydrate method produced a lower dispersion of molybdenum oxide over silica, than the $Mo(\eta 3\text{-}$

$C_3H_5)_4$ method.[96,97] Tatibouet and co-workers[98] discovered that by grafting $MoCl_5$ with silanol OH groups on $SiO_2$, the molybdenum oxide sites are more accessible than when deposited using an impregnation method. Recent studies have observed that there is no correlation between synthesis methods and structure, because after calcination there is similar molybdenum dispersion regardless of the preparation method.[82,83] The amount of molybdenum oxide on the support does influence the structure, and hence catalytic activity. Structures which have been identified are isolated octahedral (oxomolybdenum system), tetrahedral (dioxomolybdenum system) and crystalline $MoO_3$ particles, (Figure 1.5) often co-existing.[75,82,99-102]

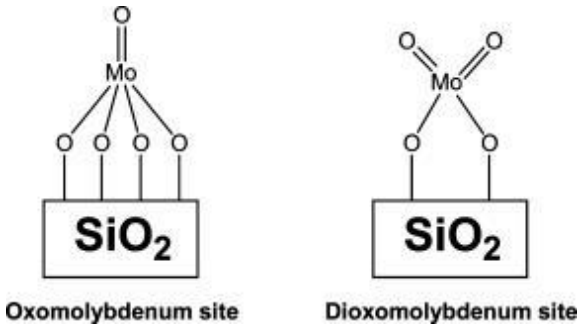


**Figure 1.5:** Structures of oxomolybdenum and dioxomolybdenm sites present on the surface of silica supported $MoO_3$.[103]

The oxidation of methanol on both systems (oxo and dioxomolybdenum) contains the same fundamental steps, where methanol dissociates onto the surface, followed by the rate determining hydrogen abstraction from the methoxy group.[103] The difference between the systems is in the mechanism of methanol oxidation. Oxomolybdenum sites undergo a bond cleavage in the Mo-O-Si sequence, which forms surface molybdenum methoxide species. The dioxomolybdenum site involves hydroxomolybdenum methoxide intermediates which are formed without the cleavage of the Mo-O-Si sequence. Seman *et al.*[104] report that at 250 °C during methanol oxidation, adsorption of methanol resulted in the formation of methoxide species on the silica support, and observed that these species

were mobile on $SiO_2$ and can migrate to the molybdenum centers, where they are oxidised to produce formaldehyde. Although the silica support is said to be inert,[104] the ability of silica to adsorb active participants in the reaction can be referred to as a non-innocent support. During the reaction, the isolated $MoO_3$ species are reported to undergo a transformation to β-$MoO_3$, where low loadings of molybdenum oxide on the support produce a high dispersion, which during the reaction, form microcrystalline β-$MoO_3$ particles (Figure 1.6), and high loadings of molybdenum form large crystalline β-$MoO_3$ particles during the reaction.

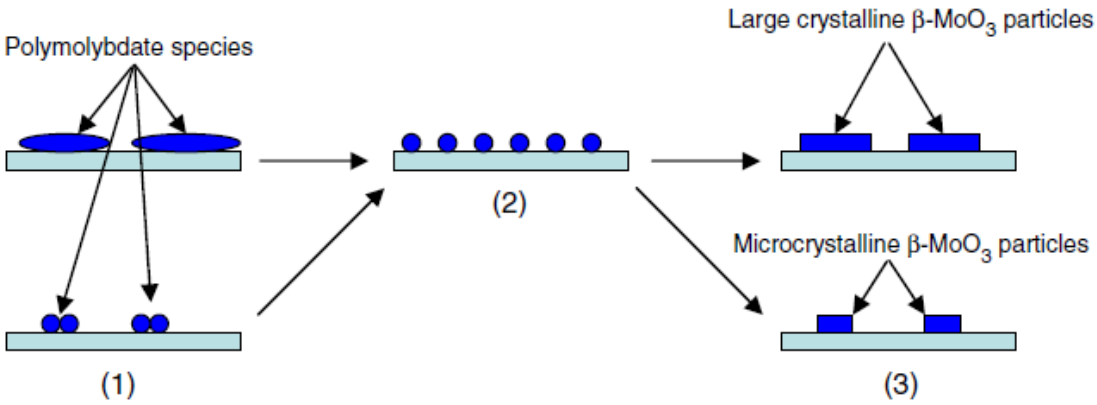


**Figure 1.6:** A schematic view of molybdenum oxide species on the silica support under ambient temperature (1), after dehydration (2) and under methanol oxidation (3).[89]

## 1.3 – Carbon monoxide (CO) oxidation

### *1.3.1 – Uses and properties of CO and $CO_2$*

Carbon monoxide is a colourless and odourless gas which is renowned for its high toxicity to humans and animals at quantities around 100 ppm. The largest source of carbon monoxide is in nature, where it is produced through photochemical reactions in the troposphere, generating on average $5x10^{12}$ kilograms per year.[105] Other natural

sources include forest fires, volcanoes and other forms of combustion. It was first observed unknowingly by a French chemist, de Lassone,[106] where he heated zinc oxide with coke but concluded mistakenly that the gas produced was hydrogen.

In general chemical terms, CO is produced form the partial oxidation of carbon containing compounds when there is not enough oxygen to produce $CO_2$. The major industrial production of CO is the heating of air at high temperatures which is passed over a bed of coke. The initial product is $CO_2$, but equilibrates with the remaining coke to produce CO. [107]

$$O_2 + 2\,C \rightarrow 2\,CO \quad (\Delta H = -221\ kJ/mol)$$

Other industrial applications to produce CO are the endothermic reaction of steam with carbon:

$$H_2O + C \rightarrow H_2 + CO \quad (\Delta H = +131 kJ/mol)$$

Also, the reduction of metal oxide cores with carbon:

$$MO + C \rightarrow M + CO$$

Carbon monoxide has many uses in the chemicals industry.[108] Hydroformylation reaction of alkenes, carbon monoxide and hydrogen produce large amounts of aldehydes, and when coupled with the Shell Higher Olefin Process in the production of linear alpha alkenes via ethylene oligomerization and olefin metathesis,[109] gives precursors to detergents. Other uses include the hydrogenation of CO to produce methanol, as well as the Monsanto process, which involves the reaction of methanol and carbon monoxide in

the presence of a homogeneous rhodium catalyst, and hydroiodic acid to give acetic acid.[110]

Carbon dioxide is a colourless gas at standard temperature and pressure but is known as 'dry ice' which is a solid below the temperature of -78.5 °C. $CO_2$ like CO, is a by-product of combustion reactions and exists naturally in the earth's atmosphere. $CO_2$ was one of the first gases to be discovered separate from air in the seventeenth century by the Flemish chemist Jan Baptist van Helmont, when charcoal was burned in a closed vessel, where he then discovered that the mass of the remaining ash was much less than the starting mass of the charcoal material. He deduced that the missing mass must have been transmuted into an invisible substance he termed a 'gas'. The properties of carbon dioxide were more thoroughly analysed in the 1750s by Joseph Black when he bubbled $CO_2$ through an aqueous solution of calcium hydroxide and precipitated calcium carbonate. Carbon dioxide is produced by a variety of industrial processes, a few of which are: methane conversion to carbon dioxide in hydrogen production plants; as a by-product of fermentation of sugar in the alcoholic beverages industry, and the thermal decomposition of calcium carbonate in the manufacture of lime. Carbon dioxide has an extremely wide range of uses from food and drink, oil recovery processes, pneumatic systems, and welding to name just a few.

### *1.3.2 – CO oxidation in relation to automotive catalysis*

By the 1960s, mass production of cars provided millions of people around the world with personal mobility, but oxidation of gasoline to $CO_2$ and $H_2O$ was far from efficient, and air pollution became a major problem in many large cities due to the by-products such as highly toxic CO, among other hydrocarbons and $NO_x$. Since legislations relating to the removal of pollutants from exhausts of automobiles initiated in California in the

1970s[111,112] were put into action, heterogeneous catalysis in this area has become the most interesting and widely researched topic by far. One of the first catalyst systems to lower the emission of such harmful fumes was a relatively simple platinum/alumina material, which at the time of discovery worked relatively well for reducing CO and hydrocarbon emissions. Due to even tighter limits for CO and hydrocarbon removal, but also due to the need to reduce $NO_x$ emissions, research was carried out to discover that the incorporation of ruthenium was a moderately efficient means of removing $NO_x$.[111-114]

Slightly more advanced catalytic systems involving platinum, palladium and ruthenium were the dual-bed converters, in which $NO_x$ was reduced in the first bed, and CO and hydrocarbons were oxidised in the second bed.[112] Again, there were further restrictions of $NO_x$ production standards in the 1980s and limitations of the dual-bed converter developed the three-way catalyst system, which is still used today. Early three way catalysts consisted of Pt and Rh dispersed at a weight ratio of 5:1 on alumina-coated cordierite monolith, with ceria added for oxygen storage. Later developments in the 1990s saw the replacement of Pt with Pd, due to the excellent $NO_x$ reduction seen with Pd,[115,116] and at the same time by segregating a portion of the Pd from ceria, resulted in better low-temperature performance.[117]

### *1.3.3 – Literature review of alternative catalysts*

Apart from CO oxidation being required for vehicles emissions removal, it has a major importance in other applications such as industrial, environmental and domestic fields. These include chemical sensors,[118] $CO_2$ lasers,[119] proton exchange membrane fuel cells[120-122] and air purification devices used by military personnel and miners.[123]

### *1.3.3.1 – Non-precious metal catalysts*

Due to the limited availability and high expense of precious metals, the search for substitute catalysts have been long sought after.[124] Mixed copper manganese oxides ($CuMnO_x$) also known as Hopcalite, has long been established as a catalyst of choice for many of the above applications, in particular the air purification devices (for the past 80 years)[125,126] which provide respiratory protection from CO poisoning.[127] In 1973, Rodgers *et al*. investigated the low temperature CO oxidation using mixed manganese oxide and copper oxide, to discover that the activity of the mixed oxides is much higher than the individual oxide activities alone. It was then suggested that this was due to the mixed oxides being able to be more easily re-oxidised by molecular oxygen after themselves being oxidised during the CO oxidation process.[126]

There are two widely accepted[128] possible reaction mechanisms for catalytic CO oxidation:

The Langmuir-Hinshelwood mechanism involves the following set of steps;

1. Competitive adsorption of reactant molecules from the gas phase onto the same surface.
2. Dissociation of the molecules on the surface.
3. Reaction between the adsorbed molecules/atoms.
4. Desorption of the reaction produce(s) to the gas phase.

The alternative is the Mars van Krevelen mechanism with the associated steps;

1. The metal/support is oxidised in a separate independent step.
2. CO molecules adsorb on the oxide from the gas phase.
3. Absorbed CO reacts with surface oxygen atoms from the oxide.
4. Produced $CO_2$ desorbs from the surface.

5. Resulting oxygen vacancies are re-filled rapidly and irreversibly by oxygen from the gas phase in a separate step (step 1 above).

The activity of CO oxidation using $CuMnO_x$ catalysts is effected by quite a broad range of phenomena as described by Taylor and co-workers[129,130] where preparation of the hopcalite catalysts by co-precipitation were varied in terms of ageing time, ageing pH, ageing temperature, copper/manganese molar ratio, and calcination temperature, and these were found to have an enormous effect on catalytic activity towards CO oxidation. Hutchings *et al*. observed that the optimum conditions for the co-precipitation preparation of $CuMn_2O_4$, is an ageing time of <30 min or >300min with a calcination temperature of 500 °C, since this catalyst reached a conversion of 88 % at 20 °C, compared to the 60 % and 77 % of calcination at 300 °C and 400 °C respectively. It has been suggested elsewhere[129] that the high activity of the un-aged or partially aged samples (0-30min), was associated with the lower crystallinity of the material, with these results consistent with previous reports where it is thought that the active form of copper manganese oxide is amorphous.[131-133] Hutchings and co-workers discussed that the precipitate initially consisted of CuO, $Cu_{1.4}Mn_{1.6}O_4$ and $Mn_2O_3$, and steadily transformed with increasing ageing time so that the amount of $Mn_2O_3$ is decreased and hence, the increased Mn incorporation into the mixed copper manganese oxide phase. This increased incorporation of the Mn was then attributed to the increased activity of the extended ageing times, possibly due to the Mn changing the iso-electric point of the surface, hence affecting its surface charge and so removes the excess sodium from the surface (known to poison the catalytic activity) which will have been retained from insufficient washing.

Although the discovery by Haruta and co-workers[134] around 25 years ago that highly dispersed gold particles on oxide supports show extremely high activity for CO oxidation

at sub-ambient temperatures, there are very few reports of promotion of hopcalite materials using precious metals such as gold. Lamb *et al.*[135] was one of the first to promote copper manganese mixed oxide with silver which enhanced the activity of the catalyst. Among the limited reports of gold promotion, Cole *et al*. observed that by using a new preparation method (deposition-precipitation) with the addition of gold, that the activity was enhanced quite dramatically. The use of 1 wt% Au (75 % conversion) saw an increase in conversion of 50 % after 120 min on stream, compared to the un-promoted $CuMnO_x$ catalyst (25 % conversion), and it was postulated that this increase in activity was due to the enhanced mobility of the active lattice oxygen species responsible for CO oxidation. A similar result was seen by Morgan and co-workers[128] where a 0.5 wt% Au loading on $CuMnO_x$ increased the activity of the catalysts with 55 % conversion achieved with the promoted catalyst, compared to 25 % conversion of the un-promoted catalyst after 100 min on stream.

#### *1.3.3.2 – Precious metal catalysts*

The use of precious metals, Pt and Rh, for CO oxidation in automotive exhaust catalysis is widespread. However, since the pioneering discovery by Haruta *et al.*[134] in 1989 that supported nanoparticles of gold oxidized CO at temperatures below 203 K (compared to >500 K for Pt and Rh),[136] there has been an extremely high volume of interest and articles including many excellent reviews[137-142] on supported gold catalysts. To date, there are a lot of controversial and unresolved issues relating to the active site, oxygen adsorption site, water effect, preparation effect, support effect and poisoning effect on activity. Due to the complex nature of the metal-support interaction when involved in CO oxidation, many single crystal studies have been investigated, but still there are conflicting reports. Saliba and co-workers,[143] report the use of Au (111) coated with

ozone for CO oxidation at 300 K, and calculated a negative activation energy of -2.5 kcal/mol, whereas, Outka *et al*.[144] report the use of a Au (110) single crystal, but observe a positive activation energy in the same temperature range as Saliba and co-workers. These model systems although providing detailed information about the surface science of the reaction are limited, since they do not include some of the important features of potential practical catalysts *i.e.* hydroxyl groups and/or water.[145]

Gold nanoparticles supported on reducible metal oxide supports ($Au/TiO_2$, $Au/Fe_2O_3$, $Au/CeO_2$) are widely accepted to be the most active catalysts, compared to non-reducible supports ($Au/Al_2O_3$, $Au/SiO_2$).[134,139,141] Bulk gold is known to be relatively inert and inactive for many oxidation reactions.[146] However, Koun Min *et al*. have shown that by using a closed recirculation system at temperatures between 249K and 294K, unsupported gold powder is active for CO oxidation, even though it is two orders of magnitude less active than supported gold nanoparticles.[147] It was suggested that the interaction of metal and support, or the nanoparticles size (mean of 3.5 nm of supported Au and mean of 76 nm diameter for unsupported Au) play a vital role in the differing activity. The choice of reducible metal oxide support for CO oxidation can sometimes be misleading due the number of conflicting results published by authors who use the same supports and same reaction conditions. One example is from Comotti *et al*.[148] who found that a $Au/ZrO_2$ catalyst for CO oxidation had poor activity, with 50 % conversion at temperatures ranging from 347–373K, which is in disagreement with Wolf *et al*.[149] who observe 50 % conversion at 253 K, which suggests that the reducibility of a support as a main factor affecting CO oxidation alone, is in doubt.

The main routes of preparation of supported gold catalysts are co-precipitation, impregnation, and deposition-precipitation. It is widely reported that the preparation

technique which produces the most active catalysts is deposition-precipitation. Colloidal-deposition is becoming an increasingly used alternative, since it is possible to produce very small nanoparticles (using a protecting agent such as PVA or glucose) which are not influenced by the support, as the nanoparticles are generated before they are deposited on the support.[148] Further pre-treatment of these catalysts such as calcination which may form cationic Au, is known to increase the nanoparticle size of the Au *i.e.* after calcination at 550 °C there is an increase of 3.8 nm (mean) to 4.9 nm (mean), and this is remarkable considering the low thermal stability of impregnation prepared Au supported catalysts.[148] Although still disputed, the role of the support in the CO oxidation reaction is reported to adsorb oxygen which can then move to the metal-support interface.[150,151]

To understand the variety of possible reasons for the activity of certain supports and nanoparticle size *etc*. in CO oxidation, it is appropriate that the possible active sites be discussed. Bond and Thompson published a review in 2000, and proposed that the active sites consist of nanoparticles incorporating both zerovalent and cationic gold, with the cationic gold positioned at the metal-support interface (Figure 1.7).[141] Haruta[152] published a review in 2002, which, based on kinetics of CO oxidation catalysed by supported gold, states there are two temperature regions which contain different kinetics and activation energies. At temperatures below 200K, the reaction catalysed by $Au/TiO_2$ takes place at the surfaces of small gold nanoparticles dispersed on the support. Above 300K, the reaction occurs at gold atoms at the perimeter sites of the supported gold nanoparticles.[145]

There are further reports by Hutchings *et al.*[153] and Guzman *et al.*[154] that agree with Bond and Thompson's proposed active sites. They state that cationic gold plays a role in CO oxidation, after discovering that no cationic gold was observed in the almost inactive catalysts. Density functional theory (DFT) has played a major role in confirming real

catalytic observations on supported Au catalysts. In general, calculations have shown that cationic,[155] zerovalent,[156] and anionic gold,[157] are all capable of adsorbing CO.

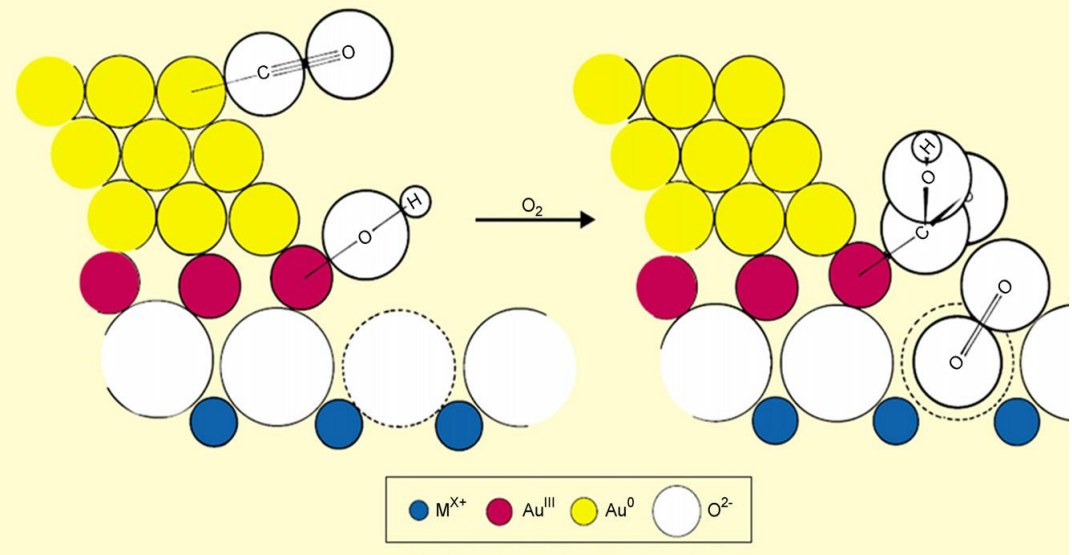


**Figure 1.7:** Proposed active site and reaction mechanism for CO oxidation (catalysed by supported gold nanoparticles).[141]

Another factor which is discussed frequently which relates to the activity of supported gold nanoparticles in CO oxidation, is the adsorption of oxygen. Stiehl and co-workers[158] discovered that molecularly adsorbed oxygen participates, by exposing $Au/TiO_2$ (110) samples to CO, and observing that more $CO_2$ was formed on the samples containing molecular oxygen. In disagreement to this however, Deng *et al.*[159] report the participation of atomic oxygen in the activity of a Au (111) catalyst. In addition to the support, particle size, and preparation techniques which affect catalytic activity, there are two other important factors which can also play a major role in activity for CO oxidation. Haruta and co-workers were one of the first research groups to observe the effect of moisture in the feed stream over $Au/TiO_2$ and $Au/Al_2O_3$ catalysts, and reported that the addition of moisture increased the catalytic activity by over four orders of magnitude at 273 K.[160,161] Calla *et al.*[162] also observed the same trend by adding 0.16 mol% water into the feed stream over the same catalysts, and observed a large increase in catalytic activity which

they suggest was due to the formation and/or regeneration of active sites. The other factor which affects catalytic activity significantly is poisoning of the catalyst by halide ions such as $Cl^-$, which are present due to the use of the gold solution $HAuCl_4$ as a precursor during the preparation. Yang *et al.* showed that the gold on the surface of a $Au/Al_2O_3$ catalyst became agglomerated with the residual presence of $Cl^-$ and this decreased the reducibility of the Au cations.[163]

## 1.4 – Research objectives

The aim of this thesis is to gain further insight into the catalytic activity of metal phosphate materials for selective methanol oxidation to formaldehyde. In particular, molybdenum phosphate and vanadium phosphate catalysts have been studied, as both the oxide forms of these metals are known to be active catalysts in many oxidation reactions, including selective methanol oxidation. However, it is known that the role of phosphorus in heterogeneous catalysis can be to increase the mobility of lattice oxygen to the surface, which could have advantages in redox process, increasing the reducibility of the metal on the surface during oxidation reactions. It is therefore appropriate to investigate the activity of metal phosphate catalysts and compare their activity to their analogous metal oxide catalysts, and also commercial catalysts such as iron molybdate used for selective methanol oxidation to formaldehyde.

This thesis also investigates the catalytic activity of supported mono-metallic and bi-metallic Au(Pd) catalysts used in CO oxidation for selective oxidation of methanol. Supported mono-metallic gold catalysts are of great interest in CO oxidation, and here, a new synthesis method of preparing very small nanoparticles of gold has been used and the resultant materials tested for CO oxidation and methanol oxidation. The use of these catalysts for methanol oxidation is not widely reported, but the few previous studies

indicate that mono-metallic gold and bi-metallic gold(palladium) catalysts are highly active due to the small nanoparticles of dispersed gold, and so these catalysts could prove to be active for methanol oxidation.

## 1.5 – References


1. S. Green, *Industrial Catalysis*, Macmillan Company, New York, **1928**.
2. J. J. Berzelius, *Årsberättelsen om framsteg i fysik och kemi*, Royal Swedish Academy of Sciences, **1835**.
3. J. F. Coindet. *Ann. Chim*. **1798**, *26*, 58–85
4. L. J. Thenard. *Ann. Chim. Phys*. **1818**, *8*, 306.
5. L. J. Thenard. *Ann. Chim. Phys*. **1818**, *9*, 96.
6. J. W. Döbereiner. *Schweigger´s J.* **1822**, *34*, 91.
7. G. Lemoine. *Ann. Chim. Phys*. **1877**, *12*, 145.
8. H. Taylor. *J. Chem. Soc.* **1944**, *66 (10,)* 1615–1617.
9. Hager, Thomas. *The Alchemy of Air*. Harmony Books, New York, **2008**.
10. P. Phillips. *Nature* **1926**, *117*, 419-421.
11. Mittash, Pier and Winkler, F.P. 571356 (**1923**) to BASF.
12. S. P. S. Andrew, *Post Congr. Symp., 17th Int. Congr. Catal., Osaka*, **1980**, paper 12.
13. G. Reuss, W. Disteldorf, O. Grundler, and A. Hilt, *Formaldehyde. In Ullmann Encyclopaedia of Industrial Chemistry, 5th Edition*; VCH Publishers, **1992**, *Vol. A11*, 619.
14. H. R. Gerberich, A. L. Stautzenberger and W. C. Hopkins. *Formaldeyde. In Encyclopaedia of Chemical Technology, 3rd Edition*; D.F.A., Eds.; Standen Editores Jonh Wiley & Sons, Inc. **1983**, *Vol. 11*, 231.
15. G. Alessandrini, P. Cariati, P. Forzatti, P. L. Villa and F. Trifiro : *Proc. 2nd. Int. Conf.* **1976**, 186.
16. K. K. Lee, A. Al-Jarallah, *Chem. Econ. Eng. Rev.* **1986**, *18 (9)*, 25-34.
17. J. R. Fair and R. C. Kmetz. *Formaldehyde. In Encyclopaedia of Chemical Processing and Design*; J. J. McKetta and W. A. Cunningham. Eds.; Marcel Dekker, Inc. **1985**, *Vol. 23*, 350.
18. A. Butlerov. *Ann. Chem.* **1859**, *111*, 242.

19. A. W. von Hofmann. *Ann. Chem.* **1868**, *145*, 357.
20. L. H. Baekeland. *Journal of Industrial and Engineering Chemistry* **1909**, *1*, 545.
21. H. Adkins, W. R. Peterson. *Journal of the American Chemical Society* **1931**, *53*, 1512.
22. S.A.R.K. Deshmukh, M. van Sint Annaland, J. A. M. Kuipers. *Applied Catalysis A: General* **2005**, *289*, 240-255.
23. A. R. Chauvel, P. R. Curty, R. Maux and C. Petitpas. *Hydr. Proc*. **1973**, *51*, 179.
24. A. B. Stiles and T. A. Koch. *Oxidation Catalysts. In Catalyst Manufacture, 2nd Edition*; Editor Marcel Dekker: New York; **1995**, *197* Chap.20.
25. M. Quain, M. A. Liaw, G. Emig. *Applied Catalysis A: General* **2003**, *238*, 211-222.
26. G. Waterhouse, G. Bowmaker and J. Metson. *Appl. Catal. A: General* **2004**, *265*, 85-101.
27. A. Andreasen, H. Lynggaard, C. Stegelmann and P. Stoltze. *Appl. Catal. A: General* **2005**, *289*, 267-273.
28. L. Lefferts and J. G. van Ommen, J. Ross. *Appl. Catal.* **1986**, *23*, 385-402.
29. R. Clayton and S. Norval. *Chem. Soc. Spec. Per. Rep*. **1980**, *3*, 70.
30. M. Kaliya, S. Brailovski, O. Temkin, Moskovko. *Kin. i. Kat*, **1978**, *19*, 1508.
31. L. Kurina, L. Novezhenova, L. Orlova, L. Koval, and T. Dobrynina, *Zh. Fiz. Khimi*. **1978**, *52*, 1507.
32. H. Liu, and E. Iglesia. *Journal of Physical Chemistry B* **2005**, *109*, 2155.
33. S. Ruf, A. May, G. Emig. *Applied Catalysis, A: General* **2001**, *213*, 203.
34. L. P. Ren. W. L. Dai. Y. Cao. K. N. Fan. *Catalysis Letters* **2003**, *85*, 81.
35. M. Bowker, R. Holroyd, A. Elliott, P. Morrall, A. Alouche, C. Entwistle and A. Toerncrona, *Catalysis Letters* **2002**, *83* (3-4).
36. P. F. Kerr, A. W. Thomas and A. M. Langer. *The American Mineralogist*, **1963**, *48*, 14.
37. G. D. Kolovertnov, G. K. Boreskov, V. A. Dzisko, B. I. Popov, D. V. Tarasova, and G. C. Belugina. *Kinet. Catal. (Engl. Transl.),* **1965**, *6(6)*, 950.
38. J-M. Leroy, S. Peirs and G. Tridot. *E´tude Physicochimique de Compose´s Ternaires*. *Comptes Rendus Acad*. Sc. Paris, series C, 218.
39. G. Alessandrini, L. Cairati, P. Forzatti, P. L. Villa and F. Trifiro. *J. Less-Comm. Met*. **1977**, *54*, 373.

40. G. M. Bartenev, G. K. Boreskov, R. R. Zakirov, B. I. Popov, E. P. Prokopev and A. D. Tsyganov. *Mossbauer Spectra. Kinet.Catal. (Engl. transl.).* **1972**, *13(1)*, 213.
41. L. Cairati, M. Carbucicchio, O. Ruggeri and F. Trifiro. *Stud. Surf. Sci. Catal*. **1979**, *3*, 279.
42. M. Carbucicchio, *J. Chem. Phys*. **1979**, *70(2)*, 784.
43. P. Forzatti, P. L. Villa, N. Ferlazzo and D. Jones. *J. Catal*. **1982**, 76, 188.
44. C. J. Machiels, U. Chowdry, W. T. A. Harrison and A. W. Sleight. *Am. Chem. Soc. Symp. Ser*. **1985**, 279.
45. P. L. Villa, A. Szabo, F. Trifiro and M. Carbucicchio. *J. Catal*. **1977**, *47*, 122.
46. M. Ai. *J. Catal*. **1978**, *52*, 16.
47. N. Pernicone. *J. Less comm. Met*. **1974**, *36*, 289.
48. F. Trifiro, S. Notarbartolo and I. Pasquon. *J. Catal*. **1971**, *22*, 324.
49. L. M. Plyasova, R. F. Klevtsova, S. V. Borisov and L. M. Kefeli. *Soviet Physics-Doklady (Engl. Transl.).* **1966**, *11(3)*, 189.
50. H. –Y. Chen. *Mat. Res. Bull*. **1979**, *14*, 1583.
51. G. Fagherazzi and N. Pernicone. *J. Catal*. **1970**, *16*, 321.
52. A. Soares, M. Portela, A. Kiennemann, L. Hilaire and J. Millet. *Appl. Catal. A: General* **2001**, *206*, 221-229.
53. M. Bowker, R. Holroyd, M. House, R. Bracey, C. Bamroongwongdee, M. Shannon and A. Carley. *Top Catal.* **2008**, *48*, 158-165.
54. M. R. Sun-Kou, S. Mendioroz, J. Fierro, J. Palacios and A. Guerrero-Ruiz, *J. Mater. Sci.* **1995**, *30*, 496.
55. J. Novakova and P. Jiru. *J. Catal*. **1972**, *27*, 155.
56. A. Soares, M. Portela, A. Kiennemann and J. Millet. *React. Kinet. Catal. Lett.* **2002**, *75* (1), 13-20.
57. P. Jiru, B. Wichterlova and J. Tichy: *Proc. 3rd International Congress on Catalysis*. **1964**, *1*,199. Amsterdam.
58. M. House, A. Carley and M. Bowker, *Journal of Catalysis* **2007**, *252*, 88-96.
59. J. M. Tatibouet and J. E. Germain. *Bull. Soc. Chim.* **1980**, *1*, 343.
60. J. M. Tatibouet and J. E. Germain. *J. Catal.* **1981**, *72*, 375.
61. J. M. Tatibouet, J. E. Germain and J. C. Volta. *J. Catal.* **1983**, *82*, 240.
62. Q. Wang and R. J. Madix. *Surface Science*, **2002**, *496(1-2)*, 51-63.
63. Bronkema and Bell, *J.Phys. Chem. C.* **2008**, *112*, 6404-6412.

64. G. S. Wong, R. R. Concepcion and J. M. Vohs. *J. Phys. Chem. B*. **2002**, *106*, 6451-6455.
65. T. Kim and I. E. Wachs. *J. Catal.* **2008**, *255(2)*, 197-205.
66. M. V. Ganduglia-Pirovano, C. Popa, J. Sauer, H. L. Abbott and A. Uhl. *J. Am. Chem. Soc.* **2010**, *132*, 2345-2349.
67. G. V. Isaguliants and I. P. Belomestnykh. *Catalysis Today* **2005**, *100*, 441.
68. G. Deo and I. E. Wachs, *J. Catal*. **1994**, *146*, 323.
69. L. J. Burcham and I. E. Wachs, *Catal. Today*, **1999**, *49*, 467.
70. P. A. Dilara and J. M. Vohs. *Surf. Sci.* **1994**, *321*, 8.
71. J. M. Sturm, D. Gobke, H. Kuhlenbeck, J. Dobler, U. Reinhardt, M. V. Ganduglia-Pirovano, J. Sauer and H.-J. Freund: *Phys. Chem. Chem. Phys*. **2009**, *11*, 3290–3299.
72. S. Guimond, D. Gobke, Y. Romanyshyn, J. M. Sturm, M. Naschitzki, H. Kuhlenbeck and H.-J. Freund, *J. Phys. Chem. C*, **2008**, *112*, 12363.
73. S. Guimond, J. M. Sturm, D. Gobke, Y. Romanyshyn, M. Naschitzki, H. Kuhlenbeck and H.-J. Freund. *J. Phys. Chem. C*, **2008**, *112*, 11835.
74. G. V. Isaguliants and I. P. Belomestnykh. *Catalysis Today* **2005**, *100*, 441.
75. W. –H. Cheng, *Journal of Catalysis* **1996**, *158*, 477-485.
76. C. Gleitzer and P. Pascal. Complements au Nouveau Trait6 de Chimie Minerale, **1976**, *5*, 89.
77. Gmelins Handbuch der Anorganischen Chemie, Molybdan, Erganzungsband, Teil B 1, Springer-Verlag, Berlin, **1975**, 86.
78. J. C. Volta, J. M. Tatibouet, C. Phichitkul and J. E. Germain. in *Proc. 8th Int. Congr. Catal.*, **1984**, *4*, Verlag Chemie and Dechema, Berlin, 45.
79. W. E. Farneth, F. Ohuchi, R. H. Staley, U. Chowdhty and A.W. Sleight. *J. Phys. Chem.*, **1985**, *89*, 2493.
80. W. E. Farneth, E. M. McCarron, A. W. Sleight and R. H. Staley. *Langmuir*, **1987**, *3*, 217.
81. W. E. Farneth, R. H. Staley and A. W. Sleight. *J. Am. Chem. Soc*. **1986**, *108*, 2327.
82. C. C. Williams, J. G. Ekerdt, J. M. Jehng, F. D. Hardcastle, A. M. Turek and I. E. Wachs. *J. Phys. Chem*. **1991**, *95***,** 8781.
83. R. D. Roark, S. D. Kohler and J. G. Ekerdt. *Catal. Lett.* **1992**, *16***,** 71.
84. T. J. Yang and J. H. Lunsford. *J. Catal.* **1987**, *103***,** 55.

85. M. Carbucicchio and F. Trifiro. *J. Catal.* **1980**, *62***,** 13.
86. C. C. Williams and J. G. Ederdt. *J. Catal.* **1993**, *141***,** 430.
87. M. Carbucicchio, F. Trifiro and A. Vaccari. *J. Catal.* **1982**, *75***,** 207.
88. K. Bruckman, B. Grzybowska, M. Che and J. M. Tatibouet. *Appl. Catal. A Gen.* **1993**, *96***,** 279.
89. G. Li, G. Xia and Z. C. Zhang. *Top. Catal.* **2009**, *52*, 1381–1387.
90. J. M. Tatibouet. *Appl. Catal. A.* **1997**, *148*, 213.
91. D. S. Kim, I. E. Wachs and K. Segawa. *Journal of Catalysis* **1994**, *146*, 268-277.
92. G. Busca. *Catal. Today.* **1996**, *27*, 457.
93. M. A. Banares and I. E. Wachs. *J Raman Spectrosc*. **2002**, *33*, 359.
94. C. Louis, M. Che and F. Bozonverduraz. *J Chim Phys Pcb* **1982**, *79*, 803.
95. M. Che, C. Louis, J. M. Tatibouet. *Polyhedron* **1986**, *5*,123.
96. J. M. Stencel, J. R. Diehl, J. R. Deste, L. E. Makovsky, L. Rodrigo, K. Marcinkowska, A. Adnot, P. C. Roberge and S. Kaliaguine. *J Phys Chem-US.* **1986**, *90*, 4739.
97. L. Rodrigo, K. Marcinkowska, A. Adnot, P. C. Roberge, S. Kaliaguine, J. M. Stencel, L. E. Makovsky and J. R. Diehl. *J Phys Chem-US*. **1986**, *90*, 2690.
98. C. Louis, J. M. Tatibouet and M. Che, *J. Catal.* **1988**, *109*, 354.
99. H. Hu, I. E. Wachs and S. R. Bare. *J. Phys. Chem.* **1995**, *99*, 10897.
100. J. –M. Jehng, G. Deo, B. M. Weckhuysen and I. E. Wachs. *J. Phys. Chem. A.* **1996**, *110*, 4.
101. C. Morterra, *G.* Magnacca and V. Bolis. *Catal. Today* **2001**, *70*, 43.
102. M. A. Banares, H. Hu and I. E. Wachs. *J. Catal.* **1994**, *150*, 407.
103. L. J. Gregoriades, J. Dobler and J. Sauer. *J. Phys. Chem. C.* **2010**, *117(7)*, 2967-2979.
104. M. Seman, J. N. Kondo and K. Domen. *J. Phys. Chem. B* **2004,** *108*, 3231 3239
105. B. Weinstock and H. Niki. *Science* **1972**, *176(4032)*, 290–2.
106. L. D. Prockop and R. I. Chichkova. *Journal of the Neurological Sciences* **2007**, *262*,122–130.
107. J. R. Rostrup-Nielsen, *J. Catal*. **1972**, *27*, 343-356.
108. C. Elschenbroich and A. Salzer. "*Organometallics : A Concise Introduction*" *(2nd Ed)* Wiley-VCH: Weinheim, **2006**.

109. Klaus Weissermel and Hans-Jurgen Arpe. *"Industrial Organic Chemistry" 3rd Ed*, John Wiley & Sons; **1997**.

110. J. H. Jones. *Platinum Metals. Rev*. **2000**, *44(3)*, 94–105.

111. K. C. Taylor, in "*Catalysis: Science and Technology"*, Springer-Verlag, Berlin, *5*, 119. **1984**.

112. H. S. Gandhi, G. W. Graham and R. W. McCabe, *J. Catal*., **2003**, *216*, 433.

113. K. C. Taylor, *Catal. Rev. Sci. Eng*. **1993**, *35*, 457.

114. N. Takahashi, H. Shinjoh, T. Iijima, T. Suzuki, K. Yamazaki, K. Yokota, H. Suzuki, N. Miyoshi, S. Matsumoto, T. Tanizawa, T. Tanaka, S. Tateishi and K. Kasahara, *Catal. Today*. **1996**, *27*, 63.

115. J. C. Summers, W. B. Williamson, M. G. Henk, *Society of Automotive Engineers*, **1988**, *97*,158.

116. J. C. Summers, J. J. White, W. B. Williamson, *Society of Automotive Engineers*. **1989**, *98*, 360.

117. J. Dettling, Z. Hu, Y. K. Lui, R. Smaling, C. Z. Wan, A. Punke, in: *A. Frennet, J.-M. Bastin (Eds.), Studies in Surface Science and Catalysis*, *96*, Elsevier, Amsterdam, **1995**, 461.

118. S. D. Gardner, G. B. Hoflund, D. R. Schryer, B. T. Upchurch, E. J. Kielin, *Langmuir* **1991**, *7*, 2135.

119. G. B. Hoflund, S. D. Gardner, D. R. Schryer, B. T. Upchurch, E. J. Kielin, *Appl. Catal. B: Environ*. **1995**, *6*,117.

120. M. Götz and H. Wendt. *Electrochim. Acta* **1998**, *43*, 3637.

121. D. T. K. Luengnaruemitchai, S. Thoa, E. Osuwan, Gulari, *Int. J. Hydrogen Energy* **2005**, *30*, 981.

122. Y. Teng, H. Sakurai, A. Ueda and T. Kobayashi. *Int. J. Hydrogen Energy* **1999**, *24*, 355.

123. S. H. Taylor and C. Rhodes. *Catal. Lett*. **2005**, *101*, 31.

124. M. Kang, M. W. Song, C. H. Lee. *Appl. Catal. A: Gen*. **2003**, *251*, 143.

125. D. R. Men-ill, C. C. Scalione. *J. Am. Chem. Soc*. **1921**, *43*, 1982–2002.

126. T. H. Rogers, C. S. Piggot, W. H. Bahlke, J. M. Jennings. *J. Am. Chem. Soc.* **1921**, *43*, 1973– 1982.

127. H. A. Jones, H. S. Taylor, *J. Phys. Chem.* **1923**, *2,* 623.

128. K. Morgan, K. J. Cole, A. Goguet, C. Hardacre, G. J. Hutchings, N. Maguire, S. O. Shekhtman, S. H. Taylor. *Journal of Catalysis* **2010**, *276*, 38–48.

129. A. A. Mirzaei, H. R. Shaterian, R. W. Joyner, M. Stockenhuber, S. H. Taylor, G. J. Hutchings. *Catal. Commun*. **2003**, *4*, 17–20.
130. A. A. Mirzaei, H. R. Shaterian, M. Kaykhaii. *Appl. Surf. Sci*. **2005**, *239*, 246–254.
131. G. J. Hutchings, A. A. Mirzaei, R. W. Joyner, M. R. H. Siddiqui, S. H. Taylor, *Catal. Lett.* **1996**, *42*, 21.
132. G. J. Hutchings, A. A. Mirzaei, R. W. Joyner, M. R. H. Siddiqui, S. H. Taylor, *Appl. Catal. A.* **1998**, *166*,143.
133. G. G. M. Schwab, S. B. Kanungo. *Phys. Chem*. **1977**, *107*, 109.
134. M. Haruta, N. Yamada, T. Kobayashi, S. Iijima. *J. Catal.* **1989**, *115*, 301.
135. A. B. Lamb, W. C. Bray, J. C. W. Frazer. *J. Ind. Eng.* **1920**, *12*, 213.
136. K. Christmann. S. Schwede, S. Schubert, W. Kudernatsch. **2010**, *11*, 1344-1363.
137. M. Haruta, *Catalysis Today*, **1997**, *36*, 153.
138. M. Haruta and M. Date. *Appl. Catal. A*, **2001**, *222*, 427.
139. M. Haruta, *Chemical Record*, **2003**, *3*, 75.
140. G. C. Bond and D. T. Thompson, *Catalysis Reviews: Science and Engineering*, **1999**, *41*, 319.
141. G. C. Bond and D. T. Thompson, *Gold Bull*. **2000**, *33*, 41.
142. G. C. Bond. *Catal. Today*, **2002**, *72*, 5.
143. N. Saliba, D. H. Parker and B. E. Koel. *Surf. Sci*. **1998**, *410*, 270.
144. D. A. Outka and R. J. Madix. *Surf. Sci*., **1987**, *179***,** 351.
145. J. C. Fierro-Gonzalez and B. C. Gates. *Catalysis Today* **2007**, *122*, 201–210.
146. T. V. Choudhary and D. W. Goodman, *Topics in Catalysis* **2002**, *21(1–3),* 25.
147. B. K. Min and C. M. Friend. *Chem Rev.* **2007**, *107(6)*, 2709-2724.
148. M. Comotti, W. –C. Li, B. Spliethoff, F. Schuth. *J. Am. Chem. Soc*. **2006**, *128*, 917.
149. A. Wolf and F. Schuth. *Appl. Catal. A.* **2002**, *226*, 1.
150. J. D. Grunwaldt and A. Baiker, *J. Phys. Chem. B,* **1999,** *103*, 1002.
151. Z. M. Liu and M. A. Vannice. *Catal. Lett*. **1997**, *43*, 51.
152. M. Haruta. *CATTECH 6,* **2002**, 102.
153. G. J. Hutchings, M. S. Hall, A. F. Carley, P. Landon, B. E. Solsona, C. J.Kiely, A. Herzing, M. Makkee, J. A. Moulijn, A. Overweg, J. C. Fierro-Gonzalez, J. Guzman, B. C. Gates, *J. Catal*. **2006**, *242*, 71.
154. J. Guzman, B. C. Gates, *J. Am. Chem. Soc*. **2004**, *126*, 2672.

155. G. Fielicke, G. von Helden, D. B. Meijer, B. Pedersen, D. M. Simard, J. Rayner, *J. Am. Chem. Soc*. **2005**, *127*, 8416.

156. Z.-P. Lui, P. Hu, *J. Am. Chem. Soc*. **2002**, 124, 14770.

157. L. D. Socaciu, J. Hagen, T. M. Bernhardt, L. Woste, U. Heiz, H. Hakkinen, U. Landman, *J. Am. Chem. Soc*. **2003**, *125*, 10437.

158. J. D. Stiehl, T. S. Kim, S. M. McClure, C. B. Mullins, *J. Am. Chem. Soc*. **2004**, *126*, 1606.

159. X. Deng, B. K. Min, A. Guloy, C. M. Friend, *J. Am. Chem. Soc*. **2005**, *127* 9267.

160. M. Date and M. Haruta. *J. Catal.* **2001**, 201, 221.

161. M. Date, M. Okumura, S. Tsubota, M. Haruta. *Angew. Chem.* **2004**, *43*, 2129.

162. J. T. Calla and R. J. Davis. *J. Catal.* **2006**, *241*, 407.

163. H. –S. Oh, J. H. Yang, C. K. Costello, Y. M. Wang, S. R. Bare, H. Kung, M. C. Kung, *J. Catal*. **2002**, *210*, 375.

# 2

# *Chapter 2 - Experimental*

## 2.1 - Introduction

This chapter contains the detailed preparation of unsupported and supported, molybdenum phosphate and vanadium phosphate catalysts. Transition metals have been added to both metal phosphate catalysts, with a view to promoting their activity in oxidation reactions. Along with the metal phosphate catalysts prepared, supported mono-metallic and bi-metallic gold(palladium) catalysts have also been prepared. The catalysts were characterised using a range of analytical techniques, and tested for partial and total oxidation reactions such as methanol oxidation and carbon monoxide oxidation respectively.

## 2.2 – Catalyst preparation

Three main synthesis methods are used to prepare the catalysts: co-precipitation, which was used to prepare the unsupported metal phosphate catalysts, incipient wetness procedure, that was used to prepare supported metal phosphate catalysts, and the sol-immobilization method, which was used to prepare supported mono-metallic and bi-metallic gold(palladium) catalysts.

Chemicals used in the catalyst preparation are reported in Table 2.1:

**Table 2.1:** Chemicals used in the preparation of catalysts.

| Chemical formula | Purity |
|---|---|
| $MoO_3$ | Sigma-Aldrich >99.5 % |
| $(NH_4)_6Mo_7O_{24}.4H_2O$ | Sigma-Aldrich 99.98 % |
| $V_2O_5$ | Sigma-Aldrich >98 % |
| $SiO_2$ | Degussa AG, Aerocat |
| $TiO_2$ | Degussa, P25 |
| $Al_2O_3$ | Condea Chemie, Puralox |
| $H_3PO_4$ | Aldrich, 85 % in $H_2O$, 99.99 % |
| $HNO_3$ | Fisher Chemical, 70 % Analytical Grade |
| $(CH_3)_2CHCH_2OH$ | Sigma-Aldrich, anhydrous, 99.5 % |
| $PdCl_2$ | Sigma Aldrich, Conc. of Pd precursor: 6.24 mg/ml |
| $HAuCl_4.3H_2O$ | Sigma Aldrich, Conc. of Au precursor: 12.25 mg/ml |
| Poly (vinyl alcohol) (PVA) | Aldrich, MW=10 000, 80 % hydrolyzed |
| $NaBH_4$ | Sigma-Aldrich, puriss 99 % |

## 2.2.1 – Unsupported molybdenum phosphate catalysts

### *2.2.1.1 - $MoO_2 \cdot HPO_4 \cdot H_2O$ – Molybdenum (VI) ortho-phosphate hydrate*

$MoO_3$ (15 g) was dissolved in phosphoric acid (45 ml), by refluxing the mixture at 180 °C until a clear, green solution formed (1.5 h). The solution was then cooled to room temperature, before $HNO_3$ (300 ml) was added, and the mixture refluxed for a further 16 h. The mixture was left to cool at room temperature, and the solid recovered by vacuum filtration, before washing with cold water (100 ml) and acetone (100 ml). The resultant $MoO_2 \cdot HPO_4 \cdot H_2O$ was then dried for 24 h at 110 °C.[1]

#### *2.2.1.2 - $(MoO_2)_2P_2O_7$ – Molybdenum (VI) pyrophosphate*

The molybdenum pyrophosphate phase can be prepared in two ways: Calcination of $MoO_2 \cdot HPO_4 \cdot H_2O$ in static air at 650 °C for 6 h, using a ramp rate of 20 °C/min. Heating $MoO_2 \cdot HPO_4 \cdot H_2O$ in nitrogen at 500 °C for 6 h (20 °C/min).

### 2.2.2 – Supported molybdenum phosphate catalysts

#### *2.2.2.1 - $(MoO_2)_2P_2O_7$ supported on $TiO_2$, $Al_2O_3$ & $SiO_2$*

The supported molybdenum pyrophosphate catalysts were prepared using the incipient wetness method. Distilled water was added to a specific amount of support to determine the amount required to fill the pores. The amount of $MoO_2 \cdot HPO_4 \cdot H_2O$ precursor needed to give the desired loading of the catalyst on the support was calculated, and dissolved in water. The solution was added to the support, and dried at 110 °C in an oven for 16 h.

To form the molybdenum pyrophosphate phase, the supported catalysts were calcined at 650 °C for 6 h in static air (20 °C/min).

### 2.2.3 – Mixed molybdenum/metal phosphate catalysts

#### *2.2.3.1 – Addition of transition metals to unsupported $(MoO_2)_2P_2O_7$*

The addition of vanadium to molybdenum pyrophosphate, was carried out using the method previously, to prepare $MoO_2 \cdot HPO_4 \cdot H_2O$ (followed by calcination). The transition metal (M) was added during the first step of the preparation in the form of the metal oxide (Table 2.1).

$MoO_3$ (5 g) and M (varying amounts) were added to a 250 ml round bottom flask, along with $H_3PO_4$ (15 ml) whilst stirring. The mixture was refluxed at 180 °C for 1.5 h. The remaining solution was cooled to room temperature, before $HNO_3$ (100 ml) was added, and refluxed at 150 °C for a further 16 h.

The mixture was cooled to room temperature, and the solid recovered by filtration, washed with acetone and water, and dried at 110 °C in an oven for 16 h. Each sample was calcined at 650 °C for 6 h in static air (20 °C/min).

#### *2.2.3.2 – Addition of transition metals to supported $(MoO_2)_2P_2O_7$*

The transition metal was added to $MoO_2 \cdot HPO_4 \cdot H_2O$ as described above (Section 2.2.3.1). The mixed molybdenum/metal phosphate precursor was supported on $SiO_2$ using the incipient wetness method, described above (Section 2.2.2.1) before calcining in static air at 650 °C for 6 h (20 °C/min) to form the supported mixed molybdenum/metal pyrophosphate catalysts.

### 2.2.4 – Unsupported vanadium phosphate catalysts

#### *2.2.4.1 – $VOHPO_4 \cdot 2H_2O$ – Vanadium phosphate dihydrate*

$V_2O_5$ (2.5 g), $H_3PO_4$ (15 ml) and distilled water (60 ml) were added to a 250 ml round bottom flask, and refluxed for 24 h. After cooling to room temperature, the mixture was filtered to recover the solid which was washed with distilled water. The solid was then refluxed for 16 h in isobutanol, and after cooling to room temperature, filtered and dried at 110 °C in an oven for 24 h.[3]

#### *2.2.4.2 – $VOHPO_4 \cdot 0.5H_2O$ – Vanadium phosphate hemihydrate*

$V_2O_5$ (5.9 g) was added to isobutanol (125 ml) in a 250 ml round bottom flask. $H_3PO_4$ (8.25 g) was then added whilst stirring, and the mixture refluxed for 16 h. After cooling to room temperature, the solid was recovered by vacuum filtration, washed with isobutanol and acetone, and dried at 110 °C in an oven for 6 h.[4]

#### *2.2.4.3 – $(VO)_2P_2O_7$ – Vanadium pyrophosphate*

The precursor ($VOHPO_4 \cdot 0.5H_2O$) prepared previously was used to prepare the vanadium pyrophosphate catalyst. The precursor was calcined at 750 °C for 2 h in nitrogen (5 °C/min), to form $(VO)_2P_2O_7$.

### 2.2.5 – Mixed molybdenum/vanadium phosphate catalysts

#### *2.2.5.1 – Addition of molybdenum during preparation of $VOHPO_4 \cdot 0.5H_2O$*

During the preparation of vanadium phosphate hemihydrates, molybdenum was introduced using different methods:

##### *2.2.5.1.1 – Co-precipitation with ammonium heptamolybdate tetrahydrate*

$V_2O_5$ (2.95 g) & $(NH_4)_6Mo_7O_{24}.4H_2O$ (required amount needed to give 0.05, 0.1, 0.5, 1 & 2 mol% Mo) were added to isobutanol (62.5 ml) in a 100 ml round bottom flask. $H_3PO_4$ (4.125 g) was then added whilst stirring, and the mixture refluxed for 16 h. After cooling to room temperature, solid was recovered by vacuum filtration, washed with isobutanol and acetone, and dried at 110 °C in an oven for 6 h.[5] The mixed $Mo/VOHPO_4.0.5H_2O$ precursor was heated at 750 °C for 2 h in nitrogen (5 °C/min), to form the mixed molybdenum/vanadium pyrophosphate material.

#### *2.2.5.1.2 – Co-precipitation with molybdenum trioxide*

$V_2O_5$ (2.95 g) & $MoO_3$ (required amount needed to acquire 2 mol% Mo) were added to isobutanol (62.5 ml) in a 100 ml round bottom flask. $H_3PO_4$ (4.125 g) was then added whilst stirring before refluxing for 16 h. After cooling to room temperature, the mixture was vacuum filtered to recover the solid, which was washed with isobutanol and acetone, and dried at 110 °C in an oven for 6 h.

The mixed Mo/$VOHPO_4.0.5H_2O$ precursor was heated at 750 °C for 2 h in a nitrogen atmosphere (5 °C/min), to form the mixed molybdenum/vanadium pyrophosphate material.

#### *2.2.5.1.3 – Incipient wetness impregnation of molybdenum*

The necessary amount (for a desired incorporation) of molybdenum was dissolved in the appropriate amount of isobutanol, and added to the precursor to form a paste.
The incipient wet material was then dried at 110 °C in an oven for 16 h.

To form the $(VO)_2P_2O_7$ phase, the mixed metal materials were heated at 750 °C for 2 h in nitrogen (5 °C/min).

## 2.2.6 – Sol immobilization of supported mono-metallic and bi-metallic gold(palladium) catalysts

#### *2.2.6.1 – Au(Pd)/$TiO_2$*

An aqueous $PdCl_2$ and $HAuCl_4$ solution of the desired concentration was prepared. The required amount of a PVA solution (1 wt%) was added so that PVA/(Au+Pd) (w/w) = 1.2. A freshly prepared solution of 0.1 M $NaBH_4$ was then added, so that $NaBH_4$/(Au +Pd)

(mol/mol) = 5, and a dark-brown sol formed. After 30 min of sol generation, the colloid was immobilized by adding $TiO_2$ (acidified to pH 1 with sulphuric acid) under vigorous stirring. The amount of support material required was calculated to give the desired total final metal loading. After 2 h, the slurry was filtered and the catalyst was washed thoroughly with distilled water (neutral mother liquors) and dried at 120 °C overnight. Mono-metallic gold catalysts were also prepared using a similar methodology. (Some batches of the supported mono-metallic gold catalysts were prepared by Saul White at Cardiff University, Wales)

#### *2.2.6.2 – Heat treatment*

The standard method of removing the stabilising ligand (PVA) is the heat treatment method, used here. The calcined catalysts were pre-treated at 200-400 °C under static air for 3 h using a heating rate of 5 °C/min.

#### *2.2.6.3 – Solvent extraction treatment*

A new method[6] of removing the stabilising ligand (PVA) whilst maintaining small gold nanoparticle size is used here. Typically, 1 g of catalyst was placed in a round bottom flask, and the desired volume (known by testing different volumes, and correlating it to studies of particle size distribution) of solvent (typically water or ethanol/THF) was added into the flask. The round bottom flask was connected to a reflux condenser, and placed in an oil bath which was heated at 90 °C, under vigorous stirring (500 rpm). The solution was left to reflux for periods of time between 30 min and 2 h. After the desired reflux period, the slurry was filtered and washed thoroughly with distilled water (2 L) and dried at 120 °C overnight.

## 2.3 – Gas Chromatography

### 2.3.1 – Methanol oxidation reactor

#### *2.3.1.1 - Overview of design*

The oxidation of methanol was conducted in a conventional flow reactor (Appendix: Figure A.1). The reactor design consists of a 5 mm *i.d.* quartz reactor tube held inside a furnace. The temperature was controlled using a thermocouple sitting just above the catalyst *i.e.* on the outlet side. The catalyst was placed inside the centre of the quartz reactor tube, supported using two equal amounts of quartz wool above and below the catalyst. The reaction mixture (gas feed) consisted of methanol, oxygen, and helium (volume% ratios of 5:10:85 were used, unless stated otherwise). Methanol was fed into the system, by passing helium through a Dreschler bottle containing methanol, which was held at 8 °C, using a water bath and chiller. After passing over the catalyst, the exhaust gas exited the reactor, and was analysed by on-line gas chromatography (GC). The exit line was heated to 120 °C, to ensure products (particularly formaldehyde) did not condense in the line before entering the gas chromatograph.

#### *2.3.1.2 - Reaction conditions*

Typically, 0.3 g of catalyst was used (unless stated otherwise) with a total gas flow of 60 ml/min, with the following composition: MeOH: $O_2$: He = 5: 10: 85 vol%. The amount of methanol used (kept outside of the explosion limits which are 6 %- 36 % in air), could be adjusted by varying the flow of helium through the Dreschler bottle, and/or by adjusting the water bath temperature. (A calibration was carried out to confirm the amount of methanol entering the system). The helium and oxygen content entering the

system were adjusted using mass flow controllers. Depending on the catalysts being tested, the furnace temperature was varied between 30 – 500 °C.

### *2.3.1.3 - Product analysis (valve setup in GC)*

Products of the methanol oxidation were analysed using a Varian Star 3400X on-line gas chromatogram. A six port injection valve (heated to 200 °C) (Figure 2.1) was used to inject a known volume of gas onto two columns in series. A Porapak Q column (80-100 mesh, 1 m) was used for the separation of HCHO (formaldehyde), $CH_3OCH_3$ (dimethyl-ether), $CH_3OH$ (methanol), $HCOOCH_3$ (methyl formate), $CH_2(OCH_3)_2$ (dimethoxy-methane) and $CO_2$ (carbon dioxide). A molecular sieve column (80-100 mesh, 2 m) was used for the separation of $O_2$ (oxygen) and CO (carbon monoxide). A second valve was used to determine which products enter the columns.

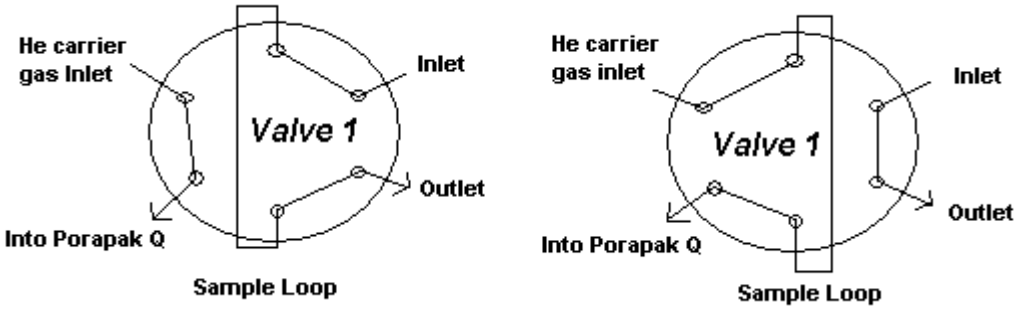


**Figure 2.1:** Schematic of GC valve setup, corresponding valve 1, either in the fill position (*left*) or in the inject position (*right).*

When the columns are set in series (Figure 2.2), the Porapak Q column outlet is linked to the inlet of the molecular sieve column, and so products are separated on both columns. Carbon dioxide and other large bulky products possibly formed, stick to the molecular sieve column, which in time, deactivates the column. To avoid this, the second valve switches to a bypass position (Figure 2.3), whereby the outlet of the Porapak Q column is no longer linked to the molecular sieve column, but instead passes through an

empty line, where the pressure is controlled using a restrictor valve to mimic the conditions of a column. By using bypass, the molecular sieve column can be switched out of series until after the $CO_2$ (and other products) elutes from the Porapak Q column.

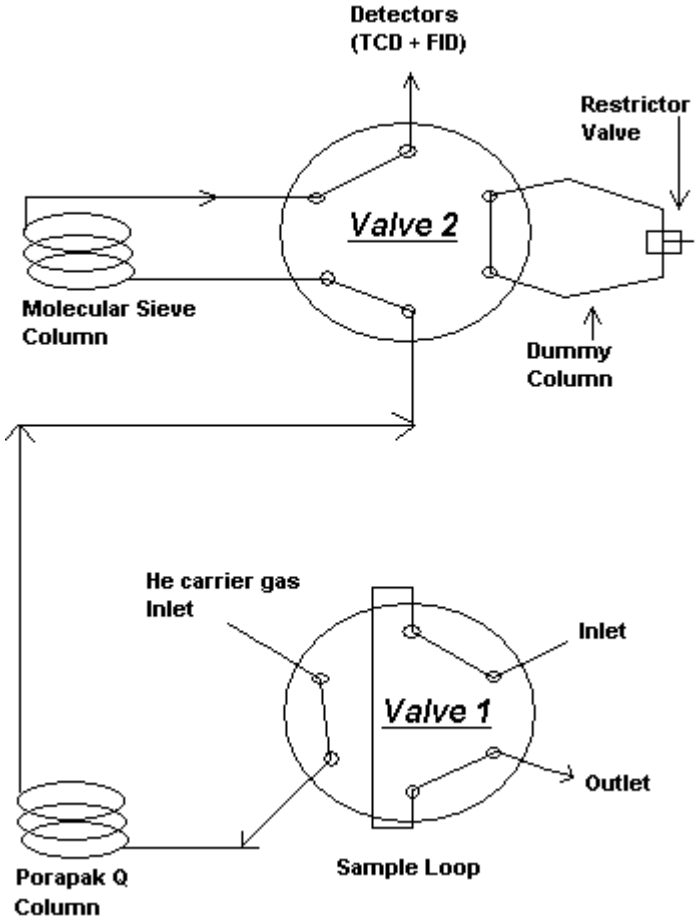


**Figure 2.2:** Schematic of GC valve setup, corresponding to the columns in series.

After the products elute from the columns, they are detected first using a thermal conductivity detector (TCD) and then a flame ionisation detector (FID), which both produce a signal which is converted using a computer so that the amount of each product can be seen as a peak on a gas chromatogram. The TCD is used to show separation of CO, $CO_2$, $H_2O$ and $O_2$, and the FID which is more sensitive to hydrocarbons, is used to analyse the separation of HCHO, $CH_3OCH_3$, $CH_3OH$, $HCOOCH_3$, and $CH_2(OCH_3)_2$.

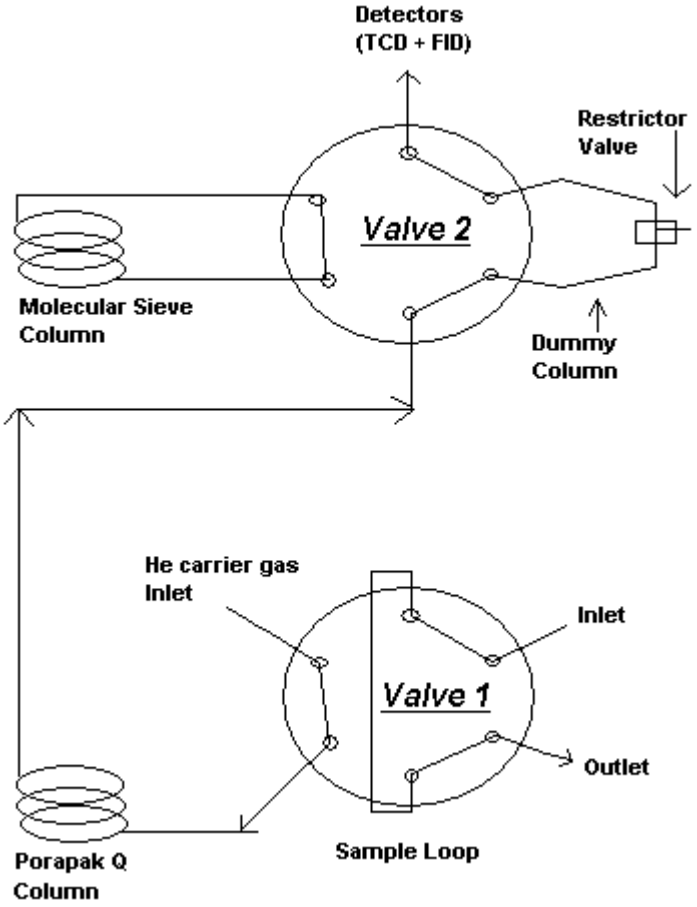


**Figure 2.3:** Schematic of GC valve setup, corresponding to the columns in bypass.

### *2.3.1.4 - Valve sequence and data handling*

To achieve the optimum separation of products from the columns with the quickest elution time possible, a temperature programme is used for the GC oven which contains the two columns. As the oven temperature increases, the product retention time will shorten, but this has a detrimental effect on the separation of product peaks on the gas chromatograms, so a finely tuned oven temperature programme is needed.

To assign the peak area on the gas chromatogram to a known amount of product (via the TCD and FID detectors), the GC needs to be calibrated beforehand. By injecting known amounts of the predicted products of the reaction into the GC, a response factor

(RF) can be calculated for different amounts of the compound injected. (RF = Known % injected/number of counts produced by the peak area.)

To determine the conversion of methanol during a reaction, the following equation is used:

$$\text{Conversion} = \frac{(MeOH_{in} - MeOH_{out})}{MeOH_{in}} \times 100$$

Where $MeOH_{in}$ is the average peak area (taken from 3 injections) at room temperature where there is no reaction of the methanol, and $MeOH_{out}$ is the average peak area recorded at a particular reaction temperature.

To determine the selectivity to each product, the following equation is used:

$$\text{Selectivity} = \frac{\text{(Amount of product (A))}}{\text{(Total amount of all products including A)}} \times 100$$

When conversion and selectivity have been calculated at a specific reaction temperature, the per pass yield of a particular product can also be calculated using the following equation:

$$\text{Yield \%} = \frac{\text{(Conversion of MeOH(\%) x Selectivity (A)(\%))}}{100}$$

### 2.3.2 – CO oxidation reactor

#### *2.3.2.1 - Overview of design*

The catalytic oxidation of CO was conducted in a flow reactor consisting of a U-shaped quartz tube, where the catalyst is placed just above one of the bends supported by quartz

wool either side of it. The tube containing the catalyst was held in a water bath which was maintained at a constant temperature of 27 °C.

CO in air was introduced from a pre-mixed cylinder (5000 ppm CO) using a mass flow controller. The GHSV used varied with specific reactions depending on the catalysts in use, and to alter the GHSV, flow of CO and the volume of catalyst used were varied. Reactants and products were analysed by on-line GC.

#### *2.3.2.2 - Sample delivery (valve setup in GC)*

The products of the reaction ($CO_2$ and $H_2O$) were analysed after the reaction using a Varian 3800, which contained a Supelco carbosieve column (3 m) which is used to separate carbon monoxide (CO), carbon dioxide ($CO_2$) and water. The reactants and products eluted from the column were analysed using a TCD.

#### *2.3.2.3 - Valve sequence and data handling*

As only one column is used, temperature and carrier gas flow rate is used to separate CO, $CO_2$ and water. The column oven was held constant at 195 °C, and CO eluted with air first, followed by $CO_2$ and water, with a total run time of 4 min.

## 2.4 - Powder X-ray diffraction (XRD)

### *2.4.1 - Theory*

X-ray diffraction is based on constructive interference of monochromatic X-rays and a crystalline sample. It is a non-destructive technique that can be used for phase identification and quantitative analysis of a sample.

X-rays are produced in a sealed vacuumed tube by firing a metal target (most commonly copper) with high energy electrons, which then interact with electrons of the target material. The high energy electrons are accelerated using a voltage at the target, so that electrons situated within inner orbitals are excited, which results in electrons being expelled from atoms. In turn, a higher energy electron (outer shell electron) drops down to fill its place, resulting in a characteristic X-ray of a specific wavelength being emitted, and filtered by a monochromator, to produce monochromatic radiation. The X-rays that are produced are concentrated into a beam, and directed at the sample, where they interact with atoms to produce constructive interference, and also diffracted X-rays.

Constructive interference is only produced when the conditions satisfy Bragg's Law.[7]

Bragg equation;

$$n\lambda = 2d \sin \theta$$

where;

- n = integer
- $\lambda$ = x-ray wavelength
- d = lattice spacing
- $\theta$ = Bragg diffraction angle (incident angle)

The conditions needed to satisfy Bragg's Law can be seen in Figure 2.4. The path length of A + B is equal to $2d\sin\theta$. When A + B is an integral number of wavelengths, *i.e.* $A + B = n\lambda$, the waves formed will be in phase, and hence interfere constructively. If $A + B \neq n\lambda$, then destructive interference is produced. By recording the $\lambda$ value produced by the reflection, the Bragg Law is used to calculate the lattice spacing (d).

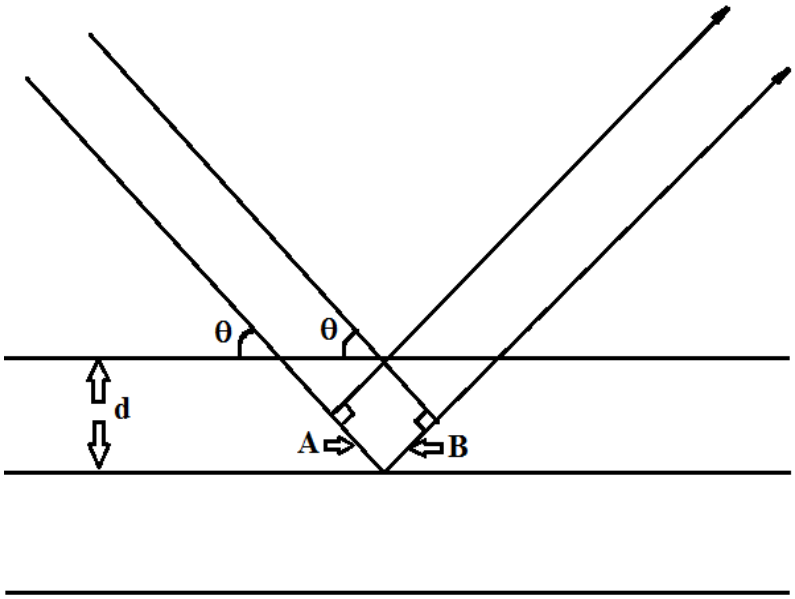


**Figure 2.4:** Reflection of X-rays when conditions satisfy Bragg's Law.

As powdered samples are used, the diffraction pattern is formed due to the random orientation of particles, where a certain crystal plane will be at an angle of θ with the incident beam, producing constructive interference. Due to the d-spacings of a sample obtained in the X-ray scan being unique to the material, the X-ray diffraction pattern produced can be compared with standard reference patterns in a database, and the material is identified.

### *2.4.2 – Experimental*

X-ray diffraction analysis was carried out on each sample using a PANalytical, XPERT Pro with CuKα radiation. Each sample was placed in a sample holder (~0.3 g) to give a flat surface. Analysis lasted around 20-30 min, before the obtained patterns are studied (to obtain information of the various phases of a material present) and compared to the JCPDS database.

## 2.5 - Raman spectroscopy

### *2.5.1 – Theory*

When the incident beam of a monochromatic laser is passed through a sample, a small number of molecules are irradiated, and this causes scattering of the light. If the frequency of the scattered light is different to the frequency of the incident light, then the Raman effect has occurred. Most collisions between photons and molecules are elastic (no change in frequency of incident and scattered light), also known as Rayleigh scattering.

The conditions needed to cause the Raman effect, is when the incident beam of light (photons) interacts with the electron cloud of a molecule. This causes an increase or decrease of energy from the incident light due to inelastic scattering. This change in energy is attributed to the energy differences of the vibrational and rotational energy levels of the molecule. Absorption of energy from the incident beam to an electron in the ground state causes it to be raised to higher (virtual) energy level, and then it promptly relaxes to a lower energy level, releasing a photon.[8] If the molecule gains energy from the incident photon, but only relaxes to an energy level above ground state (v = 1, Figure 2.5) a photon will be emitted with less energy than the incident photon, this is referred to as Stokes scattering. When the incident photon absorbs energy from the molecule which is in an initial excited state, it causes a relaxation back to the ground state, and a photon of energy greater than the incident photon emerges, it is referred to as Anti-Stokes scattering.

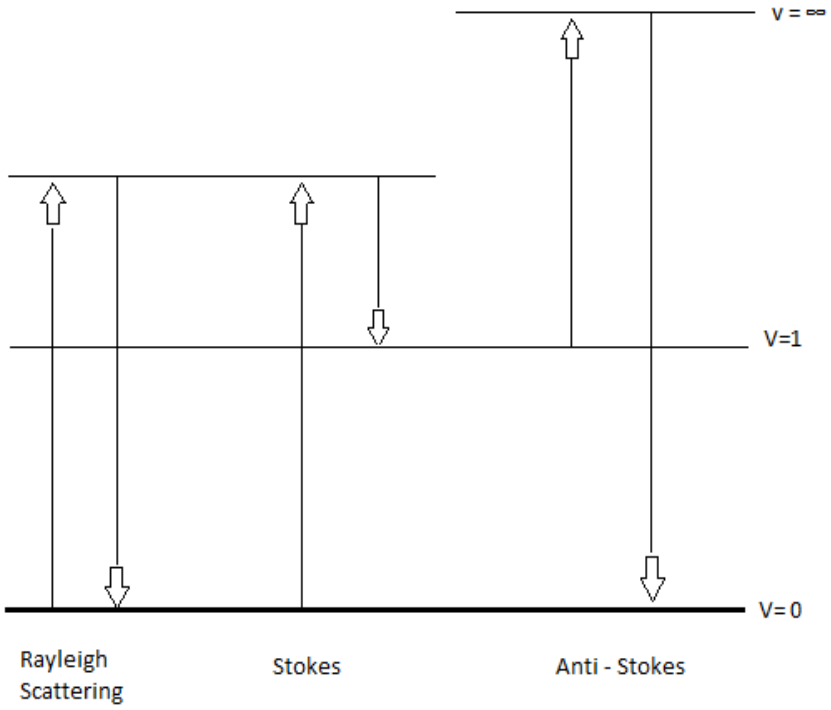


**Figure 2.5:** Energy level diagram, showing the energy increases and decreases involved in Raman and Rayleigh scattering.

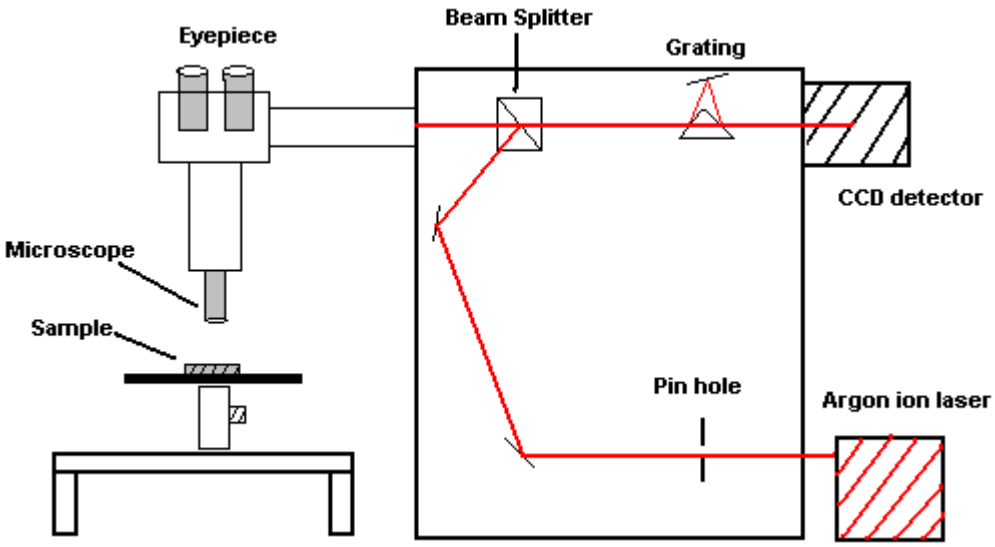


**Figure 2.6:** Schematic of a typical Raman Spectrometer.

### *2.5.2 – Experimental*

Raman spectroscopy was carried out using a Renishaw inVia Raman microscope (Figure 2.6), which is equipped with two types of lasers, a 514 nm Modu-laser (argon ion

as the active medium) with an average laser power of 25 mW, and a 785 nm Renishaw laser (argon ion). At the start of each use of the equipment, a silicon reference sample was tested for calibration. Samples to be tested were loaded on to an aluminium plate, and the sample flattened, before being analysed.

## 2.6 - Scanning electron microscopy (SEM)

### *2.6.1 – Theory*

Scanning electron microscopy is used to produce high resolution images of the bulk morphology of the samples, which can be used to analyse topography (and when coupled with Energy-dispersive X-ray spectroscopy (EDX), the chemical composition can be analysed). SEM uses a high energy electron beam, which is directed at the sample using lenses and apertures, forming secondary electrons (and primary back scattered electrons), which are then detected (Figure 2.7).

The high energy beam of electrons is produced using an electron gun, which contains a tungsten filament cathode, and electrons are emitted towards the sample. Before reaching the sample, the beam has to pass through condenser lenses, pairs of scanning coils, an objective lens and apertures, which all participate in focusing and deflecting the beam, allowing it to scan a rectangular area of the sample.

As the beam interacts with the surface of the sample, electrons lose energy due to the absorption and scattering by the sample. How far the beam penetrates the surface will depend upon the atomic number and density of the material, and on the accelerating voltage of the beam. This interaction between electrons and the sample, results in high-energy and secondary electrons being produced (along with electromagnetic radiation).

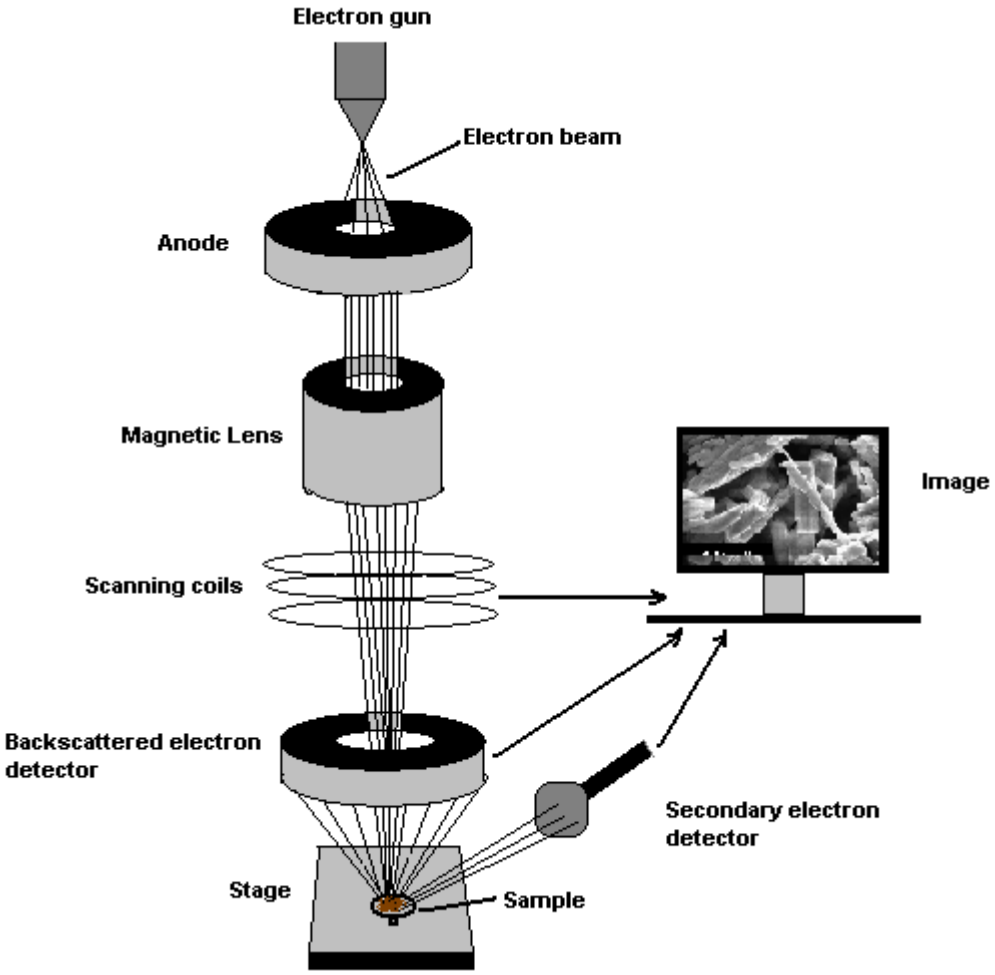


**Figure 2.7:** Schematic of Scanning Electron Microscopy (SEM).

Secondary electrons (generated using the primary electrons directed at the sample causing ionisation) have energy of less than 50 eV, whereas backscattered electrons (originating from the primary electron beam which are reflected) which have energy of greater than 50 eV. Both are detected (using detectors located at specific angles inside the equipment) and converted into an image on the viewing screen. (Figure 2.7) Although backscattered electrons produce an image much like secondary electrons, they can also be used to detect areas of the sample with different chemical compositions, *i.e.* high atomic number elements backscatter electrons more strongly than low atomic number elements, and hence appear brighter in the image produced.[9]

### *2.6.2 – Experimental*

SEM analysis was carried out using a Carl Zeiss, Evo 40 equipment. Samples were loaded onto an 8-stub carousel and a vacuum is created inside the equipment, before being analysed using either the secondary electron or the back-scattered detector.

## 2.7 – High angle annular dark field – scanning transmission electron microscopy (HAADF-STEM)

### *2.7.1 – Theory*

Scanning transmission electron microscopy (STEM) is a technique similar to SEM, which uses an electron beam to produce an image of a specimen. With STEM, the electron beam (generated by a lanthanum hexaboride filament) is focused into a narrow spot and then scanned across the sample. Advantages of using STEM over SEM are the much higher magnification, 1,000,000x compared to 100,000x respectively, and the higher spatial resolution achieved by the STEM, allowing for analysis on the atomic scale, such as a few nanometers, compared to a few micrometers using an SEM.

Annular dark field imaging is the method used to map the sample, and is very sensitive to variations in atomic number of atoms contained in the sample. A high angle annular dark field detector is used to collect electrons which are not Bragg scattered (Figure 2.8). Atomic resolution images are produced, where the contrast is directly related to the atomic number (Z-contrast image).

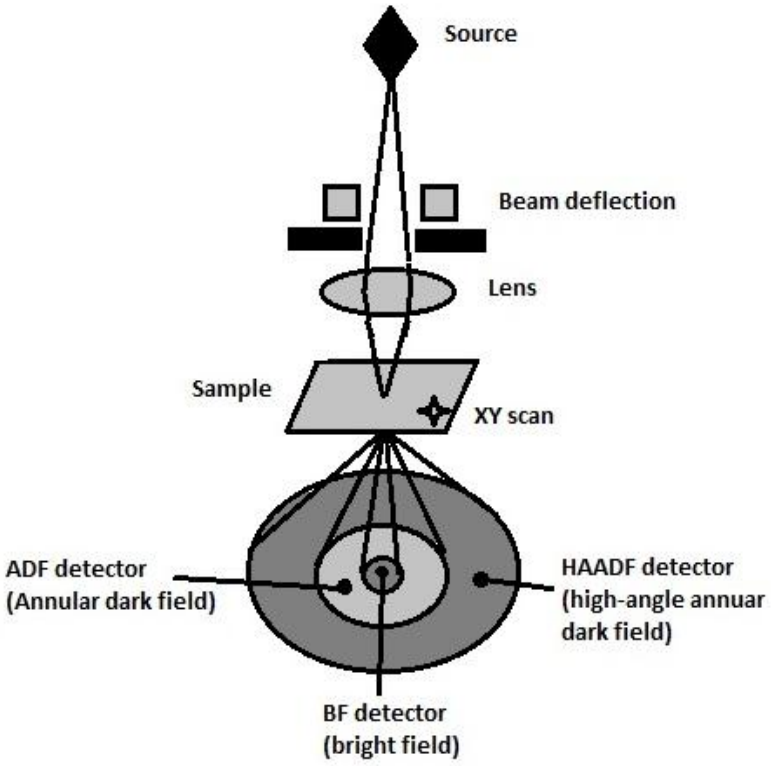


**Figure 2.8:** High-angle annular dark field – Scanning transmission electron microscope (HAADF-STEM)

### *2.7.2 – Experimental*

Catalysts were prepared for TEM/STEM analysis by dry dispersing the catalyst powder onto a holey carbon TEM grid. In the case of the starting Au-PVA and Au+Pd-PVA sols, a drop of the colloidal sol was deposited, and then allowed to evaporate, onto a 300-mesh copper TEM grid covered with an ultra thin continuous C film. High-angle annular dark field (HAADF) imaging experiments were carried out using a 200kV JEOL 2200FS transmission electron microscope equipped with a CEOS aberration corrector. (Images produced by Prof. Christopher Kiely, Lehigh University, USA)

## 2.8 - BET surface area measurement

### *2.8.1 – Theory*

The BET theory was developed by Brunauer, Emmett and Teller in 1938,[10] and is used to measure the surface area of a sample. The BET theory is an extension of the Langmuir model of adsorption, which only considers monolayer adsorption of a gas onto a surface, however, the BET theory advances from only monolayer adsorption, to multilayer adsorption. The data produced by the BET analysis are characterised by an isotherm.

The Langmuir isotherm, relates surface coverage of adsorbate molecules, to pressure of the adsorbate gas, at a specific temperature.

$$\theta = \frac{\alpha \cdot P}{1 + \alpha \cdot P}$$

Where:

θ is the percentage surface coverage of the adsorbate gas

P is the gas pressure

α is the Langmuir adsorption constant (Increases with an increase in binding energy of adsorption, and with a decrease in temperature).

Although Langmuir's isotherm is most common, other types of adsorption isotherms are observed (Figure 2.9):

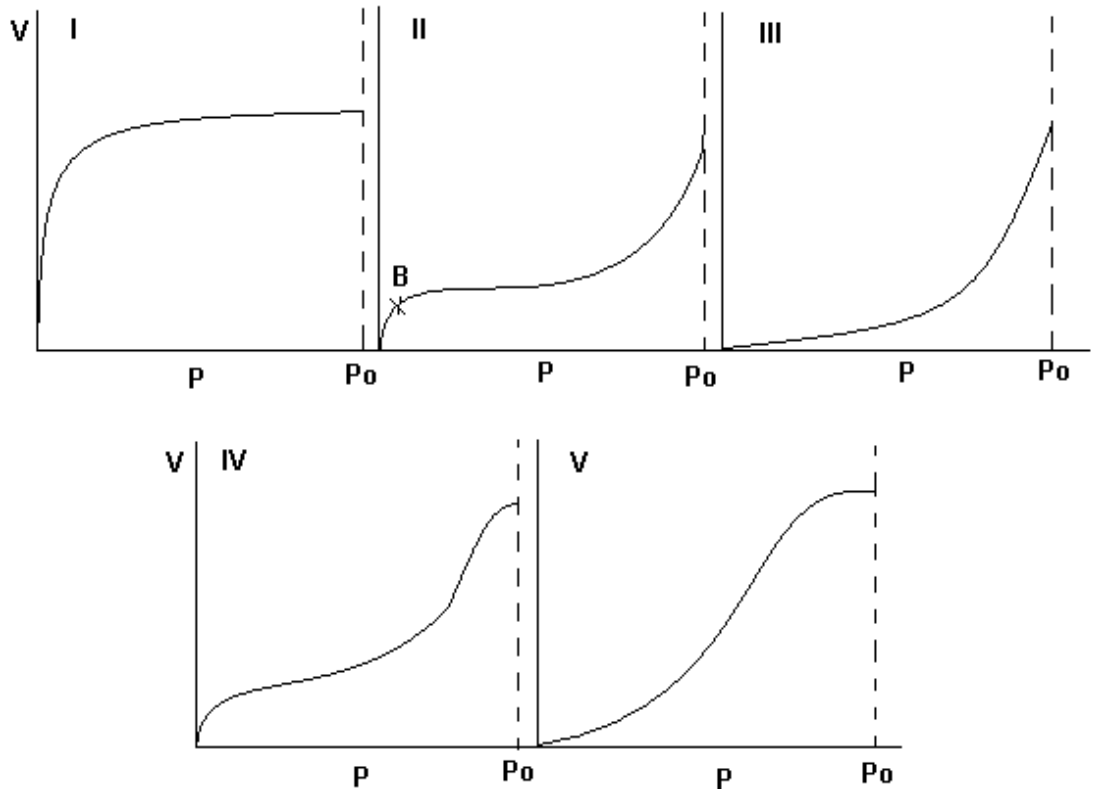


**Figure 2.9:** Five types of adsorption isotherm.

The adsorption of nitrogen onto the surface is considered to take place via physisorption, close to the condensation temperature of $N_2$ (77 K). The monolayer that is formed on the surface, is dictated by the size of the $N_2$ molecule, which is known as 0.16 $nm^2$

Figure 2.9 shows the five types of isotherms. The type II isotherm is the basis for BET theory, where at low pressure ($0.05 < P/P_o < 0.35$) there is a monolayer build up (point B) of gas on the surface, and as the pressure is increased, there is increasing multilayer adsorption.

As BET theory considers multilayer adsorption, the BET equation is used when calculating surface area:

$$\frac{1}{v\left[\left(P_o / P\right)-1\right]} = \frac{c-1}{v_m c}\left(\frac{P}{P_o}\right) + \frac{1}{v_m c}$$

Where:

$V$ = Total volume of gas adsorbed,

$V_m$ = Volume of gas corresponding to monolayer coverage,

$P$ and $P_o$ = Equilibrium and saturation pressures of adsorbates respectively,

$C$ = Constant.

The constant $C$ is based on the following equation:

$$c = e^{(H_A - H_L)/RT}$$

Where;

$H_A$ = Enthalpy of adsorption of the first layer,

$H_L$ = Enthalpy of liquefaction, which is equal to the enthalpy of adsorption of the second and subsequent layers that form on the surface.

Using the BET equation, a straight line can be plotted with $1/ v[(P_0 / P) - 1]$ on the y-axis and $P / P_0$ on the x-axis, to yield the volume of the monolayer on the surface, $V_m$, and since the size of a $N_2$ molecule is known (0.16 $nm^2$), the surface area can be calculated.

### *2.8.2 – Experimental*

A Micromeretics Gemini 2360 surface area analyser was used to carry out BET surface area analysis. All samples were degassed for 1 h at 120 °C, to remove moisture from the surface and pores of the sample, before being analysed.

## 2.9 - Temperature programmed reduction (TPR)

### *2.9.1 – Theory*

Temperature programmed reduction is a technique used in catalysis to determine the reducibility of a sample by passing a reducing gas, such as a mixture of dilute hydrogen in argon, over the sample whilst it is subjected to a programmed linear temperature ramp.

At room temperature a steady baseline on the TCD was obtained, before the temperature of the sample was increased according to the programmed temperature ramp. Hydrogen is consumed from the gas mixture by the reducible material in the sample, and there is a change in thermal conductivity of the effluent gas mixture compared to the reference of the TCD, producing a signal. During the process, hydrogen is converted to water by reacting with the sample, and so a liquid $N_2$/Isopropyl alcohol cold trap is used to remove water.

### *2.9.2 – Experimental*

TPR was carried out on each catalyst using a Quantachrome ChemBET chemisorption analyzer. Samples were weighed out and placed in a specially designed U-tube (quartz), with the catalyst held in place using two plugs of quartz wool. The system was then purged under an argon atmosphere before undergoing a pre-treatment also in an argon atmosphere (held at 120 °C for 45 min, with a temperature ramp of 5 °C/min). After

cooling, the TPR was carried out using a 10 % $H_2$ in Ar gas feed, up to a maximum of 750 °C at a specific ramp rate. The amount of $H_2$ consumed was measured using a TCD.

## 2.10 - Thermogravimetric analysis (TGA)

### *2.10.1 – Theory*

Thermogravimetric analysis, involves the measurement of weight loss from a sample as a function of temperature under a specific atmosphere. Weight loss is calculated by recording the initial mass, and recording the final mass after the experiment has finished. It is given in terms of percentage, so the species lost from the sample can be determined. TGA is also equipped with differential thermal analysis (DTA) and/or differential scanning calorimetry (DSC), which monitors the heat flow during the experiment, to determine if an endothermic or exothermic reaction is taking place (positive or negative peak in the heat flow).

### *2.10.2 – Experimental*

Analysis was conducted using a Seteram TGA 7 using ~10 mg of catalyst under a $N_2$ atmosphere. The temperature of the analysis was in the range of 40-700 °C with a ramp rate of 20 °C/min.

## 2.11 - X-ray Photoelectron Spectroscopy (XPS)

### *2.11.1 – Theory*

X-ray photoelectron spectroscopy is a surface specific quantitative spectroscopic technique, used to produce information about the surface of a sample such as the elements present, their chemical state (*i.e.* oxidation state) and relative elemental ratios.

X-rays are produced from a magnesium or aluminium source under ultra high vacuum (UHV) and are used to irradiate the sample. This bombardment of the orbitals in the specific elements, causes photoelectrons to be emitted from the top 1 to 10 nm of the surface via the photoelectric effect, which are then detected.

The binding energy of the emitted electrons can be calculated using the following equation:

$$E_{Binding} = E_{Photon} - (E_{Kinetic} + \phi_s)$$

Where:

$E_{Binding}$ = Electron binding energy of emitted electron

$E_{Photon}$ = Energy of irradiating photons

$E_{Kinetic}$ = Kinetic energy of the electron

$\phi_s$ = Spectrometer work function

As each element will have specific binding energies, they can be identified, and as the binding energies are influenced by chemical potential and polarizability, the specific binding energy determines the chemical state of the element.

### *2.11.2 – Experimental*

XPS analysis was performed using a Kratos Axis Ultra DLD photoelectron spectrometer, equipped with an aluminium monochromatic source and a dual Al/Mg achromatic source. Spectra are acquired over an area of 700x300 μm at a pass energy of 40 eV for high resolution scans. All spectra were calibrated to the C(1s) line of adventitious carbon at a binding energy of 284.7 eV.

## 2.12 - Elemental analysis

### *2.12.1 – Theory*

The weighed sample was placed into a high temperature furnace, and combusted in pure oxygen under static conditions. Elemental carbon, hydrogen and nitrogen from the sample pass through specialized reagents to produce carbon dioxide, water and nitrogen oxides. This mixture then passes through thermal conductivity detectors containing conductivity cells, where the first cell contains a water trap to measure hydrogen, the second contains a carbon dioxide trap to measure carbon, and thirdly nitrogen is measured against a helium reference.[11]

Gold weight% was measured using an inductively coupled plasma-optical emission spectroscopy analyser (ICP-OES), which uses plasma to produce excited atoms and ions, which will produce characteristic electromagnetic radiation, so that the intensity measured is attributed to the concentration of gold present on the sample.

### *2.12.2 – Experimental*

Carbon, hydrogen, nitrogen were analysed using a CE440 Elemental analyser, and ICP-OES was carried out for gold. (Elemental analysis carried out by Warwick ICP-MS facility, Warwick University, Exeter). [11]

## 2.13 - References

1. P. Kierkegaard. *Acta Chemica Scaninavica* **1958**, *12*, 1701.
2. P. Kierkegaard. *Arkiv foer Kemi* **1962**, *19*, 1–14.
3. M. T. Sananes, I. J. Ellison, S. Sajip, A. Burrow, C. J. Kiely, J. C. Volta and G. J. Hutchings. *J. Chem. Soc., Faraday Trans.* **1996**, *92*, 137.

4. F. J. C. Sanchez, R. P. K. Wells, C. Rhodes, J. K. Bartley, C. J. Kiely and G. J. Hutchings. *Phys. Chem. Chem. Phys.* **2001**, *3,* 4122-4128.
5. B.T. Pierini, E. A. Lombardo. *Catalysis Today* **2005**, *107–108*, 323–329.
6. J. A. Lopez-Sanchez, N. Dimitratos, C. Hammond, G. L. Brett, L. Kesavan, S. White, P. Miedziak, R. Tiruvalam, R. L. Jenkins, A. F. Carley, D. Knight, C. J. Kiely and G. J. Hutchings. *Nature Chemistry* **2011**, *3,* 551-556.
7. A.W. Laubengayer and H.R. Engle, *J. Amer. Chem. Soc.* **1939,** *61,* 1210.
8. *J. R. Ferraro, K. Nakamoto and C. W. Brown, (**2002**) Introductory Raman Spectroscopy. 2nd Edition,* Academic Press, London.
9. J. I. Goldstein, (**2003**) *Scanning electron microscopy and X-ray microanalysis.* 3rd Edition, Springer, New York.
10. S. Brunauer, P.H Emmet and E. Teller. *J. Am. Chem. Soc*. **1938**, *60,* 309-319.
11. Exeter Analytical, Inc. (University of Warwick), **2009**, *CE440 Elemental Analyzer,* http://www.eai1.com/theory.htm.

# 3

# *Chapter 3 – Molybdenum phosphates as new highly active catalysts for selective methanol oxidation*

## 3.1 – Introduction

Molybdenum phosphate materials have received an increasing interest in the last decade for use as new cathode materials for lithium and sodium batteries.[1] They are mainly reported as catalysts in the partial propane oxidation reaction, where they are usually promoted by metals such as silver or cerium, which produce high selectivity to propene with relatively low conversion of propane.[2-6] In general, MoPO complexes are usually built up from the linkage of $PO_4$ tetrahedra with, most of the time, $MoO_6$ octahedra.[7] One of the main characteristics of these phosphate materials, is their ability to stabilize molybdenum in various oxidation states *i.e.* $Mo^{6+}$, $Mo^{5+}$, $Mo^{3+}$ and even mixed valencies such as $Mo^{5+}/Mo^{6+}$. These redox properties make them ideal catalysts for oxidation reactions such as partial propane oxidation, and partial methanol oxidation.

Molybdenum based materials have been widely accepted as some of the most active catalysts for methanol oxidation to formaldehyde, in particular, the main commercial iron molybdate catalyst[8-10] and supported molybdenum trioxide catalysts.[11-16] Transition metal phosphate catalysts have been reported in the literature for numerous partial oxidation reactions, *e.g.* vanadyl pyrophosphate for butane oxidation to maleic anhydride,[17-19] and iron phosphate for the oxidative dehydrogenation of isobutyric acid into methacrylic

acid.[20-22] There is some evidence to suggest that the role of phosphate tetrahedra is to bind the $MO_6$ octahedra (M = transition metal) which enhances the redox properties of the catalysts, possibly due to the increase in mobility of lattice oxygen through the bulk to the surface, where it can re-oxidise the reduced surface during the reaction.[23] Utilising the high selectivity to formaldehyde using supported molybdenum trioxide, and possible improvements suggested using phosphate groups, the combination of the two as a catalyst for methanol oxidation is interesting, and a comparison can be made into the difference in activity between molybdenum oxide catalysts, and molybdenum phosphate catalysts.

This chapter will study the properties of these materials using a range of characterization techniques, and investigate their catalytic activity for selective methanol oxidation to formaldehyde. Molybdenum phosphate catalysts were prepared using methods previously reported by Kierkegaard,[24,25] and have been enhanced by promotion using transition metals, and supported using alumina, silica and titania. These are both novel procedures for these particular molybdenum phosphate catalysts.

## 3.2 – Characterisation

### *3.2.1 - Unsupported molybdenum phosphate catalysts*

#### *3.2.1.1 - ($MoO_2$·$HPO_4$·$H_2O$) – Molybdenum (VI)-orthophosphate hydrate*

Molybdenum orthophosphate hydrate was prepared using the co-precipitation method described in chapter 2 (section 2.2.1.1).

The powder X-ray diffraction (XRD) pattern of this material can be seen in Figure 3.1, which was recorded between 10 and 80 ° 2θ. The pattern corresponds well with the monoclinic structure reported in the literature,[24] and with the JCPDS database (reference

code: 00-011-0333), and shows that the material is highly crystalline, with the main reflection (-101) at 15.4 ° 2θ .

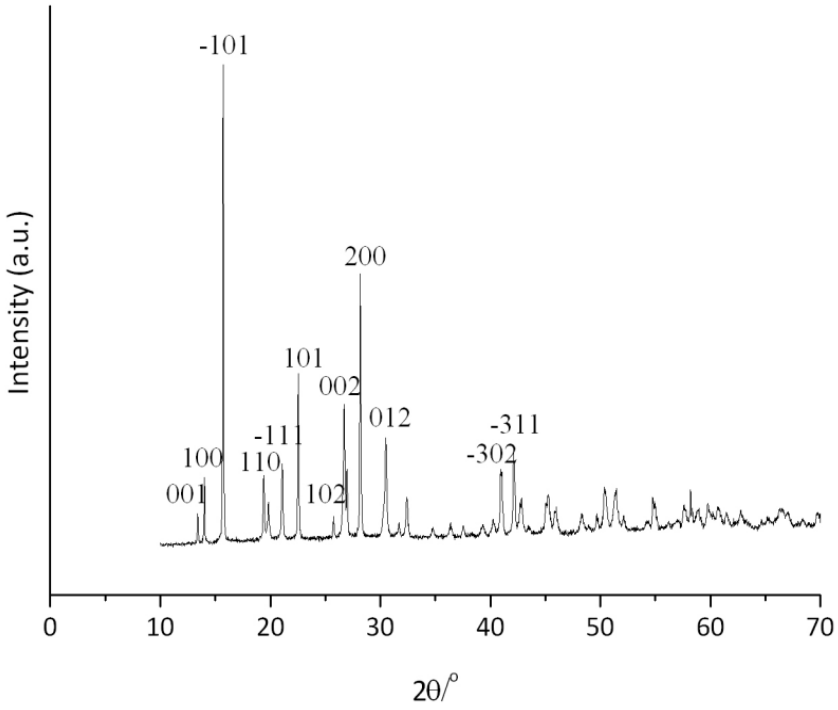


**Figure 3.1:** XRD pattern of $MoO_2 \cdot HPO_4 \cdot H_2O$.

The crystal structure of $MoO_2 \cdot HPO_4 \cdot H_2O$ consists of $PO_4$ tetrahedra binding together $MoO_6$ octahedra, in such an arrangement so as to form a chain structure, where these chains line up parallel to each other, and are held together by hydrogen atoms (Figure 3.2).

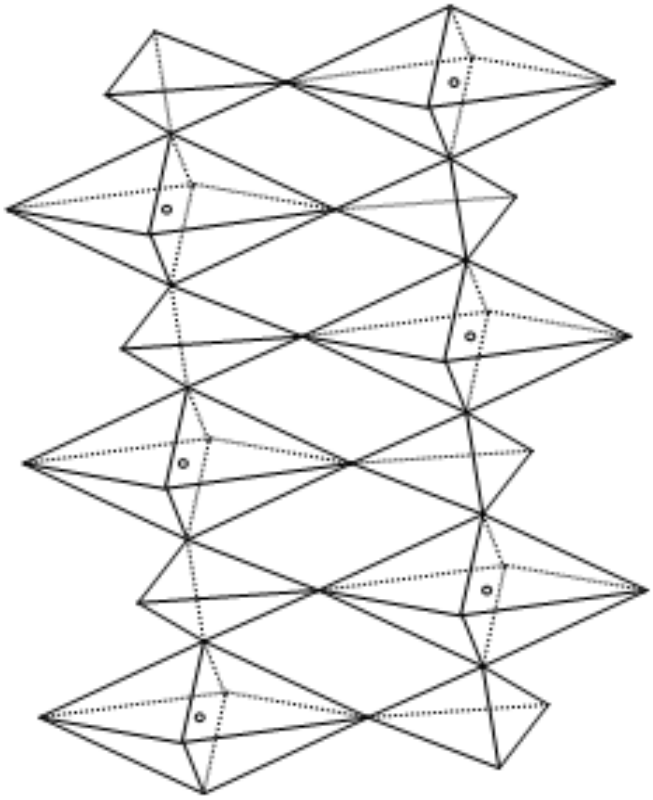

**Figure 3.2:** Schematic drawing of the crystal **s**tructure of $MoO_2 \cdot HPO_4 \cdot H_2O$. [26]

Raman spectra recorded between 200 – 1200 $cm^{-1}$ for this material confirmed the presence of the expected stretching modes, relating to the relevant species present in $MoO_2 \cdot HPO_4 \cdot H_2O$ (Figure 3.3). The peaks at 1142 and 1079 $cm^{-1}$ both correspond to $(PO_4)^{3-}$ antisymmetric stretching, with peaks at 962 and 938 $cm^{-1}$ both due to $(PO_4)^{3-}$ symmetric stretching. The final peak assignments are the Mo=O band at 1001 $cm^{-1}$ and a Mo-O-Mo band at 885 $cm^{-1}$.

Scanning electron microscopy (SEM) was used to investigate the morphology of $MoO_2 \cdot HPO_4 \cdot H_2O$ and is shown in Figure 3.4. The particles differ in size from < 2μm to > 8 μm, and have a rod shaped morphology with jagged edges.

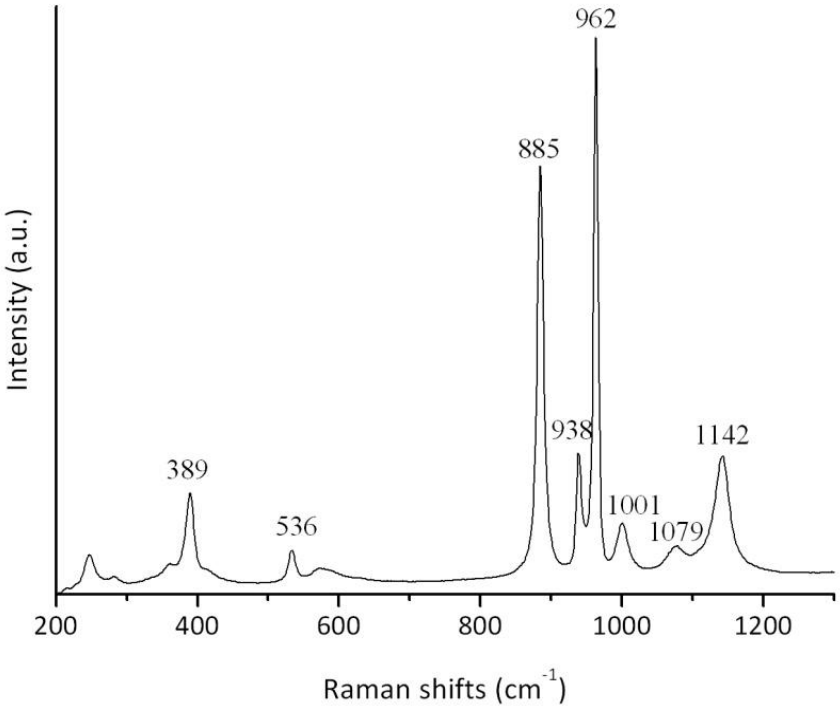


**Figure 3.3:** Raman spectra of $MoO_2.HPO_4.H_2O$.

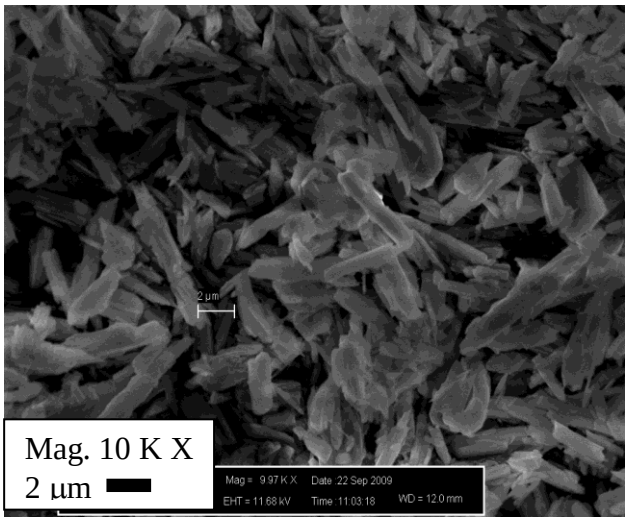


**Figure 3.4:** SEM image of $MoO_2 \cdot HPO_4 \cdot H_2O$.

### *3.2.1.2 - $(MoO_2)_2P_2O_7$ – Molybdenum pyrophosphate*

$(MoO_2)_2P_2O_7$ was prepared by calcination of $MoO_2 \cdot HPO_4 \cdot H_2O$ (section 2.2.1.2). XRD was used to confirm that $(MoO_2)_2P_2O_7$ had been synthesised correctly, and the pattern is observed in Figure 3.5. A crystalline orthorhombic $(MoO_2)_2P_2O_7$ phase is produced

(JCPDS ref. code: 01-074-1380), with a main reflection at 22 ° 2θ which corresponds to the (301) index plane. Heat treatment in an inert atmosphere such as nitrogen caused the formation of an almost identical crystalline $(MoO_2)_2P_2O_7$ phase as the calcination in air. Similar to the precursor, the $(MoO_2)_2P_2O_7$ material has a crystalline structure containing chains, but unlike the parallel chains of $MoO_2 \cdot HPO_4 \cdot H_2O$, zigzag chains are formed (Figure 3.6), which are built up of $MoO_6$ octahedra, where each octahedron shares two Mo-O vertices with other $MoO_6$ octahedra. The remaining three out of four vertices are shared with $PO_4$ tetrahedra (which link together to form $P_2O_7$ groups) and oxygen atoms.[25-27]

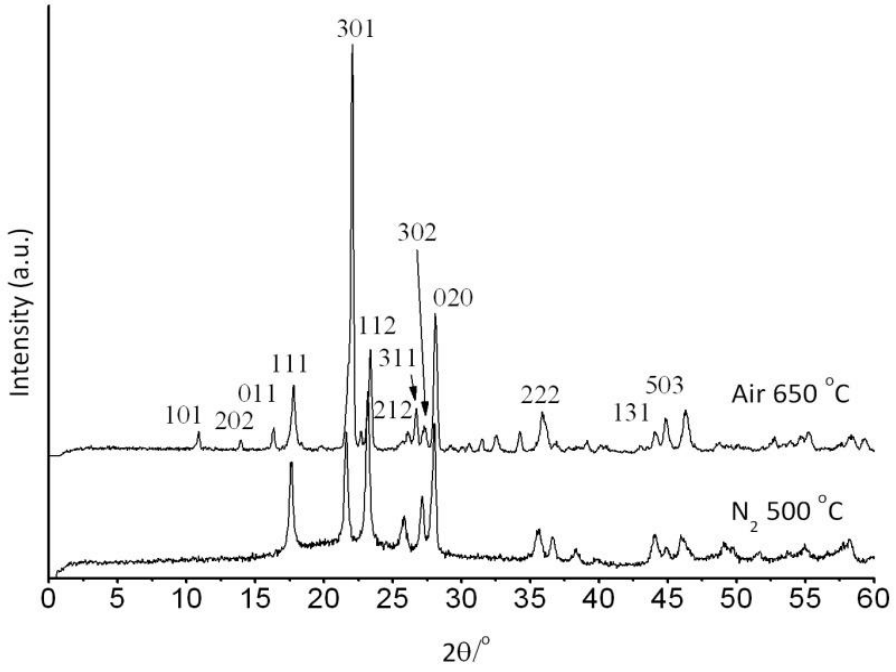


**Figure 3.5:** XRD pattern of $(MoO_2)_2P_2O_7$

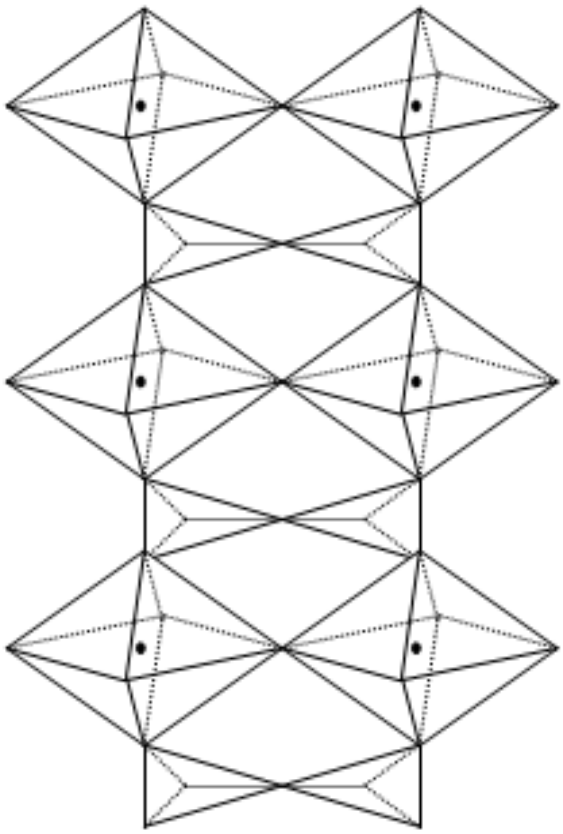

**Figure 3.6:** Schematic drawing of the crystal structure of $(MoO_2)_2P_2O_7$.[26]

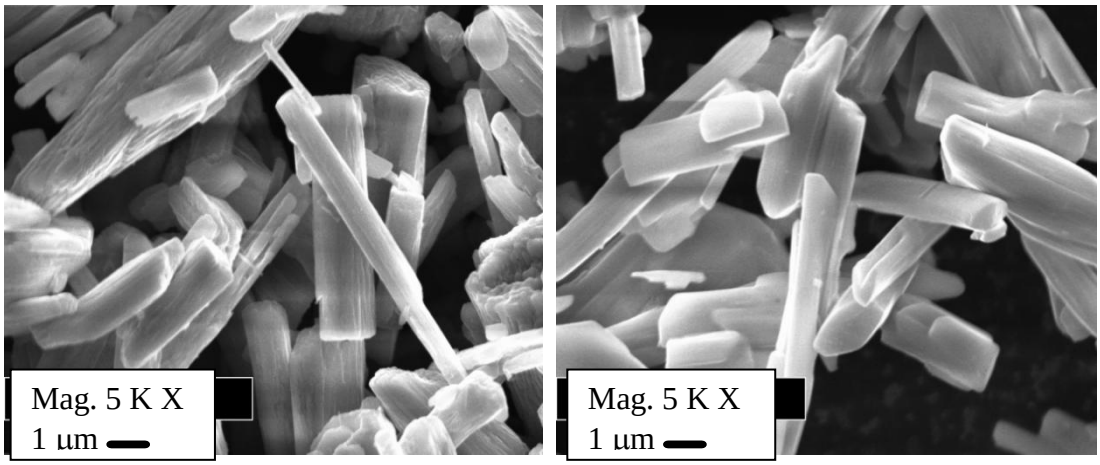


**Figure 3.7a & 3.7b:** SEM images of $(MoO_2)_2P_2O_7$ calcined (*left*) & heated in nitrogen (*right).*

SEM images of the $(MoO_2)_2P_2O_7$ material (Figure 3.7a), suggest the morphology does not change dramatically when compared with its precursor; $MoO_2 \cdot HPO_4 \cdot H_2O$. The rod structure remains, but the edges of these rods are more defined and rounded. Heat

treatment of $MoO_2 \cdot HPO_4 \cdot H_2O$ in nitrogen (Figure 3.7b) produces the same morphology as the calcined material, with the particle sizes ranging from < 2 μm to > 10 μm.

The surface area of the $(MoO_2)_2P_2O_7$ material was measured using BET surface area analysis (Table 3.1). A very low surface area of ~1 $m^2/g$ was obtained which is possibly explained by the non-porous nature of the material.

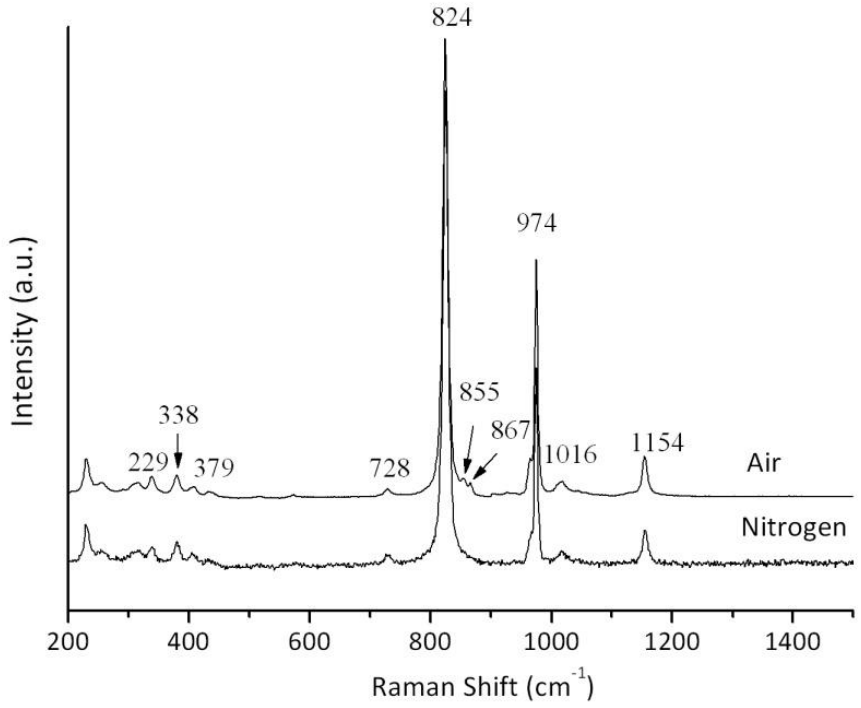


**Figure 3.8:** Raman spectra of $(MoO_2)_2P_2O_7$.

Raman spectroscopy analysis (Figure 3.8) confirmed the presence of $(MoO_2)_2P_2O_7$, with a Mo=O stretch at 1016 $cm^{-1}$ and Mo-O-Mo stretching at 824 $cm^{-1}$, as well as symmetric and anti-symmetric $(PO_4)^{3-}$ stretching at 974 $cm^{-1}$ and 1154 $cm^{-1}$ respectively. Again, heat treatment in nitrogen produced the same material as the calcination treatment.

**Table 3.1:** BET surface area measurements of unsupported molybdenum phosphate catalysts.

| Sample | BET Surface area ($m^2/g$) |
|---|---|
| $MoO_2 \cdot HPO_4 \cdot H_2O$ | 1 |
| $(MoO_2)_2P_2O_7$ | 1 |

### *3.2.2 - Supported molybdenum phosphate catalysts*

Considering the very low surface area of the molybdenum phosphate materials and their potential use as catalysts, supporting the material was attempted, as the specific supports used are known to have very high surface areas due to their morphology and/or porosity.[28-30] A number of materials were used to support molybdenum phosphate via the incipient wetness preparation method, including $Al_2O_3$, $SiO_2$ and $TiO_2$.

Characterisation of the supported materials is vital to determining the loading, surface area, and dispersion of the active phase. The XRD pattern of $(MoO_2)_2P_2O_7$ supported on $SiO_2$ (Figure 3.9) shows no indication that this phase is present (Figure 3.6). The broad reflection between 15 – 40 ° 2θ is due to the amorphous silicon dioxide support, with the sharp reflection at 44.5 ° 2θ due to an anomaly (stainless steel sample holder). The absence of reflections associated with the $(MoO_2)_2P_2O_7$ might be related to the high dispersion of the phase over the silica surface. Also, the fact that the main (most intense) index planes of the $(MoO_2)_2P_2O_7$ material appear at 22.8 ° (301) and 23.4 ° 2θ (122), which is at the centre of where the broad main silica index plane appears (15 - 40 ° 2θ), and could diminish the signal of the $(MoO_2)_2P_2O_7$ phase.

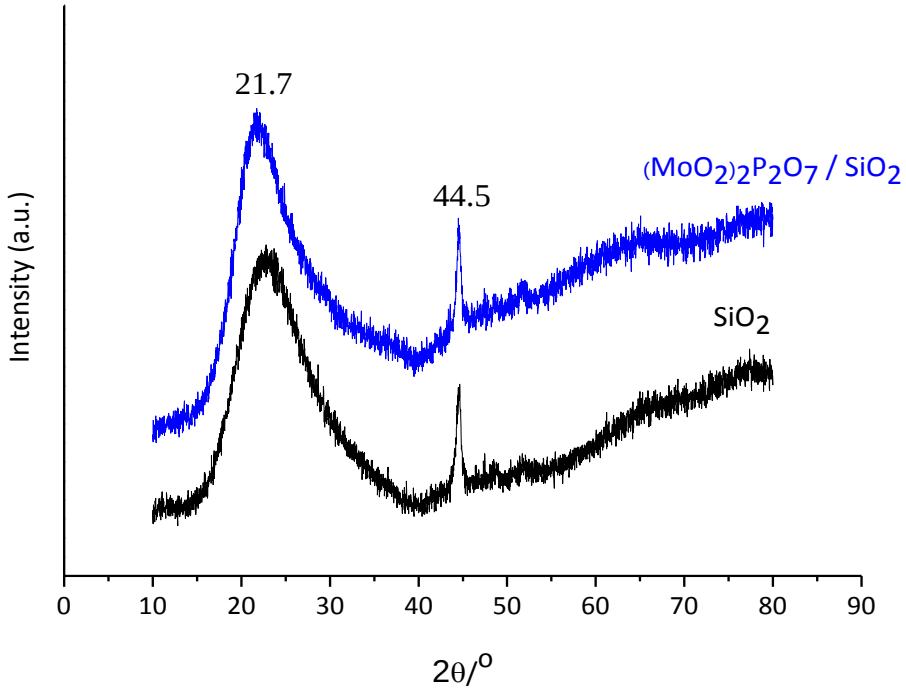


**Figure 3.9:** XRD pattern of $(MoO_2)_2P_2O_7$ (10 % loading) supported on $SiO_2$.

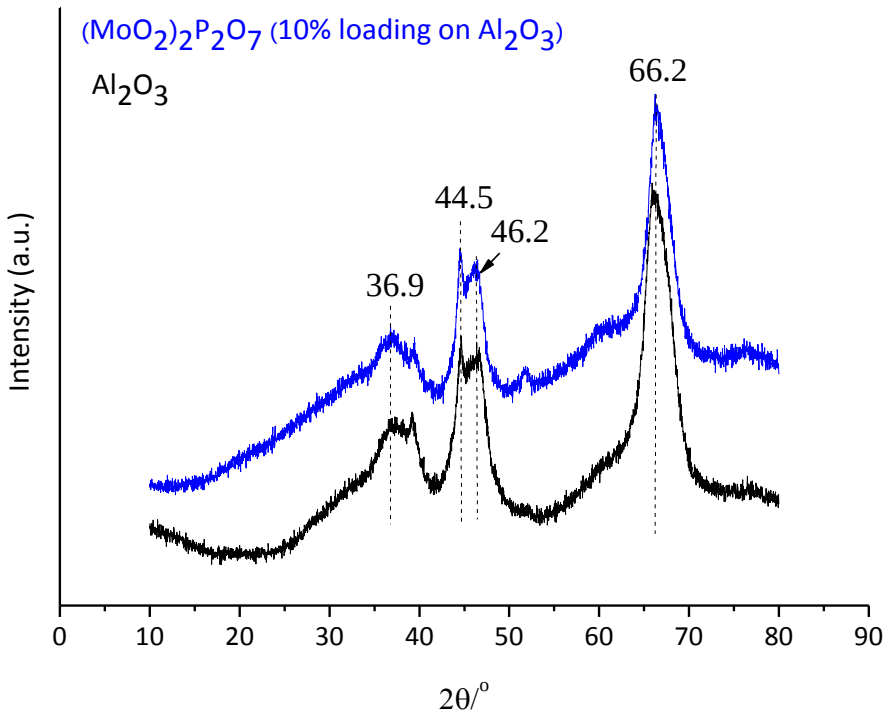


**Figure 3.10:** XRD pattern of $(MoO_2)_2P_2O_7$ (10 % loading) supported on $Al_2O_3$.

The XRD pattern of $(MoO_2)_2P_2O_7$ supported on $Al_2O_3$ (Figure 3.10) has a similar trend to the $SiO_2$ supported material, where again, $(MoO_2)_2P_2O_7$ phase reflections are not present. As before, this is possibly due to the high homogeneous dispersion of the molybdenum phosphate over the support. This is in agreement with previous studies by Casaletto *et al.*[31] who supported vanadium phosphate on $Al_2O_3$, and observed no reflections that could be assigned to the vanadium phosphate phase. The pattern of $(MoO_2)_2P_2O_7$ supported on $TiO_2$ is shown in Figure 3.11. In contrast to the other two supports, reflections consistent with the $(MoO_2)_2P_2O_7$ phase at 23.5 ° (112), 28.5 ° (020) and 31.6 ° 2θ (312) are present.

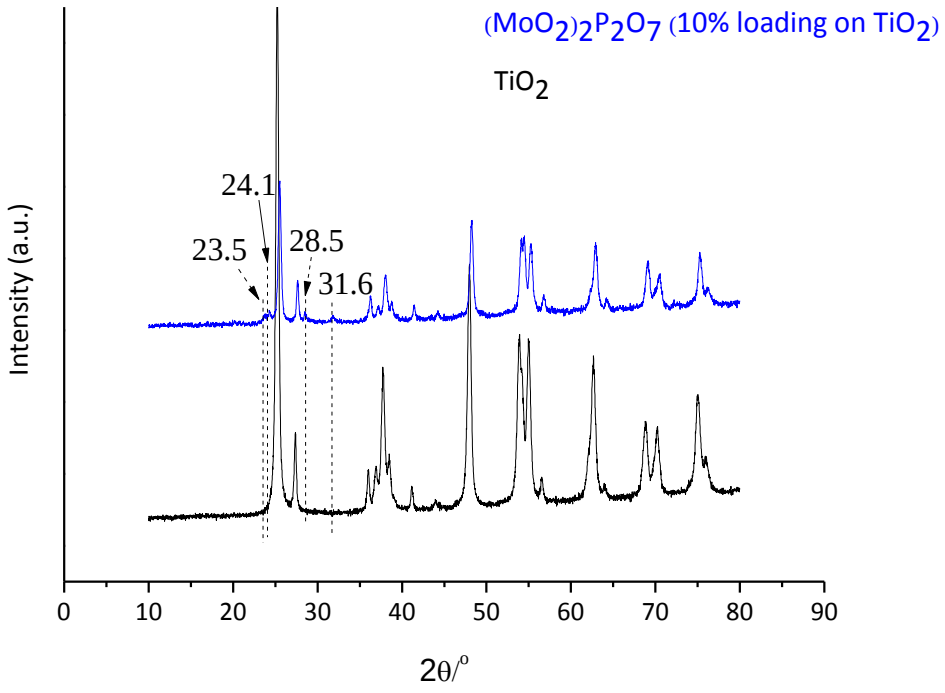


**Figure 3.11:** XRD pattern of $(MoO_2)_2P_2O_7$ (10 % loading) supported on $TiO_2$.

Raman spectroscopy can be used to confirm the presence of $(MoO_2)_2P_2O_7$, as it is a highly sensitive technique to analyse specific surface/sub-surface species in materials.

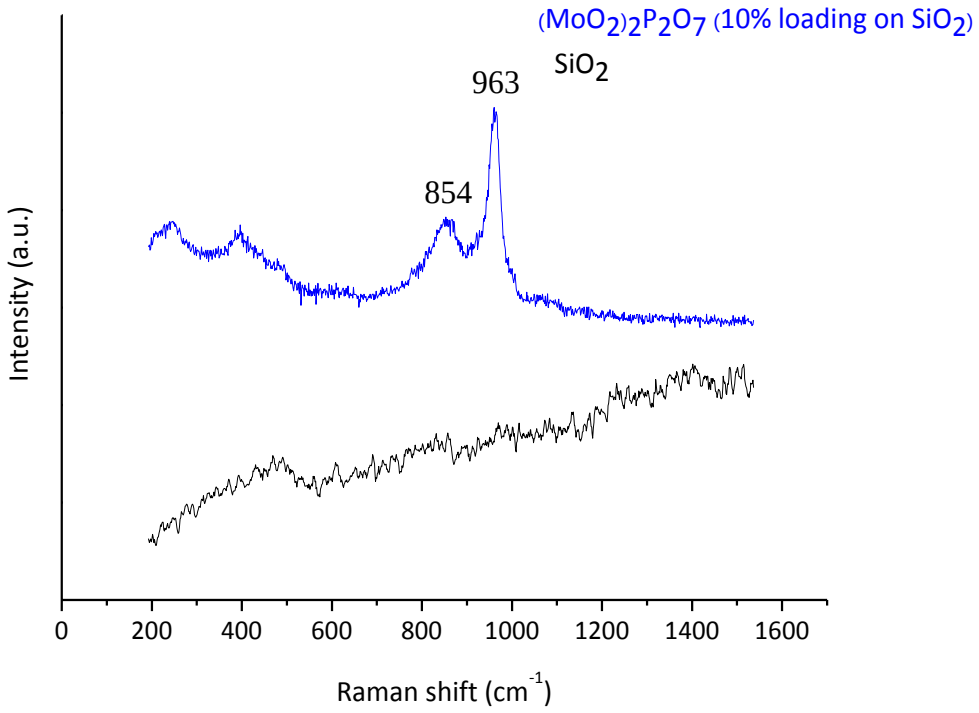


**Figure 3.12:** Raman spectrum of $(MoO_2)_2P_2O_7$ (10 % loading) supported on $SiO_2$.

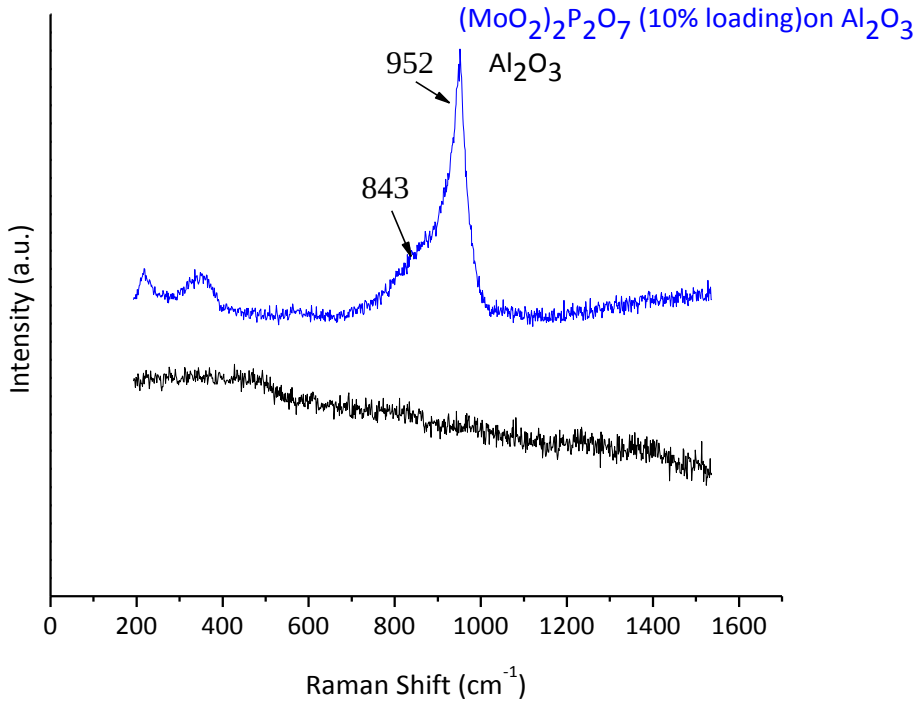


**Figure 3.13:** Raman spectrum of $(MoO_2)_2P_2O_7$ (10 % loading) supported on $Al_2O_3$.

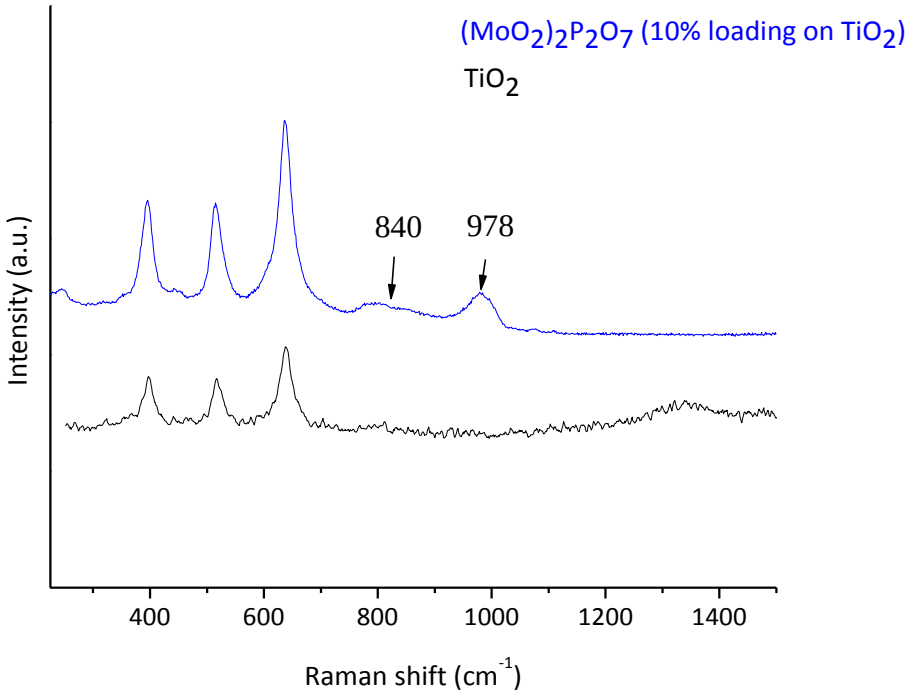


**Figure 3.14:** Raman spectrum of $(MoO_2)_2P_2O_7$ (10 % loading) supported on $TiO_2$.

Figure 3.12 displays the Raman spectrum of $(MoO_2)_2P_2O_7$ (10 % loading) supported on $SiO_2$. Analysis of the silica support only, presents no visible bands, whereas the supported $(MoO_2)_2P_2O_7$ material produces characteristic bands of $(PO_4)^{3-}$ stretching at 963 $cm^{-1}$ and Mo-O-Mo stretching at 854 $cm^{-1}$. Supporting $(MoO_2)_2P_2O_7$ on $Al_2O_3$ and $TiO_2$ produced similar results, with peaks corresponding to $(PO_4)^{3-}$ at 950 – 1000 $cm^{-1}$ and Mo-O-Mo at 840 – 860 $cm^{-1}$ present in both spectra (Figures 3.13 & 3.14).

SEM images (Figure 3.15) of supported $(MoO_2)_2P_2O_7$ on $SiO_2$ display spheres ranging in size from < 3 μm to > 15 μm. The surface of these spheres seems to be homogeneous with no particles of $(MoO_2)_2P_2O_7$ on the surface. This could be due to the $(MoO_2)_2P_2O_7$ phase being highly dispersed across the surface of the sphere, or dispersed in the pores of the silica, where in both cases these particles are too small to be analysed by XRD and hence no relevant phase is visible in the XRD pattern. BET surface area analysis (Table

3.2) of silica alone produces a high surface area of 198 $m^2/g$. Analysis of the supported $(MoO_2)_2P_2O_7$ on silica confirms the high surface area of the supported material with a measurement of 133 $m^2/g$, which suggests that the molybdenum phosphate material is coating the surface and the pores, hence reducing the overall surface area.

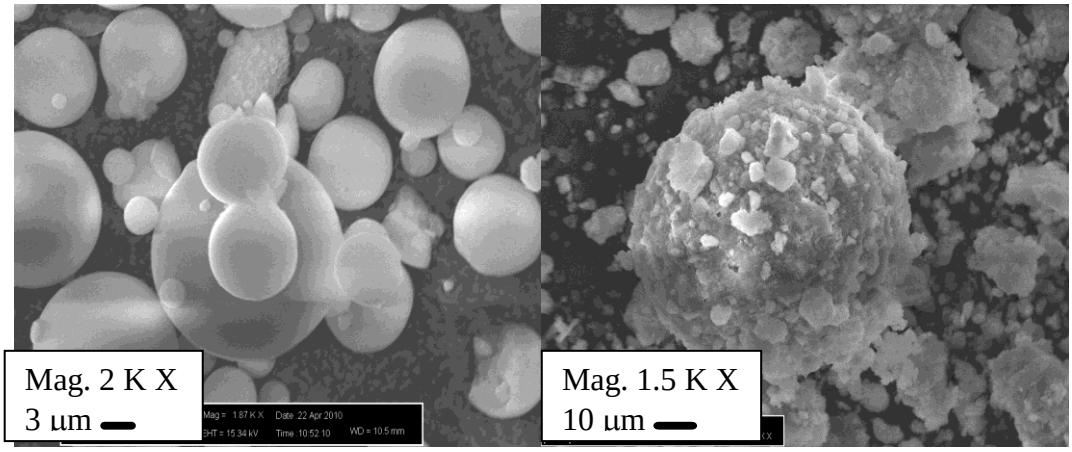


**Figure 3.15 (*left)* and 3.16 (*right)*:** SEM images of supported $(MoO_2)_2P_2O_7$ (10 % loading) on $SiO_2$ (left) and $Al_2O_3$ (*right*).

Supported $(MoO_2)_2P_2O_7$ on $Al_2O_3$ again indicates no change in morphology from the parent morphology of the support, but as with the $(MoO_2)_2P_2O_7$ loaded on $SiO_2$, the particles are too small and well dispersed to be detected by low magnification SEM analysis. The surface of these alumina spheres however, do not appear to be homogeneous, with particles sitting on the surface (Figure 3.16). After viewing the morphology of alumina alone, this was attributed to other spheres being crushed during sample preparation for SEM analysis, and becoming distributed on the surface of the intact spheres.

The surface area of the alumina supported $(MoO_2)_2P_2O_7$ material is 106 $m^2/g$, which again indicates the high dispersion of the $(MoO_2)_2P_2O_7$ material, however, the surface area of alumina alone is more than double of the supported catalyst (Table 3.2), which suggests that the $(MoO_2)_2P_2O_7$ material is coating the pores of the highly porous alumina.

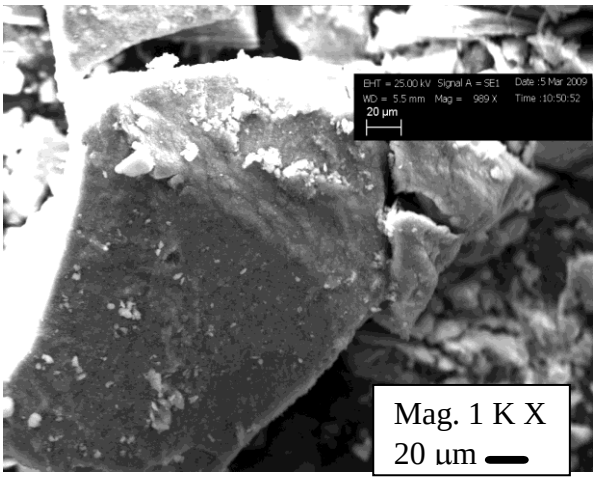


**Figure 3.17:** SEM of supported $(MoO_2)_2P_2O_7$ (10 % loading) on $TiO_2$

SEM images of the $TiO_2$ supported material (Figure 3.17) shows that it has irregular block morphology, which is characteristic of titania. The jagged blocks vary in size from < 10 μm to > 60 μm and contain small particles on the surface which, like with the alumina support, are confirmed to be smaller particles of titania (after viewing the morphology of titania alone). The surface area of the titania support (48 $m^2/g$) is much lower than the alumina and silica supports, however, when supporting the $(MoO_2)_2P_2O_7$ material, only decreases slightly to 44 $m^2/g$, which is to be expected as titania is not highly porous, and hence the majority of the supported material will be larger $(MoO_2)_2P_2O_7$ particles dispersed on the surface. The presence of these larger dispersed particles gives evidence as to the visibility of the $(MoO_2)_2P_2O_7$ phase in the XRD pattern of the titania supported material.

**Table 3.2:** BET surface area measurements of supported molybdenum phosphate catalysts

| **Material** | **BET surface area ($m^2/g$)** |
|---|---|
| $SiO_2$ | 198 |
| $Al_2O_3$ | 218 |
| $TiO_2$ | 48 |
| $(MoO_2)_2P_2O_7$ (10 % loading) on $SiO_2$ | 133 |
| $(MoO_2)_2P_2O_7$ (10 % loading) on $Al_2O_3$ | 106 |
| $(MoO_2)_2P_2O_7$ (10 % loading) on $TiO_2$ | 44 |

### *3.2.3 - Promoted molybdenum phosphate catalysts*

The use of transition metals to promote catalysts has been widely reported in the literature.[32,33] A preliminary investigation was used to study the incorporation of a range of transition metal oxides (Bi, Co, Fe, V and W), and with the comparison of catalytic results (selective methanol oxidation), vanadium provided superior activity and was studied further in this chapter. Vanadium was added in the form of vanadium pentoxide during the preparation of $MoO_2 \cdot HPO_4 \cdot H_2O$ (section 2.2.3.1), and the addition of a wide range of loadings 1, 5, 10 & 20 mol% was used so as to observe the effect on catalytic activity. This addition of transition metals to $MoO_2 \cdot HPO_4 \cdot H_2O$ is novel, and to confirm whether the phase of the material was altered or not with vanadium addition, XRD was used (Figures 3.18a & 3.18b).

The XRD pattern of $MoO_2 \cdot HPO_4 \cdot H_2O$ containing 1 mol% vanadium has the same pattern as $MoO_2 \cdot HPO_4 \cdot H_2O$ alone, with the only subtle difference being the shoulder reflection of the (111) index plane at 26.6 ° 2θ decreasing in intensity. As the amount of vanadium added is increased, the reflection at 11.9 ° 2θ gradually increases in intensity, which could be due to the vanadium forming a vanadium phosphate phase separate to the molybdenum phosphate phase present. To explore this theory, the reflection at 11.9 ° 2θ was compared with the literature and JCPDS database, to confirm that the unknown reflection corresponds to the (001) index plane of the vanadyl orthophosphate dihydrate phase: $VOPO_4.2H_2O$ (JCPDS ref. code: 00-03-1472).

Looking at the XRD patterns in more detail (Figure 3.18b) it is apparent that the shoulder reflection of the (111) plane ($MoO_2 \cdot HPO_4 \cdot H_2O$ phase) at 26.6 ° 2θ is no longer present. The reflection at 28.7 ° 2θ again corresponds to the $VOPO_4 \cdot 2H_2O$ phase, and can be indexed to the (200) plane.

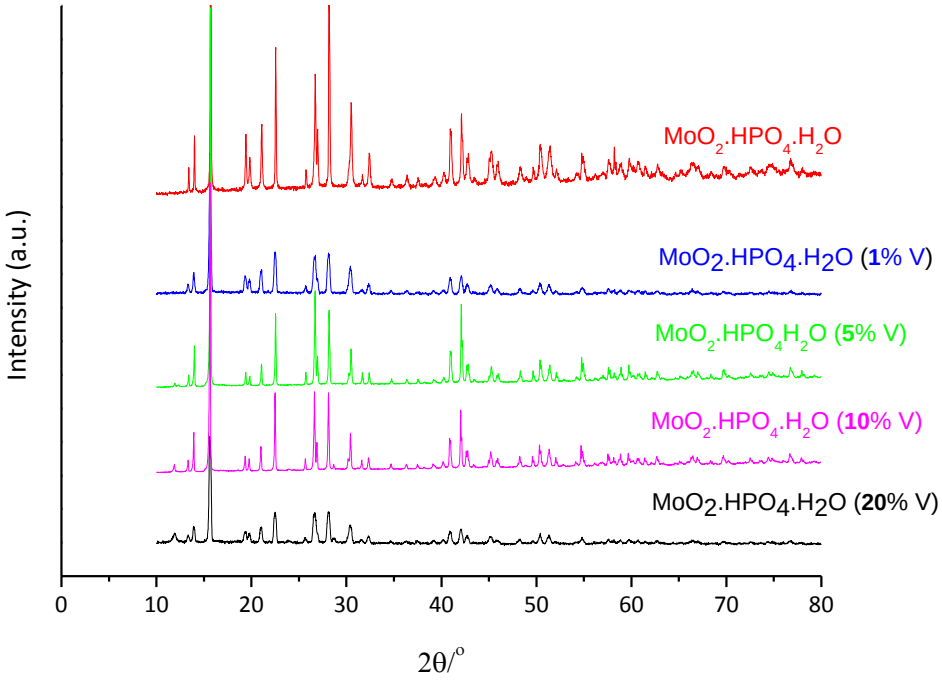


**Figure 3.18a:** XRD pattern of $MoO_2.HPO_4.H_2O$ with 1, 5, 10 and 20 % loadings of vanadium during preparation (0 – 80 ° 2θ).

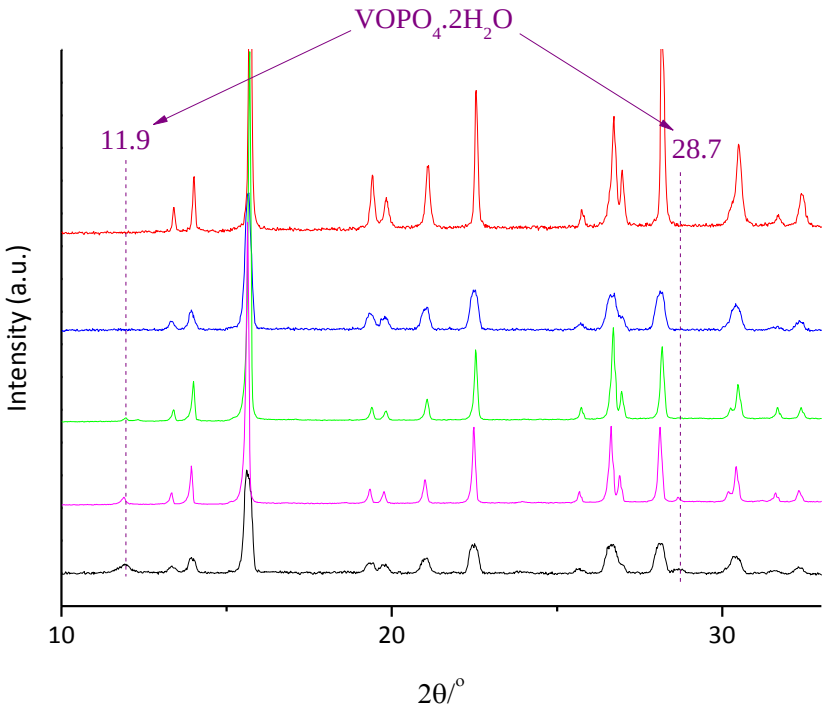


**Figure 3.18b:** XRD pattern of $MoO_2 \cdot HPO_4 \cdot H_2O$ with 1, 5, 10 and 20 mol% loadings of vanadium during preparation (10 – 33 ° 2θ).

Raman spectroscopy is important so as to discover the vanadium species present in the molybdenum phosphate structure, *i.e.* whether it is bonded to molybdenum, phosphate groups and/or oxygen atoms. Figure 3.19 shows the Raman spectra of $MoO_2 \cdot HPO_4 \cdot H_2O$ with varying amounts of vanadium added during preparation (1, 5, 10 & 20 mol%). It is clear that adding 1 mol% vanadium has little effect on the species present in the catalyst, with the only difference appearing to be the emergence of a peak at 215 $cm^{-1}$. Further addition of vanadium produces bands at 922 and 1031 $cm^{-1}$, which are characteristic of P-O stretching in $(PO_4)^{3-}$ and V-O-P stretching vibrations in $VOPO_4 \cdot 2H_2O$ respectively.[34]

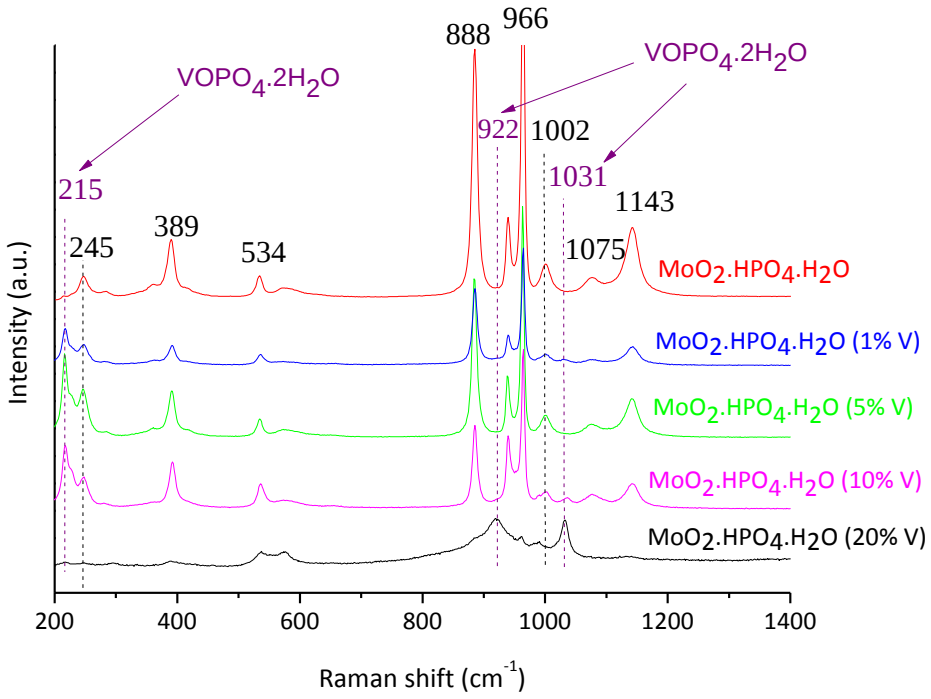


**Figure 3.19:** Raman spectrum of $MoO_2 \cdot HPO_4 \cdot H_2O$ with 1 - 20 mol% loadings of vanadium during preparation.

As previously stated, to prepare the $(MoO_2)_2P_2O_7$ phase, the precursor material must be calcined, and this same method was used with the precursors containing vanadium. To determine the effect of calcining the material on the structure, characterization was carried out using a range of techniques.

XRD analysis of the $(MoO_2)_2P_2O_7$ materials containing vanadium (Figure 3.20), show that large amounts of vanadium alters the structure of the material in some way. The addition of 1 mol% vanadium produces the same $(MoO_2)_2P_2O_7$ phase with no visible changes in the pattern, and this would suggest that the vanadium could be present in a number of forms, such as in an amorphous phase, or it could be incorporated into the structure without a change in the pattern due to the low amount added, which could provide no long range order which is needed to be detected by XRD. The Raman spectra also presents no visible difference in terms of extra bands compared to the spectra of $(MoO_2)_2P_2O_7$ alone (Figure 3.21).

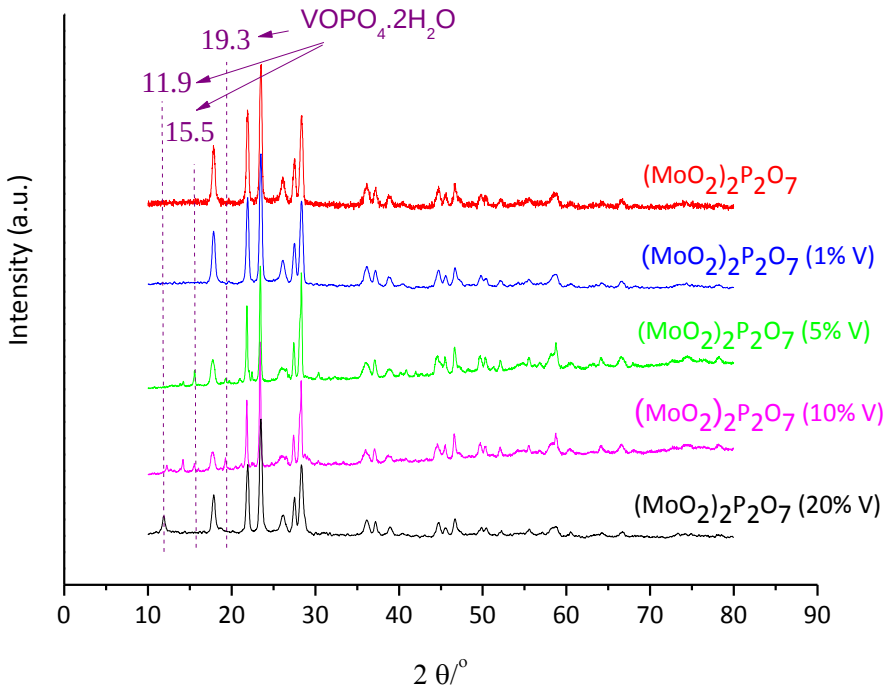


**Figure 3.20**: XRD patterns of $(MoO_2)_2P_2O_7$ containing varying amounts of vanadium (mol%).

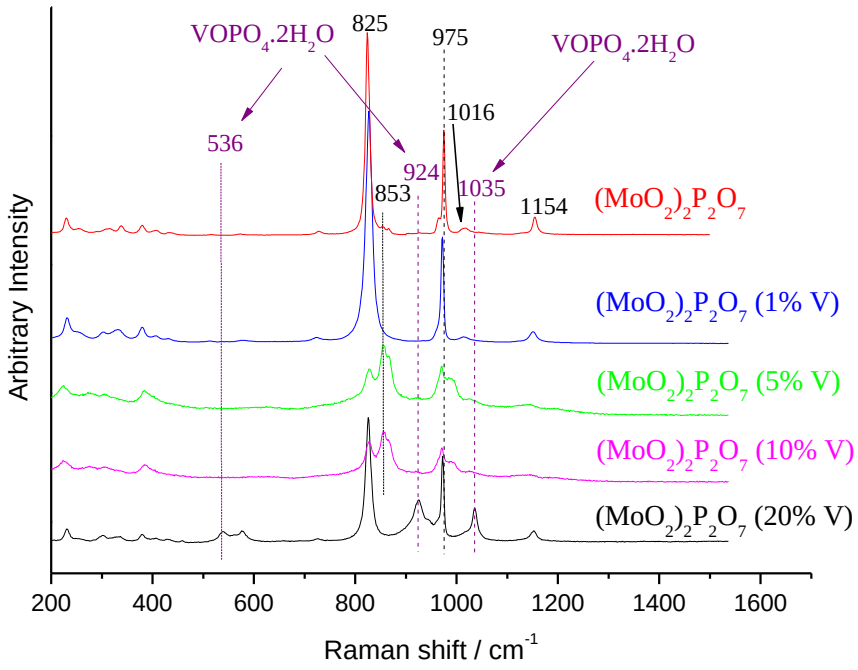


**Figure 3.21:** Raman spectra of $(MoO_2)_2P_2O_7$ containing varying amounts of vanadium (mol%).

Using X-ray photon spectroscopy (XPS) to analyse both un-promoted and 1 mol% vanadium promoted $(MoO_2)_2P_2O_7$ (Table 3.3 and 3.4 respectively) confirms the presence of vanadium on the surface of the promoted material, although present in a small amount (0.2 atomic %), XPS indicates a peak at 518.8 eV which is characteristic of $V^{5+}$ ions (consistent with the oxidation state of vanadium in $VOPO_4.2H_2O$).

**Table 3.3:** XPS data showing atomic % of elements present in $(MoO_2)_2P_2O_7$ alone.

| Element | Binding energy (eV) | Atomic % |
|---|---|---|
| O | 531.8 | 50.6 |
| C | 284.8 | 30.6 |
| P | 133.8 | 9.6 |
| Mo | 233.8 | 9.2 |

**Table 3.4:** XPS data showing atomic % of elements present in 1 mol% vanadium promoted $(MoO_2)_2P_2O_7$.

| Element | Binding energy (eV) | Atomic % |
|---|---|---|
| O | 531.8 | 53.7 |
| C | 284.8 | 26.9 |
| P | 133.8 | 10 |
| Mo | 232.8 | 9.2 |
| V | 518.8 | 0.2 |

Addition of 5 and 10 mol% vanadium produced more defined results, with the XRD pattern clearly showing the presence of vanadium as a separate phase to the $(MoO_2)_2P_2O_7$ phase (Figure 3.20). These reflections correspond to the tetragonal $VOPO_4 \cdot 2H_2O$ phase, which is formed by vanadium oxide reacting with the phosphoric acid during the co-precipitation.

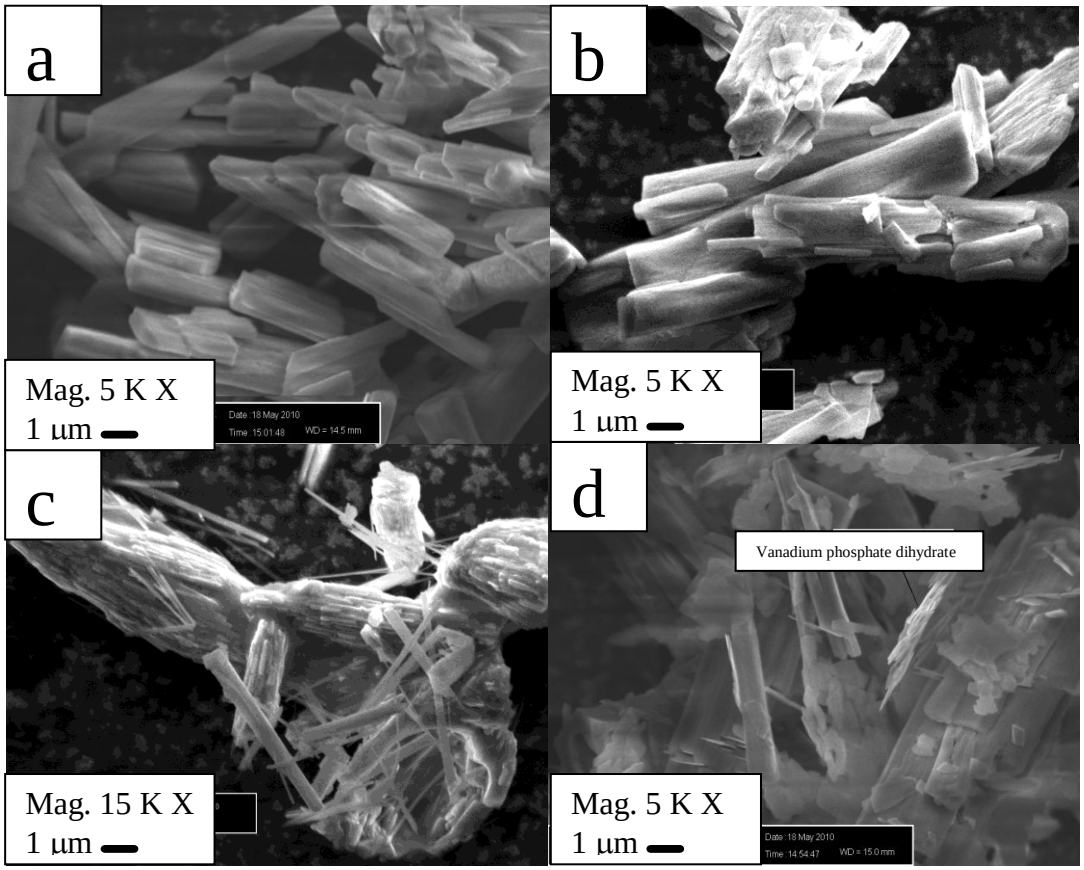


**Figure 3.22a, b, c & d:** SEM images of $(MoO_2)_2P_2O_7$ 1 mol% vanadium (*top left)*; $(MoO_2)_2P_2O_7$ 5 mol% vanadium (*top right);* $(MoO_2)_2P_2O_7$ 10 mol% vanadium *(bottom left);* $(MoO_2)_2P_2O_7$ 20 mol% vanadium (*bottom right*).

The SEM images of $(MoO_2)_2P_2O_7$ containing 1 and 5 mol% vanadium (Figure 3.22a & b) shows no indication of vanadium phosphate morphology (platelets or rosette morphology) which could suggest that vanadium has incorporated into the structure of the $(MoO_2)_2P_2O_7$ material. Addition of 10 and 20 mol% vanadium clearly indicates the presence of a separate phase in the XRD pattern with a reflection visible at 11.9 ° 2θ, corresponding to the (001) index plane of the $VOPO_4 \cdot 2H_2O$ phase (Figure 3.20). Evidence of this separate phase is also presented in the SEM images (Figure 3.22c & d) where platelets characteristic of $VOPO_4 \cdot 2H_2O$ [35] can be seen mixed with the rod structures of $(MoO_2)_2P_2O_7$. Energy dispersive X-ray (EDX) analysis was used in conjunction with SEM to confirm that the required loading of vanadium was indeed present in each sample.

Raman spectroscopy of the vanadium containing compounds (Figure 3.21) showed evidence of $VOPO_4 \cdot 2H_2O$ present in the material, becoming more clear as the vanadium content is increased. Bands are visible for the $(MoO_2)_2P_2O_7$ species (825, 975 and 1016 $cm^{-1}$), with bands at 536 and 924 $cm^{-1}$ assigned to bridging V-O-V bending [36] and $(PO_4)^{3-}$ symmetric stretching respectively.

### *3.2.4 - Supported molybdenum pyrophosphate materials containing vanadium*

XRD analysis of the silica supported materials containing low to moderate loadings of vanadium (Figure 3.23), showed no reflections that could be assigned to $(MoO_2)_2P_2O_7$ or $VOPO_4 \cdot 2H_2O$. However, in the case of high vanadium loadings (20 mol%), reflections of the $(MoO_2)_2P_2O_7$ phase are visible at 13.3 ° (200), 15.7 ° (011), 22.4 ° (202) and 28.0 ° 2θ (020). Raman spectroscopy of the supported materials containing 1 mol% vanadium (Figure 3.24) showed no bands that could be assigned to vanadium species, but does possess bands at 854 $cm^{-1}$ and 963 $cm^{-1}$ consistent with $(MoO_2)_2P_2O_7$ species. Increasing

the addition of vanadium to 20 mol% produces bands at 530, 1025 and 1140 $cm^{-1}$ which are characteristic of V-O-V bending and V-O-P stretching vibrations in $VOPO_4 \cdot 2H_2O$. BET surface area analysis of these materials indicates that the $VOPO_4 \cdot 2H_2O/(MoO_2)_2P_2O_7$ phases are coating the pores of the silica support, and hence decreasing the surface area of the support (Table 3.5).

**Table 3.5:** BET surface area measurements of unsupported and supported molybdenum pyrophosphate catalysts promoted with varying amounts of vanadium.

| Catalyst | BET surface area ($m^2/g$) |
|---|---|
| $(MoO_2)_2P_2O_7$ | 1 |
| $(MoO_2)_2P_2O_7$ 1% V | 1 |
| $(MoO_2)_2P_2O_7$ 5% V | 1 |
| $(MoO_2)_2P_2O_7$ 10% V | 1.5 |
| $(MoO_2)_2P_2O_7$ 20% V | 3 |
| $(MoO_2)_2P_2O_7$ 1% V (10% loading) on $SiO_2$ | 142 |
| $(MoO_2)_2P_2O_7$ 20% V (10% loading) on $SiO_2$ | 119 |

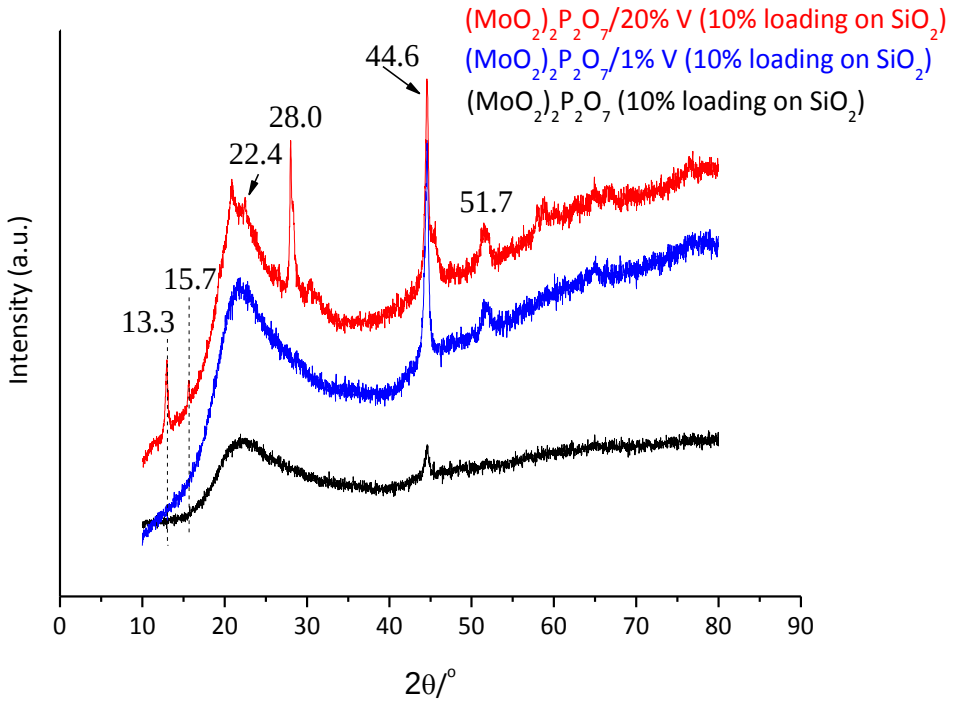


**Figure 3.23:** XRD patterns of $(MoO_2)_2P_2O_7$ with varying amounts of vanadium (mol%) supported on $SiO_2$.

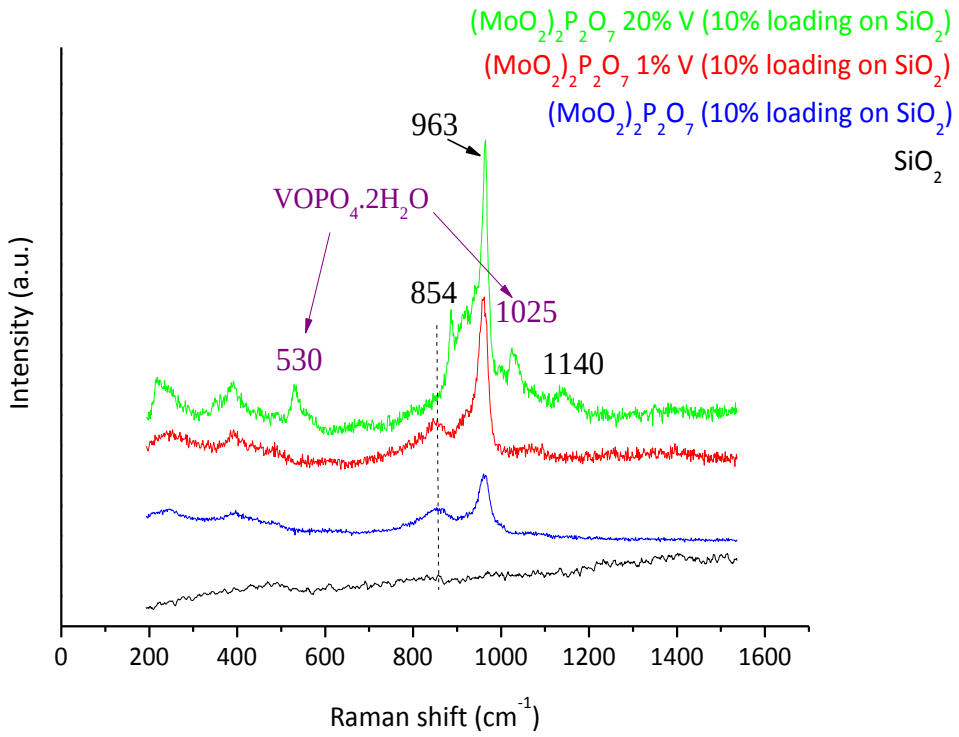


**Figure 3.24:** Raman spectra of silica supported $(MoO_2)_2P_2O_7$ containing varying amounts of vanadium (mol%).

## 3.3 – Catalytic activity

The unsupported/supported and un-promoted/promoted molybdenum phosphate catalysts were tested for the oxidation of methanol, for the formation of the partial oxidation product, formaldehyde. Dilute oxygen and methanol feeds were used so as to test outside of the methanol explosive limits (6 % - 36 % in air). To ensure that no reaction of methanol occurred at high reaction temperatures with the quartz reactor tube, a blank reaction (no catalyst) was performed (Appendix Figure A.2) which yielded no conversion of methanol at temperatures as high as 500 °C.

### *3.3.1 –Unsupported molybdenum phosphate catalysts*

To investigate the effect that the calcination of $MoO_2 \cdot HPO_4 \cdot H_2O$ has on the catalytic activity compared to the uncalcined $MoO_2 \cdot HPO_4 \cdot H_2O$, both catalysts were tested (Figure

3.25). The uncalcined catalyst maintains higher activity than $(MoO_2)_2P_2O_7$ at temperatures below 400 °C, with a conversion of 26 % methanol at 300 °C, whereas 14 % methanol is converted at the same temperature using $(MoO_2)_2P_2O_7$. At 460 °C the $(MoO_2)_2P_2O_7$ catalyst has a slightly higher activity than the $MoO_2 \cdot HPO_4 \cdot H_2O$ catalyst, with conversions of 88 % and 71 % respectively.

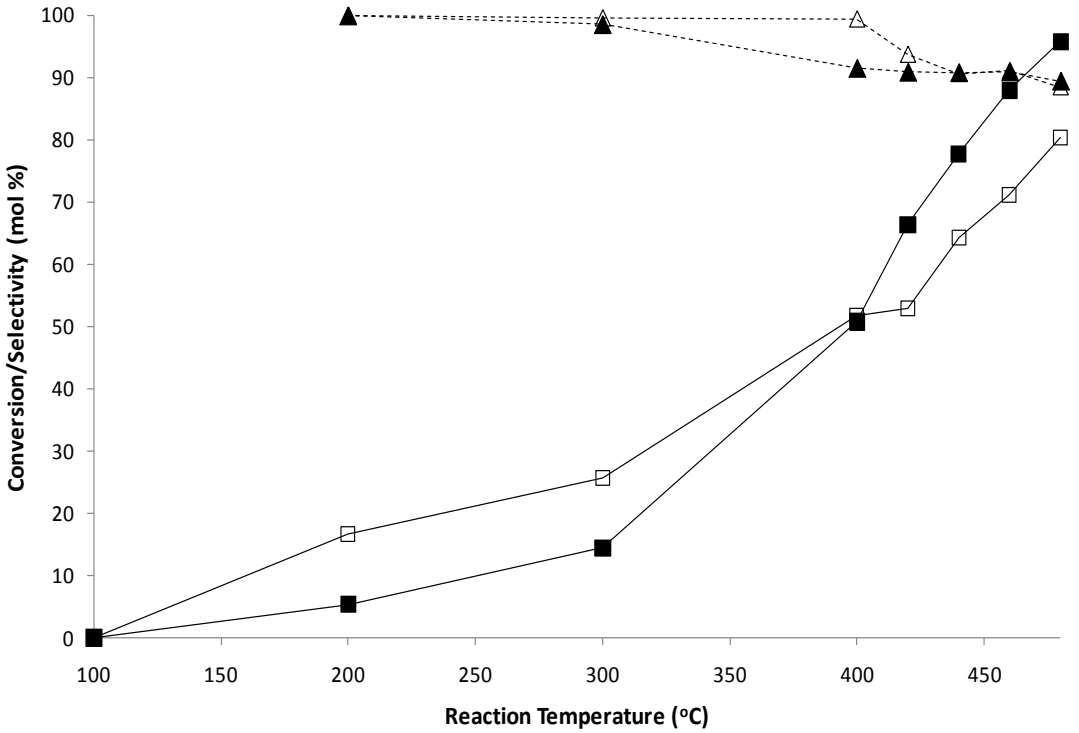


**Figure 3.25:** Methanol conversion and Formaldehyde selectivity using molybdenum phosphate precursor ($MoO_2 \cdot HPO_4 \cdot H_2O$) and molybdenum pyrophosphate $(MoO_2)_2P_2O_7$ catalysts.

= $MoO_2 \cdot HPO_4 \cdot H_2O$ methanol conversion; = $(MoO_2)_2P_2O_7$ methanol conversion;

= $MoO_2 \cdot HPO_4 \cdot H_2O$ formaldehyde selectivity; = $(MoO_2)_2P_2O_7$ formaldehyde selectivity.

### *3.3.2 –Supported molybdenum phosphate catalysts*

Supporting the $(MoO_2)_2P_2O_7$ phase is a way of improving catalytic activity of the catalysts reported frequently in the literature.[37-39] One particularly important catalyst reported in the literature for methanol oxidation is $MoO_3$ supported on $SiO_2$,[40] $Al_2O_3$ [41] and $TiO_2$. [42] These three materials were therefore singled out as potential candidates to

improve the catalytic activity of $(MoO_2)_2P_2O_7$, and these supported catalysts were prepared using the incipient wetness procedure (section 2.2.2.1).

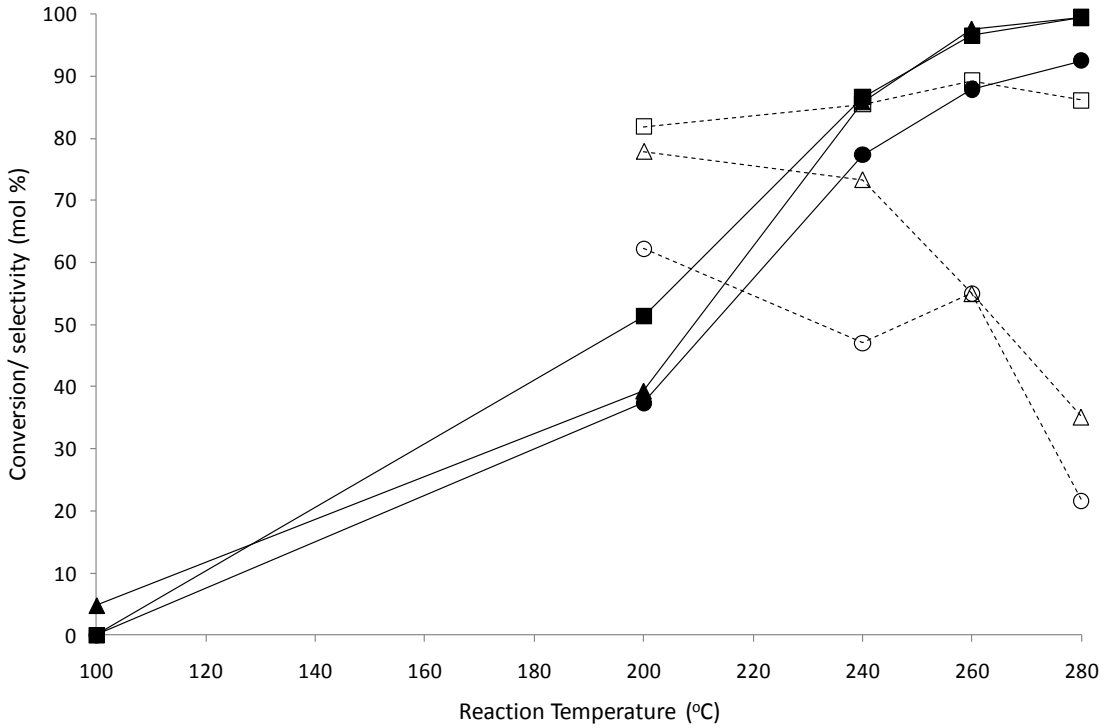


**Figure 3.26:** Methanol conversion & formaldehyde selectivity comparing $(MoO_2)_2P_2O_7$ on different supports.

■ = MeOH conversion - $(MoO_2)_2P_2O_7$ on $SiO_2$: ● = MeOH conversion - $(MoO_2)_2P_2O_7$ on $Al_2O_3$:
▲ = MeOH conversion - $(MoO_2)_2P_2O_7$ on $TiO_2$: ⊡ = FA selectivity - $(MoO_2)_2P_2O_7$ on $SiO_2$:
⊙ = FA selectivity - $(MoO_2)_2P_2O_7$ on $Al_2O_3$: △ = FA selectivity - $(MoO_2)_2P_2O_7$ on $TiO_2$.

Methanol oxidation testing (Figure 3.26) using the alumina supported catalyst yielded quite poor results, as near total methanol conversion was achieved at 280 °C, but with only 20 % formaldehyde selectivity. This is to be expected as alumina is widely known to produce high yields of dimethyl ether (Appendix Figure A.3) due to the acidic sites present on its surface.[43] The titania supported catalyst showed a similar trend with total conversion again at 280 °C, but with slightly higher formaldehyde selectivity of 40 % ($TiO_2$ activity alone Appendix Figure A.4). However, the supported catalyst with the highest activity was on silica, with total conversion achieved at 280 °C, but with

remarkably high formaldehyde selectivity compared to the other two supports, with around 85 % selectivity. ($SiO_2$ activity alone Appendix Figure A.5)

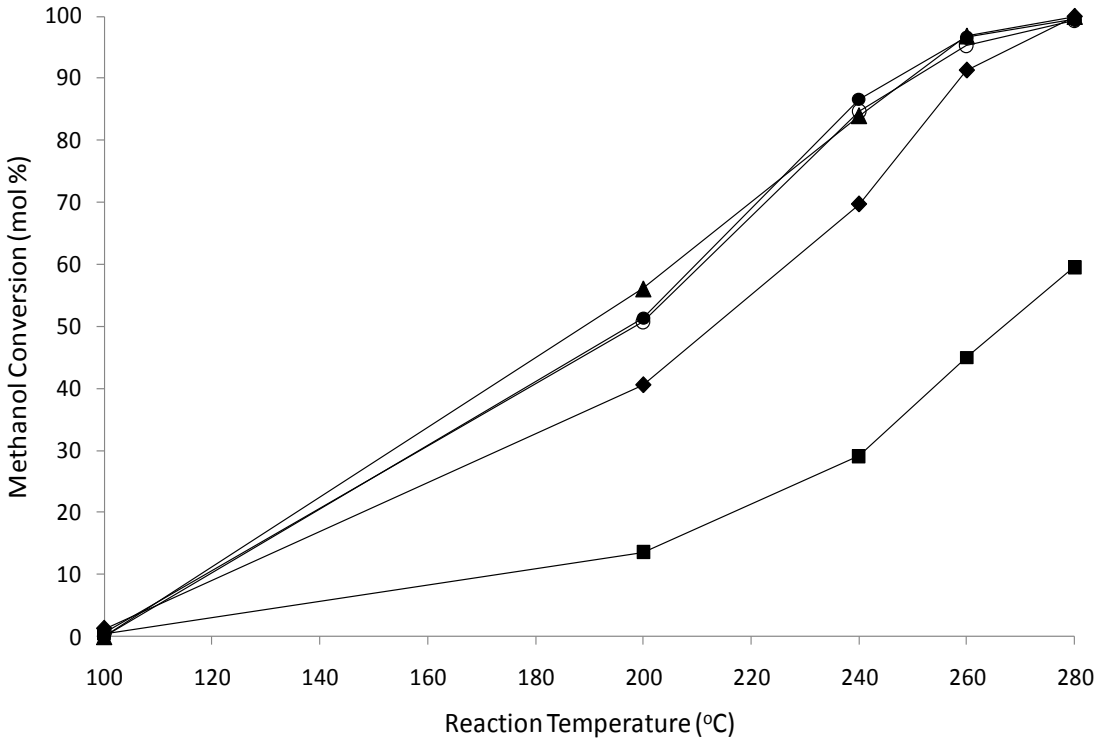


**Figure 3.27:** Methanol conversion comparing $(MoO_2)_2P_2O_7$ supported on $SiO_2$ with various loadings.

= MeOH conversion using $(MoO_2)_2P_2O_7$ supported on $SiO_2$ (1 wt% loading): = $(MoO_2)_2P_2O_7$ supported on $SiO_2$ (5 wt% loading): = $(MoO_2)_2P_2O_7$ supported on $SiO_2$ (10 wt% loading): = $(MoO_2)_2P_2O_7$ supported on $SiO_2$ (15 wt% loading): = $(MoO_2)_2P_2O_7$ supported on $SiO_2$ (20 wt% loading)

As the silica supported catalyst proved to be the best of the three in terms of high formaldehyde selectivity, varying loadings of the $(MoO_2)_2P_2O_7$ catalyst on silica were tested for methanol oxidation (Figure 3.27 & 3.28). A low loading of 1 wt% $(MoO_2)_2P_2O_7$ produces poor activity, only 30 % conversion was achieved at 240 °C, with 90 % formaldehyde selectivity (27 % yield).

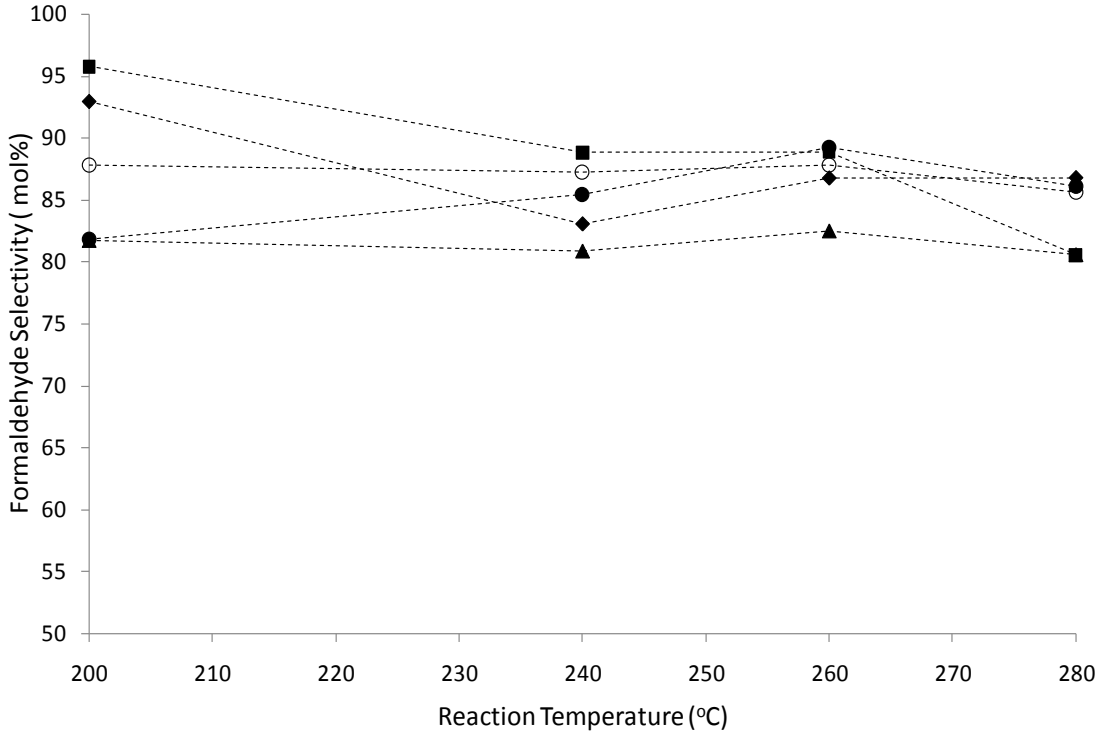


**Figure 3.28:** Formaldehyde selectivity comparing $(MoO_2)_2P_2O_7$ supported on $SiO_2$ with various loadings.

--■-- = $(MoO_2)_2P_2O_7$ supported on $SiO_2$ (1 wt% loading): --●-- = $(MoO_2)_2P_2O_7$ supported on $SiO_2$ (5 wt% loading): --▲-- = $(MoO_2)_2P_2O_7$ supported on $SiO_2$ (10 wt% loading): --⊙-- = $(MoO_2)_2P_2O_7$ supported on $SiO_2$ (15 wt% loading): --◆-- = $(MoO_2)_2P_2O_7$ supported on $SiO_2$ (20 wt% loading).

Using loadings of 5, 10, 15 and 20 wt% $(MoO_2)_2P_2O_7$ on silica therefore gives a broad range to discover the optimum loading. Using loadings of 5, 10 and 15 wt% of $(MoO_2)_2P_2O_7$, produced very similar methanol conversions at 240 °C, all at approximately 85 % conversion. However, the selectivity to formaldehyde proved to be the difference between these three loadings. It is clear that the 15 % loading of $(MoO_2)_2P_2O_7$ on $SiO_2$ has the highest formaldehyde selectivity of 88 % (75 % yield) at 240 °C, with 5 wt% loading and 10 wt% loading producing 85 % (72 % yield) and 81 % (69 % yield) respectively. (Table 3.6) The highest loading of $(MoO_2)_2P_2O_7$ on $SiO_2$ (20 wt%) produced 71 % conversion of methanol at 240 °C with 88 % selectivity to formaldehyde (63 % yield).

**Table 3.6:** Comparing formaldehyde yield at specific reaction temperatures during methanol oxidation with varying $(MoO_2)_2P_2O_7$ loadings on $SiO_2$.

| **$(MoO_2)_2P_2O_7$ loading on $SiO_2$ (wt%)** | **FA yield at 200 °C (mol%)** | **FA yield at 240 °C (mol%)** | **FA yield at 260 °C (mol%)** | **FA yield at 280 °C (mol%)** |
|---|---|---|---|---|
| **1** | 13 | 26 | 40 | 48 |
| **5** | 42 | 72 | 86 | 86 |
| **10** | 46 | 69 | 80 | 81 |
| **15** | 45 | 75 | 84 | 85 |
| **20** | 38 | 63 | 79 | 87 |

The supporting of $(MoO_2)_2P_2O_7$ on silica in a moderate amount, greatly enhances catalytic activity, however, the selectivity to formaldehyde decreases noticeably when compared to the unsupported $(MoO_2)_2P_2O_7$ catalytic activity, which produces 100 % formaldehyde selectivity at 240 °C.

### *3.3.3 – Methanol partial oxidation using vanadium promoted unsupported & supported molybdenum phosphate catalysts*

The use of transition metals have been reported in the literature to promote catalysts,[44,45] and in this study vanadium was added during a novel co-precipitation technique for this catalyst, in an attempt to incorporate it into the bulk of the molybdenum phosphate structure to potentially enhance the catalytic properties in the redox process.

Figures 3.29 & 3.30 show that the amount of vanadium added to the molybdenum phosphate has a substantial effect on activity of the catalyst. The $(MoO_2)_2P_2O_7$ catalyst without added vanadium reached 96 % conversion at 480 °C, which was similar to the catalysts that contained vanadium where conversions of ~95 % were also reached. $(MoO_2)_2P_2O_7$ containing 1 mol% vanadium showed improved activity at 400 °C, with 71 % conversion compared to the 51 % conversion without vanadium. There was no major difference in the formaldehyde selectivity but, due to the difference in conversion

at this temperature, formaldehyde yield is around 20 % higher when 1 mol% vanadium was added. The addition of 5 mol% vanadium had a similar effect to the addition of 1 mol% vanadium, although there was a slight increase in activity of the catalyst. Although the formaldehyde selectivity is high for the majority of the reaction for both catalysts containing vanadium, at 480 °C more $CO_x$ is produced which causes a decrease in formaldehyde selectivity due to its over oxidation. Addition of 20 mol% vanadium to the $(MoO_2)_2P_2O_7$ catalyst produced the highest activity at 400 °C, with nearly 25 % higher conversion, and nearly 30 % higher formaldehyde yield than the $(MoO_2)_2P_2O_7$ catalyst alone.

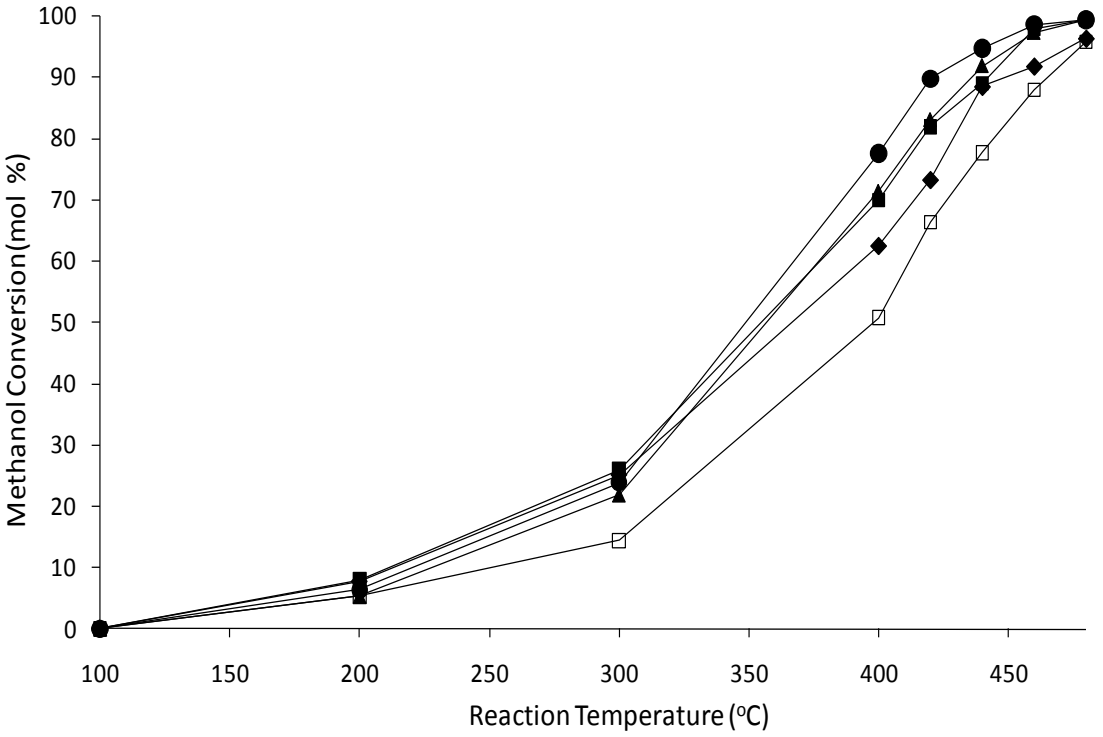


**Figure 3.29:** Methanol conversion using $(MoO_2)_2P_2O_7$ catalysts with varying amounts of vanadium.

= $(MoO_2)_2P_2O_7$: = $(MoO_2)_2P_2O_7$ 1 mol% V: = $(MoO_2)_2P_2O_7$ 5 mol% V:
= $(MoO_2)_2P_2O_7$ 10 mol% V: = $(MoO_2)_2P_2O_7$ 20 mol% V

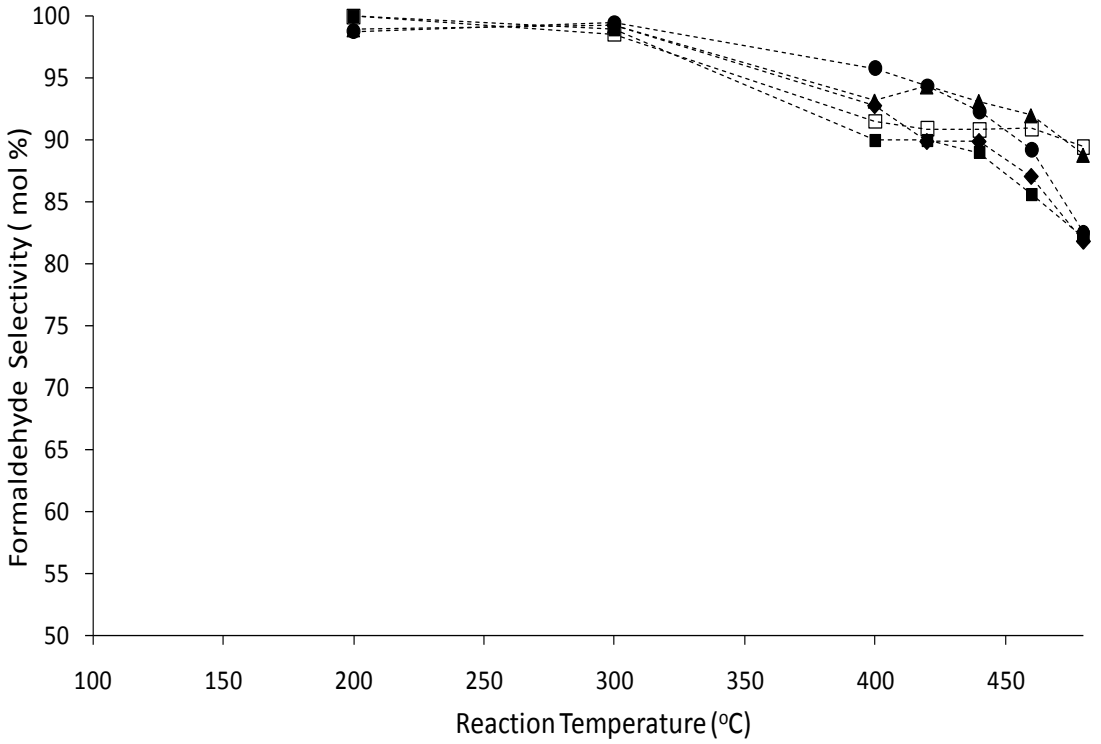


**Figure 3.30:** Formaldehyde selectivity using $(MoO_2)_2P_2O_7$ catalysts with varying amounts of vanadium.

$(MoO_2)_2P_2O_7$: $(MoO_2)_2P_2O_7$ 1 mol% V: $(MoO_2)_2P_2O_7$ 5 mol% V: $(MoO_2)_2P_2O_7$ 10 mol% V: $(MoO_2)_2P_2O_7$ 20 mol% V.

Supporting the $(MoO_2)_2P_2O_7$ catalyst using silica had a substantial effect on their effectiveness for methanol oxidation, by dramatically increasing their activity compared to the unsupported $(MoO_2)_2P_2O_7$ catalyst. The detrimental effect this had on the formaldehyde selectivity however was addressed by promoting the catalysts with vanadium, which increased the selectivity to formaldehyde. As both supporting and the addition of vanadium had positive effects on the catalytic activity of $(MoO_2)_2P_2O_7$ materials, the loading of the material on silica and the addition of vanadium were prepared and tested for methanol oxidation to formaldehyde.

Observed in Figure 3.31 is the conversion of methanol for each supported $(MoO_2)_2P_2O_7$ catalyst (10 wt% loading) containing either; 0, 1 or 20 mol% vanadium. The addition of high loadings of vanadium in this case has a detrimental effect on the activity of the

catalysts with around 20 % lower conversion, and 15 % lower formaldehyde yield for the supported catalyst containing 20 mol% vanadium at 240 °C (compared to supported un-promoted $(MoO_2)_2P_2O_7$). At low to moderate reaction temperatures (200 – 240 °C) the supported catalyst containing 1 mol% vanadium has lower activity than the un-promoted supported catalyst. However, at temperatures above 240 °C, the activity is very similar but produces formaldehyde yields of around 10 % higher than the un-promoted supported catalyst (Table 3.7).

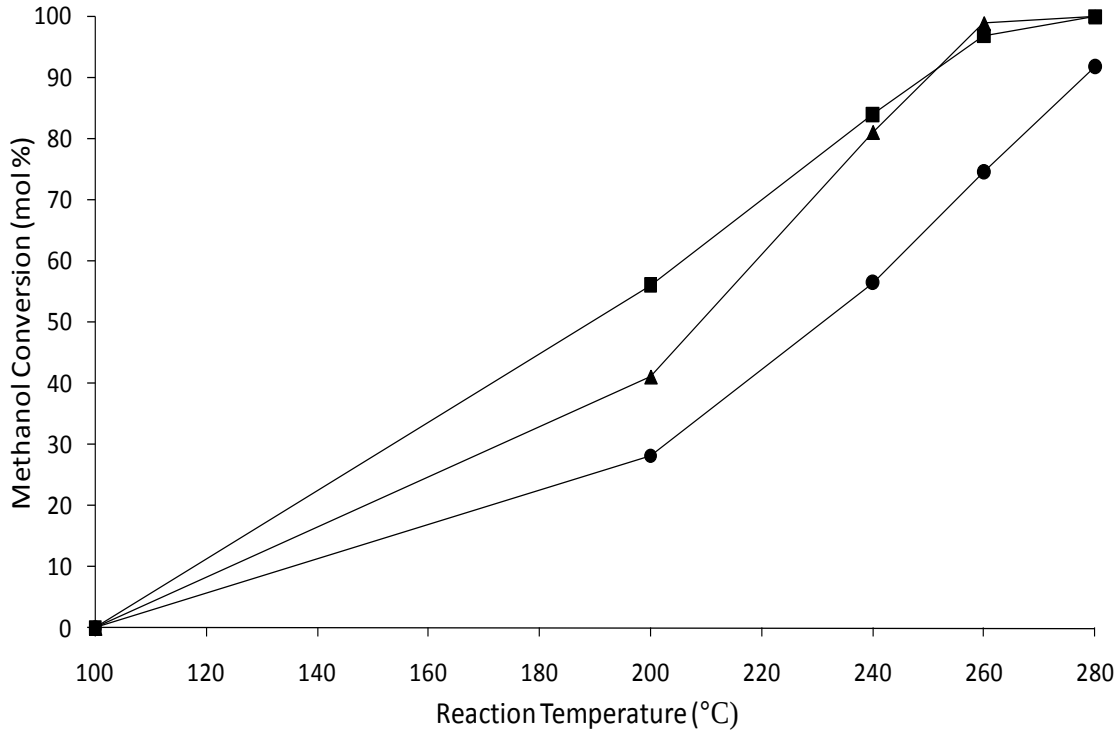


**Figure 3.31:** Comparing methanol conversion of silica supported $(MoO_2)_2P_2O_7$ with varying amounts of vanadium (mol%).

■ = $(MoO_2)_2P_2O_7$ 10 wt% loading on $SiO_2$; ▲ = 1 mol% V/$(MoO_2)_2P_2O_7$ (10 wt% loading on $SiO_2$);

● = 20 mol% V/$(MoO_2)_2P_2O_7$ (10 wt% loading on $SiO_2$)

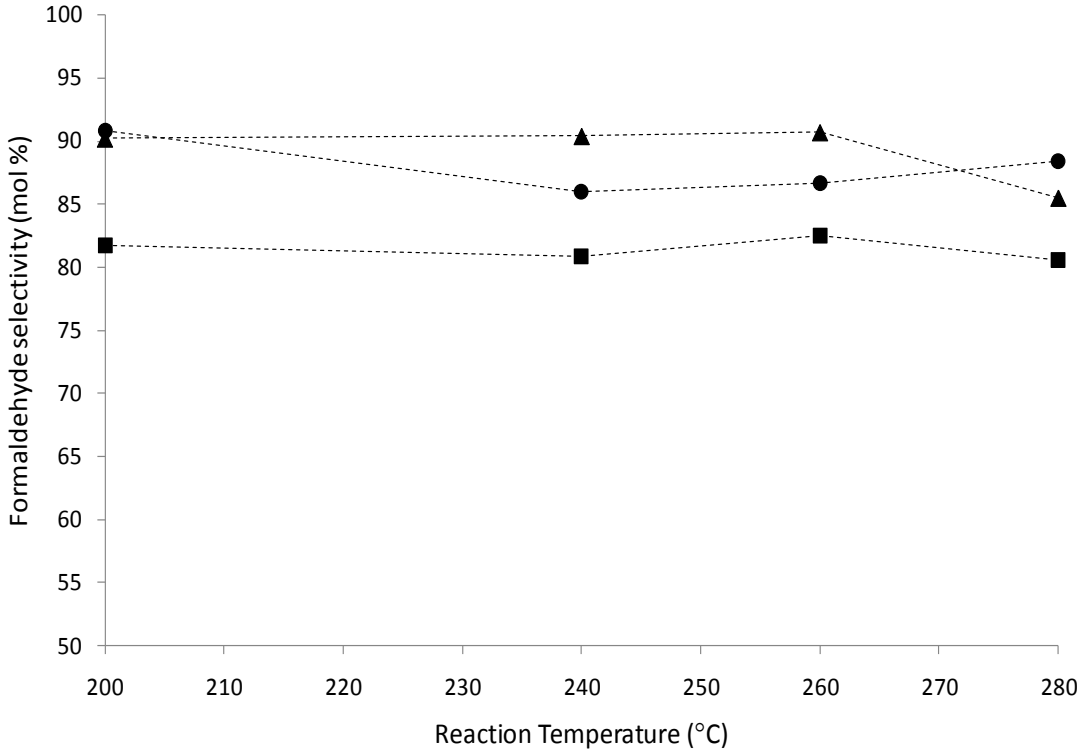


**Figure 3.32:** Comparing methanol conversion of silica supported (MoO2)2P2O7 with varying amounts of vanadium (mol%).

-■- = $(MoO_2)_2P_2O_7$ 10 wt% loading on $SiO_2$; -▲- = 1 mol% V/$(MoO_2)_2P_2O_7$ (10 wt% loading on $SiO_2$);

-●- = 20 mol% V/$(MoO_2)_2P_2O_7$ (10 wt% loading on $SiO_2$)

**Table 3.7:** Comparing formaldehyde yield at specific reaction temperatures during methanol oxidation with varying vanadium content (mol%) in supported $(MoO_2)_2P_2O_7$ on $SiO_2$ (10 wt%).

| **Vanadium content (mol%) in supported $(MoO_2)_2P_2O_7$ on $SiO_2$ (10 wt%)** | **FA yield at 200 °C (mol%)** | **FA yield at 240 °C (mol%)** | **FA yield at 260 °C (mol%)** | **FA yield at 280 °C (mol%)** |
|---|---|---|---|---|
| **0** | 46 | 69 | 80 | 81 |
| **1** | 36 | 73 | 90 | 86 |
| **20** | 24 | 48 | 64 | 79 |

## 3.4 – Discussion

### *3.4.1 – Catalytic activity of unsupported molybdenum phosphates*

Both $MoO_2 \cdot HPO_4 \cdot H_2O$ and $(MoO_2)_2P_2O_7$ catalysts show comparable formaldehyde selectivity to the $MoO_3$ catalyst (Appendix Figure A.6), however the oxide based catalyst has much higher activity than the phosphate based catalysts, with 85 % methanol conversion at 400 °C, and 51 % conversion respectively. When comparing the molybdenum phosphate catalysts with the industrial methanol oxidation catalyst, iron molybdate (Appendix Figure A.7), again, the formaldehyde selectivity is comparable (both ~ 90 %), but the activity of the iron molybdate catalyst is far greater, with total conversion reached at 300 °C compared to 13 % conversion with $(MoO_2)_2P_2O_7$ at the same temperature. The ability of the molybdenum phosphate catalysts to produce formaldehyde with such high selectivity as the commercial iron molybdate catalyst, suggests that they possess the relevant active sites to activate methanol to produce formaldehyde. Although a controversial topic, the active site of iron molybdate is thought to occur on terminal oxygen bonds, double bonded to Mo in an octahedral coordination, which allows the reacting molecules to bind, where they then undergo hydrogen abstraction with a neighbouring oxygen molecule on the surface, to produce methoxy groups which are then intermediates for formaldehyde production.[46] Further evidence is provided by Jehng *et al.*[47] who observes the decreasing intensity of Mo=O Raman bands during methanol oxidation over a supported $MoO_3$ catalyst, which was thought to be due to hydrogen bonding at this site (methoxy species) which alter the bond length, and hence frequency. These Mo=O bands are present in both molybdenum phosphate structures which is observed via a weak band at 1001 - 1016 $cm^{-1}$ in the Raman spectra (Figure 3.3 and 3.8). It would then suggest that although these sites are present, there could be a

number of factors relating to the low activity of these catalysts *i.e.* availability and/or number of these Mo=O sites, and re-oxidation of these sites after they are reduced.

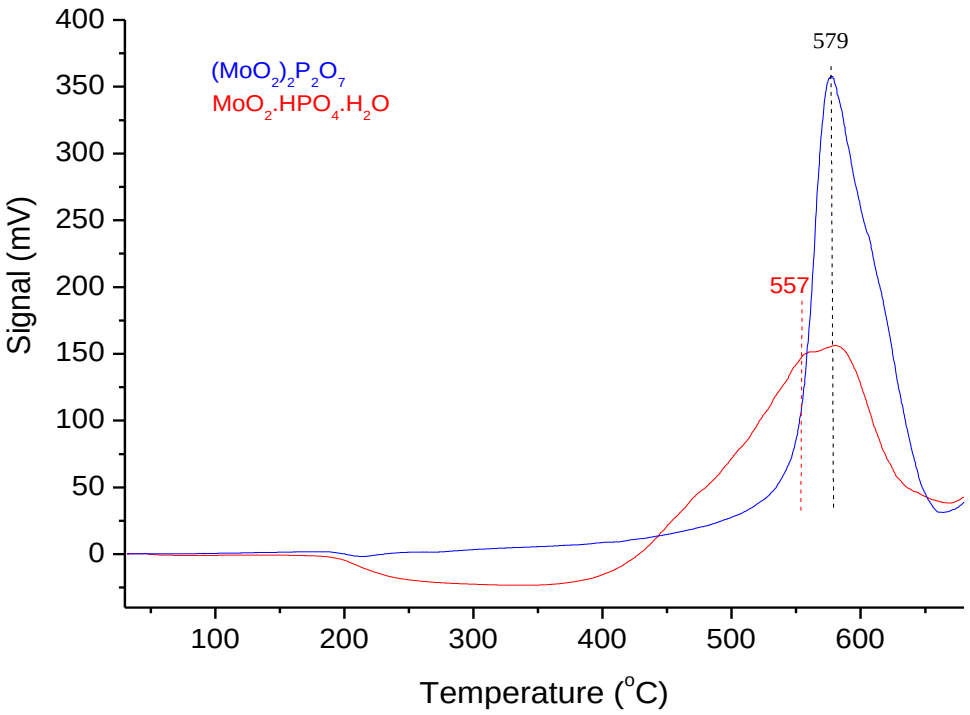


**Figure 3.33:** TPR comparing $MoO_2.HPO_4.H_2O$ and $(MoO_2)_2P_2O_7$.

Comparing the activity of both molybdenum phosphate catalysts can be investigated using temperature programmed reduction (TPR) analysis of each catalyst. As the methanol oxidation reaction to formaldehyde involves a reduction step, TPR is a useful technique to investigate molybdenum reduction. Although the specific temperatures of reduction may vary between the TPR profile and the methanol oxidation temperature profile, a relationship between the two exists, as both catalysts are under similar conditions (reducing atmosphere). For the $MoO_2 \cdot HPO_4 \cdot H_2O$ catalyst (Figure 3.33), the reduction process is initiated at around 380 °C followed by a slow increase, up to a maximum at 557 °C. The $(MoO_2)_2P_2O_7$ catalyst produces a different TPR profile, where the reduction process is initiated at a higher temperature of around 450 °C, which a sharp

increase in hydrogen consumption, to give a maximum at 579 °C. The intensity of the reduction peak for the $(MoO_2)_2P_2O_7$ catalyst is greater than for $MoO_2 \cdot HPO_4 \cdot H_2O$. The results of the TPR are indicative of the reactivity of both catalysts in the methanol oxidation reaction, since the $MoO_2 \cdot HPO_4 \cdot H_2O$ catalyst has higher activity at lower temperatures than the $(MoO_2)_2P_2O_7$ catalyst, however, at higher reaction temperatures the $(MoO_2)_2P_2O_7$ catalyst has higher activity.

Both catalysts are highly selective to the main product produced, formaldehyde, but other side products produced are low amounts of dimethyl ether and methyl formate, with the main side product being carbon monoxide, which is produced at higher temperatures due to the over oxidation of partial products such as formaldehyde. As methanol oxidation is known as a good indication of surface acidity/basicity and redox properties of the catalysts in use, the products produced by both molybdenum phosphate materials suggest that mainly redox sites are present, due to the high formation of formaldehyde and carbon monoxide, with only a limited amount of dimethyl ether which is characteristic of acidic sites on the surface.

Analysis using XPS and Raman of the fresh and ex-reactor $(MoO_2)_2P_2O_7$ catalysts produced interesting results, consistent with the activity of the catalyst in the methanol oxidation reaction. For the fresh catalyst (Table 3.8), there is confirmation that the molybdenum on the surface is in the (+6) oxidation state (233.8 eV)[48-51] with only lattice oxygen present (531.9 eV). Analysis of the ex-reactor sample gives clear evidence that the molybdenum (+6) has been reduced to molybdenum (+4), and there is a second species of oxygen present at 533.1 eV, which, when compared with literature results, is assigned to $OH^-$ groups, which provides further evidence that un-reacted methoxy groups are present on the surface.[52] There is also the possibility that the species of oxygen

present at 533.1 eV could be due to water, which is a side product in the formation of formaldehyde. From the Raman spectra (Figure 3.34) the band assigned to Mo-O-Mo stretching at 824 $cm^{-1}$, visible in the fresh catalyst, is no longer present, which contradicts the earlier suggested active site (Mo=O) by Jehng *et al.*[47] as this indicates the bridging Mo-O-Mo species could be the active site, due the decrease in intensity of the band at 824 $cm^{-1}$, and could be attributed to the un-reacted methoxy species still bonded at these sites, which will cause the site to be reduced.[47] There could also be other theories as to the loss of the Mo-O-Mo species at the surface, and this could be due to leaching of Mo from the surface, which is widely known to deactivate iron molybdate catalysts.[53] The shift of the Mo=O bond from 1016 $cm^{-1}$ in the fresh catalyst to 1002 $cm^{-1}$ in the ex-reactor catalyst however, could also suggest that this is indeed the active site proposed by Jehng *et al.* as a shift is known to occur when methoxy groups alter the length of this bond, which in turn alters the frequency.[54]

**Table 3.8:** XPS data for fresh and ex-reactor samples of $(MoO_2)_2P_2O_7$

| $(MoO_2)_2P_2O_7$ | Element | Atomic % | Binding energy (eV) | Oxidation state of metal |
|---|---|---|---|---|
| **Fresh** | Mo (3d) | 9.23 | 233.8 | +6 |
| | O (1s) | 50.23 | 531.9 | |
| **Ex-reactor** | Mo (3d) | 7.53 | 233.5 | +6 |
| | | | 231.9 | +4 |
| | O (O1s) | 60.08 | 533.1 | |
| | | | 531.7 | |

Although XPS cannot definitively confirm the loss of a particular species on the surface (Mo=O or Mo-O-Mo), the results (Table 3.8) do indicate a loss of Mo (fresh catalyst: 9.23 atomic %, ex-reactor catalyst: 7.53 atomic %). This loss can not only be assigned to leaching however, as there is a possibility that the Mo can dissolve into the bulk, or even be covered by species such as $CO_x$.

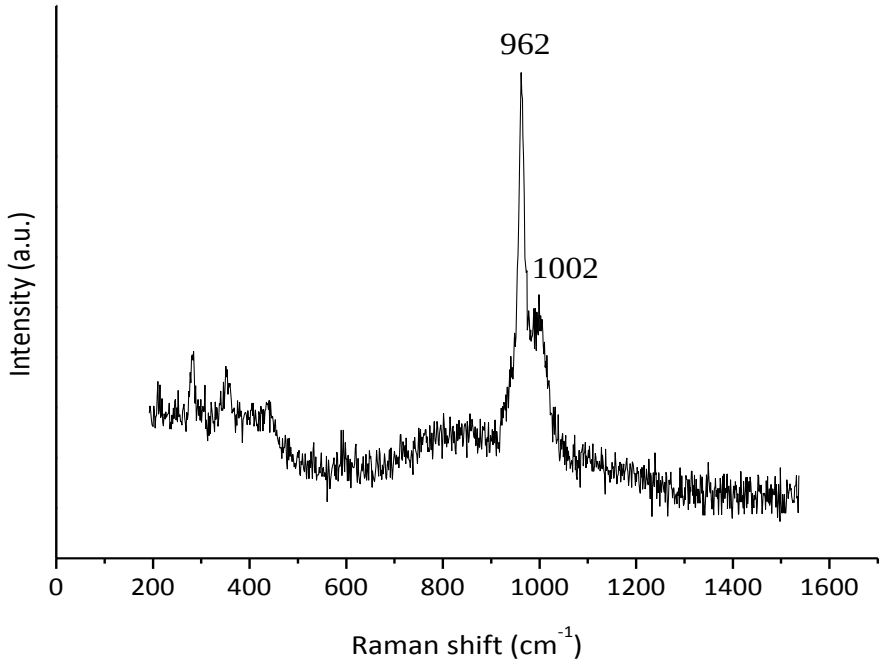


**Figure 3.34:** Raman spectra of ex-reactor $(MoO_2)_2P_2O_7$ catalyst from methanol oxidation reaction.

### *3.4.2 - Role of silica support in catalytic activity*

The remarkable increase in catalytic activity of $(MoO_2)_2P_2O_7$ supported on $SiO_2$ can be compared appropriately with the very active catalyst $MoO_3/SiO_2$ which is extensively reported in the literature as a model catalyst for investigating the catalytic mechanism of methanol partial oxidation.[55-57] There is however still controversy in identifying the structure of the molybdenum species on the silica support, and how these affect the catalytic activity. A lot of studies relate to Raman spectroscopy, particularly in-situ spectroscopy, so as to observe the potential active sites for methanol activation. It is agreed that the supporting of $MoO_3$ on $SiO_2$ improves the catalytic activity compared to the bulk $MoO_3$, an example of which was published by Cheng[58] where he observed that at 300 °C (7 % MeOH/air, 75 ml/min), bulk $MoO_3$ produced 50 % conversion of methanol compared to the 95 % conversion reached by $MoO_3/SiO_2$ (15 wt% loading). However, the drawback of supporting the material is that the formaldehyde selectivity decreases with

only 67 % selectivity compared to 79 % selectivity of the bulk $MoO_3$. The results observed for unsupported and silica supported $(MoO_2)_2P_2O_7$ follow the same trend, with the unsupported catalyst producing only 12 % conversion of methanol at 300 °C with 98 % formaldehyde selectivity, and the supported catalyst producing 99 % conversion but with 85 % formaldehyde selectivity.

Controversy exists over which Mo species exist on the surface of the silica support with two theories suggested: the oxomolybdenum system or the dioxomolybdenum system, which refers to the number of terminal oxygens bonded to the Mo centre. The fundamental steps of oxidation on both systems is the same: methanol dissociation on the surface, followed by hydrogen abstraction. The oxomolybdenum system has a different mechanism to the dioxomolybdenum system though, since cleavage of the bond in Mo-O-Si and formation of surface Mo methoxy species is the first step, followed by hydrogen abstraction in the second step. This is different to the dioxomolybdenum system where no cleavage of the Mo-Si-O bond is undertaken, and a hydroxomolybdenum methoxide intermediate is formed. Hydrogen abstraction is then affected by the OH ligand formed in the first step.[59]

It is thought that the type of Mo species on the surface depends on the amount of molybdenum present in the catalyst and on the preparation method.[60] Low loadings of molybdenum produce highly dispersed isolated Mo oxide species (Mo=O), which are characteristic of a strong band in the Raman spectra at 950 $cm^{-1}$ [40] or between 980 – 1038 $cm^{-1}$ according to Jehng *et* al.[47] Polymerised species (Mo-O-Mo) are said to occur at higher loadings of molybdenum present in the catalyst, with Raman bands at 220 $cm^{-1}$ [59] and between 880 – 950 $cm^{-1}$ present.[47]

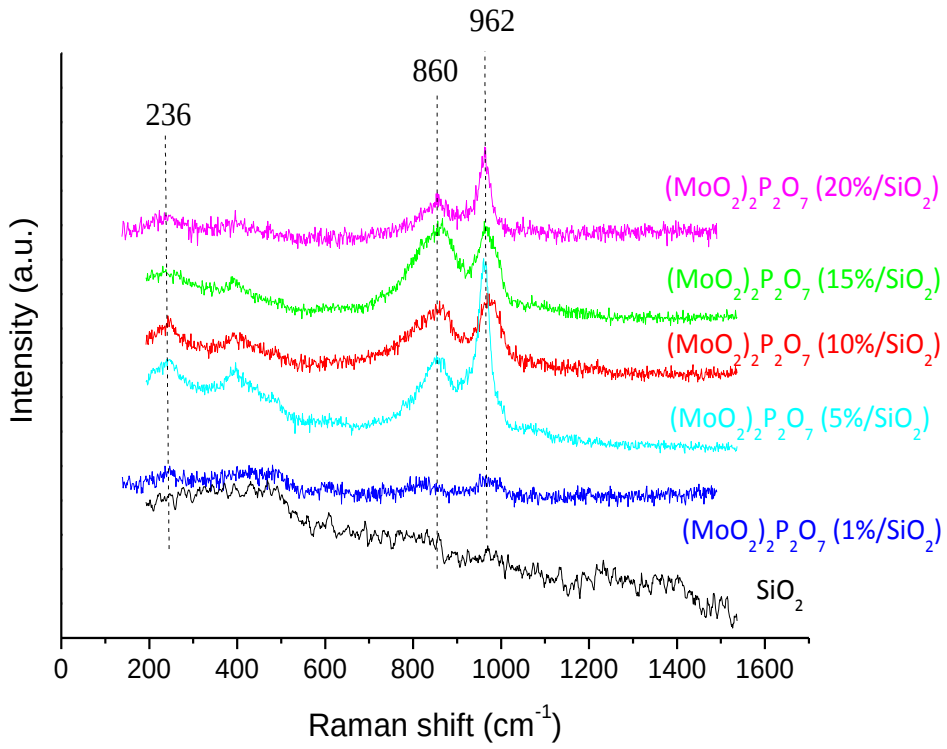


**Figure 3.35:** Raman spectrum comparing various loadings of $(MoO_2)_2P_2O_7$ on $SiO_2$.

By studying the Raman spectra of various loadings (1, 5, 10, 15 and 20 wt%) of $(MoO_2)_2P_2O_7$ on $SiO_2$ (Figure 3.35), it indicates that at low loadings (1 wt%), although very weak in intensity, the bands present at 860 $cm^{-1}$ correspond to antisymmetric bridging Mo-O-Mo stretching vibrations, which suggests that the Mo species on the surface are not isolated, but it does not necessarily mean that the $(MoO_2)_2P_2O_7$ is not highly dispersed. The band at 962 $cm^{-1}$ has previously been assigned to P-O stretching in $(PO_4)^{3-}$, however due to the broad nature of this peak, it is inconclusive whether this peak corresponds to P-O stretching or to stretching of terminal Mo=O groups, which would then propose a mixture of isolated Mo species and polymerised species. $(MoO_2)_2P_2O_7$ loading above 5 wt% reveals more of a polymolybdate structure on the surface due to the increasing intensity of the band at 860 $cm^{-1}$ (Mo-O-Mo stretching), and this is coherent with spectra reported by Jehng *et al.*[47] and Banares *et al.*[59] who observe bands at 996 and 821 $cm^{-1}$ for $MoO_3$ loaded on $SiO_2$ above 5 wt%.

The low activity of 1 wt% loading of $(MoO_2)_2P_2O_7$ on $SiO_2$, suggests that although there is high dispersion of the phase over $SiO_2$, the number of active sites present could be limited, as the majority of the surface will contain silanol groups from the support. The slight decrease in activity of the 20 wt% loading of $(MoO_2)_2P_2O_7$ on $SiO_2$ can be attributed to the aggregation of surface molybdenum species during the reaction, which is widely reported to occur with high loadings of molybdenum oxide on silica.[40,59] The increase in activity of the supported molybdenum phosphate catalysts compared to the unsupported catalyst, as well as being related to the high dispersion of the active phase over the surface, can also be due to the role of the support in the mechanism of the reaction. Although silica is considered an inert support, it does have a non-innocent role in methanol oxidation, where it is reported to act as a reservoir for methoxy species.[61] The methoxy species present on the support are mobile, and can migrate to the Mo centres to be oxidised and produce formaldehyde. The formaldehyde species can also interact with another methoxy group attached to a silanol group, to form methyl formate which is seen with the supported $(MoO_2)_2P_2O_7$ catalysts (and not with the unsupported catalysts), mainly at lower temperatures, up to a maximum at 200 °C, where above this temperature CO becomes the main side product. As well as proving to be a highly active catalyst compared to $MoO_3/SiO_2$, $(MoO_2)_2P_2O_7$ (10 wt% loading) on $SiO_2$ has comparable activity to iron molybdate, with 85 % conversion at 240 °C compared to the 50 % conversion of the industrially used iron molybdate catalyst at the same temperature. However, iron molybdate obtains high formaldehyde selectivity at this temperature (97 %) compared to the 81 % achieved by the supported molybdenum phosphate catalyst.

### *3.4.3 - Role of vanadium as a promoter in catalytic activity*

The choice of vanadium as a promoter for $(MoO_2)_2P_2O_7$ is in relation to molybdenum being used frequently as a promoter for $(VO)_2P_2O_7$ catalysts, which is known to improve the activity for *n*-butane oxidation to maleic anhydride.[62-63] It is speculated that due to the iso-structural phases of both phosphates, that there is a possibility during preparation that a small amount of Mo and V mixed phase could form. The role of the promoter in the $(VO)_2P_2O_7$ has been discussed by many authors. Ye *et al.* [64] suggest that addition of slightly electronegative ions increases the exposition of the (100) plane, which is known to be the active plane for maleic anhydride production. McCormick *et al.* suggested that the role of the promoter is to accelerate the rate of $V^{5+}$ phase formation, to yield the neighbouring $V^{5+}/V^{4+}$ couples, which are required by the Mars and van Krevelen mechanism proposed for his reaction.[62,65] There is also evidence to suggest that the addition of promoters to molybdenum phosphate materials, enhance their catalytic activity for oxidation reactions. There are reports of the use of Ce and Ag promoters enhancing the catalytic activity of Mo-P-O catalysts for propane partial oxidation to propene.[2-6] Due to the addition of vanadium to $(MoO_2)_2P_2O_7$ being a novel procedure, it is difficult to point to the exact role of vanadium in the catalytic activity of the promoted $(MoO_2)_2P_2O_7$ catalysts, but due to the structural characterization used, theories can be postulated.

It is clear that vanadium has either been incorporated into the structure of $(MoO_2)_2P_2O_7$ or it exists as a separate phase in each amount of vanadium added. At low loadings of vanadium (1 mol%), XRD and Raman spectroscopy (Figure 3.20 and 3.21) do not detect any vanadium present, and this is understandable considering that XPS only detected 0.2 atomic % on the surface (Table 3.4). This can still suggest that a small amount of V has indeed replaced Mo in the structure, however, it does not rule out the possibility that it is

sitting on the surface of the $(MoO_2)_2P_2O_7$ particles also. Addition of > 5 mol% vanadium allows the detection and confirmation of the vanadium phase present through use of XRD and Raman spectroscopy. Although at 5 mol% vanadium, the intensity of the reflections are weak, it is possible to assign the extra reflections in the $(MoO_2)_2P_2O_7$ pattern to $VOHPO_4.2H_2O$. This is entirely feasible since the preparation of the vanadyl orthophosphate dihydrate phase is very similar to the formation of the $MoO_2 \cdot HPO_4 \cdot H_2O$ material, where $V_2O_5$ is reacted with phosphoric acid under reflux conditions.[66] It is inconclusive whether the $VOHPO_4.2H_2O$ phase is separate to the $(MoO_2)_2P_2O_7$ phase or not in the sample which contains 5 mol% vanadium, but it could be a possibility that it is incorporated into the structure, as there is no visible $VOHPO_4.2H_2O$ platelet morphology in the SEM image (Figure 3.22b). The same cannot be said for the 10-20 mol% vanadium samples, as there is clear evidence that the $VOHPO_4.2H_2O$ is present in a separate phase to the $(MoO_2)_2P_2O_7$, as the characteristic platelet morphology is visible in both (Figure 3.22c & d). Although this separate morphology is present, this again does not conclude that the vanadium is only present in a separate phase, as there still could be some molybdenum replacement by vanadium ions in the $(MoO_2)_2P_2O_7$ structure.

In relation to the catalytic activity of each $(MoO_2)_2P_2O_7$ sample containing vanadium (Figure 3.29 & 3.30), it is possible to suggest the role of vanadium. In general, the addition of vanadium to the $(MoO_2)_2P_2O_7$ catalyst improves the activity, even at low loadings (1 mol%), but especially at high loadings (20 mol%). This increase in activity of the 20 mol% vanadium promoted catalyst cannot be attributed the activity of the separate phase ($VOPO_4 \cdot 2H_2O$) alone, as testing $VOPO_4 \cdot 2H_2O$ for methanol oxidation under the same reaction conditions (Appendix Figure A.8) produced a moderately active catalyst, which was not as active as the $(MoO_2)_2P_2O_7$ (20 mol% V) catalyst. At 400 °C, 41 % methanol conversion is reached with $VOPO_4 \cdot 2H_2O$ and 98 % formaldehyde selectivity,

compared to the 82 % conversion and 96 % formaldehyde selectivity produced by the $(MoO_2)_2P_2O_7$ catalyst containing 20 mol% vanadium. Therefore it can be assumed that there is a possible synergistic effect of Mo and V when combined as a catalyst. It is not known whether this increase in activity of the 20 mol% vanadium catalyst is due to the replacement of Mo ions with V ions in the structure, or the replacement of V ions by Mo in the $VOPO_4.2H_2O$ which as stated earlier is frequently reported in the literature.

XPS analysis of the fresh and ex-reactor sample of $(MoO_2)_2P_2O_7$ (20 mol% V) allows better understanding on what is happening to both metals on the surface. From Table 3.9, it is observed that in the fresh catalyst, Mo is in the +6 oxidation state, and V is in the +5 oxidation state, which are both expected for each phase. Analysis of the ex-reactor sample shows that as well as Mo being reduced from +6 → +4, the V is reduced from +5 → +4. Therefore it is clear that vanadium is involved in the methanol oxidation reaction, and comparing with theories suggested for the role of the Ag promoter in Mo-P-O catalysts, a possible role of vanadium can be postulated. As both V and Mo are able to activate/store oxygen and transform/release oxygen species, there could be a redox couple: $2V^{4+} + Mo^{6+} \leftrightarrow 2V^{5+} + Mo^{4+}$ which can improve transfer of electrons and oxygen species, as Zhang *et al.*[68] observed a similar effect during the oxidation of propane to propene using a Ag-Mo-P-O catalyst.

**Table 3.9:** XPS data for fresh and ex-reactor samples of $(MoO_2)_2P_2O_7$ (20 mol% V)

| **$(MoO_2)_2P_2O_7$ (20 mol% V)** | **Element** | **Binding energy (eV)** | **Oxidation state of metal** |
|---|---|---|---|
| **Fresh** | Mo (3d) | 233.5 | +6 |
| | V (2P 3/2) | 518.8 | +5 |
| **Ex-reactor** | Mo (3d) | 233.5 | +6 |
| | | 231.9 | +4 |
| | V (2P 3/2) | 517.3 | +4 |

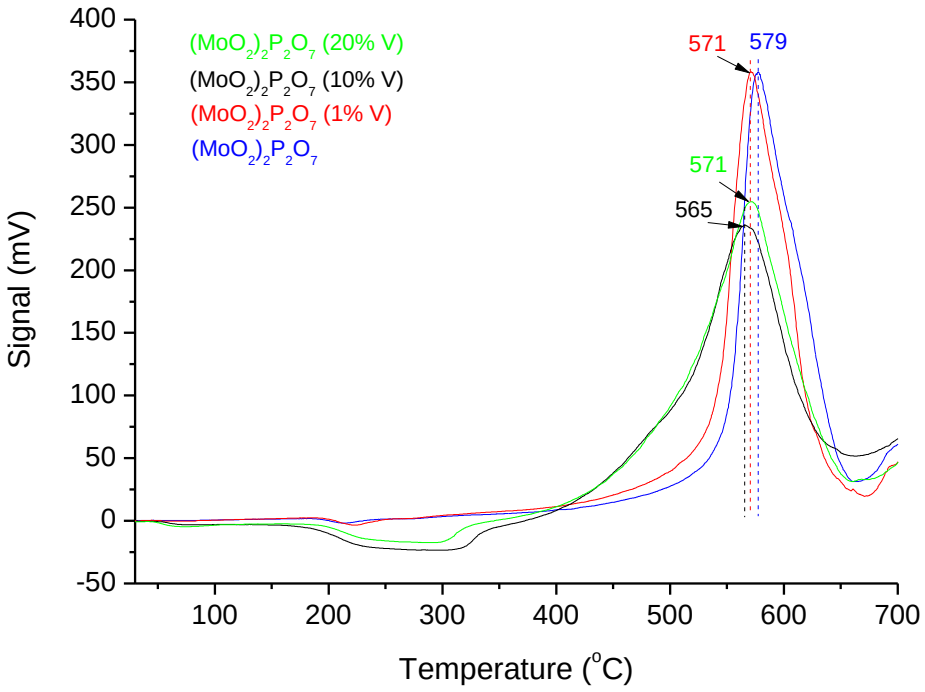


**Figure 3.36:** TPR comparing $(MoO_2)_2P_2O_7$ catalysts with varying vanadium loadings

By analysing TPR data (Figure 3.36) for the vanadium promoted $(MoO_2)_2P_2O_7$ materials, it is observed that vanadium improves the reducibility of the materials, with higher loadings of vanadium having an increased effect on reducibility, with 20 mol% vanadium obtaining higher hydrogen consumption (Table 3.10) than the un-promoted $(MoO_2)_2P_2O_7$ material.

**Table 3.10:** TPR data comparing hydrogen consumption using $(MoO_2)_2P_2O_7$ catalysts with varying amounts of vanadium (mol%).

| Vanadium mol% | On set temperature (°C) | Peak max. temperature (°C) | $H_2$ consumption μmol/g) |
|---|---|---|---|
| 0 | ~ 450 | 579 | 1646.0 |
| 1 | ~ 440 | 571 | 1692.5 |
| 10 | ~ 370 | 565 | 1806.1 |
| 20 | ~ 370 | 571 | 1923.0 |

Due to the substantial increase in activity of the silica supported $(MoO_2)P_2O_7$ compared to the unsupported catalyst, and the increase in activity due to the promotional effect of

vanadium, both 1 and 20 mol% vanadium silica supported $(MoO_2)P_2O_7$ were prepared and tested for methanol oxidation. The activity of the supported vanadium promoted $(MoO_2)P_2O_7$ catalysts however did not produce promising results as the addition of high amounts of vanadium seemed to have a negative effect on the catalytic activity.

## 3.5 – Conclusions

Molybdenum phosphate catalysts have been prepared, characterised and tested for methanol oxidation to formaldehyde, producing moderate activity and relatively high formaldehyde selectivity. Comparing with the commercial iron molybdate catalyst known for extremely high activity for methanol oxidation to formaldehyde, the $(MoO_2)_2P_2O_7$ catalyst had very poor activity, but comparable formaldehyde selectivity. Supporting the $(MoO_2)_2P_2O_7$ catalyst was attempted using silica, and was again characterised and tested. There was a significant increase in activity of the catalyst which compares well with that of the iron molybdate catalyst, however, this had a negative effect on the formaldehyde selectivity. The use of vanadium as a promoter was added during the preparation of the molybdenum phosphate materials with the aim of incorporating vanadium into the structure, which is known to improve activity, particularly for the addition of Ag to Mo-P-O catalysts which when tested for propane oxidation showed an increase in activity. This was the case with the addition of vanadium to $(MoO_2)_2P_2O_7$, where higher amounts of vanadium addition had an increasingly positive effect on the catalytic activity. Due to these positive effects of supporting and promoting $(MoO_2)_2P_2O_7$, the two were combined and produced both high activity and high formaldehyde selectivity when low amounts of vanadium were incorporated, however, the addition of high loadings of vanadium in this case had a detrimental effect on activity.

## 3.6 – References


1. Y. Uebou, S. Okada, and J. Yamaki. *J. of Power Sources* **2003**, *115*, 119–124.
2. D. Bhattacharayya, S.K. Bey, and M.S. Rao. *Appl. Catal. A* **1992**, *87*, 29.
3. M.A. Chaar, D. Patel, and H.H. Kung. *J. Catal.* **1988,** *109*, 463.
4. D. Siew Hew Sam, V. Soenen, and J.C. Volta. *J. Catal.* **1990**, *123*, 417.
5. R. H. H. Smits, K. Seshan, and J. R. H. Ross. *Stud. Surf. Sci. Catal.* **1992**, *72*, 221.
6. A. Cherrak, R. Hubaut, Y. Barbaux, and G. Mairesse. *Catal. Lett.* **1992**, *15*, 377.
7. G. Costentin, L. Savary, J.C. LAvalley, M. M. Borel and A. Grandin. *Chem. Mater.* **1998**, *10*, 59-64.
8. P.F. Kerr, A.W. Thomas, and A.M. Langer. *The American Mineralogist*, **1963**, *48*, 14.
9. G. Alessandrini, L. Cairati, P. Forzatti, P.L. Villa and F. Trifiro. *J. Less-Comm. Met.* **1977**, *54*, 373.
10. G. M. Bartenev, G. K. Boreskov, R. R. Zakirov, B. I. Popov, E. P. Prokopev and A. D. Tsyganov. *Kinet. Catal. (Engl. transl.)*. **1972**, *13* (1), 213.
11. C. C. Williams, J. G. Ekerdt, J. M. Jehng, F. D. Hardcastle, A. M. Turek and I. E. Wachs. *J. Phys. Chem.* **1991**, 95, 8781.
12. R. D. Roark, S. D. Kohler and J. G. Ekerdt. *Catal. Lett.* **1992**, *16*, 71.
13. T. J. Yang and J.H. Lunsford. *J. Catal.* **1987**, *103*, 55.
14. M. Carbucicchio and F. Trifiro. *J. Catal.* ***1980***, *62*, 13.
15. C. C. Williams and J. G. Ekerdt. *J. Catal.* ***1993***, *141*, 430.
16. R. D. Roark, S. D. Kohler, J. G. Ekerdt, D. S. Kim and I. E. Wachs. *Catal. Lett.* **1992**, *16*, 77.
17. S. Nianxue, Zhengqian Xuan, J. K. Bartley, S. H. Taylor, D. Chadwick and G. J. Hutchings. *Catalysis Letters* **2006**, *106*, 3–4.
18. Y. H. Taufiq-Yap, C. K. Goh, G. J. Hutchings, N. Dummer and J. K. Bartley. *Catalysis Lett*ers **2009**, *130*, 327–334.
19. U. Rodemerck, B. Kubias, H. W. Zanthoff, G. U. Wolf and M. Baerns. *Applied Catalysis A: General* **1997**, *153*, 217-231.
20. P. Bonnet, J. M. M. Millet, C. Leclercq and J. C. Vedrine. *Journal of Catalysis* **1996**, *158*, 128-141.
21. J. M. M. Millet, J. C. Vedrine and G. Hecquet, *Stud. Surf. Sci. Catal.* **1990**, *55*, 833.

22. M. Dekiouk, N. Boisdron, S. Pietrzyk, Y. Barbaux and J. Grimblot, *Appl. Catal*. **1992**, *90*, 61.
23. J. C. Vedrine. *Topics in Catalysis* **2000**, *11/12*, 147–152.
24. P. Kierkegaard, *Acta Chemica Scaninavica*, **1958**. *12*, 1701.
25. P. Kierkegaard. *Ark. Kemi*. **1962**, *19*, 1–14.
26. Flaiyh Farhan Al-Anazi, *Ph.D. Thesis, Cardiff University*, 2008.
27. S. E. Lister, A. Soleihavoup, R. Withers, P. Hodgkinson, J. Evans. *Inorg. Chem*. **2010**, *49*, 2290-2301.
28. A. Montesinos, T.A. Zepeda, E. Lima, B. Pawelec, J.L.G. Fierro, A. Olivas, J. A. de los Reyes H. *Applied Catalysis A: General* **2008**, *334*. 330–338.
29. K. Y. Song, M. K. Park, Y. T. Kwon, H. W. Lee, W. J. Chung and W. I. Lee. *Chem. Mater*. **2001**, *13* (7), 2349–2355.
30. J. L. G. Fierro, S. Mendioroz, J.A. Pajares, S and W. Weller. *Journal of Catalysis*, **1980**, *65, (2)*, 263-270.
31. M. P. Casaletto, L. Lisi, G. Mattogno, P. Patrono, G. Ruoppolo and G. Russo. *Applied Catalysis A: General* **2002**, *226*, 41–48.
32. T. Borowiecki and A. Golcebiowski. *Catalysis Letters*, **1994**, *25* (3-4), 309-313.
33. S. A. Kareem. *Journal of Sciences, Islamic Republic of Iran* **2002**, *13(3)*, 237-240.
34. V. V. Guliants, J. B. Benziger, S. Sundaresan, I. E. Wachs, J. M. Jehng and J. E. Roberts. *Catalysis Today* **1996**, *28*, 275-295.
35. L. Griesel, J. K. Bartley, R. P. K. Wells, G. J. Hutchings. *Journal of Molecular Catalysis A: Chemical* **2004**, *220*, 113–119.
36. R. L. Frost. *Spectrochimica Acta Part A.* **2011**, *78*, 248–252.
37. G. C. Bond and S. F. Tahir. *Applied Catalysis* **1991**, *71(1)*, 1-31.
38. J-D. Grunwaldt, M. Maciejewski, O. S. Becker, P. Fabrizioli and A. Baiker. *Journal of Catalysis* **1999**, *186*, 458–469.
39. G. G. Hlatky. *Chem. Rev.* **2000**, *100 (4)*, 1347-1376.
40. Guosheng Li, Dehong Hu, Gordon Xia and Z. Conrad Zhang. *Topics in Catalysis* **2009**, *52*, 1381–1387.
41. X. Huang, J. Liu, J. Chen, Y. Xu and W. Shen. *Catalysis Letters* **2006**, *108* (1–2), 79-86.
42. K. V. R. Chary, K. R. Reddy nd C. P. Kumar. *Catalysis Communications*, **2001**, *2 (9)*, 277-284.

43. R. S. Schiffino and R. P. Merrill. *J. Phys. Chem.* **1993**, *97 (24)*, 6425-6435.
44. B. T. Pierini and E. A. Lombardo. *Catalysis Today* **2005**, *107-108*, 323-329.
45. Mamoru Ai. *Applied Catalysis A: General* **2002**, *234 (1-2)*, 325-243.
46. Mamoru Ai. *Journal of Catalysis* **1979**, *60 (2)*, 306-315.
47. J. M. Jehng, H. Hu, X. Gao and I. E. Wachs. *Catal. Today.* **1996**, *28*, 335.
48. L.E. Firment and A. Faretti. *Surf. Sci.* **1983**, *129*, 155.
49. A. Cimino and De Angelis. *J. Catal*. **1975**, *36*, 11.
50. T.H. Fleisch and G.J. Mains, *J. Chem. Phys*. **1982**, *76*, 780.
51. W.E. Swartz, and D.M. Hercules, *Anal. Chem*. **1971**, *43*, 1774.
52. J. Haber and E. Lalik. *Catalysis Today* **1997**, *33*, 119-137.
53. B. I. Popov, V. N. Bibin and G. K. Boreskov. *Kinetics Catalysis.* **1976**, *17*, 322.
54. W. E. Farneth, E. M. McCarron, A. W. Sleight and R. H. Staley. *Langmuir* **1987**, *3*, 217.
55. J. M. Tatibouet. *Appl Catal A: General.* **1997**, *148*, 213-252.
56. G. Busca. *Catal Today*. **1996**, *27*, 457.
57. M. A. Banares and I. E. Wachs, *J Raman Spectrosc.* **2002**, *33*, 359.
58. W-H. Cheng. *J. Catal.* **1996**, *158*, 477-485.
59. M. A. Banares. H. C. Hu and I. E. Wachs. *J. Catal.* **1994**, *150*, 407-420.
60. L. E. Briand, W. E. Farneth, I. E. Wachs. *Catal. Today*. **2000**, *62*, 219
61. M. Seman. *J. Phys. Chem. B.* **2004**, *108*, 3231-3239.
62. S. Irusta, A. Boix, B. Pierini, C. Caspani and J. Petunchi. *Journal of Catalysis*. **1999**, *187*, 298–310.
63. G. J. Hutchings, R. Higgins, *J. Catal.* **1996**, *162*, 153.
64. D. Ye, A. Satsuma, A. Hattori, T. Hattori and Y. Murakami, *Catal. Today.* **1993**, *16*, 113.
65. R. McCormick, G. Alptekin, A. Herring and T. Ohno, *J. Catal.* **1997**, *172*, 160.
66. M. Trchova, P. Capkova, P. Matejka, K. Melnova, L. Benes and E. Uhlirova. *J. Solid State Chem.* **1999**, *148, 197-204.*
67. E. Kleimenov, H. Bluhm, M. Havecker, A. Knop-Gericke, A. Pestryakov, D. Teschner, J.A. Lopez-Sanchez, J. K. Bartley, G. J. Hutchings and R. Schlogl. *Surface Science* **2005**, *575*, 181-188.
68. X. Zhang, H-L. Wan, W-Z. Weng and X-D. Yi. *Applied Surface Science* **2003**, *220*, 117-124.

# 4

# *Chapter 4 – Promoted vanadium phosphate catalysts for selective methanol oxidation*

## 4.1 – Introduction

Vanadium phosphate oxide (VPO) catalysts are renowned for their superior activity for the partial oxidation of *n*-butane to maleic anhydride. Since the discovery by Bergman and Frisch in 1966,[1] where maleic anhydride was produced during n-butane oxidation using a VPO catalyst, and the commercialisation of the process by Mitsubishi Chemical Industries in 1971, it has attracted considerable interest from both industrial and academic researchers.[2] The active phase of the VPO catalysts is considered to be vanadyl pyrophosphate ($(VO)_2P_2O_7$), which is formed *via* a precursor, vanadium hydrogen phosphate hemihydrate ($VOHPO_4 \cdot 0.5H_2O$). There are frequent reports concerning the optimum P/V ratio of these catalysts, and it is believed that VPO catalysts should contain a slight excess of phosphate (P/V = 1 - 1.1)[3-5] There is an emphasis on the word slight however, as although an excess of phosphate (P/V = 1.5-3) prevents the bulk oxidation of $V^{4+}$ to $V^{5+}$, it also lowers the reducibility of $V^{4+}$, resulting in low catalytic activity.[6,7] A phosphate deficiency leads to an increased rate of $V^{4+}$ oxidation and reduction, which amounts to a more active catalyst, but this also lowers the selectivity of the catalyst dramatically, due to the increased presence of $V^{5+}$ species.[8] There are still conflicting

reports on the optimum ratio however, as Cavani *et al.*[9] report that by increasing the P/V ratio from 0.95 to 1.16, the maleic anhydride selectivity decreases, and in contrast to this, Hodnett and co-workers[10] report that maleic anhydride selectivity increased with an increase of P/V ratio from 0.95 to 1.07. The preparation route of the $VOHPO_4 \cdot 0.5H_2O$ phase has a substantial impact on the activity of the final catalyst, as the activation of this catalyst to $(VO)_2P_2O_7$ is *via* a topotactic transformation, where the morphology of the parent precursor is maintained in the final $(VO)_2P_2O_7$ catalyst.[11,12] Over the past two decades there have been many advances in the preparation routes of $VOHPO_4 \cdot 0.5H_2O$. This can generally be divided into two methodologies; the reaction of $V_2O_5$ with $H_3PO_4$ using an aqueous reducing agent, or *via* an organic route which uses alcohol as both the reducing agent and solvent, such as isobutanol.[13] The thermal activation of these $VOHPO_4 \cdot 0.5H_2O$ materials are carried out either under the reaction mixture of butane/air (if used as *n*-butane oxidation catalysts), or an inert atmosphere using Ar, He, or $N_2$ gases.

To improve the catalytic properties and mechanical resistance of these catalysts further, metal cations have been added during the preparation of the precursor. A vast amount of literature exists concerning a wide range of transition metal promoters including; Co, Ce, Ni, Zn, Bi, Cu, Zr, Mg, Ti, Mo, Nb, Fe and Cr (among others).[14-18] Despite their extensive use, the particular role of each promoter has not yet been agreed upon, with many proposals suggested. The most frequently used promoter is cobalt, as it produces consistently high activity, and is thought to have both structural and electronic effects on the $(VO)_2P_2O_7$ catalyst.[19-22] Promoters have also been proposed to increase surface area, alter the $V^{4+}/V^{5+}$ ratio, enhance the amount of energetic oxygen species at the surface, or suppress any possible formation of catalytically inactive VPO phases, *e.g.* $VO(H_2PO_4)_2$.[19, 23-27]

The active site of the $(VO)_2P_2O_7$ catalysts is still not defined and many conflicting theories have been postulated, but it is generally accepted that the active sites for *n*-butane oxidation are located on the exposed (200) planes (Figure 4.1).[28-31] The active and selective sites present on the surface of these planes are associated with vanadyl dimers, which partake in the rate limiting step of the reaction: the C-H bond cleavage. There are also other hypothetical active sites present on the surface of the (200) plane: Brønsted acid sites, such as -POH groups; Lewis-acid sites, such as $V^{4+}$ and $V^{5+}$; redox couples; bridging oxygen, such as V-O-V, V-O-P, and terminal oxygen $V^{5+}$=O, $V^{4+}$=O.[31] Vanadyl pyrophosphate catalysts are also known to be active for the selective oxidation of propane to acrylic acid,[32-35] where C-H bond cleavage is again the rate limiting step, and Ieda *et al.*[36] report a linear correlation between the oxidation activity and the surface V=O species.

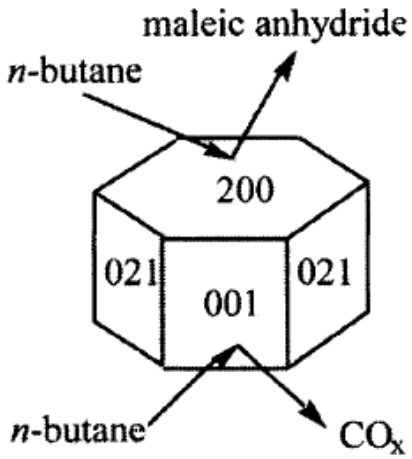


**Figure 4.1:** Selective and non-selective planes of $(VO)_2P_2O_7$ for *n*-butane oxidation.[31]

This chapter will study the catalytic activity of vanadium phosphate catalysts for the selective oxidation of methanol to formaldehyde. Although $(VO)_2P_2O_7$ materials have not been reported as catalysts for methanol oxidation, vanadium oxides are known to be active for this reaction,[37] particularly when they are supported on $TiO_2$ and $ZrO_2$.[38,39] The

addition of vanadium as a promoter to molybdenum phosphate materials in Chapter 3, also proved to enhance catalytic activity towards methanol oxidation, and so the use of vanadium based catalysts such as $(VO)_2P_2O_7$ for this reaction could provide interesting results. The VPO catalysts synthesised contained a slight excess of phosphate (P/V = 1.1), and were promoted using molybdenum, with a range of preparation methods and concentrations applied, to investigate the possible effect promoters have on the catalytic activity for the selective oxidation of methanol.

## 4.2 – Characterisation

### *4.2.1 - $VOHPO_4{\cdot}0.5H_2O$ – Vanadium hydrogen phosphate hemihydrate*

The precursor material, $VOHPO_4{\cdot}0.5H_2O$, was prepared *via* the organic synthesis route, (commonly referred to as the VPO route), using isobutanol as a reducing agent (Section 2.2.4.2).

Analysis of the X-ray diffraction pattern (XRD) of $VOHPO_4{\cdot}0.5H_2O$ (Figure 4.2) shows a highly crystalline sample, with reflections comparable with the reference pattern found in the JCPDS database (ref. code: 01-084-0761), and reported in the literature.[40] The main reflections are observed at 15.4 °, 27.0 ° and 30.4 ° 2θ, and are consistent with a series of publications by Hodnett *et al.*[41-43] The reflection observed with the largest intensity is the (220) plane, which, when more intense than the (001) plane, is characteristic of a rosette morphology, whereas a platelet morphology has the (001) plane as the most intense reflection.[44]

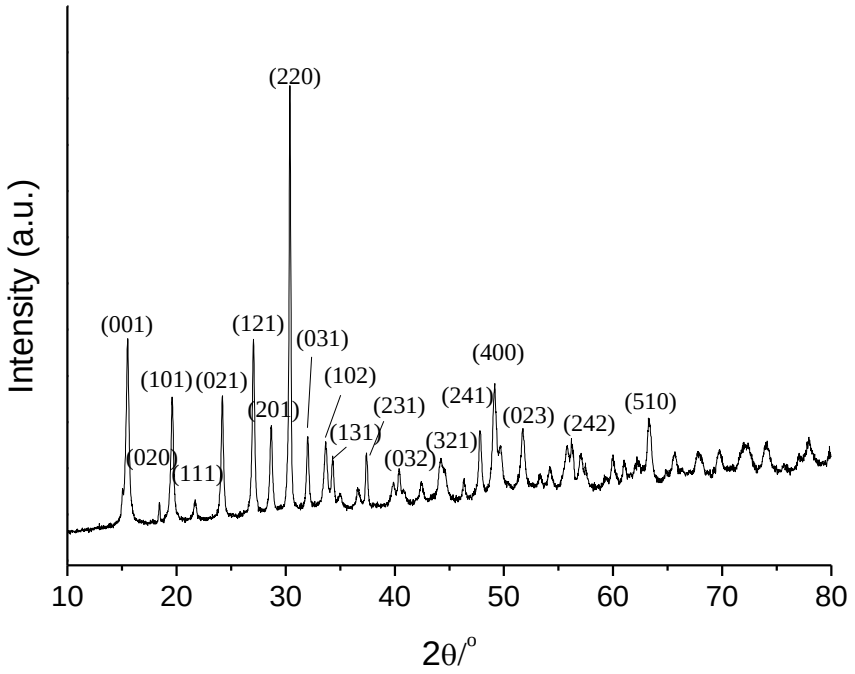


**Figure 4.2:** XRD pattern of $VOHPO_4 \cdot 0.5H_2O$.

It has been suggested that whether the platelet or the rosette morphology is obtained, depends on the preparation method, in particular the temperature used, which in turn, depends on the alcohol used (*i.e.* longer chain alcohols tend to have higher boiling points and hence, give a higher preparation temperature). Above 150 °C thick platelets form, and below 150 °C rosettes made up of aggregated small platelets form.[45] The organic synthesis route using isobutanol is known to produce a crystalline platelet morphology, in which the plates agglomerate to form a rosette. The use of *sec*-butyl alcohol or *t*-butyl alcohol, results in well-formed platelets of the precursor, where no agglomeration occurs.[46,47]

Characteristic peaks of $VOHPO_4 \cdot 0.5H_2O$ were present in the Raman spectra at 985, 1106 and 1152 $cm^{-1}$ (Figure 4.3). The peak observed at 985 $cm^{-1}$ dominates the spectra, and has been assigned to P-O stretching, with the less intense bands at 1106 and 1152 $cm^{-1}$ assigned to V-O-P stretching. Coupled vibrations of V-O and P-O can be seen at 344

$cm^{-1}$. The presence of these bands are to be expected, with the well-known structure of $VOHPO_4 \cdot 0.5H_2O$ possessing $[VOHPO_4]$ layers, which are hydrogen bonded *via* $HPO_4^{2-}$ groups, reported by Torardi *et al*.[48] and Leonowicz *et al*.[49]

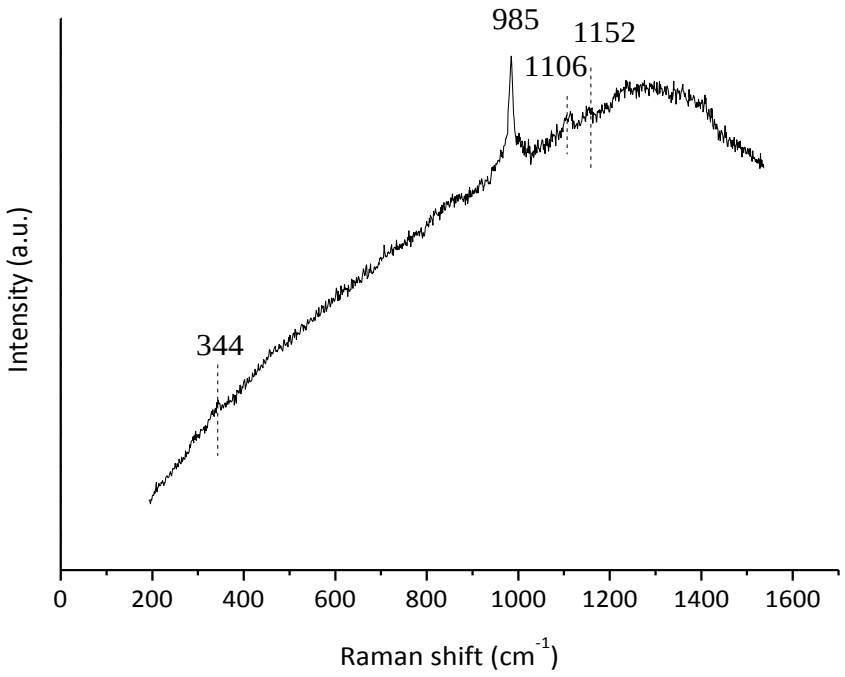


**Figure 4.3:** Raman spectrum of $VOHPO_4 \cdot 0.5H_2O$

Formation of a rosette morphology resulting from the transition of the reactants ($V_2O_5$, $H_3PO_4$, and isobutanol), to $VOHPO_4 \cdot 0.5H_2O$ can be tracked by *in situ* XRD combined with SEM, according to Hodnett *et al*.[50] They observe the dehydration of $VOHPO_4 \cdot 2H_2O$ to $VOHPO_4 \cdot H_2O$ which causes strain to develop in the platelets, which subsequently causes delamination, where the edges of the platelets curl up and separate out. These exposed delamination edges provide a nucleation point for epitaxial growth of the $VOHPO_4 \cdot 0.5H_2O$ phase, and the resulting rosette morphology (Figure 4.4).

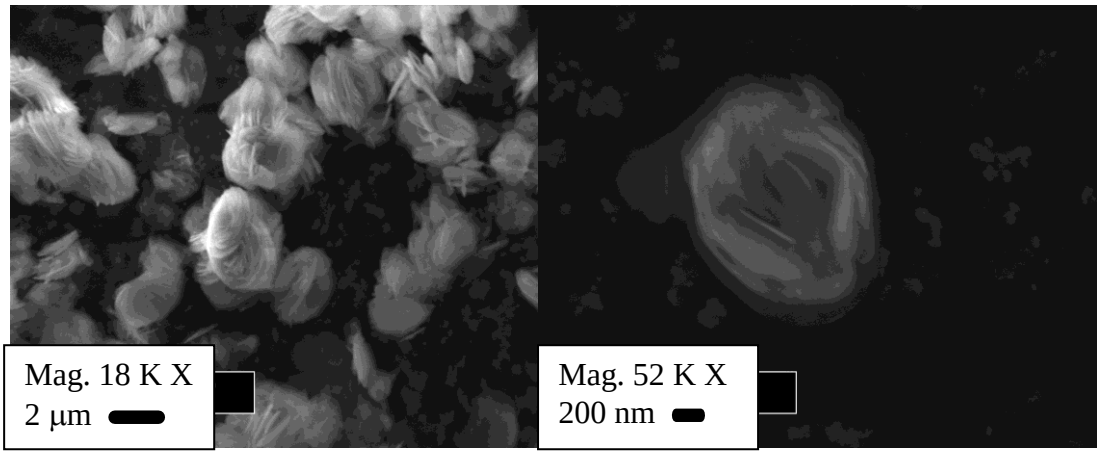


**Figure 4.4:** SEM images of $VOHPO_4 \cdot 0.5H_2O$.

### *4.2.2 – $(VO)_2P_2O_7$ – Vanadyl pyrophosphate*

The formation of the $(VO)_2P_2O_7$ material *via* the $VOHPO_4 \cdot 0.5H_2O$ precursor, has been extensively reported[41] to undergo topotactic transformation whilst maintaining the morphological appearance of the of the parent precursor.

The XRD pattern of the $(VO)_2P_2O_7$ material is illustrated in Figure 4.5, with the main reflections observed at 23.0 ° and 28.4 ° 2θ which represent the crystallographic planes (200) and (022) respectively. This is consistent with the JCPDS database (ref. code: 01-070-5865) and literature data.[12,23,45] The pattern consists of the $(VO)_2P_2O_7$ phase, which, when using the heat treatment in an inert atmosphere (750 °C, $N_2$), is to be expected. The use of a reduction/oxidation atmosphere (butane/air) forms $(VO)_2P_2O_7$ in addition to some $V^{5+}$ vanadium phosphate phases: $\alpha_I$, $\alpha_{II}$-$VOPO_4$, β - $VOPO_4$, γ - $VOPO_4$ and δ - $VOPO_4$.[50]

Raman spectroscopy analysis of the material (Figure 4.6) provides evidence that $(VO)_2P_2O_7$ and $VOHPO_4 \cdot 0.5H_2O$ possess similar species, with the band at 931 $cm^{-1}$ assigned to P-O-P stretching, and bands at 1131 and 1181 $cm^{-1}$ corresponding to V-O-P stretching.

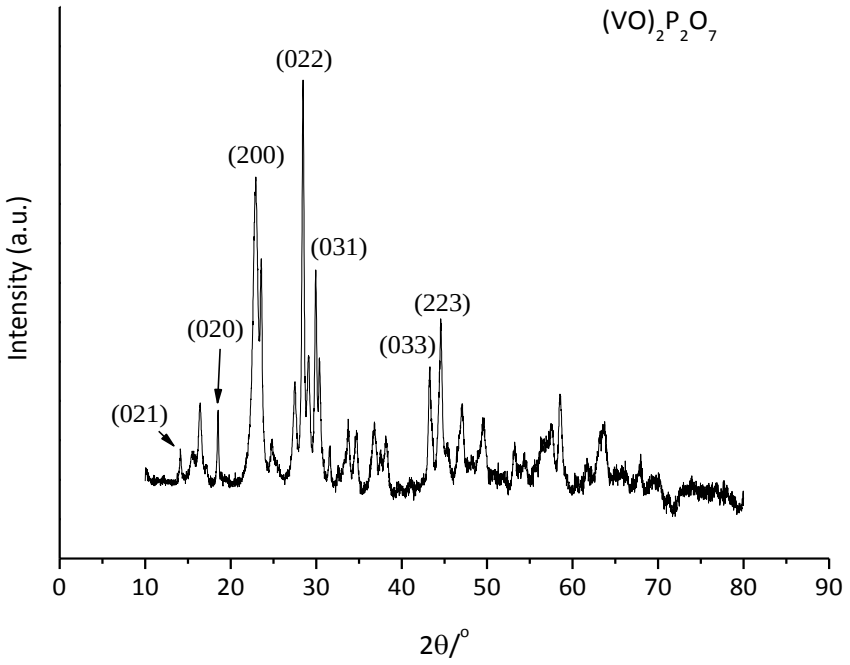


**Figure 4.5:** XRD pattern of $(VO)_2P_2O_7$.

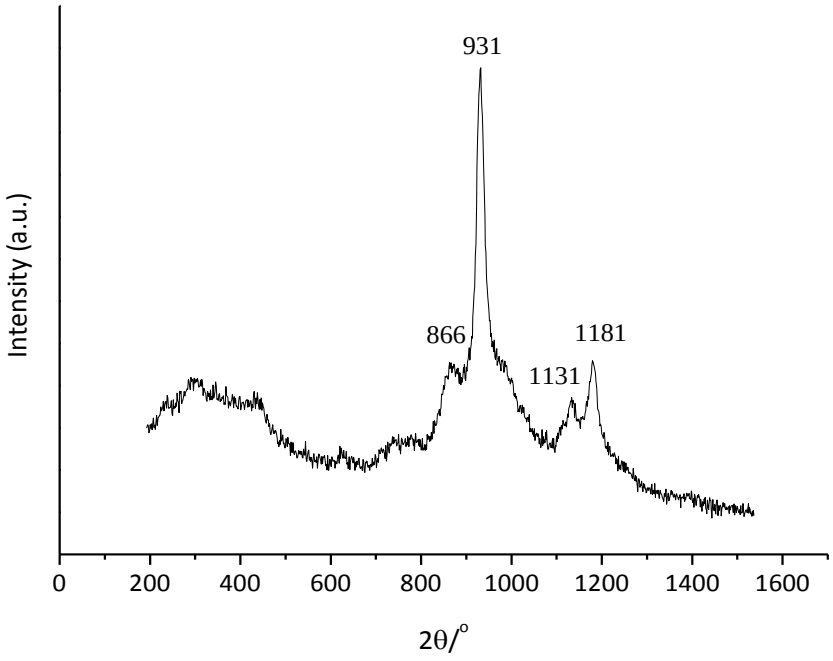


**Figure 4.6:** Raman spectrum of $(VO)_2P_2O_7$.

### *4.2.3 – Addition of molybdenum to vanadium phosphates*

Molybdenum has been introduced to $VOHPO_4 \cdot 0.5H_2O$ using the addition of molybdenum trioxide and ammonium molybdate tetrahydrate (Section 2.2.5). Both procedures involve introducing molybdenum during the phosphation step of the preparation of the precursor (co-precipitation). However, to see the effect of molybdenum addition after the preparation of $VOHPO_4 \cdot 0.5H_2O$, the incipient wetness method has also been used (impregnation).

The $VOHPO_4 \cdot 0.5H_2O$ materials and the corresponding $(VO)_2P_2O_7$ materials have been characterised using a range of techniques, in order to study the effect molybdenum has on the structure and properties of the vanadium phosphate materials.

#### *4.2.3.1 – Addition of molybdenum oxide*

XRD studies determines the effect molybdenum (2 mol%) has on the $VOHPO_4 \cdot 0.5H_2O$ structure, either by incorporation, or as a separate phase to make a mixed phase material. Comparing the precursor XRD pattern with the modified molybdenum containing precursor pattern (Figure 4.7a), the main phase present was indeed the $VOHPO_4 \cdot 0.5H_2O$, with no shifts in $2\theta$ of the overall pattern, or of any particular reflection. This suggests that molybdenum ions have not displaced vanadium ions in the structure (or *vice versa*), which would cause a change in crystallite size and hence a shift in $2\theta$.

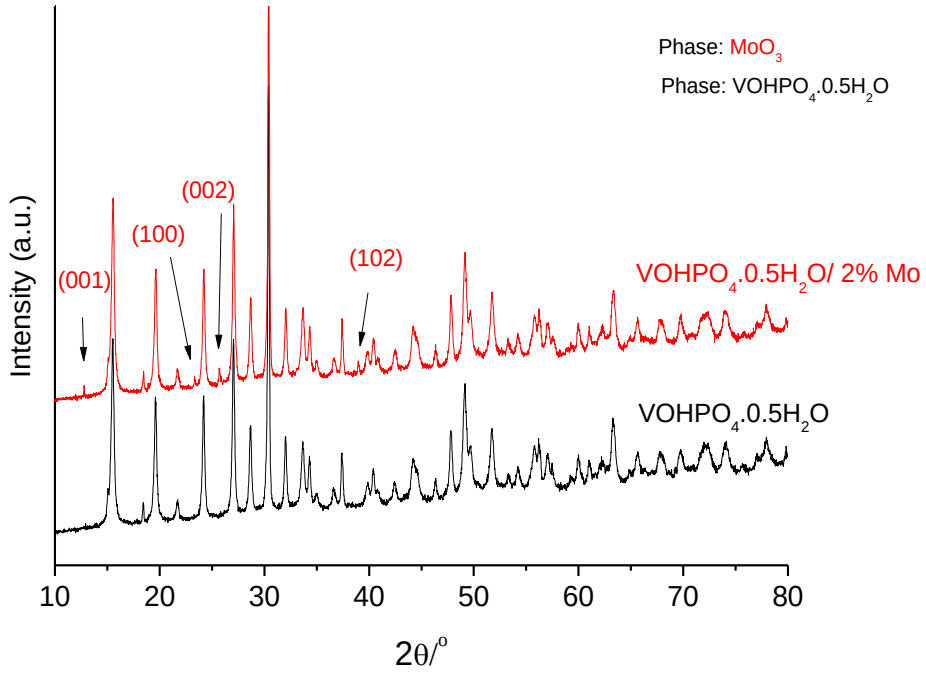


**Figure 4.7a:** XRD patterns of un-promoted $VOHPO_4 \cdot 0.5H_2O$ and $VOHPO_4.0 \cdot 5H_2O$ containing 2 mol% $MoO_3$.

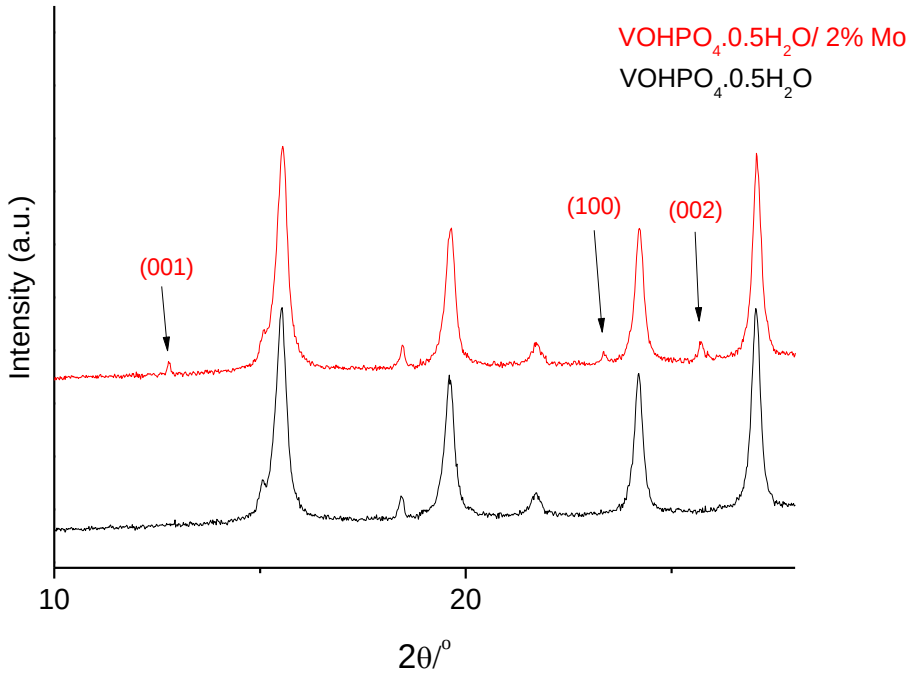


**Figure 4.7b:** XRD patterns of un-promoted $VOHPO_4 \cdot 0.5H_2O$ and $VOHPO_4 \cdot 0.5H_2O$ containing 2 mol% $MoO_3$. (Range of 10 – 28 $^o$ 2θ).

However, extra reflections are observed (Figure 4.7b) at 12.8 °, 23.4 °, 25.8 ° and 38.8 ° 2θ, which are representative of the crystallographic planes (001), (100), (002) and (102) respectively of $MoO_3$ ( JCPDS database ref. code: 05-0508). It is apparent that the reactant $MoO_3$, has remained unaltered and exists as a separate phase, possibly clustered on the surface of $VOHPO_4 \cdot 0.5H_2O$. However, this does not rule out that a small portion of molybdenum added has become incorporated into the structure, as previous studies reveals incorporation below a promoter loading of 0.13 mol% is undetectable by XRD.[51]

Raman spectroscopy analysis (Figure 4.8) of the mixed compound shows the bands associated with $VOHPO_4 \cdot 0.5H_2O$ (985, 1104 and 1152 $cm^{-1}$), but with an extra weak band at 818 $cm^{-1}$ assigned to Mo-O-Mo stretching, which is expected for high loadings of $MoO_3$ as it is not highly dispersed, and hence forms polymeric structures consistent with a bridging Mo-O-Mo species.[52]

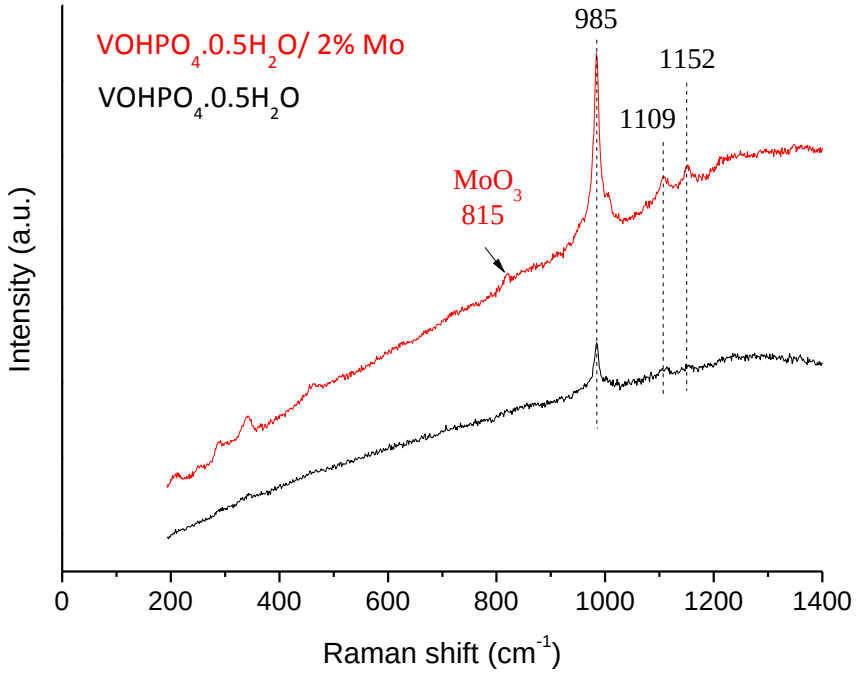


**Figure 4.8:** Raman spectra of $VOHPO_4 \cdot 0.5H_2O$ prepared with 2 mol% $MoO_3$ (co-precipitation).

The preparation method and XRD pattern suggest that the mixed phase compounds will consist of a rosette morphology, and this was observed using SEM analysis (Figure 4.9). Low resolution analysis of the mixed vanadium phosphate compound indicates no $MoO_3$ morphology, which suggests that molybdenum oxide clusters are dispersed over the surface of the $VOHPO_4 \cdot 0.5H_2O$ rosettes, although high resolution studies are needed to confirm this.

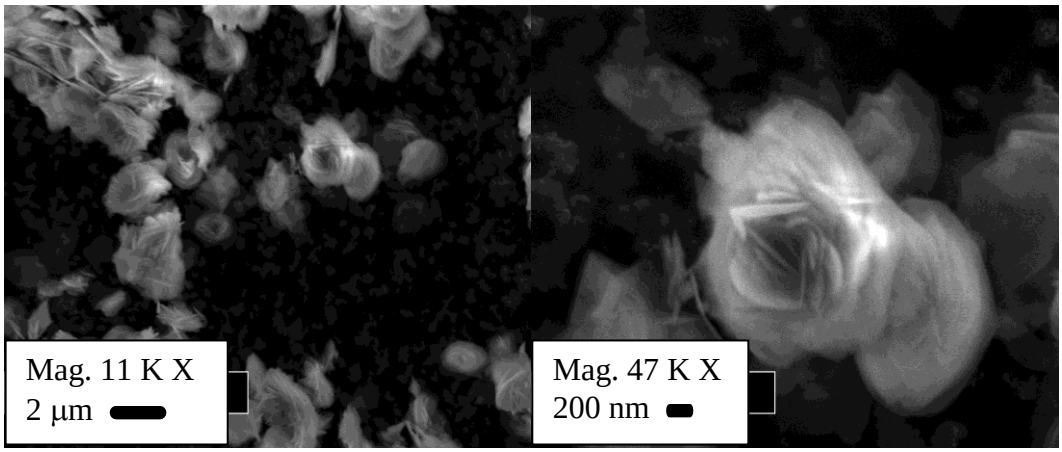


**Figure 4.9:** SEM images of $VOHPO_4 \cdot 0.5H_2O$ containing 2 mol% $MoO_3$.

To study the effect of heat treatment on the material, $VOHPO_4 \cdot 0.5H_2O$ containing Mo was heated under a nitrogen atmosphere at 750 °C, to form $(VO)_2P_2O_7$. The $MoO_3$ reflections (Figure 4.10) have disappeared, and only the crystalline $(VO)_2P_2O_7$ phase was detected. There are subtle differences in the intensities of some reflections of the $(VO)_2P_2O_7$ phase, such as the decrease in intensity of the (200) plane, which is frequently reported in the literature upon the addition of promoters.[36]

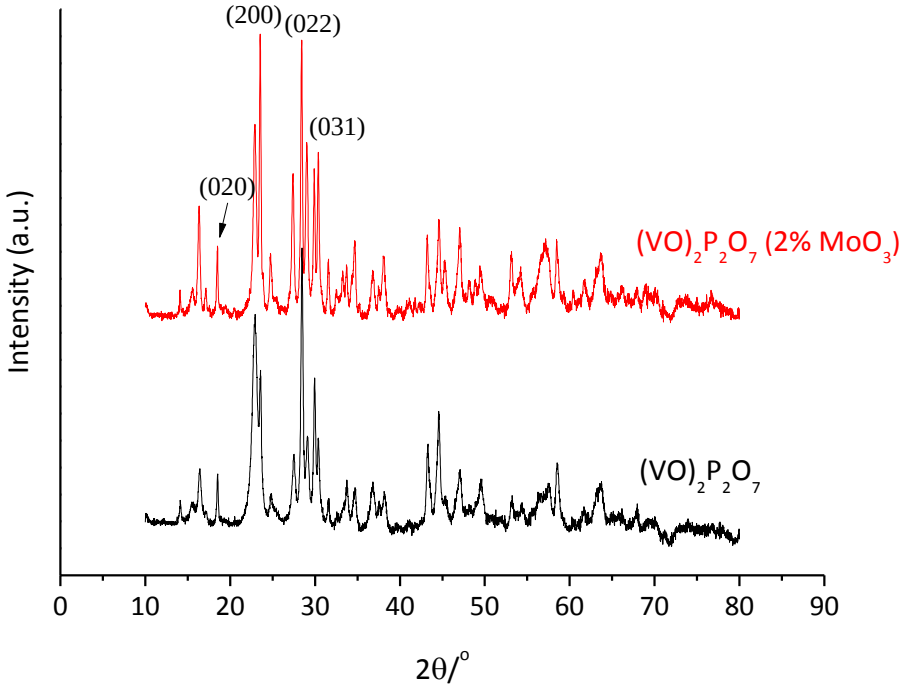


**Figure 4.10:** XRD patterns of $(VO)_2P_2O_7$ containing 2 mol% $MoO_3$.

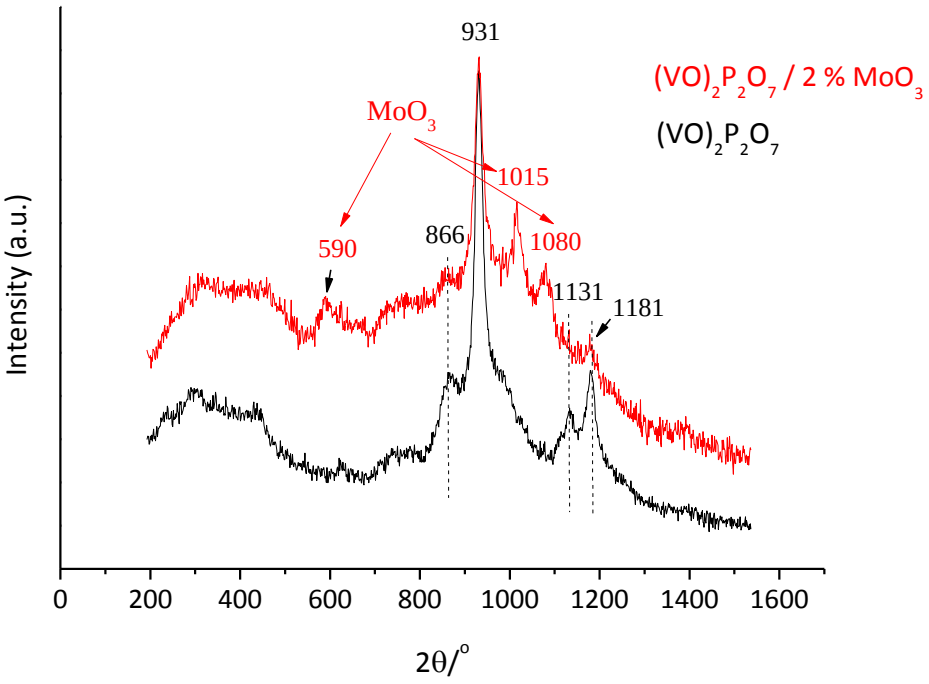


**Figure 4.11:** Raman spectra of $(VO)_2P_2O_7$ containing 2 mol% $MoO_3$.

Raman spectroscopy is a highly sensitive technique for detecting species present in materials, and this was the case for $(VO)_2P_2O_7$ containing 2 mol% $MoO_3$ (Figure 4.11), as a characteristic band of molybdenum oxide at 1015 (Mo=O) was observed among the bands corresponding to species present in $(VO)_2P_2O_7$ (931 and 1181 $cm^{-1}$).

### *4.2.3.2 – Addition of ammonium heptamolybdate tetrahydrate*

#### *4.2.3.2.1 - Co-precipitation method*

The use of molybdenum as a promoter for vanadium phosphate catalysts has been previously reported in the literature, with the main preparation method the co-precipitation of $V_2O_5$, $H_3PO_4$ and isobutanol with the metal salt, to form $Mo/VOHPO_4{\cdot}0.5H_2O$.[53] Using a similar synthesis, ammonium heptamolybdate tetrahydrate was added in various concentrations, ranging from 0.05 - 2 mol% Mo (Section 2.2.5.1.1). Another method reported,[52] involved the addition of the metal salt to $VOHPO_4{\cdot}0.5H_2O$ using the incipient wetness procedure, and this has also been studied (Section 2.2.5.1.3).

Characterisation techniques such as Raman spectroscopy, XRD, and SEM was used to analyse both the $VOHPO_4{\cdot}0.5H_2O$ and $(VO)_2P_2O_7$ materials containing molybdenum, to attempt to observe the effect on structure and morphology of the precursor and also to study the effect on the materials after heating to high temperatures.

The addition of low amounts of molybdenum salt (0.05 - 1 mol% Mo) had no visible effect on the structure of the $VOHPO_4{\cdot}0.5H_2O$ material, as the only observed phase present in the pattern was $VOHPO_4{\cdot}0.5H_2O$ (Figure 4.12a & b), with no molybdenum oxide or molybdenum phosphate phases detected. This does not rule out the formation of amorphous compounds or surface layers as XRD is unable to detect these. This is

consistent with previous results, which disclose that XRD patterns are unchanged after adding the molybdenum salt during the co-precipitation of the $VOHPO_4 \cdot 0.5H_2O$ material.[53]

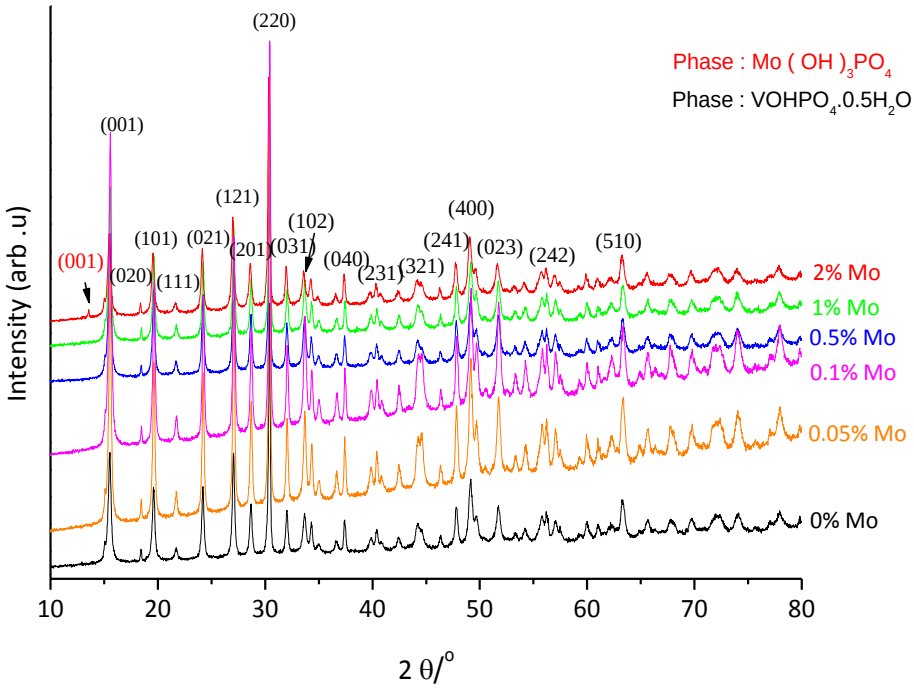


**Figure 4.12a:** XRD of $VOHPO_4 \cdot 0.5H_2O$ containing varying amounts of molybdenum. (co-precipitation method)

However, the addition of molybdenum salt at 2 mol%, causes an extra reflection among the main $VOHPO_4 \cdot 0.5H_2O$ phase, detected at 14 ° 2θ and which was assigned to the (001) plane of the molybdenum orthophosphate hydrate phase, $MoO_2 \cdot HPO_4 \cdot H_2O$ (sometimes written as $Mo(OH)_3PO_4$). This suggests that the excess molybdenum salt has reacted with the phosphoric acid to form $MoO_2 \cdot HPO_4 \cdot H_2O$, which is identical to the phase produced in Chapter 3. This could be a separate phase from the $VOHPO_4 \cdot 0.5H_2O$ phase, although closer analysis of the XRD pattern illustrated in Figure 4.12b, indicates that molybdenum ions have been incorporated into the $VOHPO_4 \cdot 0.5H_2O$ structure to a degree, as there is a

slight shift of the pattern to lower 2θ. This is typical when a larger ion displaces a smaller ion in the crystal structure increasing the crystallite size.

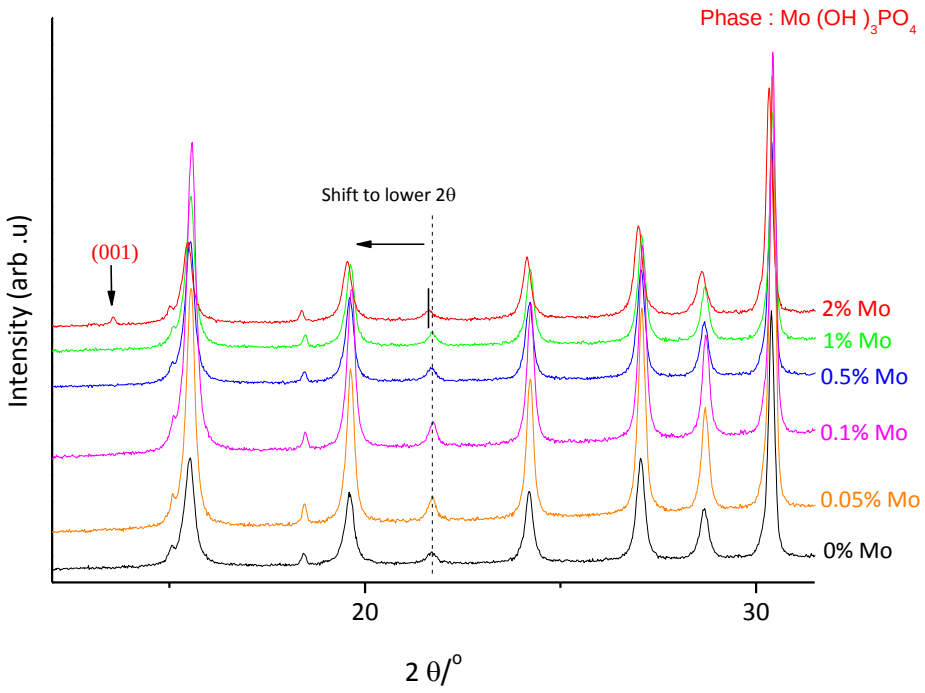


**Figure 4.12b:** XRD pattern of $VOHPO_4 \cdot 0.5H_2O$ containing varying amounts of molybdenum (co-precipitation method). (Range of 12 – 31.5 ° 2θ).

Raman spectroscopy analysis of the molybdenum containing $VOHPO_4 \cdot 0.5H_2O$ materials (Figure 4.13) showed the characteristic bands at 983, 1111 and 1157 $cm^{-1}$ of the vanadium phosphate material with no bands present for molybdenum phosphate species which could be obscured due to the high background in the spectra. The high background is due to fluorescence of these materials, which can occur when isobutanol molecules become trapped between the layers in the $VOHPO_4 \cdot 0.5H_2O$ structure,[54] which leads to difficulty in detecting low intensity bands which might correspond to the molybdenum phosphate species. An alternative theory could be that, due to the low percentage of molybdenum present, it could be widely dispersed across the material, and the intensity

of the bands could be reduced by the overwhelming intensity of the vanadium phosphate species present.

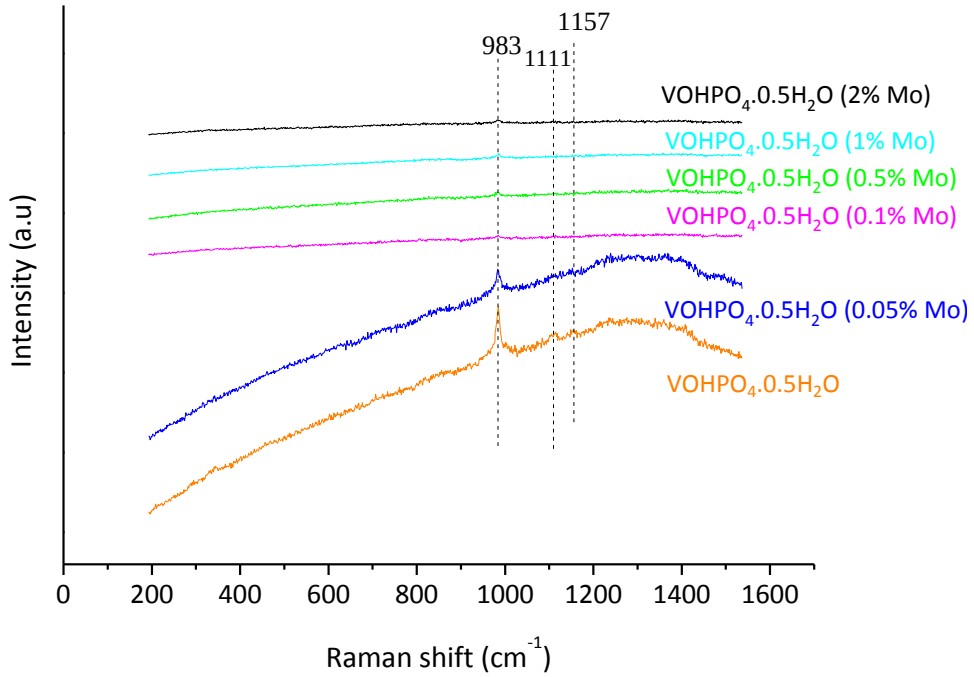


**Figure 4.13:** Raman spectra of $VOHPO_4 \cdot 0.5H_2O$ containing various amounts of molybdenum (co-precipitation method).

The appearance of the $MoO_2 \cdot HPO_4 \cdot H_2O$ phase and the shift to lower 2θ in the XRD pattern of the $VOHPO_4 \cdot 0.5H_2O$ containing 2 mol% molybdenum, could indicate slight morphological changes. SEM analysis of this material (Figure 4.14) showed no morphological changes however, when compared to the rosette morphology of the un-doped $VOHPO_4 \cdot 0.5H_2O$ material. (Figure 4.4)

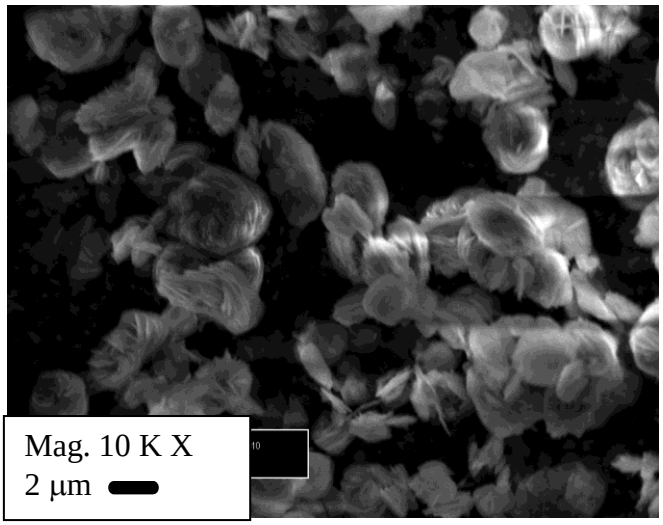


**Figure 4.14:** SEMs of $VOHPO_4 \cdot 0.5H_2O$ with (2 mol% Mo (co-precipitation method)

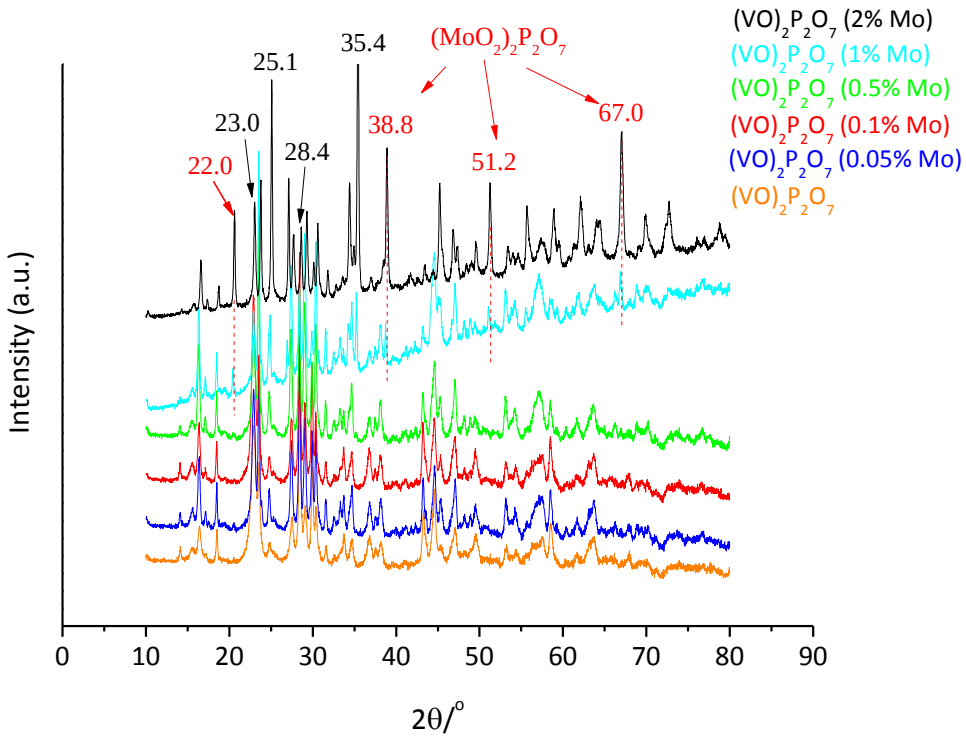


**Figure 4.15:** XRD pattern of $(VO)_2P_2O_7$ containing various amounts of molybdenum. (co-precipitation method).

Heat treatment of the molybdenum promoted $VOHPO_4 \cdot 0.5H_2O$ at 750 °C in a nitrogen atmosphere, produced only the $(VO)_2P_2O_7$ phase when molybdenum loadings were relatively low (0.05 – 0.5 mol%), as observed in Figure 4.15. The addition of 1 mol% Mo produced reflections which can be assigned to the molybdenum pyrophosphate phase,

$(MoO_2)_2P_2O_7$.(JCPDS database (ref code: 01-074-1380). The reflections observed appear at 22.0 °, 38.8 °, 51.2 ° and 67.0 ° 2θ which correspond to the index planes, (202), (403), (315) and (335) respectively. These became more prominent with the addition of 2 mol% Mo, which could suggest that a mixed molybdenum and vanadium phosphate phase may have been formed, as these two pyrophosphates are iso-structural.[55]

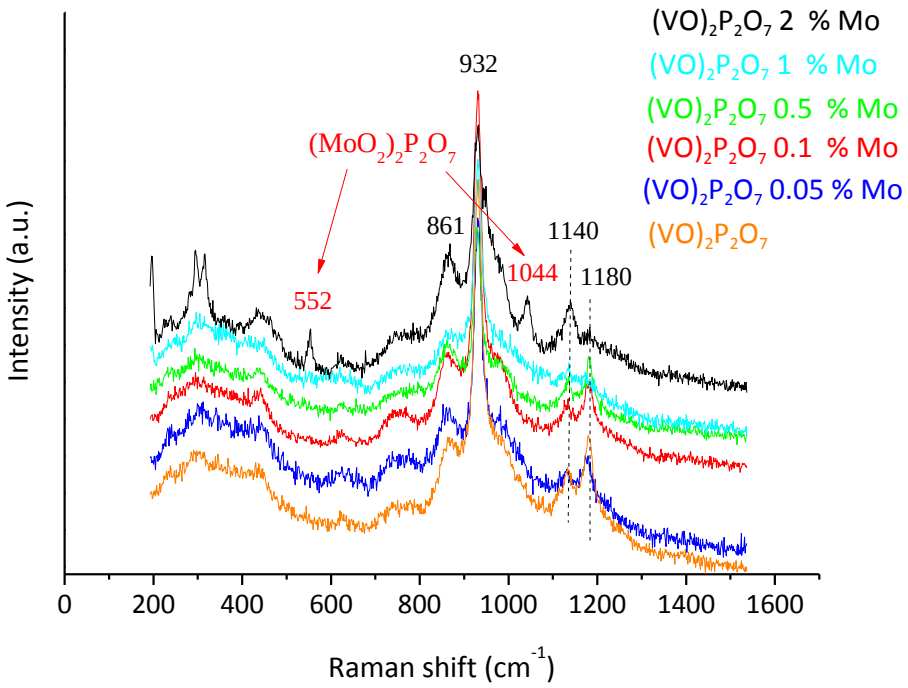


**Figure 4.16:** Raman spectra of $(VO)_2P_2O_7$ containing various amounts of molybdenum. (co-precipitation method).

Raman spectroscopy studies of the molybdenum promoted $(VO)_2P_2O_7$ materials (Figure 4.16) showed that no molybdenum species were present in the materials containing 0.05 to 1 mol% Mo. However, with the addition of 2 mol% Mo there are characteristic bands at 522 $cm^{-1}$ assigned to bending modes in molybdenum oxide, and at 1044 $cm^{-1}$, which corresponds to Mo=O stretching. The presence of these molybdenum mono-oxo species suggests that the Mo centres are isolated either on the surface, or throughout the bulk structure of the $(VO)_2P_2O_7$.

#### *4.2.3.2.2 - Incipient wetness method*

The XRD pattern of $VOHPO_4 \cdot 0.5H_2O$ containing 2 mol% Mo added *via* the impregnation procedure (Figure 4.17), produced a very similar pattern to that observed for the co-precipitation addition of ammonia molybdate tetrahydrate (Figure 4.12), with the presence of the (001) crystallographic plane at 13.6 ° 2θ representative of the $MoO_2 \cdot HPO_4 \cdot H_2O$ phase. There were, however, additional reflections for the material prepared using the incipient wetness method at 12.8 ° and 26.4 ° 2θ. The (111) plane at 26.4 ° 2θ is characteristic of the $MoO_2 \cdot HPO_4 \cdot H_2O$ phase, and the (001) plane at 12.8 ° 2θ is attributed to the $MoO_3$ phase. It is then apparent that the molybdenum has replaced vanadium in the structure of $VOHPO_4 \cdot 0.5H_2O$, to form the $MoO_2 \cdot HPO_4 \cdot H_2O$ phase, although there was a small amount of molybdenum present as $MoO_3$, which could suggest that this material is dispersed on the surface of $VOHPO_4 \cdot 0.5H_2O$.

Heat treatment of this material (containing 2 mol% Mo – impregnation) to form the active phase $(VO)_2P_2O_7$, produced an XRD pattern (Figure 4.18) very similar to that of the $(VO)_2P_2O_7$ material containing 2 mol% Mo added *via* co-precipitation, with additional reflections present at 21.9 ° and 38.7 ° 2θ, characteristic of the (202) and (403) crystallographic planes of the $(MoO_2)_2P_2O_7$ phase respectively. This could be expected, as the heat treatment of $MoO_2 \cdot HPO_4 \cdot H_2O$ in a nitrogen atmosphere above 650 °C, forms the $(MoO_2)_2P_2O_7$ phase (Figure 3.5).

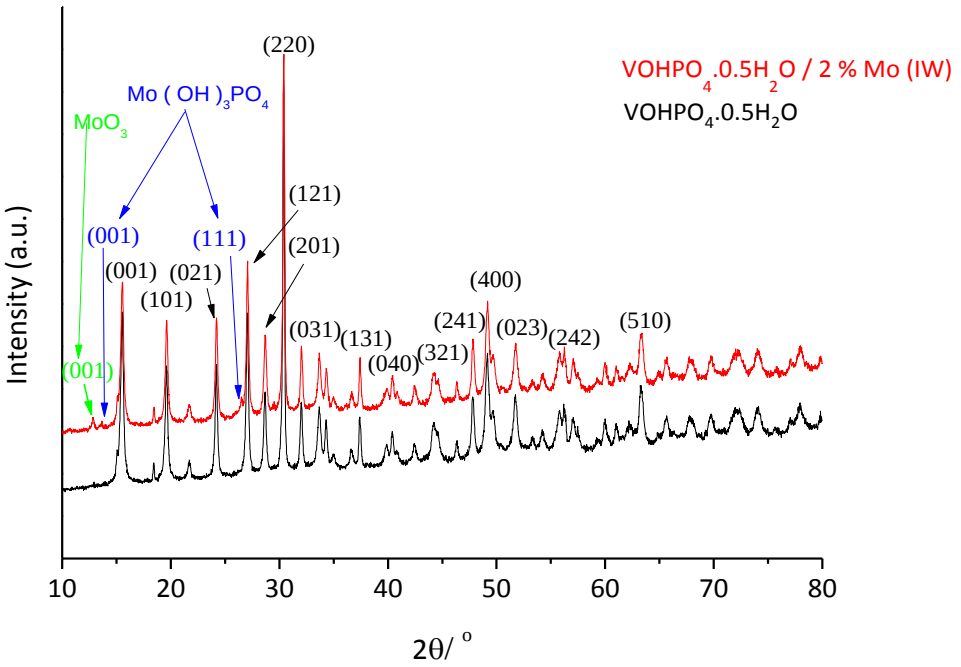


**Figure 4.17:** XRD patterns of $VOHPO_4 \cdot 0.5H_2O$ with 2 mol% molybdenum (*via* impregnation method).

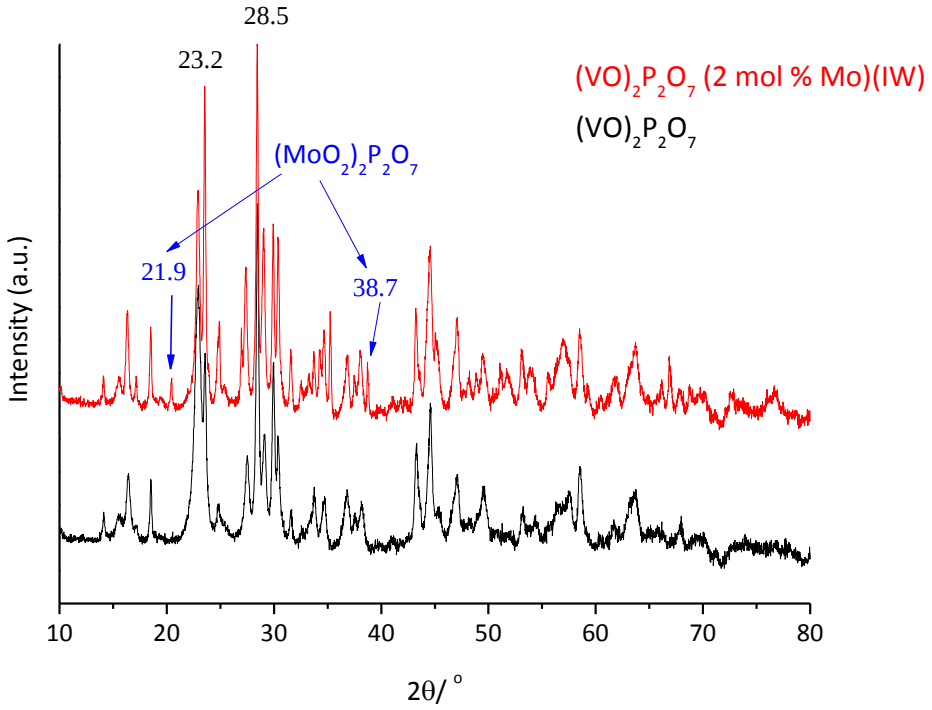


**Figure 4.18:** XRD patterns of $(VO)_2P_2O_7$ containing 2 mol% molybdenum (*via* impregnation method).

Raman spectroscopy analysis (Figure 4.19) of the mixed $(VO)_2P_2O_7/(MoO_2)_2P_2O_7$ material contained an Mo=O stretching band at 1037 $cm^{-1}$.

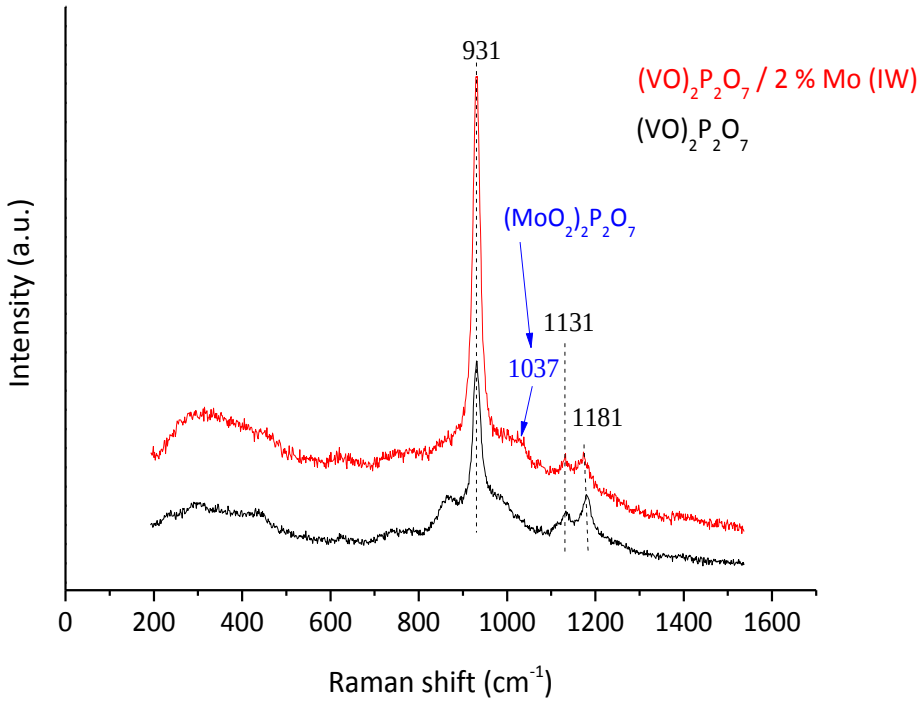


**Figure 4.19:** Raman spectra of $(VO)_2P_2O_7$ containing 2 mol% molybdenum (*via* impregnation method).

Studying the morphology of this material using SEM (Figure 4.20) showed that the morphology did not change dramatically, as the rosette morphology was maintained after the addition of 2 mol% Mo, which was consistent with the addition of Mo using the co-precipitation method (Figure 4.14).

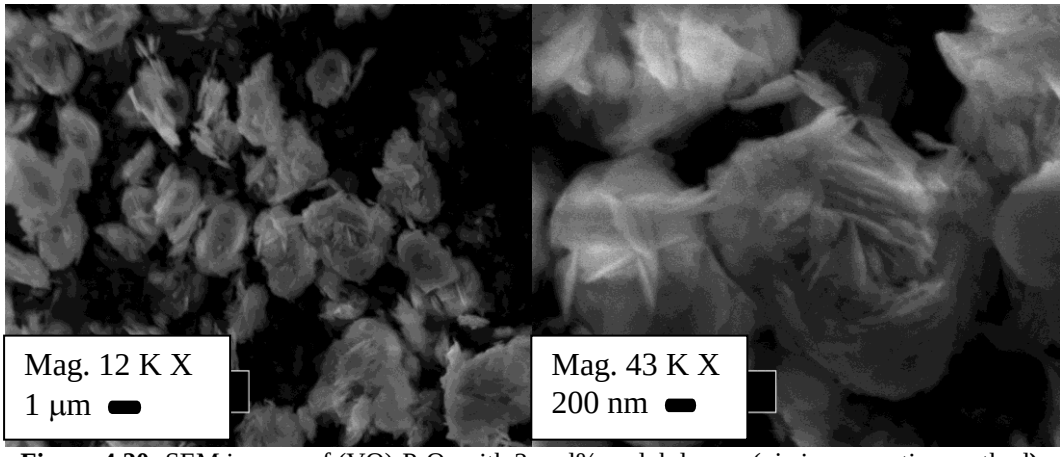


**Figure 4.20:** SEM images of $(VO)_2P_2O_7$ with 2 mol% molybdenum (*via* impregnation method**).**

## 4.3 – Catalytic activity

The VPO materials, both un-promoted and promoted were tested as catalysts for the selective oxidation of methanol to formaldehyde. As stated previously, vanadium oxide based catalysts are frequently reported in the literature as active catalysts for the selective oxidation of methanol, and so comparisons between the activity of the phosphate based catalysts reported in this chapter could determine whether phosphate groups play a role in increasing activity. The catalytic activity of these VPO catalysts will also be compared to the industrial catalyst used for methanol oxidation to formaldehyde, iron molybdate.

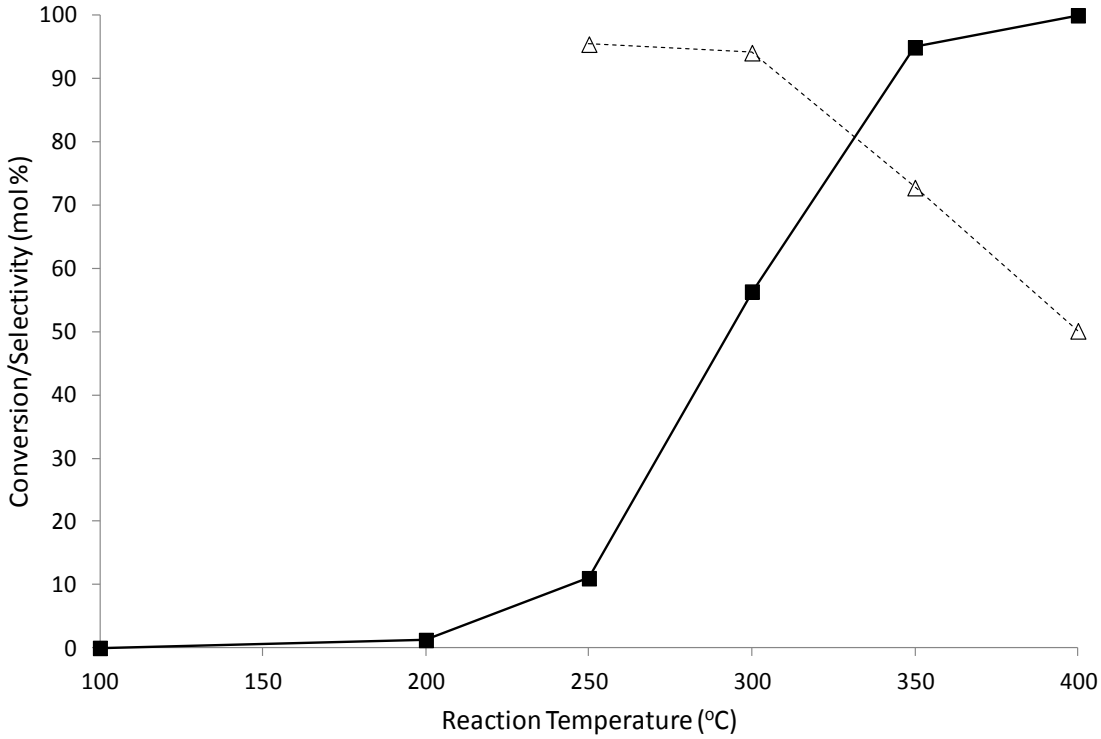


**Figure 4.21:** Catalytic Activity of a $V_2O_5$ catalyst during selective oxidation of methanol.

= Methanol conversion (mol%); = Formaldehyde selectivity (mol%)

The reaction of methanol over $V_2O_5$ (Figure 4.21) begins at ~200 °C, initially forming methyl formate (100 % selectivity). From 250 °C to 300 °C the catalyst has high selectivity to formaldehyde, with a 53 % yield at 300 °C. Above 300 °C methanol

conversion increased rapidly to around 95 % conversion (350 °C), although the selectivity to formaldehyde decreased as the formation of $CO_x$ increased. Near total conversion was reached at 400 °C.

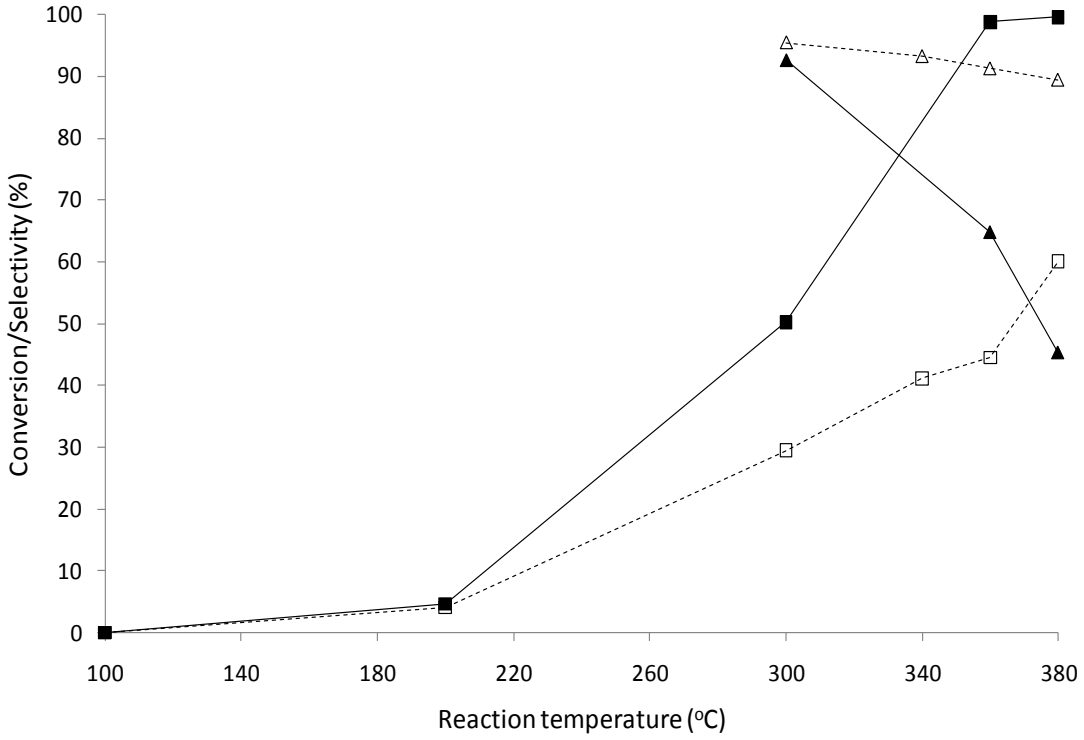


**Figure 4.22:** Methanol partial oxidation using $VOHPO_4 \cdot 0.5H_2O$ and $(VO)_2P_2O_7$ catalysts.

-□- = Methanol conversion ($VOHPO_4 \cdot 0.5H_2O$); —■— = Methanol conversion ($(VO)_2P_2O_7$);

-△- = Formaldehyde selectivity ($VOHPO_4 \cdot 0.5H_2O$); —▲— = Formaldehyde selectivity ($(VO)_2P_2O_7$)

The reaction profile of both $VOHPO_4 \cdot 0.5H_2O$ and $(VO)_2P_2O_7$ catalysts (Figure 4.22) was similar to that of the vanadium oxide (Figure 4.21, Table 4.1a & b), with the light off temperature (temperature at which catalytic reaction is initiated) at 200 °C. High selectivity to formaldehyde at 300 °C was observed, which decreased as the temperature was increased further. $VOHPO_4 \cdot 0.5H_2O$ as a catalyst for butane oxidation is known to be inactive initially, but is transformed to the active phase $(VO)_2P_2O_7$ over a relatively long period of time (>72 h), under specific conditions (*n*-butane/air mixture). This was not the case with methanol oxidation as the reaction begins at 200 °C over $VOHPO_4 \cdot 0.5H_2O$. In

contrast to $V_2O_5$, the increase in conversion was moderate as the temperature of the reaction was increased, with only 30 % conversion at 300 °C, compared to the 60 % conversion at the same temperature with $V_2O_5$ (same GHSV).

It is clear that although the reaction over $(VO)_2P_2O_7$ began at the same temperature as $VOHPO_4 \cdot 0.5H_2O$, the activity of the $(VO)_2P_2O_7$ catalyst above 200 °C was substantially higher than $VOHPO_4 \cdot 0.5H_2O$, with 50 % conversion at 300 °C, and 99 % conversion at 360 °C, compared to 30 % (300 °C) and 44 % (360 °C) conversion using $VOHPO_4 \cdot 0.5H_2O$. For butane oxidation to maleic anhydride, it has been reported that the active phase is $(VO)_2P_2O_7$,[56,57] and this also appears to be the case for the oxidation of methanol to formaldehyde.

**Table 4.1a:** Comparison of methanol converted using $V_2O_5$, $VOHPO_4 \cdot 0.5H_2O$, $(VO)_2P_2O_7$ and Iron molybdate catalysts, during methanol oxidation.

| **Reaction Temperature (°C)** | **$V_2O_5$ (Conversion mol%)** | **$VOHPO_4 \cdot 0.5H_2O$ (Conversion mol%)** | **$(VO)_2P_2O_7$ (Conversion mol%)** | **Iron Molybdate (Conversion mol%)** |
|---|---|---|---|---|
| **200** | 2 | 4 | 5 | 7 |
| **250** | 11 | 17 | 30 | 55 |
| **300** | 58 | 30 | 51 | 100 |
| **360** | 97 | 45 | 99 | 100 |
| **380** | 100 | 60 | 100 | 100 |

**Table 4.1b:** Comparison of formaldehyde selectivity and yield using $V_2O_5$, $VOHPO_4 \cdot 0.5H_2O$, $(VO)_2P_2O_7$ and Iron molybdate catalysts, during methanol oxidation.

| **Reaction Temperature (°C)** | **$V_2O_5$ (mol%)** | | **$VOHPO_4 \cdot 0.5H_2O$ (mol%)** | | **$(VO)_2P_2O_7$ (mol%)** | | **Iron Molybdate (mol%)** | |
|---|---|---|---|---|---|---|---|---|
| | **Selectivity** | **Yield** | **Selectivity** | **Yield** | **Selectivity** | **Yield** | **Selectivity** | **Yield** |
| **200** | 0 | 0 | 0 | 0 | 0 | 0 | 100 | 7 |
| **250** | 96 | 11 | 0 | 0 | 0 | 0 | 95 | 52 |
| **300** | 94 | 55 | 96 | 29 | 94 | 48 | 93 | 93 |
| **360** | 65 | 63 | 93 | 42 | 60 | 59 | 83 | 83 |
| **380** | 53 | 53 | 92 | 55 | 47 | 47 | 75 | 75 |

These results for the $(VO)_2P_2O_7$ catalyst give a clear indication that adding phosphate groups provides no real advantage for the methanol oxidation reaction, since the activity and selectivity to formaldehyde of $(VO)_2P_2O_7$ and $V_2O_5$ are very similar. The catalytic activity of the $VOHPO_4 \cdot 0.5H_2O$ catalyst only gave 30 % methanol conversion at 300 °C which does not compare well with the ~99 % conversion achieved with the industrial iron molybdate catalyst (Table 4.1a & b). However, $VOHPO_4 \cdot 0.5H_2O$ was highly selective to formaldehyde at this temperature, which was similar to the iron molybdate, both achieving ~95 % selectivity at 300 °C.

### *4.3.1 – Molybdenum promoted vanadium phosphate catalysts*

The promotion of VPO has been widely studied for many transition metals including Co, Cr, Fe and Bi.[15-18] Molybdenum containing materials are known to be active methanol oxidation catalysts *i.e.* present in iron molybdate, supported molybdenum oxide and now supported molybdenum phosphate catalysts. Therefore, VPO was prepared with the promotion of Mo using a range of techniques, such as the addition of molybdenum

trioxide and ammonium heptamolybdate tetrahydrate *via* co-precipitation and incipient wetness, and the materials tested as catalysts for methanol oxidation.

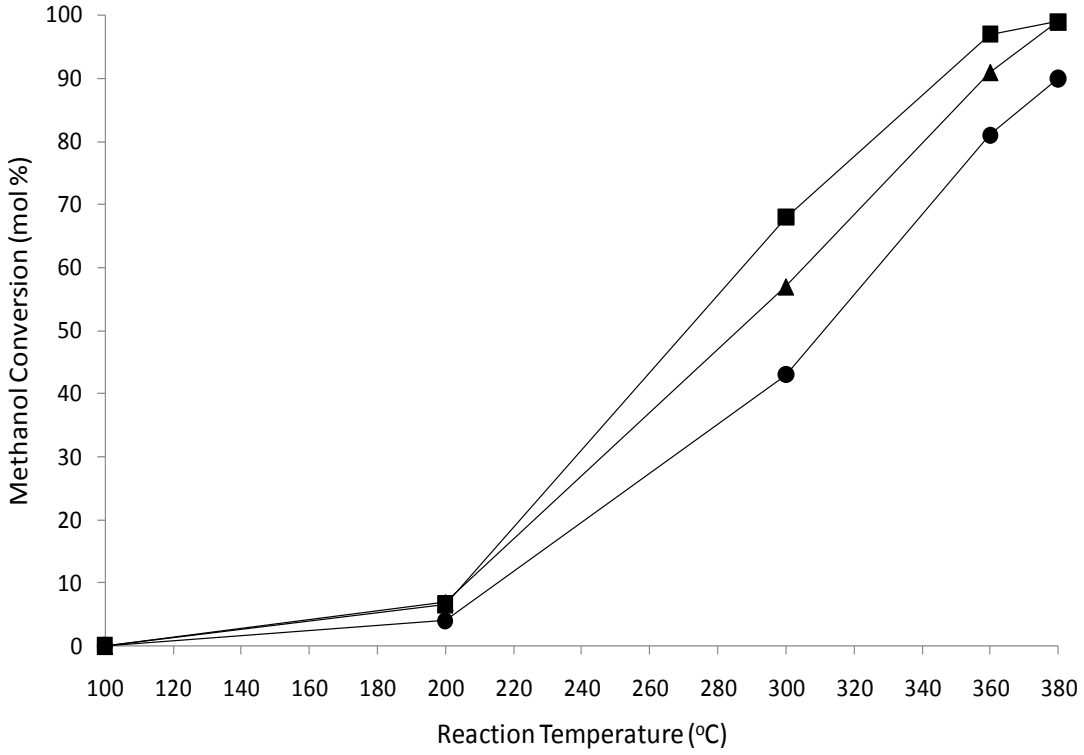


**Figure 4.23:** Methanol conversion using $(VO)_2P_2O_7$ containing 2 mol% molybdenum added *via* various preparation methods.

■ = $(VO)_2P_2O_7$ (2 mol% Mo – ammonium heptamolybdate tetrahydrate co-precipitation);
▲ = $(VO)_2P_2O_7$ (2 mol% Mo – ammonium heptamolybdate tetrahydrate Incipient wetness);
● = $(VO)_2P_2O_7$ (2 mol% Mo – $MoO_3$ co-precipitation).

To compare the effect that the synthesis method had on catalytic activity, 2 mol% Mo was added in each case. It was observed that molybdenum added *via* the ammonium heptamolybdate tetrahydrate co-precipitation method gave the highest activity, with the lowest activity seen for the addition of $MoO_3$ during the co-precipitation synthesis (Figure 4.23 & Table 4.2a). At 300 °C, 68 % conversion of methanol was reached (ammonium heptamolybdate tetrahydrate co-precipitation prepared catalyst), whereas with the addition of ammonium heptamolybdate tetrahydrate *via* incipient wetness and

the addition of $MoO_3$ *via* co-precipitation, only 57 % and 43 % conversion were reached respectively.

**Table 4.2a:** Comparison of methanol converted; 2 mol% ammonium heptamolybdate tetrahydrate (AHM) co-precipitation & incipient wetness prepared catalysts, as well as 2 mol% $MoO_3$ incipient wetness prepared catalyst, during methanol oxidation.

| **Reaction Temperature (°C)** | **2 mol% AHM – co-precipitation Conversion (mol%)** | **2 mol% AHM Incipient wetness Conversion (mol%)** | **2 mol% $MoO_3$ - Co-precipitation Conversion (mol%)** |
|---|---|---|---|
| **200** | 7 | 7 | 4 |
| **300** | 69 | 55 | 42 |
| **360** | 98 | 90 | 81 |
| **380** | 100 | 100 | 89 |

**Table 4.2b:** Comparison of formaldehyde selectivity and yield using 2 mol% ammonium heptamolybdate tetrahydrate (AHM) co-precipitation & incipient wetness prepared catalysts, as well as 2 mol% $MoO_3$ incipient wetness prepared catalyst, during methanol oxidation.

| **Reaction Temperature (°C)** | **2 mol% AHM – co-precipitation** | | **2 mol% AHM Incipient wetness** | | **2 mol% $MoO_3$ - Co-precipitation** | |
|---|---|---|---|---|---|---|
| | Selectivity (mol%) | Yield (mol%) | Selectivity (mol%) | Yield (mol%) | Selectivity (mol%) | Yield (mol%) |
| **200** | 79 | 6 | 72 | 5 | 82 | 3 |
| **300** | 94 | 65 | 87 | 48 | 86 | 36 |
| **360** | 82 | 80 | 80 | 72 | 74 | 60 |
| **380** | 74 | 74 | 70 | 70 | 62 | 55 |

The main product produced by all three catalysts was formaldehyde (Figure 4.24 & Table 4.2b), with ammonium heptamolybdate tetrahydrate co-precipitation promotion producing the highest selectivity over the temperature profile, compared to the two other preparation methods. At 300 °C, 94 % formaldehyde selectivity was achieved when adding ammonium heptamolybdate tetrahydrate *via* co-precipitation, which was 8 % and 9 % higher than the ammonium heptamolybdate tetrahydrate incipient wetness (87 %) and the $MoO_3$ (86 %) synthesis methods respectively.

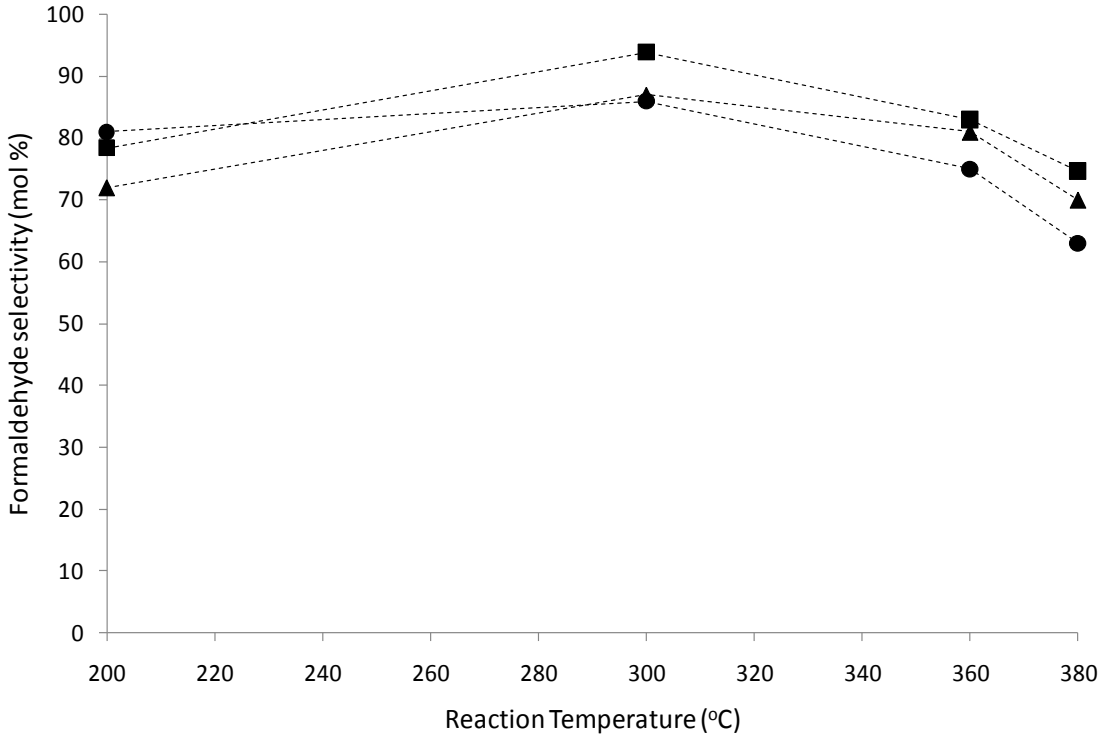


**Figure 4.24:** Formaldehyde selectivity using $(VO)_2P_2O_7$ containing 2 mol% molybdenum added *via* various preparation methods.

-■- = $(VO)_2P_2O_7$ (2 mol% Mo – ammonium heptamolybdate tetrahydrate co-precipitation);
-▲- = $(VO)_2P_2O_7$ (2 mol% Mo – ammonium heptamolybdate tetrahydrate Incipient wetness);
-●- = $(VO)_2P_2O_7$ (2 mol% Mo – $MoO_3$ co-precipitation).

The addition of ammonium heptamolybdate tetrahydrate *via* the co-precipitation synthesis method gave the catalyst which had the highest activity towards methanol oxidation and the highest formaldehyde yield (Table 4.2a & b). Therefore, to study the effect on catalytic activity of varying the concentration of Mo added during the synthesis, this methodology was used to prepare catalysts with 0.05 to 2 mol% Mo. The activity data achieved using these catalysts is shown in Figure 4.25. The light off temperature of each catalyst was just below 200 °C, with the addition of molybdenum having no major benefit to the activity of the catalyst. The most notable deviation from the standard $(VO)_2P_2O_7$ catalyst at this temperature, was the high formaldehyde selectivity achieved with the addition of ≤0.5 mol% Mo. A formaldehyde selectivity of ~99 % was reached

with the 0.5 and 1 mol% Mo promoted catalysts, whereas only 78 % formaldehyde was reached with the addition of 2 mol% Mo. Other side products detected for the 2 mol% promoted $(VO)_2P_2O_7$ catalyst at 200 °C were, di-methyl ether (14 %) and methyl formate (9 %), whereas the un-promoted $(VO)_2P_2O_7$ catalyst produced only 4 % selectivity to methyl formate. This indicates that high amounts of molybdenum added to the $(VO)_2P_2O_7$ catalyst create a more acidic catalyst surface compared to the redox sites on un-promoted $(VO)_2P_2O_7$, as the product di-methyl ether is a good indication of the acid character of a catalyst.

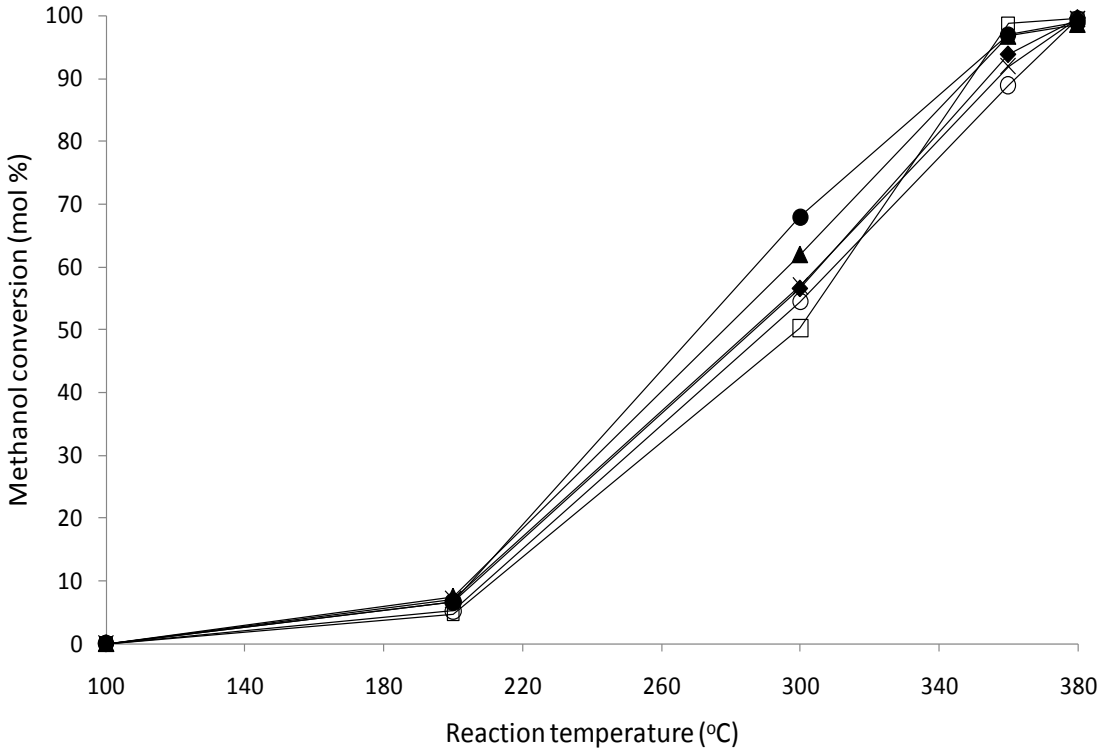


**Figure 4.25:** Methanol partial oxidation using vanadium pyrophosphate catalysts with varying molybdenum mol%.

= $(VO)_2P_2O_7$; = $(VO)_2P_2O_7$ (0.05 mol% Mo); = $(VO)_2P_2O_7$ (0.1 mol% Mo);
= $(VO)_2P_2O_7$ (0.5 mol% Mo); = $(VO)_2P_2O_7$ (1 mol% Mo); = $(VO)_2P_2O_7$ (2 mol% Mo).

An increase in reaction temperature to 300 °C produced a more clear indication of the promotional effect that molybdenum has on the $(VO)_2P_2O_7$ catalyst. Addition of Mo in

amounts as low as 0.1 mol%, increased the conversion of methanol by 6 % (compared to the non-promoted $(VO)_2P_2O_7$), and further addition of molybdenum to the $(VO)_2P_2O_7$ catalyst increased the conversion further, with 62 % and 68 % achieved when adding 1 mol% and 2 mol% Mo respectively, compared to the 50 % reached with the un-promoted catalyst at this temperature. Near total conversion of methanol was reached at 380 °C for all promoted and non-promoted catalysts, which suggests that the promotional effect of molybdenum at this temperature has been nullified, possibly due to sintering of the molybdenum clusters.

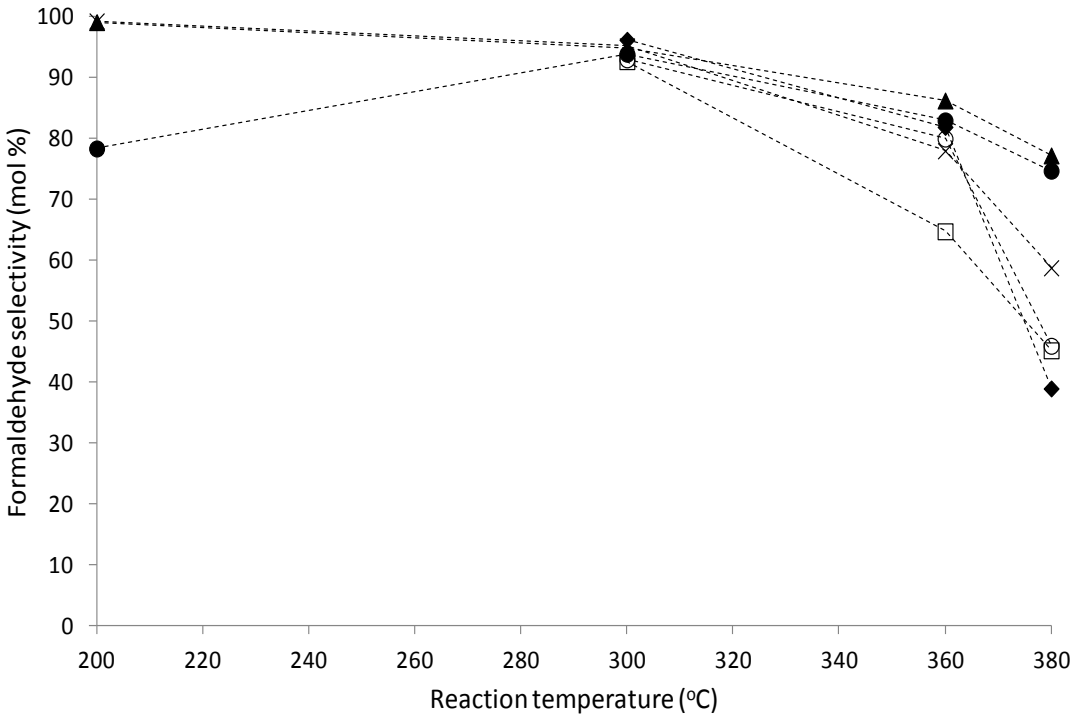


**Figure 4.26:** Formaldehyde selectivity using vanadium pyrophosphate catalysts with varying molybdenum mol%.

-□- = $(VO)_2P_2O_7$; -⊖- = $(VO)_2P_2O_7$ (0.05 mol% Mo); —◆— = $(VO)_2P_2O_7$ (0.1 mol% Mo);

-✕- = $(VO)_2P_2O_7$ (0.5 mol% Mo); -▲- = $(VO)_2P_2O_7$ (1 mol% Mo); -●- = $(VO)_2P_2O_7$ (2 mol% Mo).

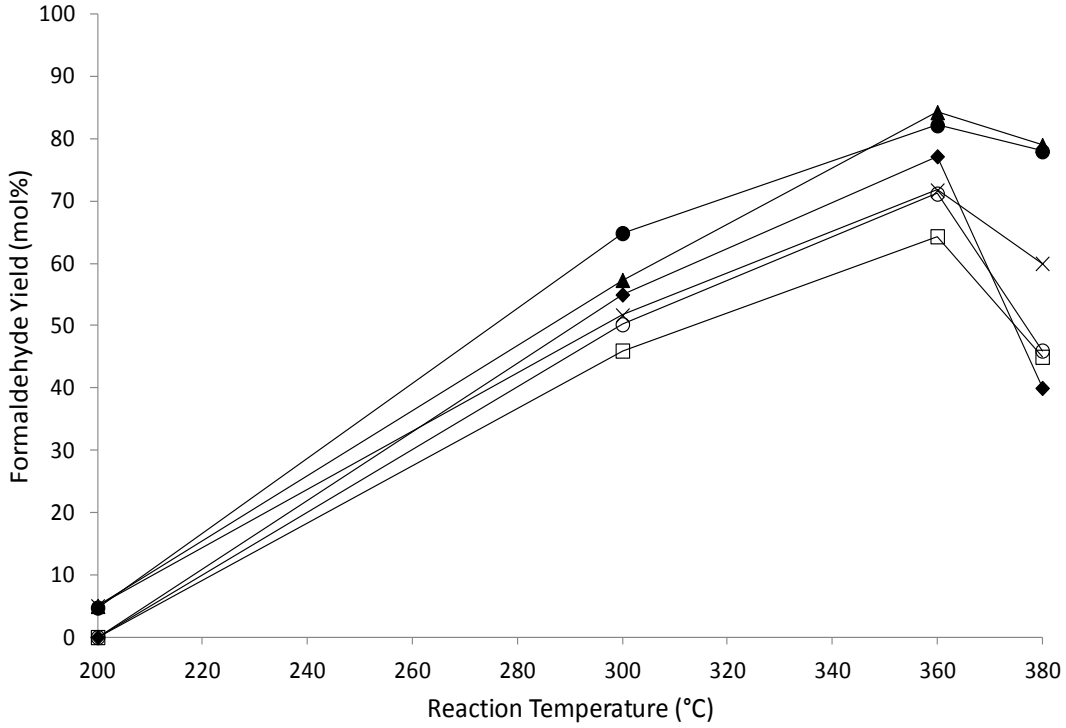


**Figure 4.27:** Formaldehyde yield achieved using vanadium pyrophosphate catalysts with varying molybdenum mol%.

= $(VO)_2P_2O_7$; = $(VO)_2P_2O_7$ (0.05 mol% Mo); = $(VO)_2P_2O_7$ (0.1 mol% Mo);
= $(VO)_2P_2O_7$ (0.5 mol% Mo); = $(VO)_2P_2O_7$ (1 mol% Mo); = $(VO)_2P_2O_7$ (2 mol% Mo).

Concurrent to higher activity produced when molybdenum was added to the $(VO)_2P_2O_7$ catalysts, formaldehyde selectivity was also enhanced throughout the reaction (Figure 4.26). As stated previously, at 200 °C, (doping) with 0.5–2 mol% molybdenum promotes the formation of formaldehyde as the main product, whereas no formaldehyde was produced by the non-doped catalyst at this temperature. At a higher temperature of 300 °C, formaldehyde selectivity over the doped and un-doped catalysts was high, with around 94 % selectivity. At even higher temperatures the promotional effect of molybdenum was observed more clearly. At 360 °C, un-promoted $(VO)_2P_2O_7$ gave 65 % selectivity to formaldehyde, compared to 80 % and 82 % selectivity achieved with low Mo additions of 0.05 and 0.1 mol% respectively. Promotion with 1 and 2 mol% Mo

increased the selectivity further at this temperature, with 86 % and 83 % formaldehyde selectivity respectively. The main by-product of the reaction with these catalysts was CO, with small amounts of $CO_2$, di-methyl ether and methyl formate.

## 4.4- Discussion

### *4.4.1 - Molybdenum as a promoter: effect of introduction method and concentration on the catalytic activity*

The organic synthesis method used to prepare $VOHPO_4 \cdot 0.5H_2O$ catalysts was preferred over the aqueous route, as it is known to produce a catalyst (after thermal activation) with the highest activity and selectivity for the selective oxidation of *n*-butane to maleic anhydride.[58,59] Analysis of $VOHPO_4 \cdot 0.5H_2O$ and $(VO)_2P_2O_7$ catalysts using a range of characterization techniques indicated that highly crystalline phases were formed, with the XRD diffraction pattern only containing reflections associated with $(VO)_2P_2O_7$. This is due to the method used to activate the precursor, $VOHPO_4 \cdot 0.5H_2O$ to the final catalyst. Typically, the chosen method of transforming the precursor to the active catalyst for *n*-butane oxidation is *via* heat treatment under the reaction conditions. However, this is known to produce a variety of different vanadium phosphate phases (*e.g.* $VOPO_4$ polymorphs and $(VO)_2P_2O_7$). By heat treating the precursor in a nitrogen atmosphere, pure $(VO)_2P_2O_7$ is produced (Figure 4.5) and so the activity of the catalyst for methanol oxidation can be attributed to this phase. The oxidation state of vanadium in both $VOHPO_4 \cdot 0.5H_2O$ and $(VO)_2P_2O_7$ is $V^{4+}$, but the structural differences between the two compounds could cause a substantial difference in activity. The $HPO_4$ groups and water molecules present between the two dimensional layers of $VOHPO_4 \cdot 0.5H_2O$ could hinder the mobility of lattice oxygen needed to re-oxidse the reduced metal centers at the surface,

with the three dimensional structure of $(VO)_2P_2O_7$ allowing for higher mobility throughout the structure and hence increasing activity.

The use of promoters added to $(VO)_2P_2O_7$ catalysts for *n*-butane oxidation has been widely studied in the literature, with improvements in the catalytic properties and mechanical resistance of the catalysts being observed.[53] Molybdenum has been reported as a promoter for $(VO)_2P_2O_7$ catalysts in *n*-butane oxidation with promising results, showing a substantial increase in maleic anhydride selectivity compared with the un-promoted $(VO)_2P_2O_7$ catalyst.[53] The promotional effect of molybdenum on the catalytic activity for the methanol oxidation reaction, and its ability to be incorporated into the vanadium phosphate structure makes it attractive as a dopant. Molybdenum was added *via* various preparation methods and in different concentrations, in the hope that the catalytic properties of the $(VO)_2P_2O_7$ catalysts could be enhanced for selective methanol oxidation to formaldehyde.

In an initial study, $MoO_3$ was introduced into the co-precipitation of $VOHPO_4 \cdot 0.5H_2O$. The aim was to replace vanadium ions in the $(VO)_2P_2O_7$ structure, and introduce redox couples ($V^{4+}/Mo^{5+}$) at the surface to improve the reducibility of the metal centers. The combination of XRD and Raman spectroscopy studies on both the precursor and the active $(VO)_2P_2O_7$ catalyst indicated that $MoO_3$ existed as a separate phase to the vanadium phosphate, with reflections attributed to $MoO_3$ in the diffraction pattern, and no shift in 2θ to suggest any cation replacement. However, the use of Raman spectroscopy suggested Mo could be present as a separate phase to $(VO)_2P_2O_7$, as the $(PO_4)^{3-}$ bands at 1080 $cm^{-1}$ are indicative of $MoOPO_4$. The absence of a shift in 2θ could be due to the isolated nature of Mo species, as observed by the band at 1015 $cm^{-1}$ which are attributed to Mo=O species.

The introduction of ammonium heptamolybdate tetrahydrate during the phosphation step in preparing $VOHPO_4 \cdot 0.5H_2O$ is a known method reported by Pierini *et al.*[53] to increase the selectivity towards maleic anhydride during *n*-butane oxidation. XRD studies on the addition of 2 mol% Mo to $VOHPO_4 \cdot 0.5H_2O$ produced extra reflections associated with $MoO_2 \cdot HPO_4 \cdot H_2O$. Heat treatment of this material formed $(VO)_2P_2O_7$ as well as $(MoO_2)_2P_2O_7$ (Figure 4.15). The presence of the molybdenum phosphate phase indicated that a mixed phase was formed, upon analyzing the XRD pattern of Mo/ $VOHPO_4 \cdot 0.5H_2O$ more closely (Figure 4.12b), it was clear that there was a shift in the whole pattern towards lower 2θ. These have been assigned to the replacement of vanadium ions by molybdenum ions in the structure.

Another synthesis method for promoted vanadium phosphate catalysts was with ammonium heptamolybdate tetrahydrate, *via* the impregnation method, also proposed by Pierini *et al.* Again, XRD analysis of the promoted material indicated reflections attributed to $MoO_2 \cdot HPO_4 \cdot H_2O$, but also the presence of $MoO_3$ (Figure 4.17). Unlike for the co-precipitation addition of ammonium heptamolybdate tetrahydrate, there was no shift in 2θ, which does not rule out that a small amount of vanadium was replaced by molybdenum forming a solid solution. This has been frequently reported in the literature, where Zazhigalov[60] observed the formation of cobalt phosphate. Hutchings[55] suggests that, based on the fact that molybdenum phosphate and vanadium phosphate are iso-structural phases, a small amount of solid solution of Mo and V mixed phase could be formed, but it is more likely that the molybdenum phosphate is present as a separate phase to the vanadium phosphate material. In addition to the extra reflections associated with $MoO_2 \cdot HPO_4 \cdot H_2O$, there are reflections assigned to $MoO_3$, which could indicate that the un-reacted ammonium heptamolybdate tetrahydrate is present as isolated $MoO_3$ species on the surface.

To compare the effect of both the preparation technique and the molybdenum reagent used to promote the $(VO)_2P_2O_7$, the three catalysts ($MoO_3$ method, ammonium heptamolybdate tetrahydrate method – co-precipitation and impregnation each containing 2 mol% Mo) were tested and compared with the un-promoted catalyst (Figure 4.24a & b). Comparing the catalysts at 300 °C gave a clear indication of the effect Mo has on the activity. Un-promoted $(VO)_2P_2O_7$ gave 50 % methanol conversion, whereas the addition of Mo *via* the co-precipitation introduction of ammonium heptamolybdate tetrahydrate gave 68 % conversion. Impregnation of ammonium heptamolybdate tetrahydrate also increased the activity of the catalyst to 57 % conversion. However, the introduction of $MoO_3$ during the co-precipitation caused a decrease in activity of the catalyst, with only 43 % conversion at the same temperature. The three promoted catalysts all gave excellent selectivity to formaldehyde over the reaction profile, with around 86 % selectivity, which was comparable to the un-promoted $(VO)_2P_2O_7$ catalyst. It is not until at higher temperatures that the positive effect of Mo promotion becomes apparent. At temperatures above 360 °C, the formaldehyde selectivity of the molybdenum promoted catalysts maintained the high selectivity, whereas, with the un-promoted catalyst there is a decrease in selectivity.

By comparing the catalytic activity for all three promoted catalysts to the characterization data, it is clear that the presence of $MoO_3$ in $(VO)_2P_2O_7$ has a negative effect on activity. The XRD analysis of the $MoO_3$ promoted catalyst in particular, indicated that it was not incorporated into the vanadium phosphate structure, and combined with Raman analysis, indicated that it was present as isolated species on the surface. Molybdenum oxide ($MoO_3$) is widely known to exhibit high selectivity to formaldehyde (during methanol oxidation)[61] and surface Mo atoms in iron molybdate catalysts are deemed as the active sites for the selective oxidation of methanol to

formaldehyde.[62,63] The increase in formaldehyde selectivity over the $MoO_3$ promoted catalyst at higher reaction temperatures therefore suggests that Mo is involved in the reaction, but it must hinder the activity of the $V^{4+}$ active sites in some way. One possibility could be that $MoO_3$ blocks active sites on the surface. The heat treatment of the $MoO_3/VOHPO_4{\cdot}0.5H_2O$ to form $(VO)_2P_2O_7$ requires high temperature (750 °C) which could sinter the Mo species across the surface leading to large clusters of $MoO_3$ which limit the number of active sites available for formaldehyde production, but these clusters could potentially block active sites or reduce the mobility of oxygen across the surface. This could also explain the lower activity of catalysts prepared using the impregnation method of adding ammonium heptamolybdate tetrahydrate compared to the co-precipitation synthesis technique. XRD analysis of the impregnated $VOHPO_4{\cdot}0.5H_2O$ material also contains reflections attributed to $MoO_3$. The bands associated with isolated Mo=O species are observed in the Raman spectra (Figure 4.19), which again, could be due to the sintering of $MoO_3$ as the precursor is heat treated to 750 °C to form $(VO)_2P_2O_7$. However, the impregnation method of promoting ammonium heptamolybdate tetrahydrate does improve the activity and selectivity of the catalyst compared to the un-promoted $(VO)_2P_2O_7$, which indicates Mo is present in a different phase, or contained in the structure of $(VO)_2P_2O_7$ where the Mo cannot sinter, which enhances the catalytic activity. Again, using XRD to study the phases present, $(MoO_2)_2P_2O_7$ is observed. Catalysts promoted using ammonium heptamolybdate tetrahydrate and the co-precipitation method, gave substantially higher activity than the un-promoted catalyst. Analysis of the diffraction pattern (Figure 4.12b) of the $VOHPO_4{\cdot}0.5H_2O$ material containing 2 mol% Mo (added *via* co-precipitation) indicates that there was substitution of V ions in the lattice by Mo ions, determined by an increase in crystallite size and hence a shift to lower 2θ. Pierini *et al.*[53] suggested that the increase in maleic anhydride

selectivity over Mo promoted $(VO)_2P_2O_7$ catalysts, was due to increasing exposure of the (200) plane (which contains the active sites), increasing Lewis acidity, and generation of $V^{5+}$ centers close to the $V^{4+}$ center of $(VO)_2P_2O_7$. It has been agreed by other authors that $V^{5+}$ (in a limited and controlled amount) enhances the activity of $(VO)_2P_2O_7$ catalysts for *n*-butane oxidation.[7, 64] The high activity of $V_2O_5$ for methanol oxidation (Figure 4.21) is known to be influenced by the strength and number of V=O bonds present and also the acidity of the surface vanadium oxide phase.[65] It is then possible to relate the enhanced activity of the Mo promoted catalysts (ammonium molybdate tetrahydrate co-precipitation method) to the increase in Lewis acidity at the surface, but also due to the generation of $V^{5+}$ centers which are also present in the active $V_2O_5$ catalyst. It is possible that the incorporation of molybdenum ions into the $(VO)_2P_2O_7$ structure gives an increase in lattice oxygen mobility to the surface to re-oxidize the reduced metal centers, which would increase the activity of the catalyst. Another theory could be the development of $V^{4+}/Mo^{6+}$ redox couples at the surface which could aid in enhancing the reducibility of the vanadium by donating electrons.

Due to the increased activity of the $(VO)_2P_2O_7$ catalyst containing 2 mol% Mo added *via* AHM co-precipitation, the loadings of Mo were varied to determine the optimum promotion loading. As Pierini *et al.*[53] reported a considerable increase in maleic anhydride selectivity by introducing loadings as low as 1 mol%, a range of loadings from 0.05–2 mol% were tested for methanol oxidation. A clear correlation between increased loading of molybdenum and increased activity and formaldehyde selectivity can be observed (Figure 4.25 & 4.26), which indicates the positive effect molybdenum has on the $(VO)_2P_2O_7$ catalysts.

To further understand the role of molybdenum in the activity of the promoted catalysts towards methanol oxidation, XPS analysis was performed (all binding energies obtained were referenced to the C1s binding energy at 284.8 eV). Firstly fresh and ex-reactor samples of the un-promoted $(VO)_2P_2O_7$ catalyst were studied (Table 4.3).

**Table 4.3:** XPS data of fresh and ex-reactor $(VO)_2P_2O_7$ catalysts.

| **$(VO)_2P_2O_7$** | **Element** | **Binding Energy (eV)** | **Oxidation State** |
|---|---|---|---|
| **Fresh** | V (2P 3/2) | 517.3 | +4 |
| | O (1s) | 530.9 | - |
| **Ex-reactor** | V (2P 3/2) | 517.3 | +4 |
| | O (1s) | 532.5 | - |

The difference in binding energy between the +5 and +4 oxidation state of vanadium is around 1 eV, and the use of peak fitting software is needed to determine the accurate interpretation of each spectra.[66,67] Therefore, there are many conflicting reports of binding energies for the two oxidation states,[68-70] but by using the C1s binding energy as a reference the oxidation state of vanadium in both the fresh and ex-reactor sample of $(VO)_2P_2O_7$ were found to be +4. Although the oxidation states are the same, it is difficult to assess whether there is only $V^{4+}$ present, as a small amount of $V^{5+}$ cannot be ruled out. The noticeable differences between the fresh and ex-reactor samples are the different oxygen species in both samples, and also the decrease in the amount of vanadium. The oxygen species present in the fresh sample (530.9 eV) can be attributed to lattice oxygen in the structure of $(VO)_2P_2O_7$, however, the O1s binding energy of the ex-reactor sample shifted to 532.5 eV, which, as seen with the ex-reactor samples of molybdenum phosphate catalysts in Chapter 3, can be assigned to –OH groups on the surface, which

could be due to un-reacted methoxy groups on the surface, or water formed as a byproduct.[71] The decrease in the amount of $V^{4+}$ between the fresh and ex-reactor samples suggests that this particular species is involved in the reaction, and can be reduced to $V^{3+}$.

**Table 4.4:** XPS analysis of fresh Molybdenum promoted $(VO)_2P_2O_7$ catalysts.

| **$(VO)_2P_2O_7$ Mo loading (mol%)** | **Element** | **Binding energy (eV)** | **Oxidation State** |
|---|---|---|---|
| **0.1** | V (2P 3/2) | 517.5 | +4 |
| | Mo (3d) | - | - |
| | O (1s) | 531.8 | - |
| **1** | V (2P 3/2) | 517.3 | +4 |
| | Mo (3d) | 233.6 | +6 |
| | O (1s) | 531.8 | - |
| **2** | V (2P 3/2) | 517.2 | +4 |
| | Mo (3d) | 233.5 | +6 |
| | O (1s) | 531.9 | - |

XPS analysis was also performed on the fresh Mo promoted samples (Table 4.4). The +6 oxidation state of Mo found in all promoted samples agrees with the XRD results where reflections associated with the $(MoO_2)_2P_2O_7$ phase are present. Molybdenum is known to activate and store oxygen species, like vanadium, and the presence of both in close proximity to each other could provide redox couples: $V^{4+} + Mo^{6+} \leftrightarrow V^{5+} + Mo^{4+}$ which could enhance the activity of the catalyst. The increased activity for the higher loadings of vanadium could correlate with an increase in amount of these redox couples across the surface.

## 4.5 – Conclusions

Promoted vanadium phosphate catalysts have been prepared, characterized and tested for methanol oxidation to formaldehyde with promising results. No literature exists for the use of $(VO)_2P_2O_7$ for selective methanol oxidation, as it is principally used as the main industrial catalyst for *n*-butane oxidation to maleic anhydride. One of the main techniques to improve $(VO)_2P_2O_7$ catalysts involves the use of transition metal promoters, in particular cobalt, that substantially improves maleic anhydride selectivity. Another promoter that has been used is molybdenum and this has been studied in this chapter to promote $(VO)_2P_2O_7$ for their use as catalysts for selective methanol oxidation (reported for the first time). A variety of synthesis methods were used to introduce the Mo into the VPO structure, with characterization and catalytic testing confirming that the ideal method of promotion was using ammonium heptamolybdate tetrahydrate, which when added *via* co-precipitation, formed a solid solution of $(MoO_2)_2P_2O_7/(VO)_2P_2O_7$. This leads to an increase in activity, but also to an increase in formaldehyde selectivity. Although the highest loading of Mo added was 2 mol% (which showed the highest activity and formaldehyde selectivity), higher loadings of molybdenum could be used as there is a correlation between increasing Mo concentration and increasing activity/selectivity. Compared to the bulk $V_2O_5$ catalyst (frequently reported in the literature), the presence of phosphate groups do not enhance the activity towards methanol oxidation, as the catalytic activity of both $V_2O_5$ and $(VO)_2P_2O_7$ are similar.

## 4.6 – References

1. R. I. Bergman, and N. W. Frisch. *US Patent* **1966**, *3*, 293, 268.
2. Wu-HSun Cheng. *Applied catalysis A: General* **1996**, *147*, 55-67.
3. F. Trifiró. *Catal. Today* **1993**, *16*, 91.

4. H. S. Horowitz, C. M. Blackstone, A. W. Sleight and G. Teufer. *Appl. Catal.* **1988**, *38*, 193.
5. L. M. Cornaglia, C. Caspani and E. A. Lombardo. *Appl. Catal*. **1991**, *74*, 15.
6. M. O'Connor, F. Dason and B. K. Hodnett. *Appl. Catal*. **1990**, *64*, 161.
7. G. Centi, F. Trifiró, J. R. Ebner and V. M. Franchetti. *Chem. Rev*. **1988**, *88*, 55.
8. F. Cavani, G. Centi and F. Trifiró. *La Chimica & L'Industria*. **1992**, *74*, 182.
9. F. Cavani, G, Centi and F. Trifiró. *L. Chem. Commun*. **1985**, 492.
10. B. K. Hodnett, P. Permanne and B. Delmon. *Appl. Catal.* **1983**, *6*, 231.
11. N. Duvauchelle, E. Kesteman, F. Oudet, and E. Bordes. *J. Solid State Chem.* **1998**, *137*, 311-324.
12. C. J. Kiely, A. Burrows, G. J. Hutchings, K. E. Bere, J. C. Volta, A. Tuel, M. Abon, *Faraday Discuss*. **1996**, *105*, 103-118.
13. F. Cavani. G. Centi, F. Trifiró. *Appl. Catal.* **1984**, *9*, 191-202.
14. B. Pierini, G. Sola, J. Petunchi. *Catal. Today* **1992**, *15*, 537.
15. C. Carrara, S. Irusta, E. Lombardo, and L. Cornaglia. *Applied Catalysis A: General* **2001**, *217*, 275–286.
16. M. T. Sananes-Schulz, F. Ben Abdelouahab, G. J. Hutchings, and J. C. Volta. *J. Catal.* **1996**, *163*, 346–353.
17. Y. H. Taufiq-Yap and A. A. Abdul Ghani. *Chin. J. Catal*. **2007**, 28 (12), 1037–1040.
18. C. K. Goh, Y. H. Taufiq-Yap, G. J. Hutchings, N. Dummer and J. Bartley. *Catalysis Today* **2008**, *131*, 408–412.
19. S. Sajip, J. K. Bartley, A. Burrows, M. T. Sananes-Schulz, A. Tuel, J. C. Volta, C. J. Kiely and G. J. Hutchings. *New J. Chem*. **2001**, *25 (1)*, 125.
20. N. Govender, H. B. Friedrich and M. J. van Vuuren. *Catal. Today* **2004**, *97*, 315.
21. A. Cruz-Lopez, N. Guilhaume, S. Miachon and J. A. Dalmon. *Catal. Today* **2005**, *949*, 107–108.
22. Y. H. Taufiq-Yap. *J. Natur. Gas Chem*. **2006**, *15*, 144.
23. G. J. Hutchings. *J. Mater. Chem*. **2004**, *14*, 3385–3395.
24. L. Sartoni, A. Delimitis, J. K. Bartley, A. Burrows, H. Roussel, J. M. Herrmann, J. C. Volta, C. J. Kiely and G. J. Hutchings. *J. Mater. Chem.* **2006**, *16*, 4348–4360.
25. A. M. Duarte de Farias, W. de A. Gonzalez, P. G. Pries de Oliveira, J. G. Eon, J. M. Herrmann, M. Aouine, S. Loridant, J. C. Volta. *J. Catal.* **2002**, *208*, 238–246.

26. P. Nagaraju, N. Lingaiah, P. S. Sai Prasad, V. Narayana Kalevaru, A. Martin. *Catal. Commun.* **2008**, *9*, 2449–2454.
27. A. Delimitis. *Applied Catalysis A: General* **2010**, *376*, 33–39.
28. P. Ruiz and B. Delmon. *Catal. Today* **1987**, *1*, 2.
29. G. Centi. *Catal. Today* **1993**, *16*, 1.
30. F. Cavani and F. Trifiró. *Catal. Today* **1994**, *11*, 246.
31. V. V. Guliants, M. A. Carreon, *Vanadium-Phosphorus-Oxides: from Fundamentals of n-Butane to Synthesis of New Phases on Catalysis* **2005**, *Vol. 18*, RSC Publishing, Cambridge, 1.
32. M. Ai. *J. Catal*. **1986**, *101*, 389.
33. Y. F. Han, H. M. Wang, H. Cheng and J. F. Deng. *Chem. Commun*. 1999, *521*.
34. J. K. Novakova, E. G. Derouane. *Catal. Today* **2003**, *81*, 247.
35. G. Landi, L. Lisi and J. C. Volta. *Chem. Commun*. **2003**, 492.
36. S. Ieda. *Proceedings of 15th Saudi-Japan Joint Symposium Dhahran, Saudi Arabia, November 27-28*, **2005**.
37. J. M. Tatibouët and J. E. Germain. *Bull. Soc. Chim.* **1980**, 343.
38. J. M. Tatibouët and J. E. Germain. *J. Catal.* **1981**, *72*, 375.
39. Q. Wang and R. J. Madix. *Surface Science*, **2002**, *496 (1-2)*, 51-63.
40. H. Imai, Y. Kamiya and T. Okuhara. *J. Catal.*, **2008**, *255*, 213-219.
41. L. O'Mahony, J. Henry, D. Sutton, T. Curtin, B. K. Hodnett. *Applied Catalysis A: General* **2003**, *253*, 409–416.
42. L. O'Mahony, D. Sutton and B. K. Hodnett. *Catal.Today* **2004**, *91–92*, 185–189.
43. L. O'Mahony, T. Curtin, J. Henry, D. Zemlyanov, M. Mihov and B. K. *Hodnett. Applied Catalysis A: General* **2005**, *285*, 36–42.
44. C. J. Kiely, A. Burrows, S. Sajip, G. J. Hutchings, M. T. Sananes, A. Tuel and J. C. Volta, *J. Catal.* **1996**, *162*, 31–47.
45. Wen-Sheng Dong, J. K. Bartley , N. F. Dummer, F. Girgsdies, Dansheng Su, R. Schlögl , J. C Volta and G. J. Hutchings. *J. Mater. Chem*. **2005**, *15*, 3214–3220.
46. H. S. Horowitz, C. M. Blackstone, A. W. Sleight and G. Teufer. *Appl. Catal.* **1988**, *38*, 193.
47. E. Kestemann, M. Merzouki, B. Taouk, E. Bordes, R. Contractor and G. Poncelet. *Stud. Surf. Sci. Catal.* **1995**, *91*,707.
48. C. C. Torardi and J. C. Calabrese. *Inorg. Chem*. **1984**, *23*, 1310.

49. M. E. Leonowicz, J. W. Johnson, J. F. Brody, H. F. Shannon and J. M. Newsam, *J. Solid State Chem.* **1985**, *56*, 370
50. Zhi-Yang Xue and Glenn L. Schrader. *J. Phys. Chem. B* **1999,** *103,* 9459-9467
51. L. Cornaglia, C. Carrara, J. O. Petunchi, E. A. Lambardo, *Stud. Surf. Sci. Catal.* **2000**, *130*, 1727.
52. S. Irusta, A. Boix, B. Pierini, C. Caspani, and J. Petunchi. *J. Catal.* **1999**, *187***,** 298–310.
53. B. T. Pierini and E. A. Lombardo. *Catalysis Today* **2005**, *107–108*, 323–329.
54. F. B. Abdelouahab, R. Olier, M. Ziyad and J. C. Volta. *J. Catal.* **1995**, *157*, 687.
55. G. Hutchings and R. Higgins. *J. Catal.* **1996**, *162*, 153.
56. G. Busca and G. Centi. *J. Am. Chem. Soc.* **1989**, *111*, 46.
57. G. Centi and F. Trifiró. *Chem. Eng. Sci.,* **1990**, *45,* 2589.
58. J. R. Ebner and M. R. Thompson, *In Structure-Activity and Selectivity Relationships in Heterogeneous Catalysis*, ed., Elsevier, Amsterdam, **1991**, *31*.
59. L. M. Cornaglia, C. A. Sanchez and E. A. Lombardo. *Appl. Catal*. **1993**, *95*, 117.
60. V. A. Zazhigalov, J. Haber, J. Stoch, A. Pyatnitzkaya, G. A. Komashko, V. M. Belousov, *Appl. Catal. A.* **1993**, *96*, 135.
61. A. P. V. Soares, M. Portela, A. Kiennemann, L. Hilaire and J. M. M Millet. *Applied Catalysis A: General*, **2001,** *206,* 221-229.
62. L. I. Abaulina, G. N. Kustova, R. F. Klevtsova, B. I. Popov, V. N. Bibin, V. A. Melekhina, V. N. Kolomiichuk and G. K. Boreskov, *Kinet. Catal*. (*Engl. Transl*.) **1976**, *17 (5)*, 1126.
63. M. R. Sun-Kou, S. Mendioroz, J. L. G. Fierro, J. M. Palacios and A. Guerrero-Ruiz. *J. Mater. Sci.* **1995**, *30*, 496.
64. G. Bergeret, M. David, J. P. Broyer, J. C. Volta and G. Hecquet. *Catal. Today* **1987**, *1*, 37.
65. G. Deo and I. E. Wachs. *J. Catal.* **1994**, *146*, 323-334.
66. M. Abon, K. E. Bere, A. Tuel and P. Delishere. *J. Catal*. **1995**, *156*, 28.
67. P. Delishere, K. E. Bere and M. Abon. *Appl. Catal. A: Gen*eral **1998**, *172*, 295.
68. J. Mendialdua, R. Casanova and Y. Barbaux. *J. Electron. Spectrosc. Relat. Phenom*. **1995**, *71*, 249.
69. M. Demeter, M. Neumann and W. Reichelt. *Surf. Sci.* **2000**, *41*, 454–456.

70. G. Silversmit, D. Depla, H. Poelman, G. B. Marin and R. De Gryse. *J. Electron Spectroscopy and Related Phenomena* **2004**, *135*, 167–175.

71. J. Haber and E. Lalik. *Catalysis Today* **1997**, *33*, 119-137.

# 5

# *Chapter 5 – Methanol and carbon monoxide oxidation using supported mono and bi-metallic gold/palladium catalysts*

## 5.1 – Introduction

Since the pioneering discovery by Haruta *et al.* in 1989,[1] where supported gold nanoparticles were found to be highly active catalysts for CO oxidation at room temperature or below, there has been an increasing interest into how this usually inert metal can perform so well in this oxidation reaction. It is now widely accepted that the size of gold nanoparticles have a major role in determining how active the supported catalyst is in CO oxidation, with smaller nanoparticles being favoured for high activity.[2-6] Therefore, it is clear that the preparation method and the particular support used, is of high importance in determining the size of the gold nanoparticles. The impregnation method using $HAuCl_4$ often produces large metallic gold particles (>20 nm) after thermal treatment. The growth in particle size after thermal treatment is thought to occur as the interaction between the gold particles and the support is weak, which leads to sintering of the particles.[7]

The two main methods to achieve small nanoparticles of gold on an oxide support, are the co-precipitation and the deposition-precipitation methods.[8,9] In the past decade, an

adaptation of the deposition method has become increasingly popular, which involves the use of stabilising molecules, such as poly vinyl alcohol (PVA) [10] or urea,[11] which prevent particle growth during preparation. However, the removal of the stabilising molecule from the catalyst is crucial, as it has the negative effect of blocking potential active sites. The most frequently reported methods are the use of thermal and oxidative treatments, but these lead to large particle growth due to sintering, which negates the effects of using the ligand in the first place.[12,13] In this chapter, a new method of removing the stabilising ligand using solvent extraction is studied using high resolution microscopy, and compared with the thermal treatment method for catalysts used in CO oxidation and selective methanol oxidation.

In recent years there have been highly cited publications associated with the use of gold as a catalyst for methanol oxidation.[14-16] Gold supported on an oxide such as titania is reported in the literature as a catalyst for the oxidation of methanol to hydrogen, due to the use of hydrogen in fuel cell applications.[17,18] Chang *et al*. discovered that the catalytic properties of the gold nanoparticles depends on the particle size, oxidation state, nature of the oxide support and the interaction between the nanoparticles and the support.[19] Therefore, due to the major influence nanoparticle size has on catalytic activity, methanol oxidation is another ideal reaction to observe the effect that the solvent extraction treatment has on catalytic activity, compared to the standard thermal treatment method. Mono-metallic Au/$TiO_2$ and also bi-metallic Au(Pd)/$TiO_2$ catalysts were tested for this reaction, to study whether there is a synergistic effect, as palladium catalysts are also known to be active in the partial oxidation of methanol to hydrogen,[20] as well as methanol electro-oxidation.[21,22]

The characterization and CO oxidation testing (in this chapter) using 1 wt% $Au/TiO_2$ catalysts (prepared using thermal and solvent extraction treatments) were carried out by co-workers at the Hutchings group at Cardiff Catalysis Institute, and is published in the journal: Nature Chemistry.[23] A small number of CO oxidation catalytic tests which are observed in the Nature Chemistry article were repeated by myself and are highlighted in the figure captions..

## 5.2 – Characterisation - *Removal of PVA and its effect on gold particle size*

Sol immobilization was used to prepare 1 wt% $Au/TiO_2$ (refer to Chapter 2 for preparation), using the stabilising ligand polyvinyl alcohol (PVA). However, the methods used to remove the stabilising ligand (to expose the active sites on the surface) have been varied, so that the size of the gold nanoparticles can be correlated with the methods used to remove the ligand, heat treatment or solvent extraction using water. Each catalyst has been characterised before and after each treatment using a range of analytical techniques.

Laser Raman spectroscopy is an ideal technique for analysing the relative amount of PVA present in each catalyst, as it can detect the presence of C-C, C-H and O-H bond stretches, which are characteristic of PVA. For the solvent extraction treatment, as the reflux time is increased, the amount of PVA removed increases, and this can be seen in Figure 5.1. The more noticeable peaks present with PVA occur between 800 – 2000 $cm^{-1}$ (Table 5.1a), and it is clear that when no treatment is applied, *i.e.* non-refluxed spectra in Figure 5.1, the main bands characteristic of PVA are prominent, which is to be expected, since the catalyst has only been dried at 120 °C, which is insufficient to remove noticeable amounts of PVA. A reflux time of 15 minutes can also be said to have little effect, as there is no major decrease in intensity of the PVA bands when compared to the

non-refluxed catalyst. Refluxing for 30 and 60 minutes however, has had a more obvious effect and there is a more noticeable decrease in intensity of the PVA bands.

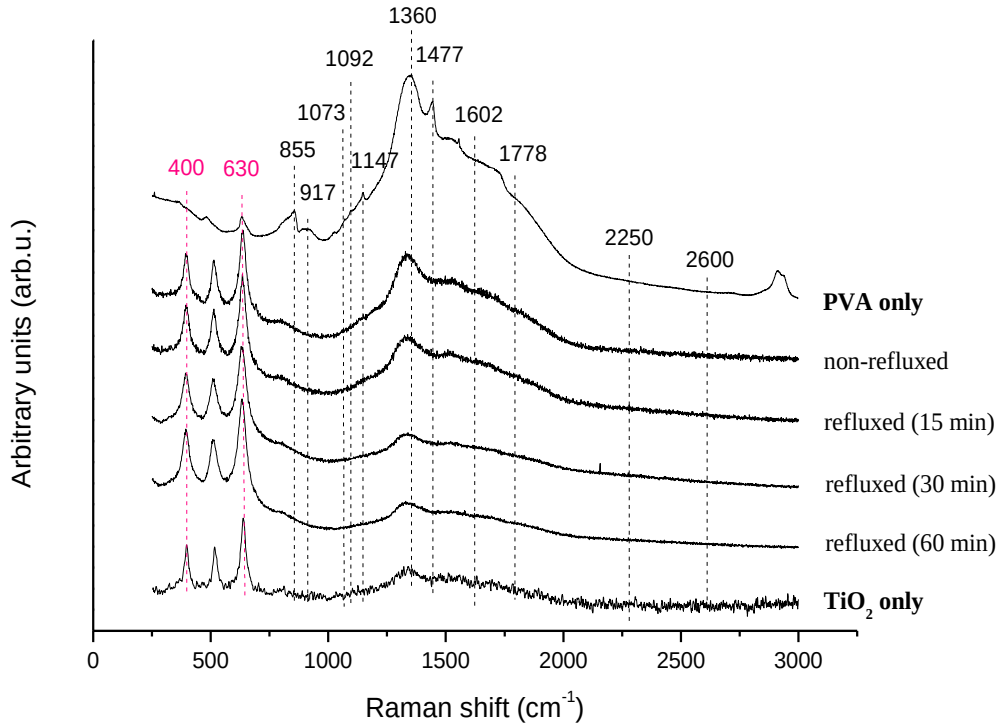


**Figure 5.1:** Raman spectra for the refluxed series of 1 wt% $Au/TiO_2$: PVA only, 1 wt% $Au/TiO_2$ – non-refluxed, 1 wt% $Au/TiO_2$ – 15 min reflux, 1 wt% $Au/TiO_2$ – 30 min reflux, 1 wt% $Au/TiO_2$ – 60 min reflux, & $TiO_2$ only. (Analysis peformed by Gareth Whiting)

Evidence to support these results was found when elemental analysis was carried out on each material in the series. There is a slight decrease in the amount of carbon, from 0.59 to 0.57 wt% (Table 5.2) when comparing the non-refluxed to the 30 min reflux, and a marked difference can be observed after 60 min of reflux treatment, with 0.44 wt% carbon detected, suggesting a large loss of PVA from the catalyst. Gold elemental analysis of the catalyst was used so as to ensure that by removing the PVA from the catalyst surface, no gold was lost in the process, and it is clear that gold has indeed remained intact, *i.e.* ~1 wt% for non-refluxed and each reflux treated materials (Table 5.3).

**Table 5.1a.** Band assignments for the Raman spectrum of polyvinylalcohol (PVA).

| Assignment | Frequency ($cm^{-1}$) |
|---|---|
| C-C stretch | 855 |
| C-C stretch | 917 |
| C-O stretch, O-H bend | 1073 |
| C-O stretch, O-H bend | 1092 |
| C-O stretch, C-C stretch | 1147 |
| C-H bend, O-H bend | 1360 |
| C-H bend, O-H bend | 1477 |
| C-H stretch, O-H bend | 1602 |
| C-H stretch | 1778 |
| C-O stretch, C-H bend | 2250 |
| C-H stretch | 2600 |

**Table 5.1b.** Band assignments for the Raman spectrum of $TiO_2$ (P25).

| Assignment | Frequency ($cm^{-1}$) |
|---|---|
| Anatase crystalline phase | 144 |
| Short range order of the octahedrally co-ordinated titanium | 400-410 |
| Short range order of the octahedrally co-ordinated titanium | 600-630 |

**Table 5.2:** Elemental analysis of 1 wt% Au/$TiO_2$ (non-refluxed, 30 min water reflux, and 60 min water reflux).[23]

| Elemental Analysis | Non-refluxed (wt%) | 30 min Reflux (wt%) | 60 min Reflux (wt%) |
|---|---|---|---|
| **Carbon** | 0.59 | 0.57 | 0.44 |
| **Gold** | 1.02 | 1.01 | 1.02 |

**Table 5.3:** Carbon content of 1 wt% Au/$TiO_2$ non-treated, and calcined samples (200, 300 and 400 ºC calcined in air).[23]

| Calcination temperature | Non-treated | 200 °C | 300 °C | 400 °C |
|---|---|---|---|---|
| **Carbon (wt%)** | 0.59 | 0.25 | 0.04 | 0.03 |

It could be expected that the heat treatment method of removing the PVA from the catalyst will prove to be the most efficient, since this is one of the main methods used in the literature for removing such stabilising ligands. From Raman spectroscopy (Figure 5.2) and elemental analysis (Table 5.3) it is clear that this is the case for the 1 wt% $Au/TiO_2$ catalysts calcined at various temperatures. It seems that a temperature of 200 °C is not sufficient enough to remove large amounts of PVA from the catalyst, as there is only a minor decrease in intensity of the characteristic PVA bands when compared with the non-treated catalyst. However, by increasing the calcination temperature above 300 °C, there is clear increase in the amount of PVA removed. Elemental analysis (Table 5.3) shows that there is virtually no carbon left on the catalyst calcined at 300 °C (0.04 wt%) and 400 °C (0.03 wt%). Further insight into the temperature required to remove the PVA was determined using thermogravametric analysis (TGA) (Figure 5.3), which was confirmed to be 300-400 °C.

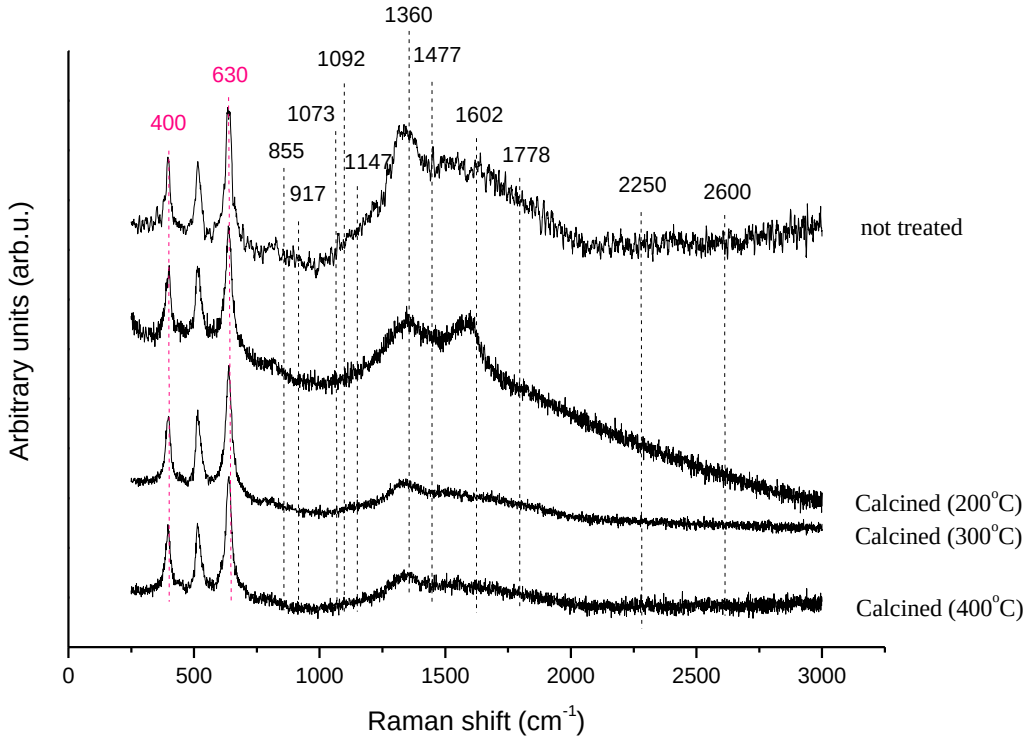


**Figure 5.2:** Raman spectra for the calcined series of 1 wt% $Au/TiO_2$ , 1 wt% $Au/TiO_2$ – non-treated, 1 wt % $Au/TiO_2$ – calcined at 200 °C, 1 wt% $Au/TiO_2$ – calcined at 300 °C, 1 wt% $Au/TiO_2$ – calcined at 400 °C.[23] (Analysis repeated by Gareth Whiting)

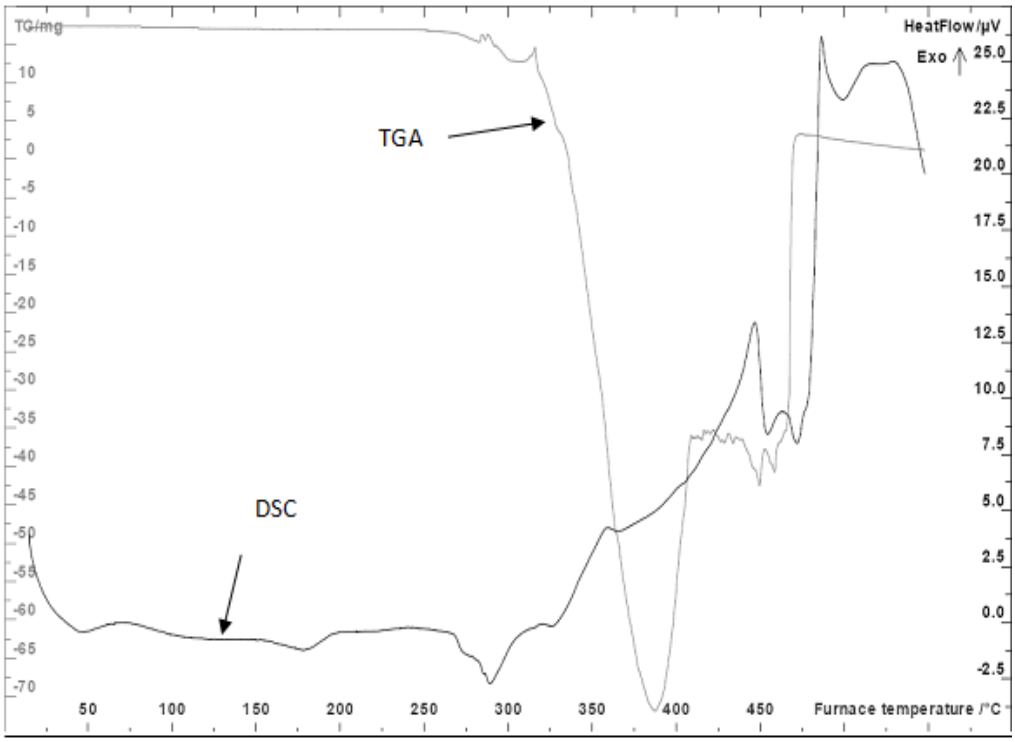


**Figure 5.3:** TGA analysis of a 1 wt% $Au/TiO_2$ catalyst prepared using PVA.[23]

A major disadvantage of using heat treatment to remove the stabilising ligand, is that it often causes the gold nanoparticles to sinter, which usually reduces the activity of the catalysts. To explore whether this was the case for the solvent extraction treated catalysts (and to confirm sintering with the heat treated series of catalysts), scanning transmission electron microscopy (STEM) analysis was used to determine the gold particle size in the 1 wt% $Au/TiO_2$ catalysts. (Provided by Dr. Christopher Kiely – Lehigh University)

A high angle annular dark field (HAADF) image of the starting Au-PVA colloid (drop of the colloidal sol deposited on the mount from solution) is shown in Figure 5.4a, and the corresponding particle size distribution is shown in Figure 5.4b, where the median gold nanoparticle size is 2.7 nm.

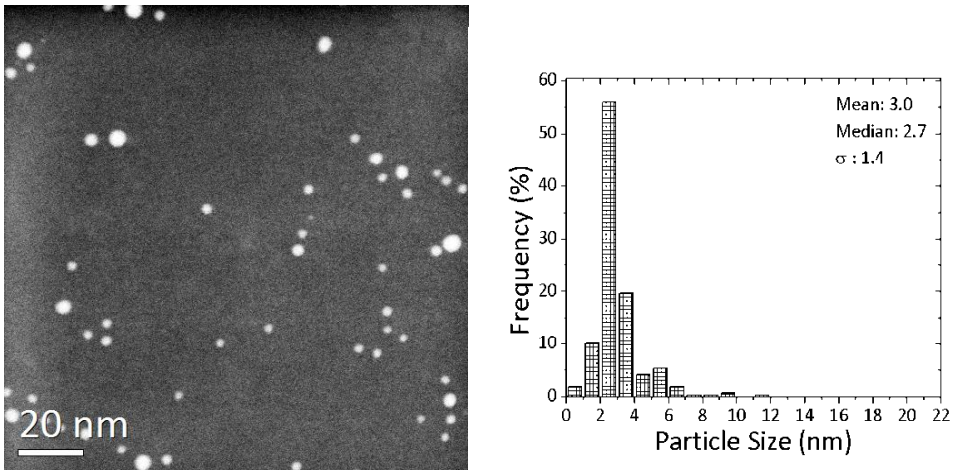


**Figure 5.4:** (**a**) HAADF image of the starting Au/PVA colloid *(left)*; (**b**) corresponding particle size distribution *(right)*.[23]

The HAADF image of the starting Au-PVA colloid immobilized on $TiO_2$, and then dried at 120 °C with corresponding gold particle size distribution, is shown in Figure 5.5a and 5.5b respectively. The median particle size has increase to 3.5 nm (compared to the non-dried Au-PVA colloid), which is probably due to the heat treatment when drying at 120 °C, but the deposition on the support could also have a role in effecting the particle size. Atomic resolution HAADF images of the Au particles in this sample presented in Figure 5.6(a-c), show that they display a mixture of cub-octahedral (Figure 5.6a), singly twinned (Figure 5.6b) and multiply twinned (Figure 5.6c) morphologies, with the twinned variants predominant.

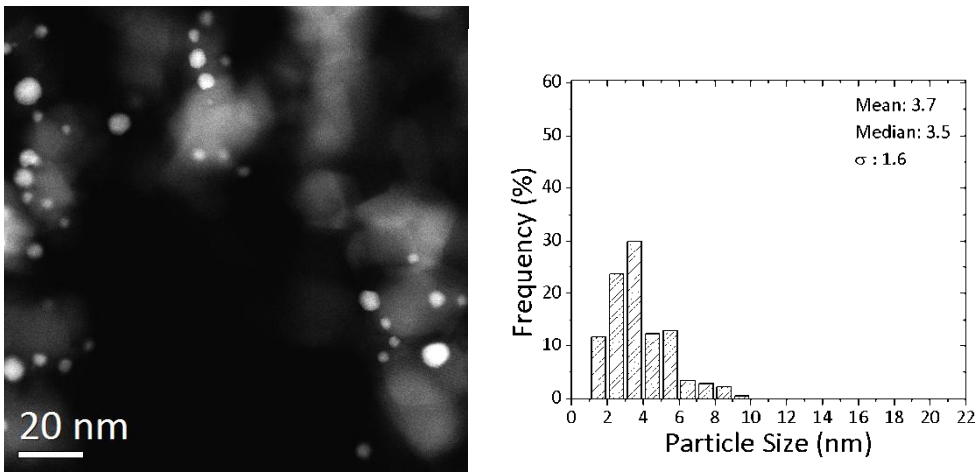


**Figure 5.5:** (**a**) HAADF image of 1wt% Au/$TiO_2$ immobilized & dried at 120 °C *(left)*; (**b**) corresponding particle size distribution *(right)*.[23]

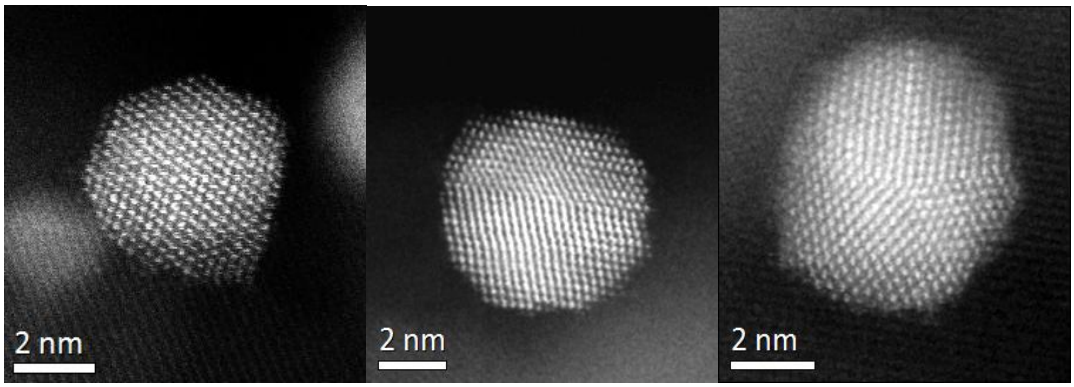


**Figure 5.6a, b & c:** HAADF STEM images of the immobilized sol on $TiO_2$ dried at 120 °C showing characteristic (**a**) cub-octahedral *(left)*, (**b**) singly twinned *(centre)* and (**c**) multiply twinned *(right)* morphologies.[23]

Representative low magnification HAADF images of the Au immobilized on $TiO_2$, and water refluxed at 90 °C for time periods of 30, 60 and 120 min, are presented in Figures 5.7a, 5.8a and 5.9a respectively, with the corresponding particle size distribution shown in Figures 5.7b, 5.8b and 5.9b respectively. From the particle size distributions, it is clear to see that the longer the reflux reaction time, the larger the particle size: 30 min (3.7 nm), 60 min (4.2 nm) and 120 min (5 nm). After refluxing for 30 min, there was only a slight increase in the median particle size (3.7 nm) compared with the standard dried (120 °C) immobilized catalyst (3.5 nm).

When looking at Raman spectroscopy (Figure 5.1) and carbon analysis data (Table 5.2) where only a slight decrease in carbon wt% is observed after refluxing for 30 min (0.57 to 0.55 wt%), it is then reasonable to suggest that 30 minutes is not long enough to remove the PVA, and so, allow the particles to coalesce. Refluxing for 60 min at 90 °C appears to be the optimum conditions. A significant amount of PVA is removed (Table 5.2 & Figure 5.1), with only a minor increase in median particle size from 3.5 to 4.2 nm.

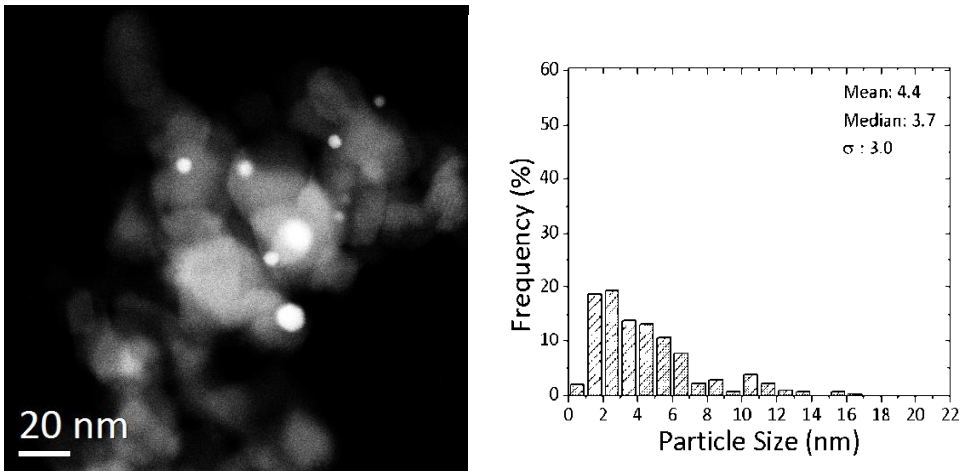


**Figure 5.7a (*left)* & 5.7b (*right)*:** Low magnification STEM-HAADF image of Au immobilized on $TiO_2$ & water refluxed at 90 °C, 30 min with corresponding particle size distribution.[23]

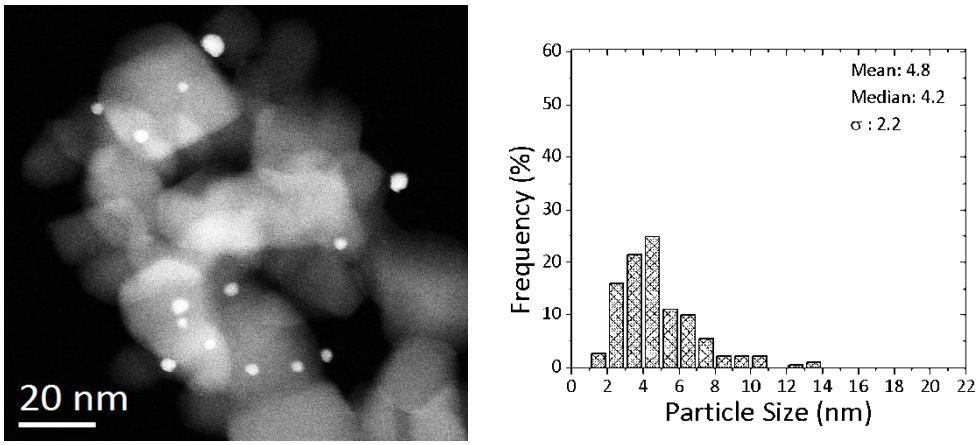


**Figure 5.8a (*left)* & 5.8b (*right)*:** Low magnification STEM-HAADF image of Au immobilized on $TiO_2$ & water refluxed at 90 °C, 60 min with corresponding particle size distribution.[23]

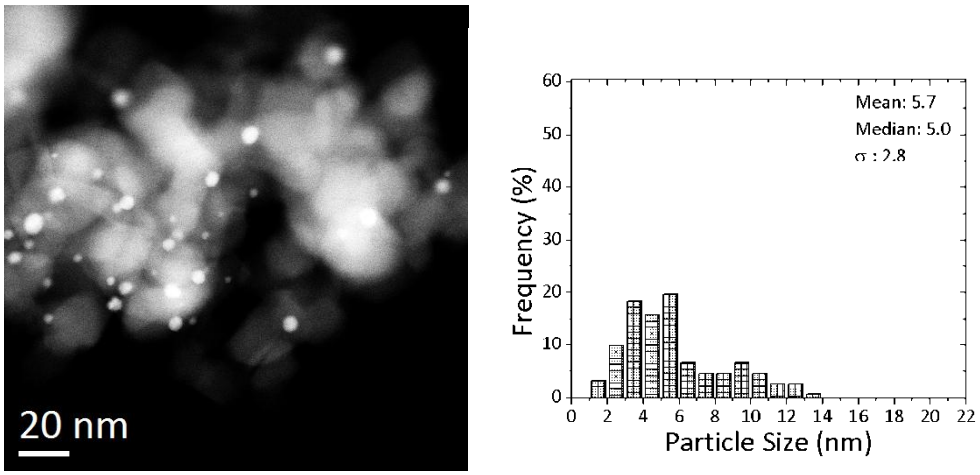


**Figure 5.9a (*left)* & 5.9b (*right)*:** Low magnification STEM-HAADF image of Au immobilized on $TiO_2$ & water refluxed at 90 °C, 120 min with corresponding particle size distribution.[23]

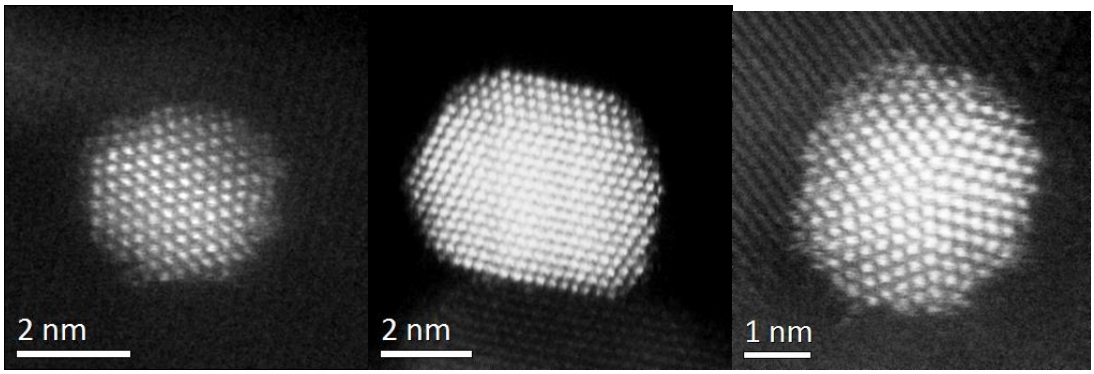


**Figure 5.10 a (*left),* b (*middle)* & c *(right)*:** Representative atomic resolution HAADF STEM images of the immobilized sol on $TiO_2$ refluxed at 90 °C, 60 min showing characteristic (**a**) cub-octahedral, (**b**) singly twinned and (**c**) multiply twinned morphologies.[23]

The mild water reflux treatment has a minor influence on the gold particles, with the atomic resolution HAADF images (Figure 5.10 (a-c)) indicating that the cub-octahedral, singly twinned and multiply twinned particles are still present after refluxing for 60 minutes. As stated previously, it is expected that the gold particle size will increase upon heat treatment, with increasing temperature producing increasingly large particles. Using HAADF STEM, it was possible to image this trend for the calcined 1 wt% $Au/TiO_2$ series (200, 300 & 400 °C). At a moderate temperature of 200 °C (Figures 5.11a & b), the median particle size has increased from 3.5 nm to 4.7 nm. Although the temperature is moderate, Raman spectroscopy and carbon analysis (Figure 5.2 & Table 5.3) showed that around half of the PVA had been removed which is enough for the particles to coalesce slightly. After heat treatment at 300 °C the median particle size increased to 5.1 nm (Figure 5.12a & b) and calcining at 400 °C caused the particle size to increase greatly to 10.2 nm. This is a major increase, and confirms that the gold particles sinter at high temperature, which contradicts the effect of using the PVA to keep the small particles.

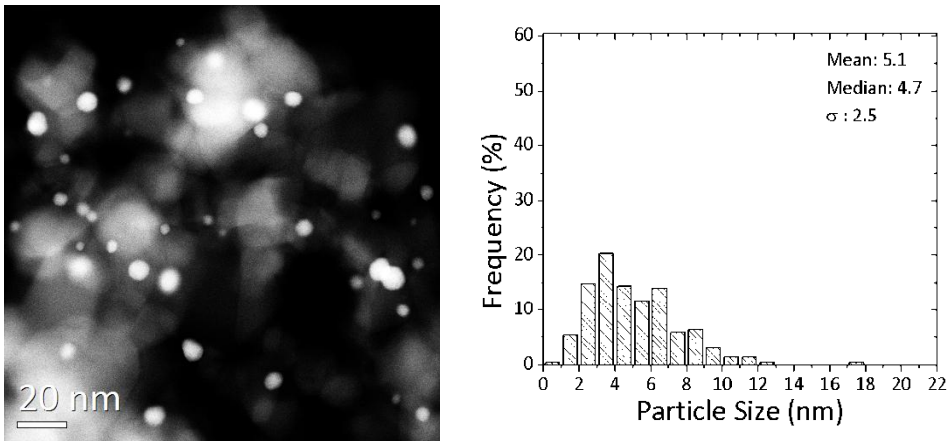


**Figure 5.11a (*left)* & b (*right)*:** Low magnification STEM-HAADF image of Au immobilized on $TiO_2$ & calcined for 3 h at 200 °C with corresponding particle size distribution.[23]

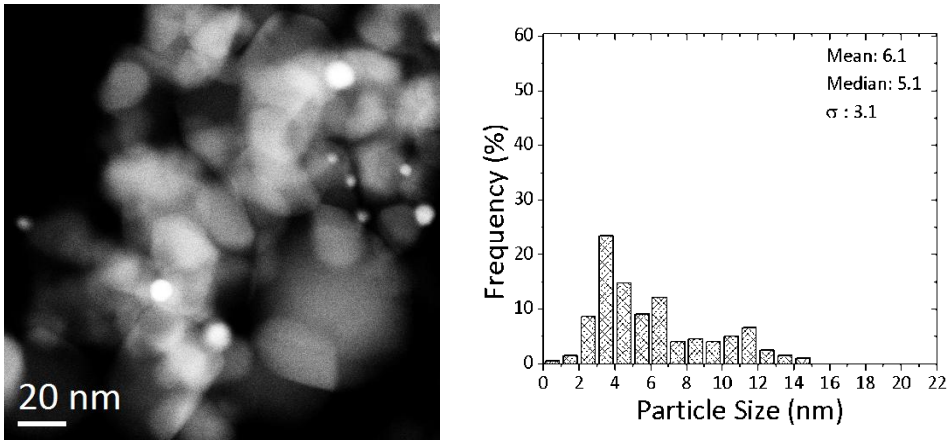


**Figure 5.12a (*left)* & b (*right)*:** Low magnification STEM-HAADF image of Au immobilized on $TiO_2$ & calcined for 3 h at 300 °C with corresponding particle size distribution.[23]

Atomic resolution HAADF images of the samples heat treated at different temperatures show that they retained a mixture of cub-octahedral, decahedral and icosahedral gold particles. However, the distribution of the different gold particle morphologies changed from the non-treated sample, and the cub-octahedral morphology became more dominant as the calcination temperature was increased. It is also noticeable that the heat treated samples showed an increased tendency to form flatter and more extended interface structures with the underlying $TiO_2$ support particles with temperature (Figure 5.14 a-c).

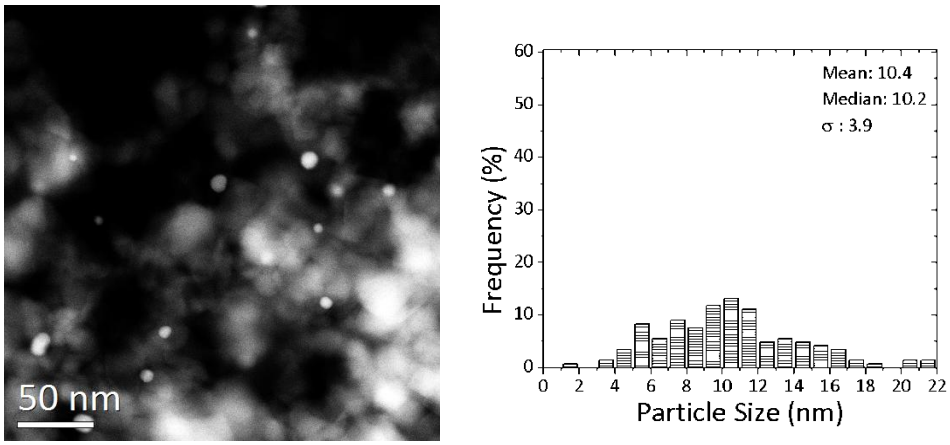


**Figure 5.13a (*left)* & b (*right)*:** Low magnification STEM-HAADF image of Au immobilized on $TiO_2$ & calcined for 3 h at 400 °C with corresponding particle size distribution.[23]

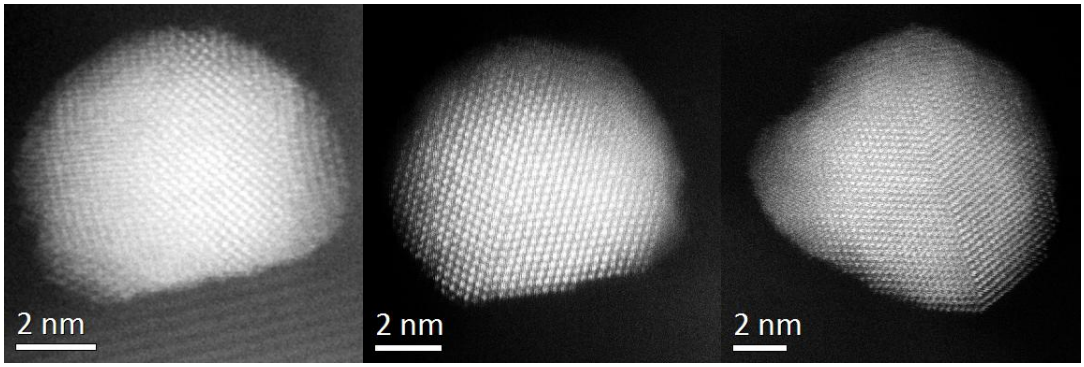


**Figure 5.14a (*left),* b *(middle)* & c *(right):*** Representative atomic resolution HAADF STEM images of the immobilized sol on $TiO_2$ calcined at 400 °C.[23]

As expected, the solvent extraction treatment of the 1 wt% $Au/TiO_2$ catalysts provided sufficient removal of the stabilising ligand, PVA, whilst maintaining reasonably small gold particle size, with an optimum reflux time of 60 minutes. The heat treatment method of removing the PVA resulted in considerably larger gold particle size than the solvent extraction method, with higher temperatures forcing the greater particle size.

## 5.3 - CO oxidation

To understand how the removal of the PVA stabilising ligand (in various amounts depending on treatment method) affected the activity of the catalysts, carbon monoxide oxidation was used as a test reaction. $Au/TiO_2$ is a widely reported catalyst for this

reaction, known for its high activity, with smaller nanoparticles of gold (<5 nm) being highly favourable.

### *5.3.1 – Water reflux treatment*

CO oxidation at ambient temperature is greatly influenced by the size of the gold nanoparticles on the particular support, with larger gold particles (>5 nm) less efficient for the reaction.[2-6] In theory, the water reflux treated 1 wt% Au/$TiO_2$ catalysts should have much higher activity than the heat treated catalysts, as the gold nanoparticle size is much smaller compared to the heat treated catalyst series, which have substantially increased particle size, for example; 60 min reflux treatment at 90 °C producing a median particle size of 4.2 nm, compared to a heat treatment of 400 °C for 3 hours giving a median particle size of 10.2 nm (Figures 5.7b-5.13b). As the 1 wt% Au/$TiO_2$ water refluxed catalysts were prepared under a range of conditions such as reflux temperature, amount of solvent used and time of reflux, the full range of catalysts were tested for CO oxidation to determine the optimum conditions of catalyst preparation using this treatment method.

To discover the reflux temperature which produces the highest activity for CO oxidation, a range of temperatures were used from 60 – 100 °C. Figure 5.15 shows that the catalyst treated at 90 °C for 60 min gave 100 % CO conversion. The general trend states that low reflux temperatures seem to be insufficient to remove the PVA from the surface of the catalyst, therefore exposing less active sites for CO oxidation and hence, reducing activity (*i.e.* 60 °C reflux gave 34 % CO conversion).

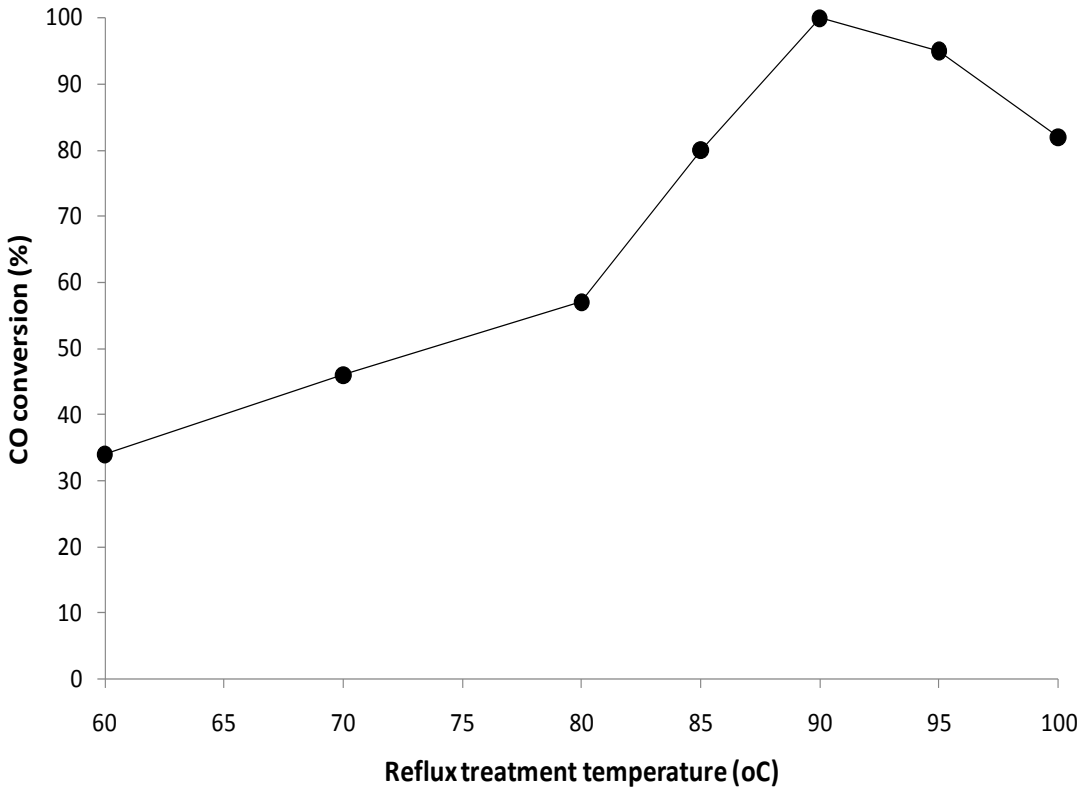


**Figure 5.15:** Comparison of water reflux temperature with catalyst activity for CO oxidation: GHSV of 6,000 $h^{-1}$, catalyst (50 mg) reflux time 60 min. [23] (Test repeated by Gareth Whiting)

The amount of water used during the reflux pre-treatment was varied to determine the effect on the catalyst activity. A low volume of solvent (50 mL) produced the lowest CO conversion (40 %), with a high conversion (70 %) reached with a volume of 200 mL or above. (Figure 5.16 – catalysts prepared and tested by Ceri Hammond).

Considering that water reflux treatment at 90 °C produced the most active catalyst (Figure 5.15), the optimum conditions for the CO oxidation reaction were studied using this pretreatment step (Figure 5.17 - prepared and tested by Ceri Hammond). By altering the flow rate of CO to achieve gas hourly space velocities (GHSVs) between 12,000 $h^{-1}$ and 6,000 $h^{-1}$, it was observed that low flow rates lead to an increase in activity of the catalyst, which is to be expected.

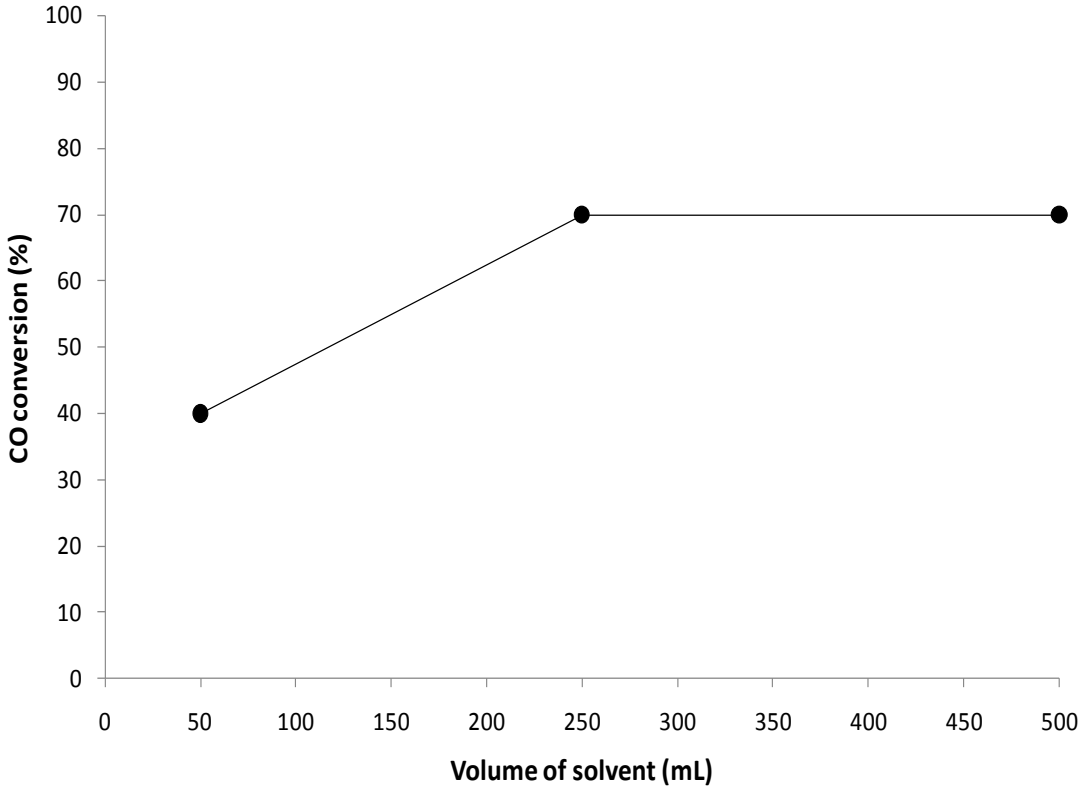


**Figure 5.16:** Effect of volume of reflux solvent used on CO oxidation performance for PVA stabilized 1wt% $Au/TiO_2$ catalyst. Reaction conditions: GHSV of 12,000 $h^{-1}$ catalyst (50 mg). (Prepared and tested by Ceri Hammond).[23]

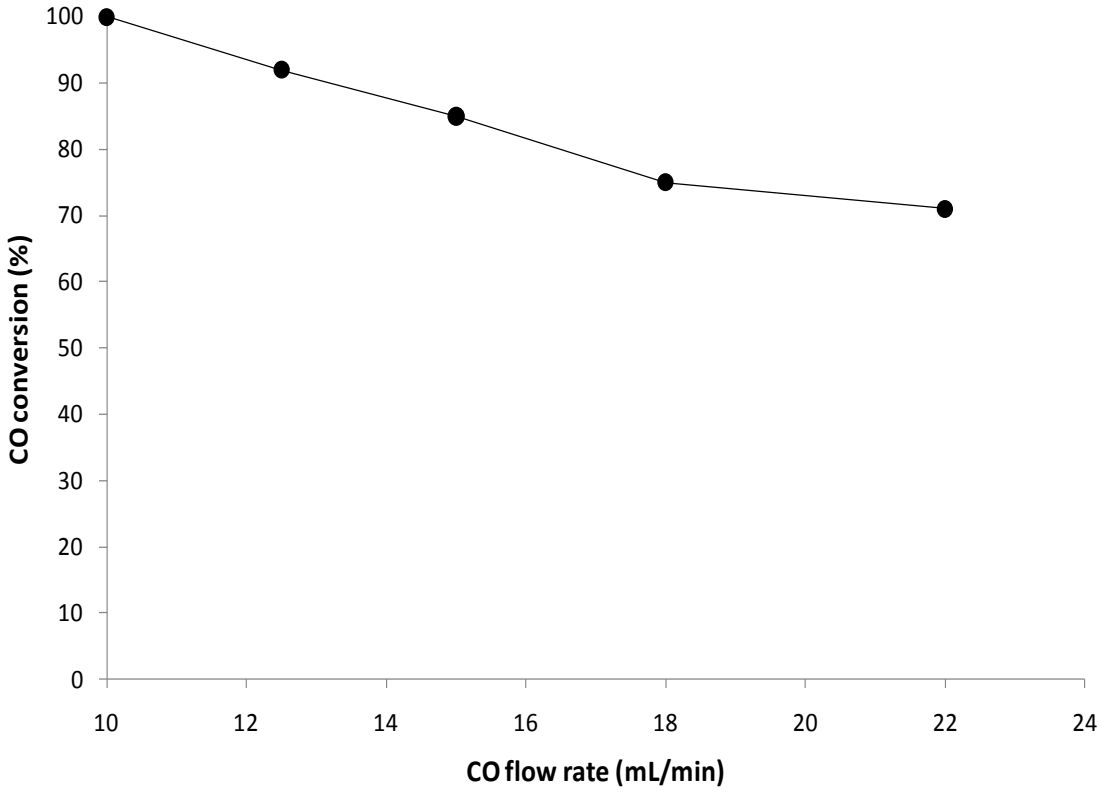


**Figure 5.17:** Effect of varying flow rate for CO oxidation on a standard Au-PVA/$TiO_2$ catalyst refluxed at 90 °C in water for 60 min. GHSV between 12,000 $h^{-1}$ and 6,000 $h^{-1}$ catalyst (50 mg). (Prepared and tested by Ceri Hammond).[23]

Particle size distributions of the catalysts refluxed in water for different time periods (Figure 5.7b - 5.9b), confirmed that a short reflux time (30 min) produced the smaller median particle size (3.7 nm), with longer reflux times *i.e.* 120 min, producing a larger median particle size (5 nm). Considering that CO oxidation is heavily influenced by gold particle size, it could be expected that the lower reflux times which give the smallest nanoparticles will produce the highest catalytic activity. However, the CO oxidation results (Figure 5.18) show the trend is the opposite, with the order of activity: non-refluxed <30 min <60 min <120 min. This can only be attributed to the amount of PVA remaining on the surface blocking active sites needed for the oxidation reaction to take place. Shorter reflux times removed less PVA than longer reflux times, as seen from the carbon analysis (Table 5.2) of the materials and Raman spectroscopy (Figure 5.1).

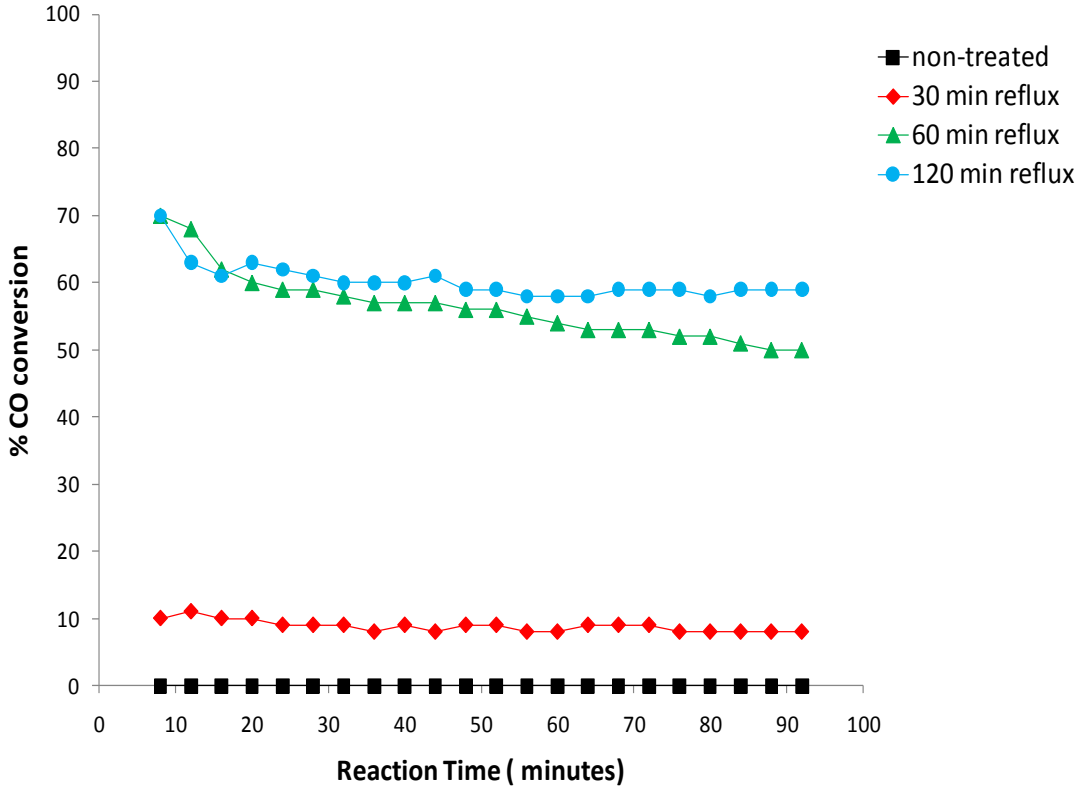


**Figure 5.18:** Comparison of reflux time with water: ■ non-treated, ♦ 30 min, ▲ 60 min, ● 120 min.[23]
(Catalytic tests repeated by Gareth Whiting)

### *5.3.2 – Heat treated catalysts*

It has been previously reported that heat treatment of $Au/TiO_2$ catalysts causes the Au nanoparticle size to increase greatly with increasing temperature, due to sintering of the particles.[7] This has proved to have a detrimental effect on catalyst activity for CO oxidation, with larger particles proving inactive catalysts for the reaction. Therefore, it is expected that the heat treated series of 1 wt% $Au/TiO_2$ catalysts will not be as active as the water reflux treated catalysts, which maintain a low Au nanoparticle size after treatment.

Catalytic testing was performed under reaction conditions (described in Chapter 2), that allow differences in activity to be clearly observed (*i.e.* not total CO conversion). However, further studies have shown that conditions can be optimized to achieve total CO conversion for the water reflux-treated catalyst, unlike the heat-treated or non-treated PVA coated samples.

It is clear from Figure 5.19 that the activity of the heat treated catalysts was low (<10 % conversion), with >40 % conversion of CO for the water refluxed catalyst. This is coherent with the characterization data (Figure 5.8b, 5.11b, 5.12b and 5.13b), which shows that the gold nanoparticle size of the heat treated samples is much higher than in the water reflux treated samples, which lowers the activity of the catalysts.

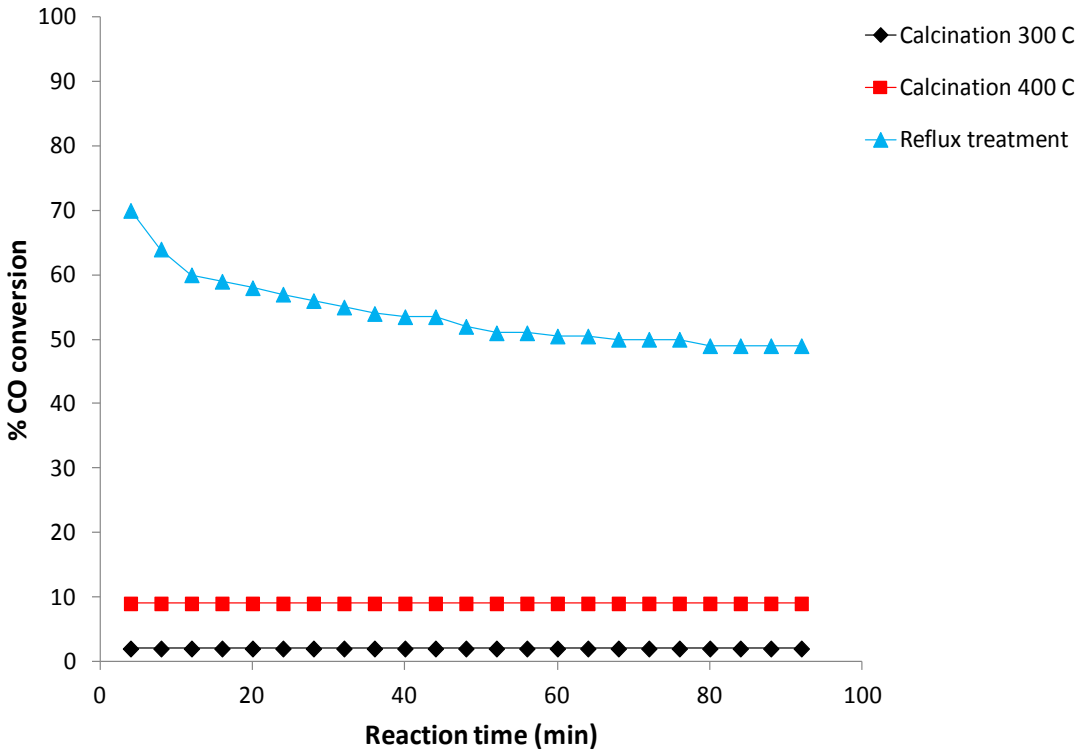


**Figure 5.19:** Comparison of CO conversion activity for catalysts prepared using: ▲ reflux treatment; and air oxidation at: ♦ 300 °C; ■ 400 °C (calcined in flowing air at 300 & 400 °C for 3 h), GHSV of 12,000 $h^{-1}$, catalyst (50 mg).[23] (Catalytic tests repeated by Gareth Whiting)

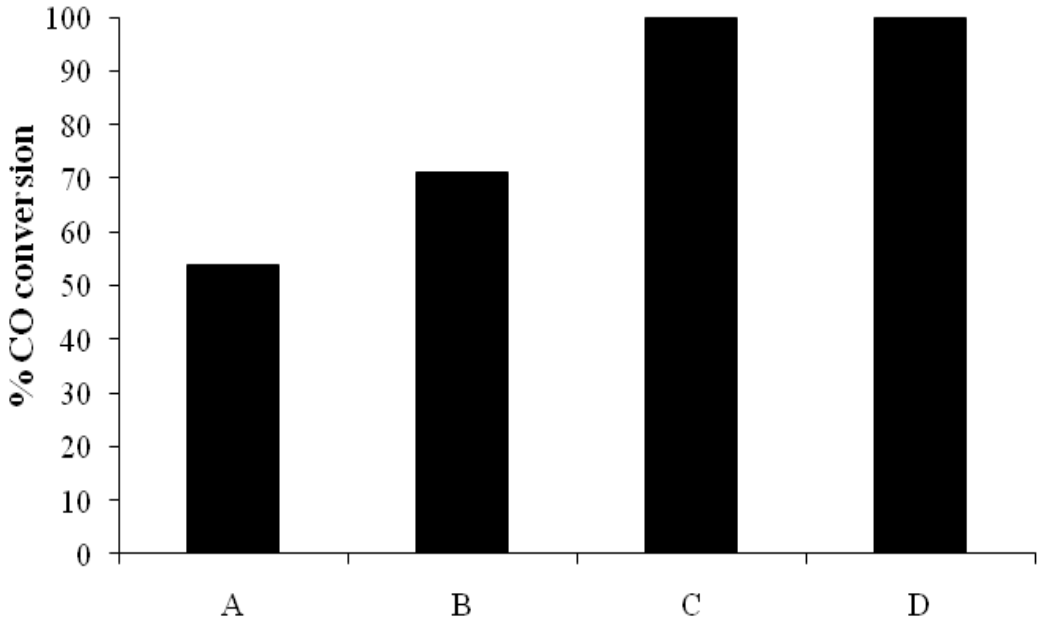


**Figure 5.20:** Catalytic activity of 1 wt% $Au/TiO_2$ after a series of pre-treatments. Entry A: Calcination (200 °C, 3 h, static air), B: Reflux (90 °C, 1 h), C: Reflux and calcination (200 °C, 3 h, static air); D: Reflux and heat treatment with $H_2$ (200 °C, 3 h, 5 % $H_2$/Ar), GHSV = 24000 $h^{-1}$, catalyst (50 mg). (Catalysts prepared and tested by Saul White).[23]

Comotti *et al.*[24] discovered that by testing 1 wt% $Au/TiO_2$ for CO oxidation in catalytic cycles (prepared using PVA under similar conditions to the materials prepared here) produced substantially increased activity upon each additional cycle. Further investigation suggested that the water reflux treated $Au/TiO_2$ needs to be thermally activated to improve the activity. By calcining the 1 wt% $Au/TiO_2$ catalyst in air for 4 h, and then undergoing CO oxidation cycling, no change was noted between the initial and following runs, contributing to Comotti *et al.* theory that the organic matter *i.e.* PVA on the surface of the catalyst inhibits the activity of the catalyst and upon thermal activation is removed. As seen by the carbon analysis (Table 5.3) for the heat treated catalysts prepared here, large amounts of PVA are removed by this treatment process, agreeing with Comotti *et al.* theory. To study whether the activity of the solvent extraction treated catalysts could be improved by thermal activation for CO oxidation, 1 wt% $Au/TiO_2$ catalysts refluxed at 90 °C for 60 minutes underwent a range of thermal treatment conditions. (Figure 5.20). By heating the reflux treated catalyst in air at 200 °C for 3 h and also heating a reflux treated catalyst in hydrogen at 200 °C for 3 h, before testing for CO oxidation. As expected, there is a visible increase (Figure 5.20) in activity for the thermally activated catalysts compared to standard reflux treated catalysts and standard heat treated catalysts, agreeing with Comotti *et al.* that PVA inhibits the activity of the catalyst. Carbon analysis further supports this theory whereby, a further ~50 % of PVA is removed (Table 5.3) when comparing the amount of carbon remaining in the reflux treated catalyst (0.44 %) to the catalyst heat treated at 200 °C (0.25 %).

## 5.4 - Selective methanol oxidation to methyl formate

In the past five years, there has been an increasing interest in the use of gold based catalysts for use in the selective oxidation of methanol, towards products such as methyl formate[14-16,25] and hydrogen.[26] As with CO oxidation, mono-metallic $Au/TiO_2$, and now bi-metallic $Au(Pd)/TiO_2$ catalysts, have been prepared using the same heat and solvent extraction treatments, and tested for methanol oxidation, to observe the effect that PVA removal and Au nanoparticle size have on catalytic activity and selectivity.

### *5.4.1 – Effect of reaction conditions on catalytic activity*

#### *5.4.1.1 - Mono-metallic $Au/TiO_2$*

The mono-metallic $Au/TiO_2$ catalyst refluxed in water at 90 °C for 60 minutes proved to have superior CO oxidation activity compared to the catalysts refluxed at other temperatures and time periods (Figure 5.15). Therefore this catalyst was initially chosen to compare to the catalytic activity of heat treated, and the non-treated catalysts. As the median particle size distribution shows (Figure 5.8b, Figures 5.11b-13b), there was a clear increase in gold particle size for the heat treated catalysts when compared with the non-treated and water refluxed catalysts. Although gold particle size is known to have a significant impact on CO oxidation activity, the effect of particle size on catalytic activity for methanol oxidation has not yet been reported.

For an initial test, the non-treated, heat treated series and water refluxed (90 °C/60 min) $Au/TiO_2$ catalysts were tested, using a methanol to oxygen feed ratio of 1:2. Figure 5.21a shows that the catalytic activity of both treated and non-treated catalysts at low temperatures (<100 °C) are extremely low (<10 % conversion). At 150 °C, a clearer indication of the comparable activity was noticeable. The $Au/TiO_2$ catalyst heat treated at

200 °C showed the highest activity (29 % conversion), followed be the non-treated catalyst (13 % conversion), with the water refluxed catalyst producing the poorest activity (10 % conversion). Total conversion is achieved by all $Au/TiO_2$ catalysts by 200 °C. The main product produced by each catalyst at low temperature (<150 °C) is methyl formate (Figure 5.21b), with the main product being CO at higher temperatures.

As the selectivity towards methyl formate decreases so dramatically at temperatures >100 °C, studies were carried out changing the mass of catalyst, oxygen concentration in the feed, and adjusting the total flow rate over the catalyst.

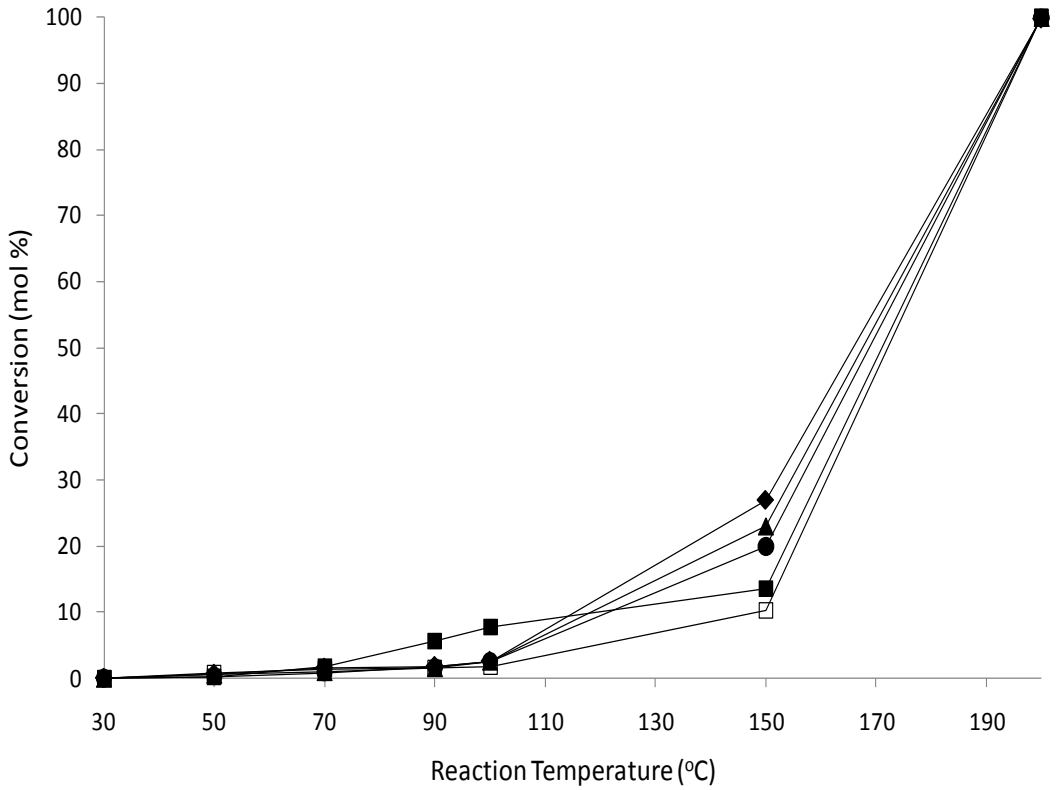


**Figure 5.21a:** Methanol conversion over $Au/TiO_2$ catalysts prepared using sol immobilization, but treated in various methods. (5 % MeOH; 10 % $O_2$; 85 % He).

■ = Non-treated; □ = Reflux (90 °C/60 min); ◆ = Calcined 200 °C; ▲ = Calcined 300 °C; ● = Calcined 400 °C.

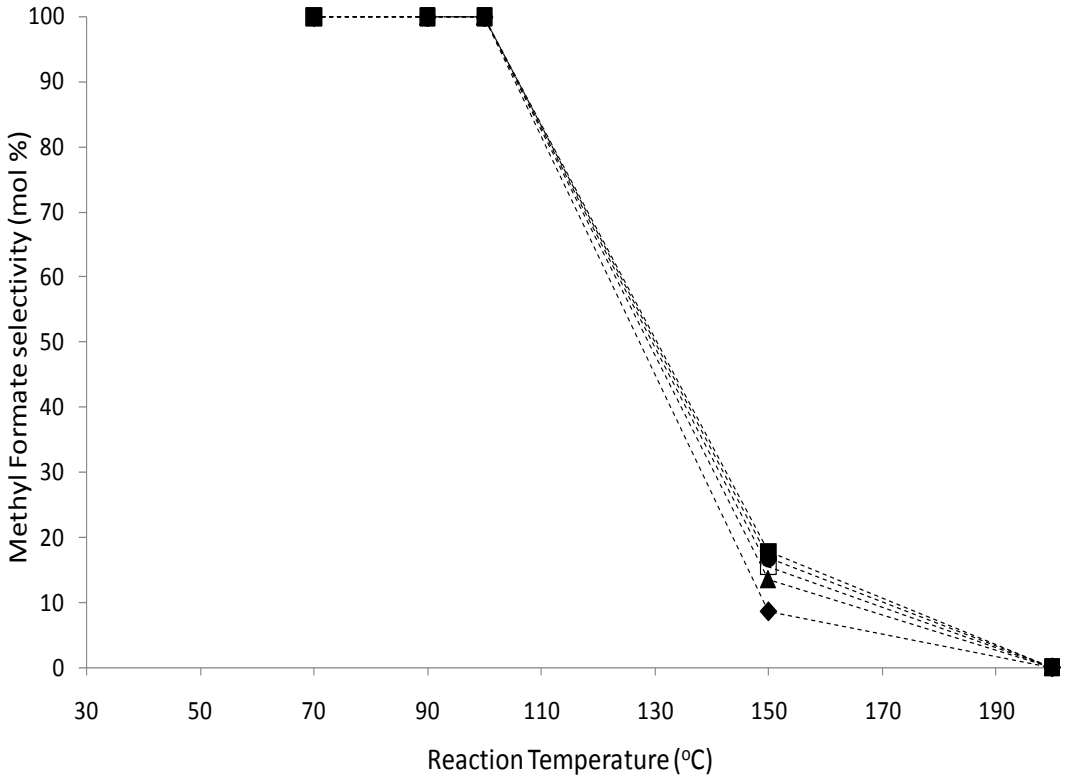


**Figure 5.21b:** Methyl formate selectivity produced using 1 wt% $Au/TiO_2$ catalysts treated using various methods.

= Non-treated; = Reflux (90 °C/60 min); = Calcined 200 °C;
= Calcined 300 °C; = Calcined 400 °C.

To observe the effects of these changes under reaction conditions, the same catalyst was used, 1 wt% $Au/TiO_2$ (90 °C/60 min). By reducing the amount of oxygen in the feed from 10 vol% to 2.5 vol% (to achieve a methanol to oxygen ratio of 2:1), the methyl formate selectivity at temperatures >100 °C increased substantially for the majority of $Au/TiO_2$ catalysts (Figure 5.22b) although, as expected, due to the lower amount of oxygen present in the feed, the catalytic activity of each catalyst at temperatures above 150 °C dramatically decreased (Figure 5.22a). In most cases a 70 % loss of activity was recorded compared to the activity of the same catalysts when using a methanol to oxygen ratio of 1:2 (Figure 5.21a). However, at 150 °C or below, the catalytic activity was maintained (compared to the 10 vol% oxygen conditions), and an increase in methyl formate selectivity is achieved. By adjusting the mass of catalyst used, and altering the total flow

rate of the reactant feed, a minimal change in methyl formate selectivity was recorded, with a large increase of methanol conversion for each catalyst. Therefore, a methanol to oxygen ratio of 2:1 was determined as the optimum reaction conditions with a total flow rate of 60 ml/min.

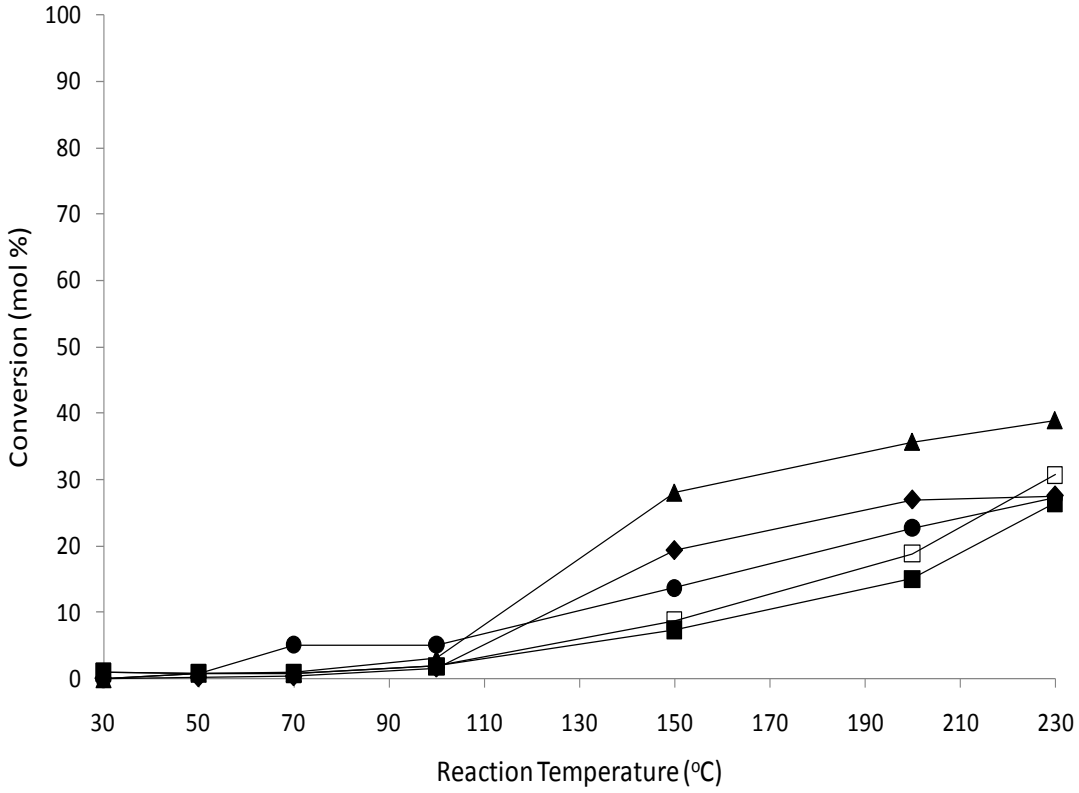


**Figure 5.22a:** Methanol conversion over $Au/TiO_2$ prepared using various treatment methods. (5 % MeOH; 2.5 % $O_2$; 92.5 % He).

= Dried; = Reflux (90 °C/60 min); = Calcined 200 °C; = Calcined 300 °C; = Calcined 400 °C.

Figure 5.22a shows that the highest activity was seen for the heat treated catalysts. The low activity of the reflux treated catalyst and the non-treated catalyst, (as well as the gold particle size distribution studies on each of the samples), suggest that small gold nanoparticles are not as important for the oxidation of methanol. The amount of PVA covering the surface could also play a major role in catalytic activity. Carbon analysis of the fresh non-treated, heat treated and water refluxed 1 wt% $Au/TiO_2$ catalysts (Tables

5.2 and 5.3) shows that a substantial amount of PVA still remains on the non-treated (0.59 wt%) and water refluxed catalyst (0.44 wt%) compared to the 200 °C (0.25 wt%) and 300 °C (0.04 wt%) heat treated catalysts.

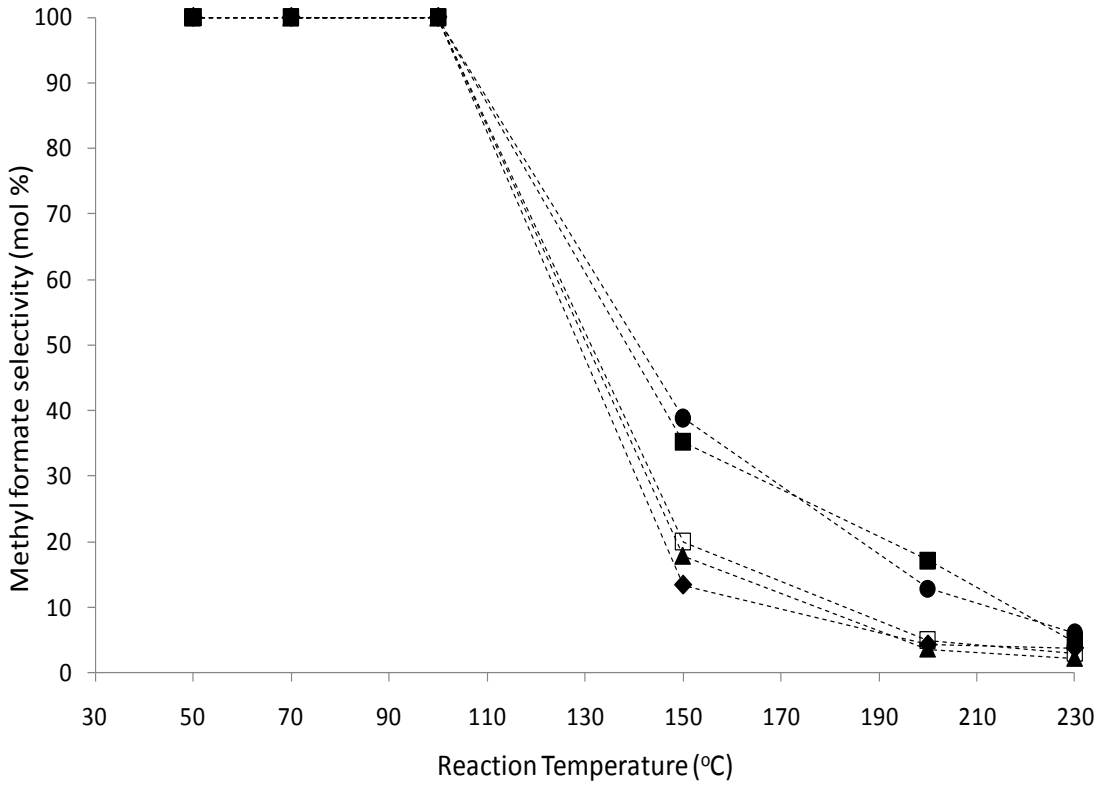


**Figure 5.22b:** Methyl formate selectivity produced using $Au/TiO_2$ catalysts treated using various methods.

-■- = Non-treated; -□- = Reflux (90 °C/60 min); -◆- = Calcined 200 °C; -▲- = Calcined 300 °C; -●- = Calcined 400 °C.

Unlike the CO oxidation reaction which is performed at a consistently low temperature, the oxidation of methanol undergoes a temperature increase throughout the experiment. Therefore, an *in situ* heat treatment of each material can be said to occur as the reaction takes place, and as with previous CO oxidation results (and also recorded by Comotti *et al.*[24]), thermal activation removes PVA from the catalyst. It would therefore be reasonable to suggest that the activity of the water refluxed 1 wt% $Au/TiO_2$ would be similar to the activity of the 200 °C heat treated catalyst at a reaction temperature of

200 °C, however this is not the case, with the heat treated catalyst achieving higher activity than the reflux treated catalyst.

### *5.4.1.2 - Bi-metallic Au(Pd)/$TiO_2$*

The use of palladium based catalysts has been reported in the literature for the elecrocatalytic oxidation of methanol.[20-22] These bi-metallic Au(Pd)/$TiO_2$ treated and non-treated series of catalysts were found to have a dramatically lower activity than the mono-metallic Au/$TiO_2$ catalysts for CO oxidation. However, for many oxidation reactions Au(Pd) catalysts are known to have a higher activity than mono-metallic Au catalysts and so bi-metallic Au(Pd)/$TiO_2$ catalysts prepared using the same methodology as the Au/$TiO_2$ catalysts were studied for the partial oxidation of methanol.

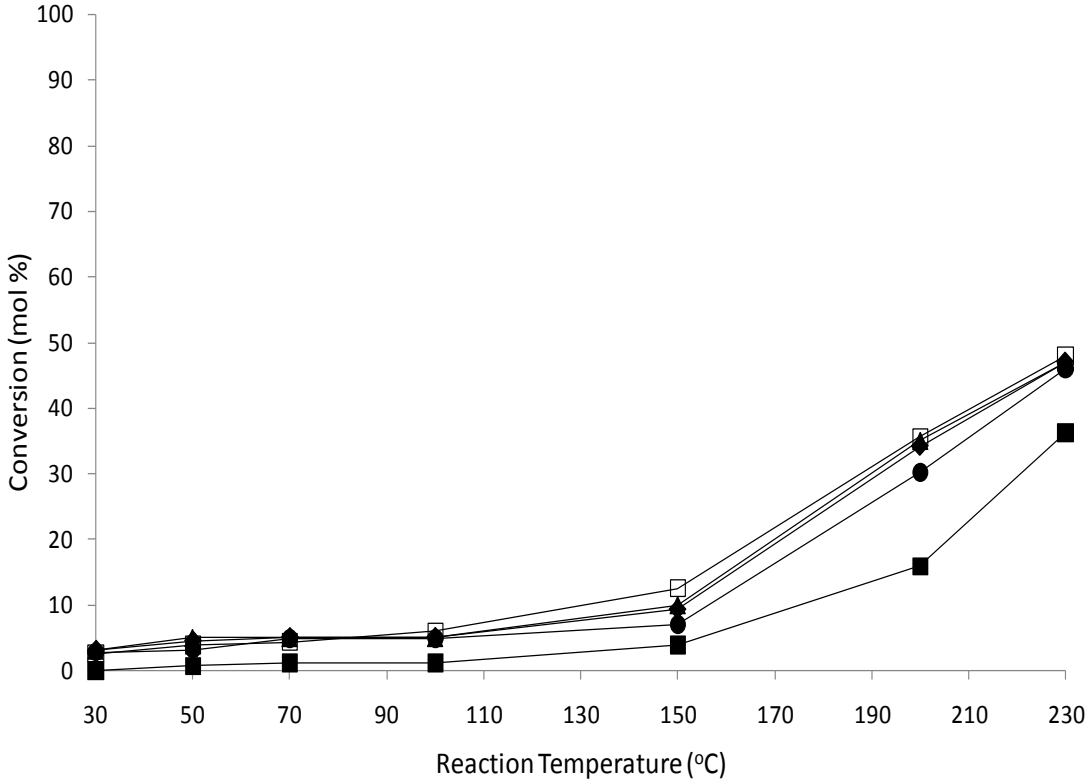


**Figure 5.23a:** Methanol conversion over Au(Pd)/$TiO_2$ prepared using various treatment methods. (5 % MeOH; 2.5 % $O_2$; 92.5 % He).

■ = Non-treated; ⊟ = Reflux (90 °C/60 min); ◆ = Calcined 200 °C; ▲ = Calcined 300 °C; ● = Calcined 400 °C.

Figure 5.23a shows the catalytic activity of non-treated, heat treated, and solvent extraction treated Au(Pd)/$TiO_2$ catalysts. It is clear that there is a synergistic effect for the bi-metallic catalysts, as the catalytic activity was higher at lower temperatures (<100 °C) than the corresponding mono-metallic Au/$TiO_2$ catalysts. The most interesting result was the activity of the water reflux (90 °C/60 min) treated Au(Pd)/$TiO_2$ catalyst which achieved the highest activity compared to the non-treated and heat treated catalysts, whilst maintaining a higher methyl formate selectivity than the other catalysts (Figure 5.23b). The non-treated catalyst showed the lowest activity, with only 4 % methanol conversion at 150 °C compared to the 13 % conversion achieved by the reflux treated catalyst. As with the mono-metallic catalysts, this result probably indicates that the remaining PVA on the catalysts surface (of the non-treated material) blocks the potential active sites. The heat treated catalysts all maintain similar activity throughout, with the 400 °C treated catalysts showing lower activity than the 200 and 300 °C treated catalysts, possibly due to the larger gold/palladium particle size.

Noticeably with these bi-metallic Au(Pd)/$TiO_2$ catalysts, is their improved activity compared to the mono-metallic Au/$TiO_2$ catalysts at temperatures of 50 °C or below, with 100 % selectivity to methyl formate. For the water reflux treated Au(Pd)/$TiO_2$ catalyst, 2.5 % conversion and 100 % methyl formate selectivity was achieved at 30 °C. Research by Wittstock *et al.*[14] studied a nanoporous gold monolith as a catalyst for the partial oxidation of methanol (methanol to oxygen ratio of 2:1), which produced surprisingly high activity at low temperatures, *i.e.* 10 % conversion and 100 % methyl formate selectivity at room temperature (~20 °C). This is the only article to report this high activity and high product selectivity at such a low temperature for methanol oxidation, and so improving the activity of the water reflux treated Au(Pd)/$TiO_2$ catalyst further is an interesting prospect. The commercial production of methyl formate is via the

carbonylation of methanol and catalyzed by sodium methoxide, using temperatures around 100 °C. The main disadvantage of this process however, is that impurities in the carbon monoxide source (for carbonylation of methanol) are detrimental to the sodium methoxide catalyst, and so discovering alternative methods of producing high yields of methyl formate is necessary.

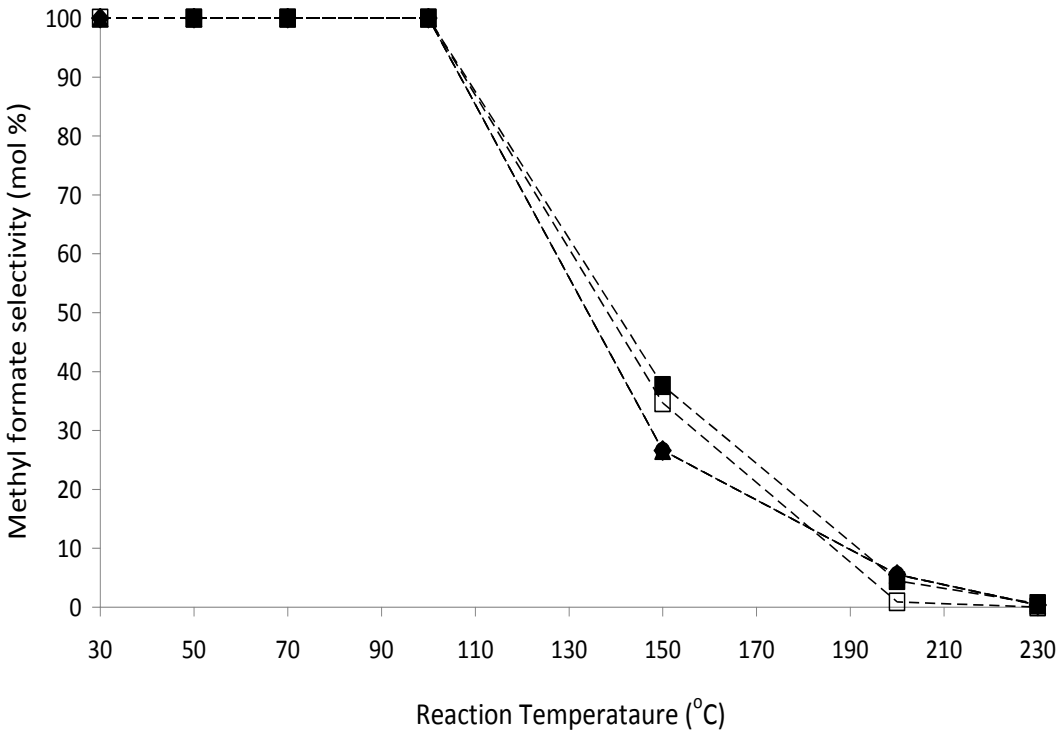


**Figure 5.23b:** Methyl formate selectivity produced using Au(Pd)/$TiO_2$ catalysts treated using various methods.

-■- = Non-treated; -□- = Reflux (90 °C/60 min); -◆- = Calcined 200 °C; -▲- = Calcined 300 °C; -●- = Calcined 400 °C.

### *5.4.2 – Effect of catalytic cycles on activity of Au(Pd)/$TiO_2$ catalysts*

Comotti *et al.*[24] found that there is a need to thermally activate the supported gold catalyst (for CO oxidation) by *in situ* heating the catalyst up to a required temperature, and then decreasing the temperature (cycle). This pre-treatment gave a 90 % increase in activity for a 1 wt% Au/$TiO_2$ catalyst, prepared using PVA after thermally activating the

catalyst. Following this discovery by Comotti *et al.*[24] studies on the Au(Pd)/$TiO_2$ catalysts were performed using this methodology for the selective oxidation of methanol.

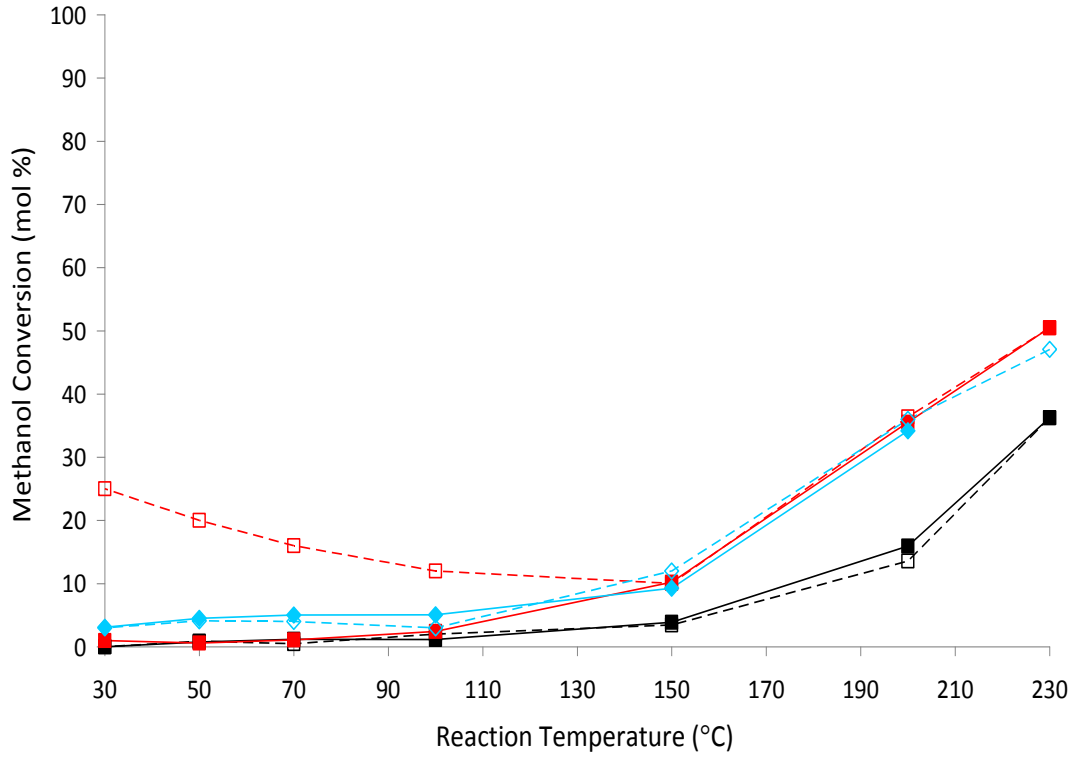


**Figure 5.24:** Methanol conversion for catalytic cycles over Au(Pd)/$TiO_2$ catalysts, treated using various methods.

= Au(Pd)/$TiO_2$ (non-treated) increasing reaction temperature; = Au(Pd)/$TiO_2$ (non-treated) decreasing reaction temperature; = Au(Pd)/$TiO_2$ (reflux 90 °C/60min) increasing reaction temperature; = Au(Pd)/$TiO_2$ (reflux 90 °C/60min) decreasing reaction temperature; = Au(Pd)/$TiO_2$ (Calcined at 200 °C) increasing reaction temperature; = Au(Pd)/$TiO_2$ (Calcined at 200 °C) decreasing reaction temperature.

Three catalysts were studied; non-treated, reflux treated and 200 °C heat treated (Figure 5.24). Surprisingly, the non-treated Au(Pd)/$TiO_2$ catalytic activity remained stable after thermal activation, which indicates that the removal of PVA (by *in situ* heat treatment) did not have a substantial effect on activity, as the fresh non-treated Au(Pd)/$TiO_2$ catalyst contains the greatest amount of PVA and should lose a substantial amount during the heating process of the reaction. The same was observed for the 200 °C heat treated

catalyst, although this is expected since the reaction temperature used for thermal activation is only slightly above this (230 °C), so any PVA will have already been removed during the pre-treatment. It is interesting that the water reflux treated Au(Pd)/$TiO_2$ catalytic activity increases considerably after *in situ* thermal activation, with 25 % conversion and 60 % selectivity towards methyl formate at room temperature (~30 °C) (initial activity before *in situ* thermal activation; ~1 % conversion with 100 % methyl formate selectivity). The bi-metallic Au(Pd)/$TiO_2$ catalyst produced a 15 % methyl formate yield compared to the 10 % yield produced by Wittstock *et al.*[14] with a nanoporous Au monolith catalyst under the same conditions.

### *5.4.3 – Stability analysis of Au(Pd)/TiO2 catalyst treated via the solvent extraction treatment process*

To ensure that the catalytic activity of the Au(Pd)/$TiO_2$ reflux treated catalyst at each temperature after *in situ* thermal activation is stable, two temperatures were selected where there is a noticeable increase in catalytic activity after the activation (30 and 70 °C), and these were held for ~20 hours. Figure 5.25 shows the stability of the catalytic activity of the bi-metallic catalyst at 30 °C. A fresh catalyst was heated up to 230 °C under the standard conditions described previously, and then decreased to 30 °C and held for 18 h. There was a decrease in activity from 25 to 20 % methanol conversion after 18 h, but on average 22.5 % methanol conversion is achieved. It is also noticeable that the methyl formate selectivity increases over time, with a decrease in CO selectivity.

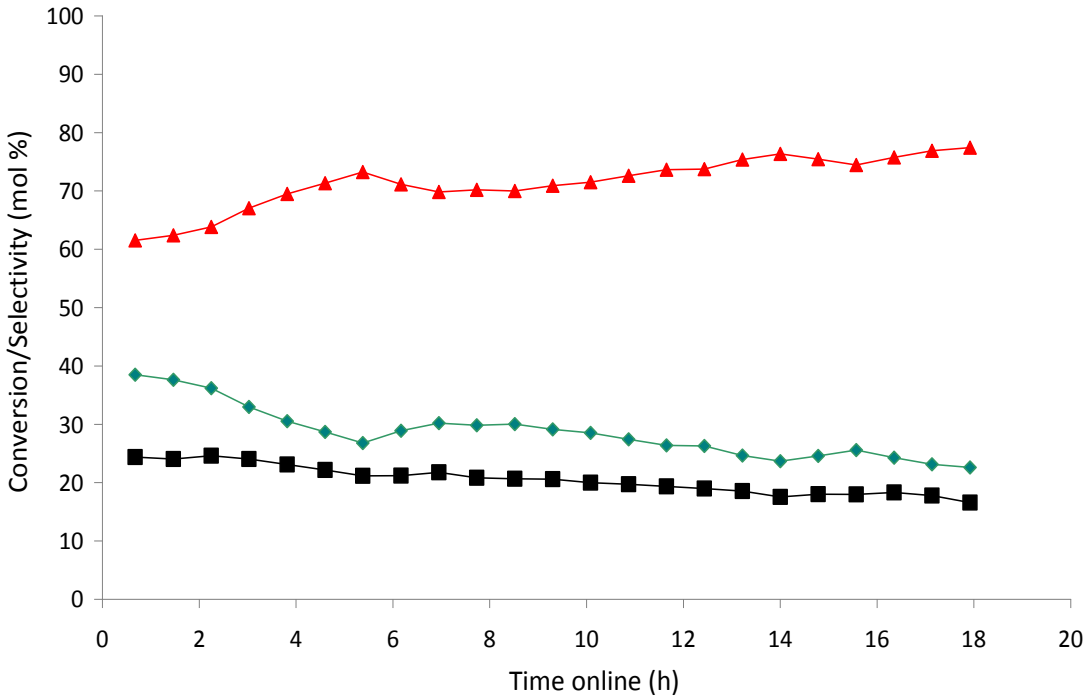


**Figure 5.25:** Methanol selective oxidation using Au(Pd)/$TiO_2$ (reflux 90 °C/60min) catalyst. After increasing temperature to 230 °C and then decreasing to 30 °C, temperature held for 16.5h and conversion and selectivity recorded.

= Methanol conversion; = Methyl formate selectivity; = Carbon dioxide selectivity

At a temperature of 30 °C, it is possible that methanol is collecting on the surface of the catalyst due to it condensing. Therefore, the experiment was repeated using a fresh Au(Pd)/$TiO_2$ catalyst, and held at 70 °C after thermal activation to avoid any possible condensation. Figure 5.26 shows that the activity and selectivity towards methyl formate are both stable over a period of 22 h, which is in agreement with the stability results achieved by Wittstock *et al.*[14] who reported a decrease in conversion of ~6 % over every 24 hours during 7 days testing (reaction temperature of 60 °C).

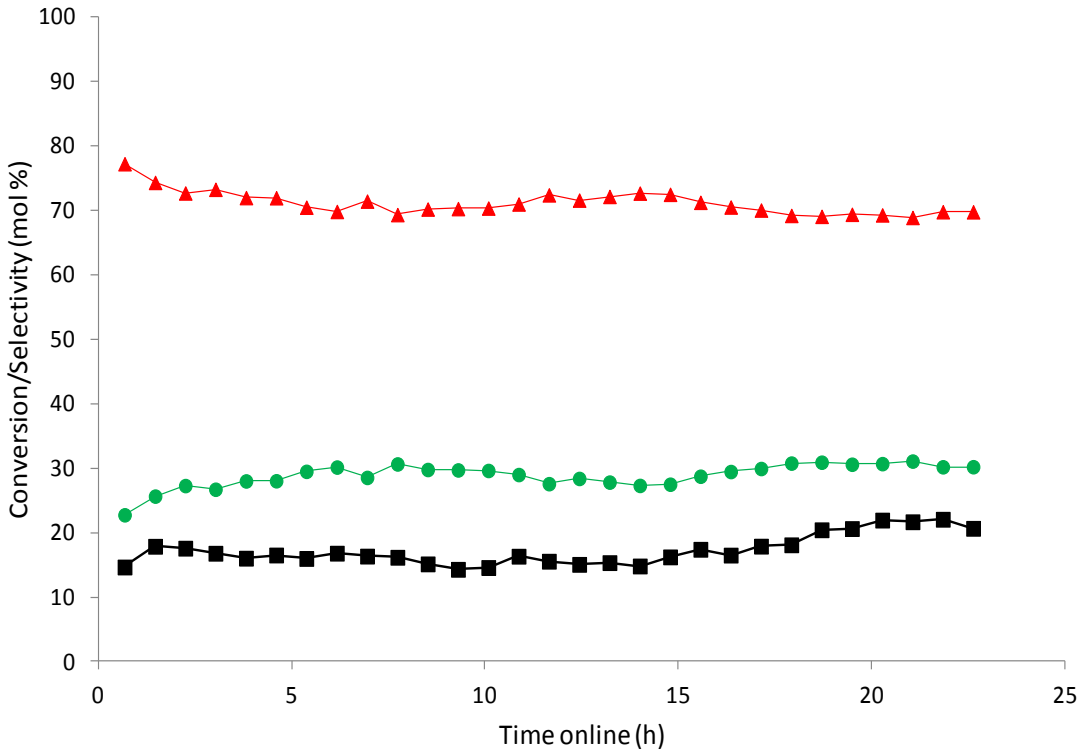


**Figure 5.26:** Methanol selective oxidation using Au(Pd)/$TiO_2$ (reflux 90 °C/60min) catalyst. After increasing temperature to 230 °C and then decreasing to 70 °C, temperature held for 16.5h and conversion and selectivity recorded.

= Methanol conversion; = Methyl formate selectivity; = Carbon dioxide selectivity.

### *5.4.4 – Reproducibility analysis of Au(Pd)/TiO2 catalysts prepared via the solvent extraction treatment process*

Although the catalytic activity of the water reflux treated Au(Pd)/$TiO_2$ catalyst was confirmed to be stable, further studies were performed in order to determine the reproducibility of the *in situ* thermal activation procedure. It was observed (Figure 5.27a) that the catalytic activity of a fresh reflux treated Au(Pd)/$TiO_2$ catalyst was substantially lower compared to the activity achieved after *in situ* thermal activation. The activity of this used catalyst when tested the following day, can be seen in Figure 5.27b. It is clear, that the catalyst has not maintained its high activity at low temperatures (70 °C), and has reverted back to the catalytic activity comparable to the fresh Au(Pd)/$TiO_2$ catalyst (Figure 5.24).

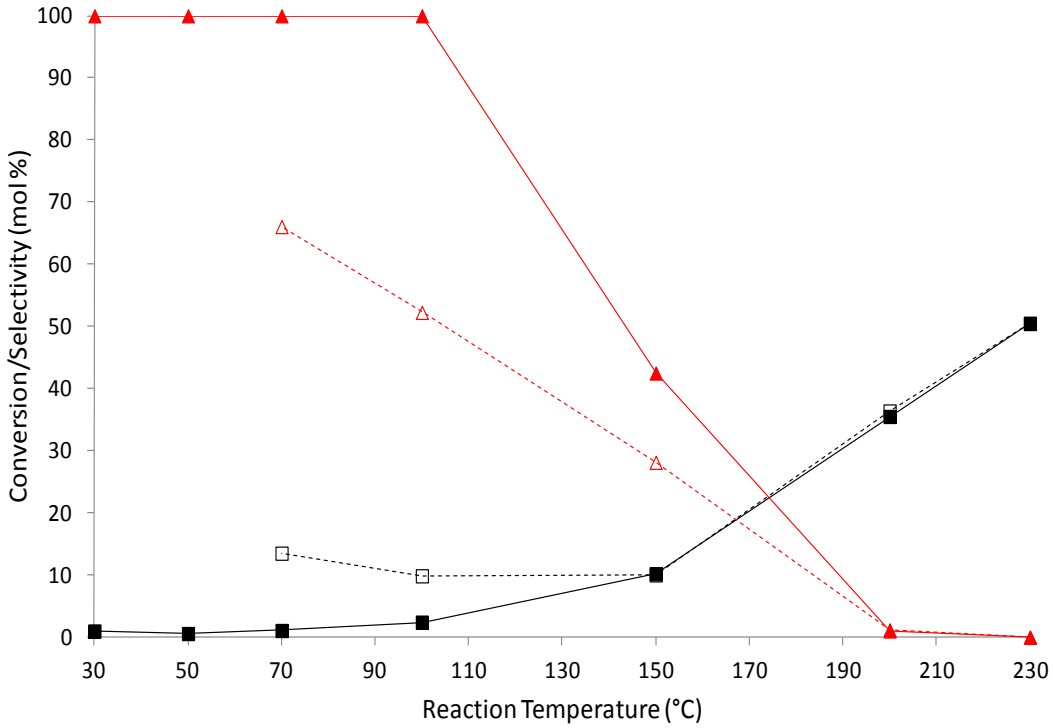


**Figure 5.27a:** Catalytic cycle using Au(Pd)/$TiO_2$ (reflux 90°C/60min) catalyst.

= Methanol conversion during increasing reaction temperature; = Methanol conversion during decreasing reaction temperature; = Methyl formate selectivity during increasing reaction temperature; = Methyl formate selectivity during decreasing reaction temperature.

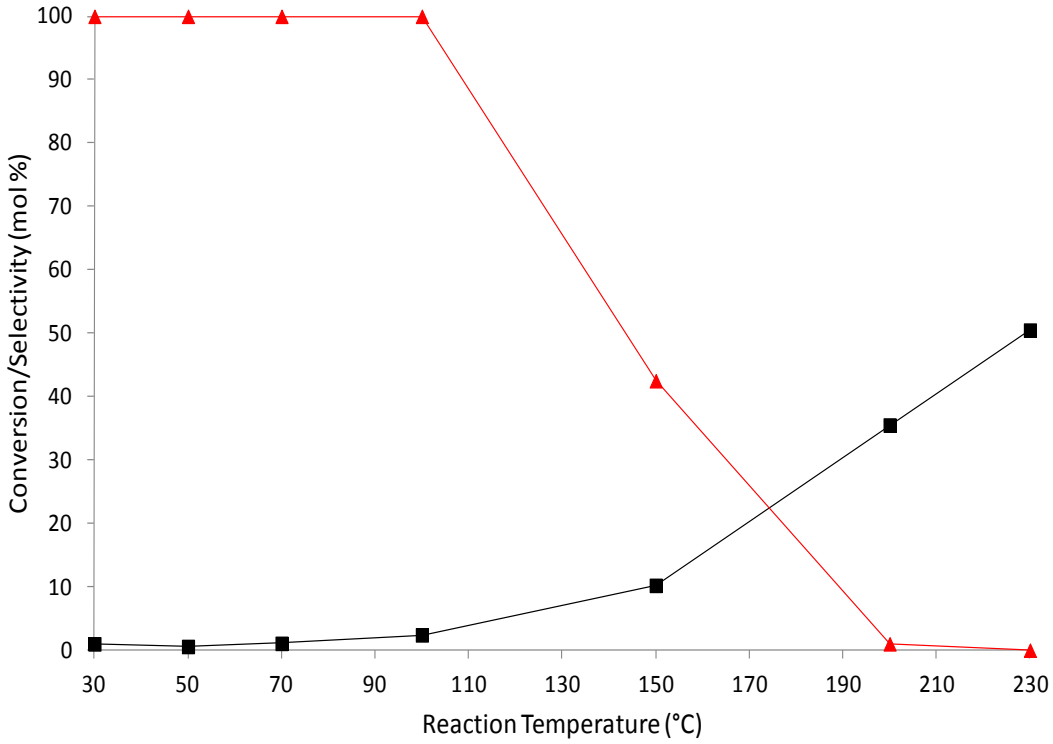


**Figure 5.27b:** Second test using (used catalyst) Au(Pd)/$TiO_2$ (reflux 90 °C/60 min) catalyst.

= Methanol conversion; = Methyl formate selectivity

To determine whether the catalysts had been modified after testing, Raman spectroscopy was carried out. Figure 5.28 shows that the fresh Au(Pd)/$TiO_2$ catalysts showed the relevant bands associated with $TiO_2$ (Table 5.1b), whereas after *in situ* thermal activation (used) these are not visible, suggesting that there could be a covering of condensed methanol or $CO_x$ on the $TiO_2$ at the surface (due to the low temperatures used during the final stages of the reaction). To study whether this theory was likely, TGA analysis was performed (air atmosphere) on the used catalyst, but no noticeable mass loss was recorded. Further investigation into whether a substance was covering the catalyst surface, led to the heating of catalyst under a pure oxygen atmosphere (which was performed *in situ* in the reactor). Figure 5.28 shows that there is a reappearance of the $TiO_2$ bands, suggesting that the substance covering the surface of the catalysts has been removed.

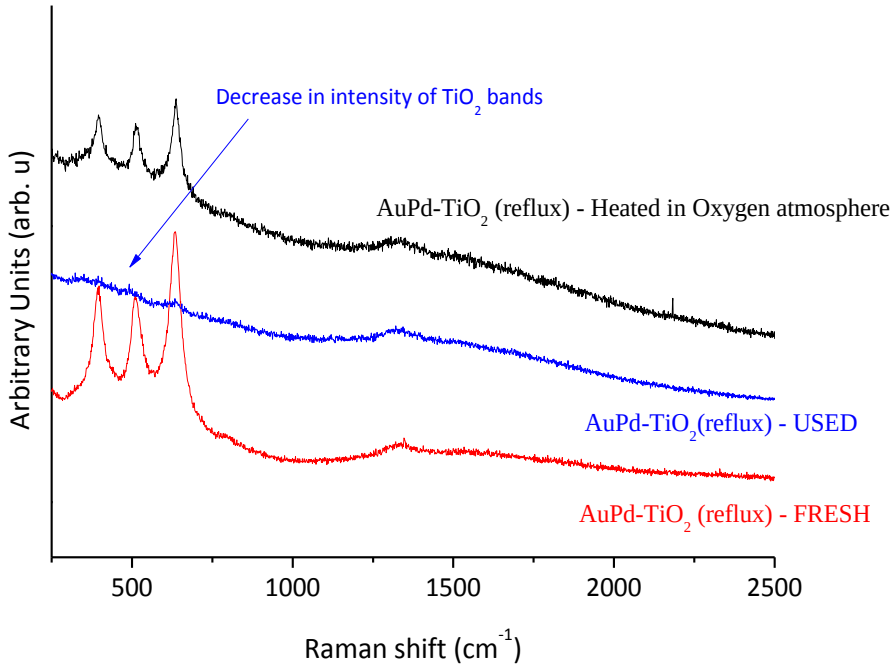


**Figure 5.28:** Raman spectra of Fresh, Used and $O_2$ heat treated used Au(Pd)/$TiO_2$ (reflux treated) catalysts.

To determine whether the catalyst was reactivated after heating under an oxygen atmosphere, the methanol oxidation reaction was repeated. It is observed in Figure 5.29 that the catalytic activity of the bi-metallic catalyst has returned to the activity that was obtained after *in situ* thermal activation. Upon this discovery, further studies were performed, where the heat treatment of a fresh catalyst in an oxygen atmosphere, outside the oxidation reactor (*ex situ* in a furnace) was carried out, before testing it for methanol oxidation. Figure 5.30 shows that the activity of the *ex situ* heat treated catalyst does not resemble the activity seen for the *in situ* heat treated catalyst (Figure 5.29). This indicates that heating the catalyst does not seem to play a role in changing the catalysts activity, which could be caused by an unidentified species on the surface.

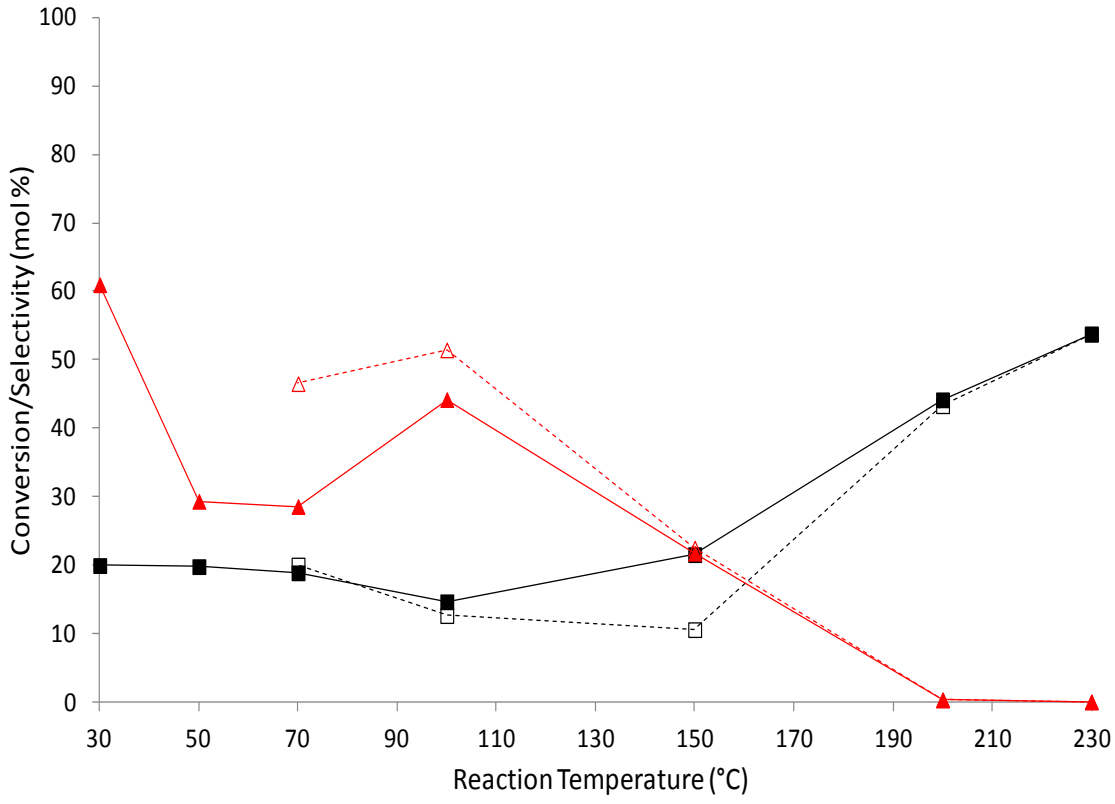


**Figure 5.29:** Second test of (used) Au(Pd)/$TiO_2$ (reflux 90°C/60min) catalyst which has been heated (*in situ)* to 230 °C in $O_2$ after first reaction.

= Methanol conversion during increasing reaction temperature; = Methanol conversion during decreasing reaction temperature; = Methyl formate selectivity during increasing reaction temperature; = Methyl formate selectivity during decreasing reaction temperature.

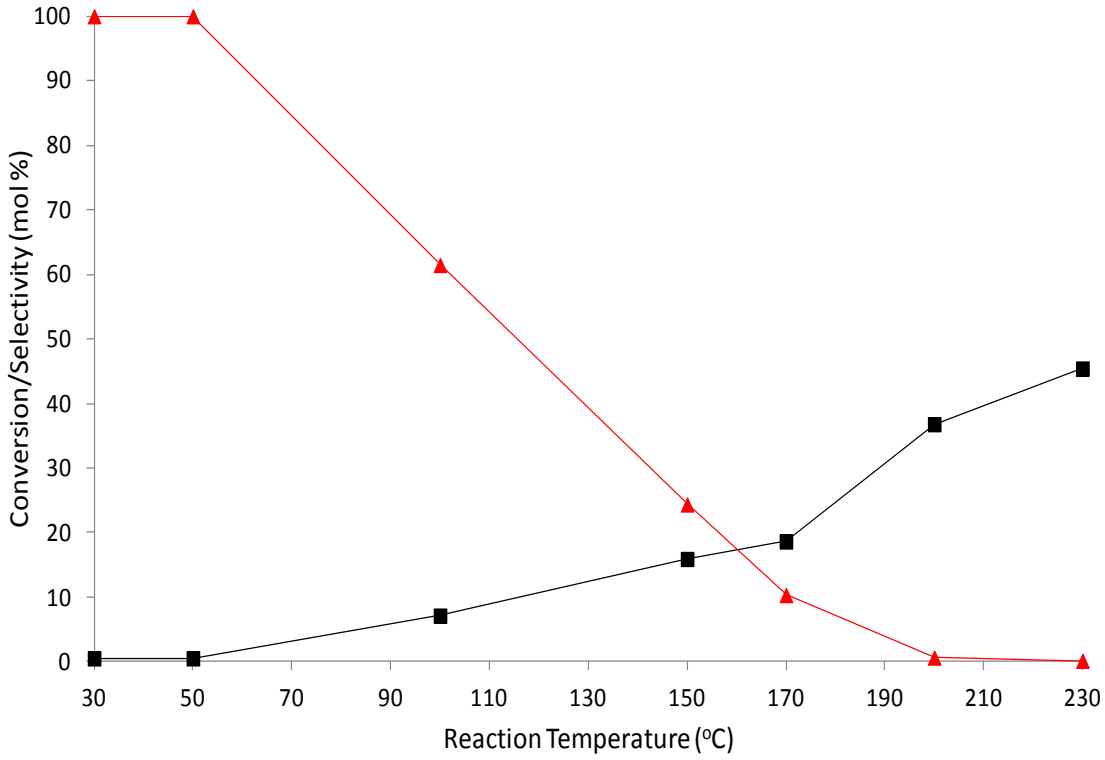


**Figure 5.30:** Methanol oxidation using a reflux treated Au(Pd)/$TiO_2$ catalyst, *ex situ* heated in an oxygen atmosphere to 230 °C. (In a furnace separate to the reactor).

The exact cause of the loss in activity from the end of the reaction and its re-use in the next experiment is not clear. However, the postulation that there are adsorbed species on the surface of the catalyst after (*in* situ) thermal activation needs more detailed analysis. TEM, and in particular XPS could provide detailed information on the structure of the metal particles and also the species present on the surface (with their relevant ratios and oxidation states).

Figures 5.31a, b and c, show low magnification TEM images of a fresh reflux treated Au(Pd)/$TiO_2$ catalyst, accompanied by the *in situ* and *ex situ* heat treated catalysts. Due to the low magnification, it is difficult to determine whether there is a change in structure of the gold or palladium particles on the surface between the three catalysts, and more detailed studies need to be carried out to study this feature. However, the average particle

size distribution of the catalysts indicate that there is no major increase in size, when comparing the fresh, *in situ* and *ex situ* heat treated catalysts. The minimal difference in particle size between the fresh and the 200 °C heat treated catalysts was expected, as the particle size distribution of the fresh $Au/TiO_2$ (Figure 5.8b) and the 200 °C heat treated $Au/TiO_2$ (Figure 5.11b) are very similar. (4.8 and 5.1 nm respectively).

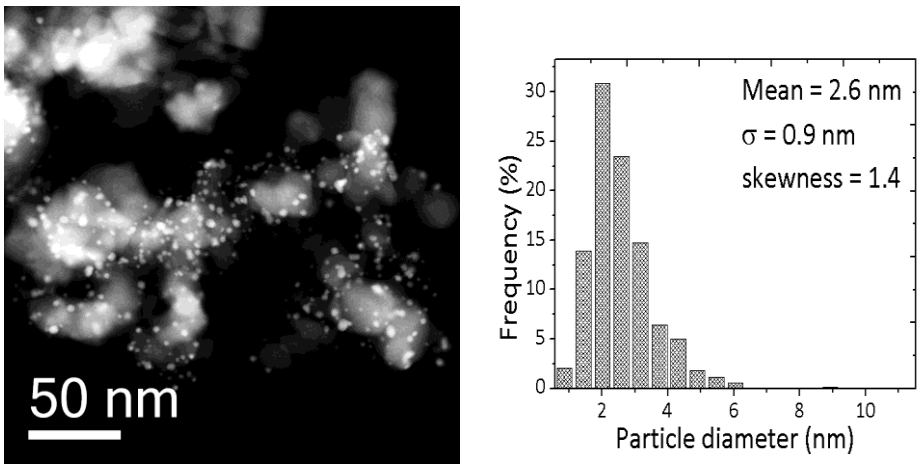


**Figure 5.31a:** TEM image and particle size distribution of fresh reflux treated $Au(Pd)/TiO_2$ catalyst. (data provided by Qian He)

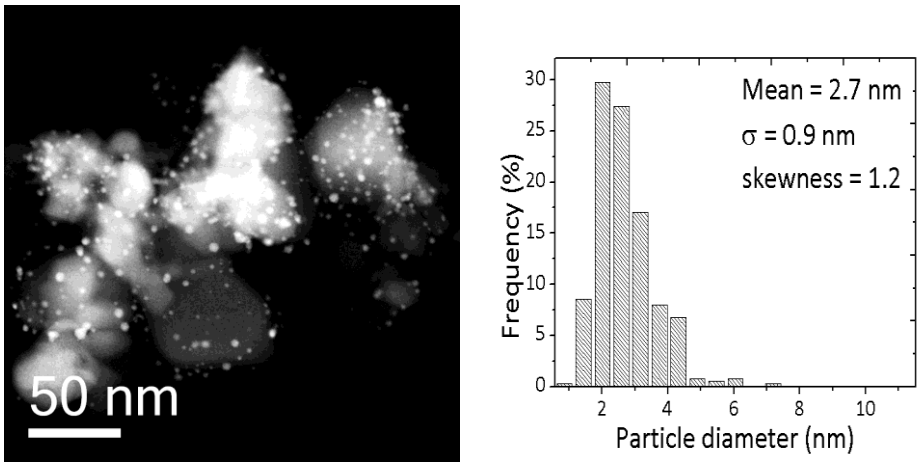


**Figure 5.31b:** TEM image and particle size distribution of used *in situ* heated reflux treated $Au(Pd)/TiO_2$ catalyst. (data provided by Qian He)

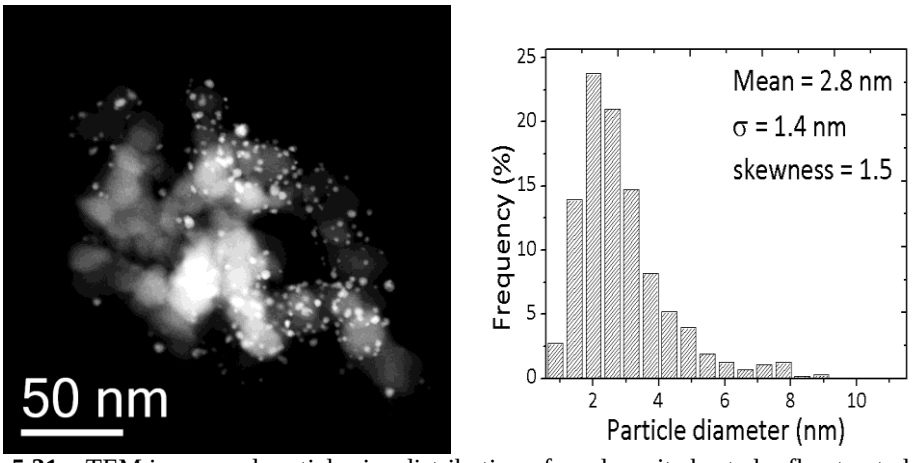


**Figure 5.31c:** TEM image and particle size distribution of used *ex situ* heated reflux treated Au(Pd)/$TiO_2$ catalyst. (data provided by Qian He).

To study whether the formation of surface species are the cause of the change in activity, detailed XPS analysis of the fresh, *in situ* and *ex situ* heat treated catalysts was carried out. Table 5.4 shows that the amount of each element in the fresh and *ex situ* heat treated samples are very similar, which could explain the similarity in observed activity for the oxidation of methanol. A substantial difference is observed in the Au 4f spectra, with an 800 % increase in the amount of Au observed for the *ex situ* heat treated sample.

The most important result observed (taking into consideration the difference in catalytic activity of each material) in the XPS analysis however, was the amount of oxygen species present in the *in situ* heat treated sample compared to the *ex situ* heat treated sample, and the fresh sample. A 29.5 % increase in the oxygen species present in the *in situ* heat treated sample, compared to the fresh sample, indicates a substantial change in oxygen species on the surface. Further analysis of the particular oxygen species present between the three samples is shown in Figures 5.31a, b and c.

**Table 5.4:** XPS analysis of reflux treated Au(Pd)/$TiO_2$ catalyst, fresh, *in situ* heated in $O_2$ after reaction, *ex situ* heating in $O_2$ in a furnace (separate to oxidation reactor).

| Catalyst | O 1s (At %) | Ti 2p (At %) | Pd 3d (At %) | Au 4f (At %) |
|---|---|---|---|---|
| **Fresh** | 44 | 15.5 | 0.3 | 0.2 |
| ***In situ*** | **57** | 19.5 | 0.2 | 0.2 |
| ***Ex situ*** | 44 | 15 | 0.2 | **1.8** |

It was found that the oxygen species present in both the fresh and *ex situ* heat treated samples (Figure 5.31a and c) are very similar, with three main species visible at binding energies of 529.7, 531.8 and 533.2 eV, whereas the three main species present in the *in situ* heat treated sample are at 529.7, 531.1 and 533.2 eV. The peak present at 531.1 eV is not visible without the use of peak fitting software, however, when taken into consideration, the peak is quite substantial, and therefore it is appropriate to assign it to an extra species, which is not present in the fresh or *ex situ* samples. A binding energy of 531.1 eV closely relates to the 531.2 – 531.4 eV observed by Carley *et al.*[27] and Schön[28] which has been assigned to formate groups (or OH groups observed by Hovarth *et al.*[29])

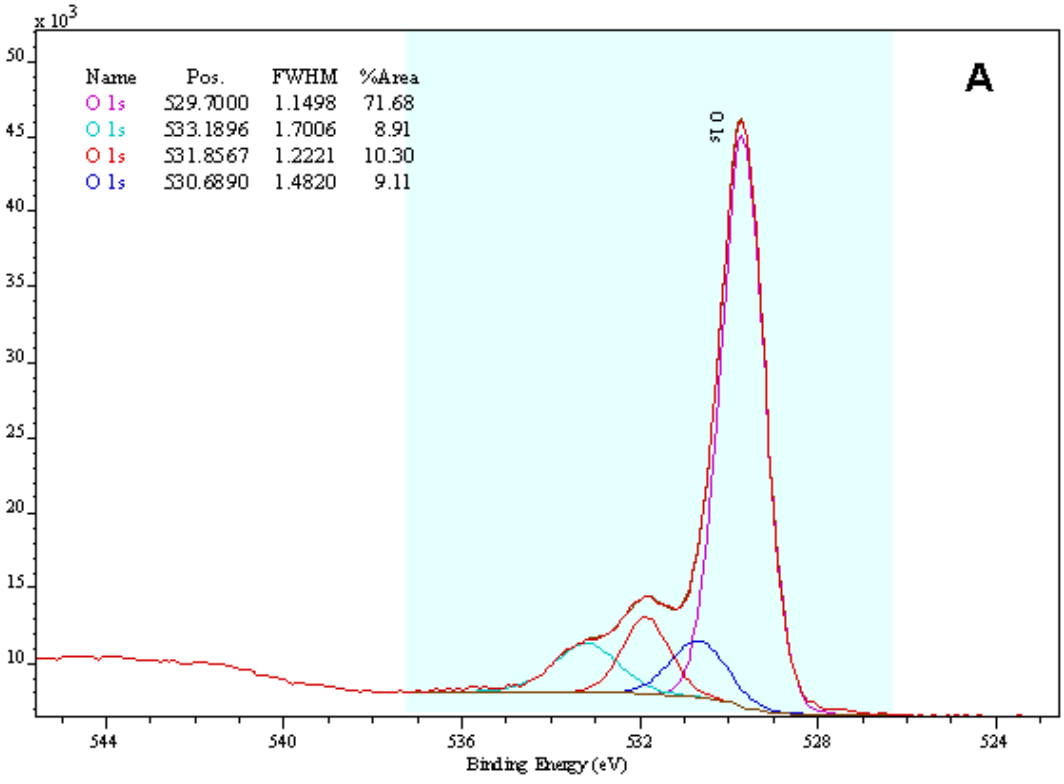

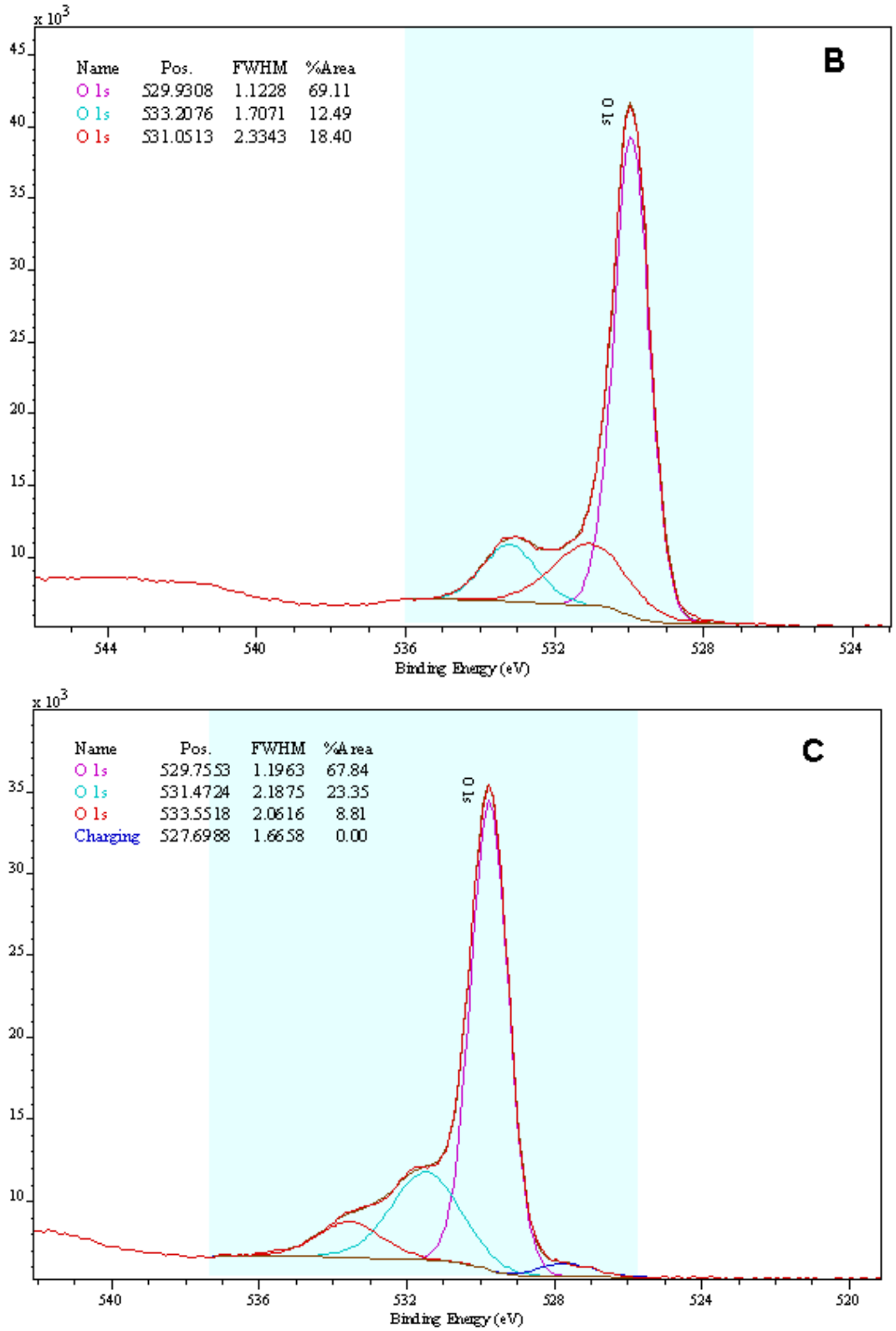


**Figures 5.31(A, B, C): A:** XPS spectra of O 1s (Fresh Au(Pd)/$TiO_2$); **B:** XPS spectra of O 1s (Used *in situ* heated Au(Pd)/$TiO_2$); **C:** XPS spectra of O 1s (*ex situ* heated Au(Pd)/$TiO_2$)

Assuming that the species present at 531.1 eV is indeed formate groups present on the surface, it can be postulated that these formate species, associated with methyl formate, could be bound to active sites on the surface, blocking potential active sites. This could explain why the activity of the catalyst is not reproducible in the consecutive reaction with methanol. The return to the high activity and reappearance of the $TiO_2$ (Figure 5.28) after heat treating with oxygen also adds weight to this theory, as these conditions could remove the methyl formate present on surface, and expose the active sites which are then able oxidise methanol readily in the next reaction.

A detailed theoretical study has been performed by Bingjun Xu *et al.* into the mechanism of methanol oxidation on gold active sites.[25] Although this may not be the only mechanism to form methyl formate on gold active sites, using this study it is possible to observe how methyl formate covering the surface and blocking potential active sites could lead to deactivation of the catalyst. It is reported that the O-H bond in methanol is activated by a reaction with adsorbed atomic oxygen to form an alkoxy molecule, which then undergoes β-H elimination to form formaldehyde. The formaldehyde molecule then reacts with another alkoxy bonded to an adjacent active site, to form an adsorbed hemiacetal. Further β-H elimination from the hemiacetal produces methyl formate. Therefore, if the methyl formate does not desorb from the surface at the low temperature used towards the termination of the methanol oxidation reaction, the reaction to form another methyl formate molecule on an adjacent active site becomes improbable.

Further XPS analysis is needed on the *in situ* used sample, which when treated in an oxygen atmosphere and heat, returns to the highly active catalyst observed at the end of the reaction. This would confirm whether the peak at 531.1 eV reduces in size or

disappears, and hence the methyl formate groups blocking potential active sites would be removed.

## 5.5 – Conclusions

Supported mono-metallic and bi-metallic gold/palladium nanoparticles have been prepared using the sol immobilisation technique, using heat and solvent extraction treatments to remove the PVA stabiliser and achieve small nanoparticle size. The catalysts were then characterized and tested for carbon monoxide and methanol oxidation. The standard method of removing the stabilising ligand before catalyst testing is the heat treatment method which is known to lead to particle growth. In this study a new method using solvent extraction has been used, to maintain a small nanoparticle size. As gold nanoparticle size is known to have a major effect on the activity towards CO oxidation, this was an ideal reaction to test whether the new solvent extraction method produced higher activity catalysts than the heat treatment method. Using high resolution TEM analysis, the particle size of the catalysts prepared using the solvent extraction method were found to be substantially smaller than those prepared using the heat treatment method. The small particle size produced extremely high activity towards CO oxidation compared to the heat treated and non-treated catalysts.

As supported gold catalysts are known to be active towards methanol oxidation, this was another ideal test, to study whether the solvent extraction method achieved higher activity than the heat treated method. A correlation between activity and particle size was determined which has not been previously reported for methanol oxidation. Both mono-metallic $Au/TiO_2$ catalysts and bi-metallic $Au(Pd)/TiO_2$ catalysts were tested and it was determined that there was a promotional effect as the bi-metallic catalysts showed higher activity than the mono-metallic catalysts. Further studies using the bi-metallic catalysts

led to the discovery that *in situ* thermal activation of the water refluxed Au(Pd)/$TiO_2$ catalyst, gave ~20 % methanol conversion with ~60 % methyl formate selectivity at room temperature. This result is comparable to the high profile result achieved by Wittstock *et al.*[14] in 2010 where 10 % conversion is reached with 100 % methyl formate selectivity at room temperature.

## 5.6 – References


1. M. Haruta, N. Yamada, T. Kobayashi; S. Iijima. *J. Catal*. **1989**, *115*, 301.
2. N. Lopez, T. V. W. Janssens, B. S. Clausen, Y. Xu, M. Mavrikakis, T. Bligaard and J. K. Norskov. *J. Catal.* **2004**, *223*, 232–235.
3. R. Zanella, S. Giorgio, C.-H. Shin, C. R. Henry and C. Louis. *J. Catal*. **2004**, *222*, 357–367.
4. G. R. Bamwenda, S. Tsubota, T. Nakamura and M. Haruta. *Catal. Lett.* **1997**, 44, 83.
5. M. Valden, X. Lai and D.W. Goodman. *Science* **1998**, *281*, 1647.
6. A. I. Kozlov, A. P. Kozlova, H. Liu and Y. Iwasawa. *Appl. Catal. A* **1999**, *182*, 9.
7. H. H. Kung, M. C. Kung and C. K. Costello. *J. Catal.* **2003**, *216*, 425.
8. M. Haruta, H. Kageyama, N. Kamijo, T. Kobayashi and F. Delannay. *Stud. Surf. Sci. Catal.* **1988**, *44*, 33.
9. M. Hurata. *Catal. Surv. Jpn.* **1997**, 61.
10. A. Beck, A. Horvath, Gy. Stefler, R. Katona, O. Geszti, Gy. Tolnai, L. F. Liotta, and L. Guczi. *Catal. Today* **2008**, *139*, 180-187.
11. M. A. P. Dekker, M. J. Lippits and B. E. Nieuwenhuys. *Catal. Lett.* **1996**, *56*, 195.
12. J. D. Grunwaldt, C. Kiener, C. Wögerbauer and A. Baiker, A. *J. Catal.* **1999**, *181*, 223-232.
13. S. Tsubota, T. Nakamura, K. Tanaka and M. Haruta. *Catal. Letters* **1998**, 56**,** 131-135.
14. A. Wittstock, V. Zielasek, J. Biener, C. M. Friend and M. Baumer. *Science* **2010**, *327 (5963)*, 319-322.
15. Bingjun Xu, Xiaoying Liu, J. Haubrich, R. J. Madix, and C. M. Friend. *Angew. Chem. Int. Ed.* **2009**, *48*, 4206 –4209.

16. Bingjun Xu, Xiaoying Liu, J. Haubrich and C. M. Friend. *Nature Chem.* **2010**, *2*, 61-65.
17. F.-W. Chang, L. S. Roselin and T.-C. Ou. *Appl. Catal. A*, **2008**, *334*, 147–155.
18. T.-C. Ou, F.-W. Chang, L. S. Roselin, *J. Mol. Catal. A* **2008**, *293*, 8–16.
19. Feg-Wen Chang, Ti-Cheng Ou, L. S. Roselin, Wun-Syong Chen, Szu-Chia Lai, Hsiao-Min Wu. *J. Mol. Catal. A Chemical* **2009**, *313*, 55–64.
20. M. L. Cubeiro and J. L. G. Fierro. *Appl. Catal. A: General* **1998**, *168*, 307-322.
21. Mei Wang, Dao-jun Guo, Hu-lin Li. *Journal of Solid State Chemistry* **2005**, *178*, 1996–2000.
22. F. Kadigran, B. Beden, J. M. Leger and C. Lamy. *J. Electroanal. Chem.* **1981**, *125*, 89-103.
23. J. A. Lopez-Sanchez, N. Dimitratos, C. Hammond, G. L. Brett, L. Kesavan, S. White, P. Miedziak, R. Tiruvalam, R. L. Jenkins, A. F. Carley, D. Knight, C. J. Kiely and G. J. Hutchings. *Nature Chemistry* **2011**, *3*, 551-556.
24. M. Comotti, Wen-Cui Li, B. Spliethoff, and F. Schuth. *J. Am. Chem. Soc.* **2006**, *128*, 917-924.
25. Bingjun Xu, J Haubrich, T. A. Baker, E. Kaxiras, and C. M. Friend. *J. Phys. Chem. C* **2011**, *115*, 3703–3708.
26. Q-bo Chen, Lai-tao Luo and Xiaomao Yang. *Indian Journal of Chemistry*. **2008**, *47A*, 1317-1322.
27. A. F. Carley, A. W. Owens, M. K. Rajumon, M. W. Roberts and S. D. Jackson. *Catal. Lett.* **1996**, *37*,79.
28. G. Schön. *Surface. Science* **1973**, *35*, 96.
29. D. Horvath, L. Toth and L. Guczi. *Catalysis Letters* **2000**, *67*, 117–128.

# 6

# *Chapter 6 – Conclusions and future work*

## 6.1 – Conclusions

### 6.1.1 – *Selective methanol oxidation to formaldehyde*

The main objective of this thesis involved the selective oxidation of methanol to formaldehyde using molybdenum and vanadium phosphate catalysts. Formaldehyde is a highly valuable compound as it is used largely in the textiles industry, and also in the manufacture of many desired materials such as paper, fertilizers and embalming agents, among others.[1] Currently there are two main catalysts used industrially to produce high yields of formaldehyde from methanol, which are silver and iron molybdate. Important companies such as ICI, Degussa and BASF all adopt the silver catalyst during the production of formaldehyde.[2] Iron molybdate however, is the preferred choice by the majority of industries due to its clear economical advantages. The oxidation of methanol to formaldehyde over a silver catalyst operates at temperatures around 650-680 °C, with ~99 % conversion of methanol and 90 % selectivity to formaldehyde.[3-5] Not only is iron molybdate economically more viable to purchase, but it also operates at much lower reaction temperatures; <400 °C, achieving ~99 % conversion and >95 % formaldehyde selectivity. There are however drawbacks in the use of both iron molybdate and silver catalysts. Apart from the high reaction temperature needed to achieve high yields of

formaldehyde when employing the silver catalyst, it is also subject to contamination with methanol impurities.[6] Iron molybdate catalysts produce an advantage over silver in this aspect, as it is not known to be easily contaminated, but does deactivate over a period of time due to molybdenum volatilisation, and so needs to be replaced every 1-2 years.[7,8]

Amongst the two main catalysts used for methanol oxidation to formaldehyde, many other catalytic systems have attempted to record high yields of formaldehyde. Ruf *et al.*[9] studied the catalytic activity of evaporated sodium catalysts which produced 45 % methanol conversion and 40 % formaldehyde selectivity, whereas Ren *et al.*[10] report 10 % conversion and 99 % selectivity using a mixed Ag-$SiO_2$-MgO-$Al_2O_3$ catalyst, which are evidently less active than either silver or iron molybdate catalysts. As well as the large research interest into improving both of these catalysts, there is a vast amount of literature concerning alternative catalysts for the selective oxidation of methanol to formaldehyde. Relevant to the work carried out in this thesis, the most frequently reported catalysts are molybdenum and vanadium based. Although molybdenum trioxide as a bulk catalyst has been reported to be active for this reaction, it is mainly reported to be supported on silica. Work studied by Cheng[11] revealed that at a reaction temperature of 300 °C, bulk $MoO_3$ produces 50 % conversion of methanol, but when supported on silica (15 wt%), conversion increased to 95 %, clearly indicating the benefit of supporting the active material. The disadvantage of supporting $MoO_3$ however, was seen by the diminishing formaldehyde selectivity, which dropped to 67 % selectivity (supported) compared to 79 % selectivity achieved with bulk $MoO_3$. Serman *et al.*[12] report that although the silica support is in fact inert in the oxidation of methanol alone, it is suggested to have a non-innocent role when applied as a support for $MoO_3$. At 250 °C, it was revealed that adsorption of methanol resulted in the formation of methoxide species

on the silica support, which are mobile, and can migrate to molybdenum centres to be oxidised to formaldehyde.

As well as supported molybdenum oxides, vanadium oxides have also been extensively used as active catalysts for the selective oxidation to formaldehyde. Tatibouet and Germain[13] discovered that bulk $V_2O_5$ as a catalyst produces appreciable selectivity to formaldehyde with 97 % selectivity, but this is only viable at low methanol conversions. As with $MoO_3$ the most frequently reported $V_2O_5$ catalysts are supported on a range of metal oxide supports such as $TiO_2$ and $ZrO_2$, among others, with the activity of the vanadia strongly dependent on the support used. Niskala *et al.*[14] have reported the use 3 wt% $V_2O_5$ on $SiO_2$ and 3 wt% $V_2O_5$ on $SiO_2/TiO_2$ (10 wt%) as active catalysts for the oxidation of methanol to formaldehyde. At a reaction temperature of 480 °C the $V_2O_5/SiO_2$ catalyst achieves 75 % selectivity at a conversion of 82 %, but the use of a mixed oxide support of $SiO_2/TiO_2$ and a lower reaction temperature of 410 °C, 96 % formaldehyde selectivity is produced at 91 % conversion.

Taking the above approaches, and those presented in this thesis into account, it is evident that the supported molybdenum phosphate and promoted vanadium phosphate catalysts provide a promising step forward in the selective oxidation of methanol to formaldehyde. Chapter 3 investigated the catalytic activity of $(MoO_2)_2P_2O_7$ catalysts which were prepared using a co-precipitation technique based on the preparation method for the extensively researched $(VO)_2P_2O_7$ catalysts (known for high activity for *n*-butane oxidation to maleic anhydride). When comparing to the activity reported by Cheng for $MoO_3$, it is clear that the presence of phosphate groups do not enhance the molybdenum based catalysts. Unlike the 50 % methanol conversion and 79 % formaldehyde selectivity for $MoO_3$, $(MoO_2)_2P_2O_7$ produced only 15 % conversion but with 100 % formaldehyde

selectivity. The low activity of $(MoO_2)_2P_2O_7$ was attributed to the very low surface area (~1 $m^2/g$), and so the catalyst was supported using $Al_2O_3$, $SiO_2$ and $TiO_2$. The supported $(MoO_2)_2P_2O_7$ catalyst which achieved the highest activity and formaldehyde selectivity was 15 wt % $(MoO_2)_2P_2O_7\backslash SiO_2$. By supporting the $(MoO_2)_2P_2O_7$ catalyst on $SiO_2$, a significant increase in activity was achieved with ~99 % conversion and 87 % formaldehyde selectivity, compared with 15 % conversion and 100 % selectivity produced by bulk $(MoO_2)_2P_2O_7$ . The major negative in supporting the active catalyst is the decrease in formaldehyde selectivity. As with studies reported by Cheng, where 15 wt% $MoO_3/SiO_2$ achieved 95 % conversion and 67 % formaldehyde selectivity (at 300 °C), the 15 wt% $(MoO_2)_2P_2O_7/SiO_2$ catalyst synthesised in this thesis achieves 99 % conversion but with appreciably higher formaldehyde selectivity of 85 % (at the same reaction temperature). As well as achieving considerably higher yields of formaldehyde compared to supported $MoO_3$, the activity of $(MoO_2)_2P_2O_7/SiO_2$ is comparable to that of the commercial iron molybdate catalyst, which produces 92 % formaldehyde selectivity at ~99 % methanol conversion at 300 °C (Appendix Figure A.7). To investigate the loss of formaldehyde selectivity when supporting the molybdenum phosphate catalysts, promotion using transition metals were studied. As supported vanadium based catalysts are known as active catalysts for methanol oxidation to formaldehyde, vanadium was introduced during the synthesis of molybdenum phosphates using $V_2O_5$, with the aim of incorporating vanadium into the structure, which is known to improve activity. Characterization of the V promoted $(MoO_2)_2P_2O_7$ materials discovered that a mixed phase of $VOPO_4.2H_2O/(MoO_2)_2P_2O_7$ was formed, with a range of vanadium concentrations added. As expected, the promotion of vanadium (1 mol%) increased both activity and formaldehyde selectivity, with 71 % conversion at a reaction temperature of 400 °C compared to 51 % conversion achieved with the un-promoted $(MoO_2)_2P_2O_7$

catalyst at this temperature. Not only was conversion increased, but formaldehyde selectivity was around 20 % higher with the vanadium promoted catalyst. High concentrations of vanadium (20 mol%) increased the activity and selectivity still further, with 25 % higher conversion and 30 % higher selectivity than the un-promoted catalyst. Due to the enhancements by both supporting and promoting $(MoO_2)_2P_2O_7$, these were combined, resulting in a 1 mol% vanadium promoted $(MoO_2)_2P_2O_7/SiO_2$ catalyst achieving remarkably high activity and selectivity at an optimum reaction temperature of 260 °C, with 99 % methanol conversion and 92 % formaldehyde selectivity, sufficiently higher than that of iron molybdate which produces only 75 % conversion and 92 % formaldehyde selectivity at the same reaction temperature.

In relation to the promotional effect of vanadium, and its known activity for methanol oxidation to formaldehyde with supported vanadium oxide catalysts, $(VO)_2P_2O_7$ materials were prepared and their catalytic activity recorded in chapter 4. When comparing to the catalytic activity of bulk $V_2O_5$, again no noticeable advantage of phosphate groups was seen, as both $V_2O_5$ and $(VO)_2P_2O_7$ have comparable activity. $(VO)_2P_2O_7$ is a highly active catalyst for the oxidation of *n*-butane to maleic anhydride, however the use of this catalyst has not been reported for its use in methanol oxidation surprisingly. A significant amount of research reveals the use of transition metal promoters as a means of enhancing catalytic activity further, and this idea was used here to promote $(VO)_2P_2O_7$ catalysts for methanol oxidation. Molybdenum was chosen as a promoter, and introduced in the synthesis of $(VO)_2P_2O_7$ using a range of techniques. Both molybdenum oxide and molybdenum salt were studied using both co-precipitation and incipient wetness impregnation, and the materials thoroughly characterized and tested. The addition of 2 mol% vanadium using the co-precipitation addition of ammonium heptamolybdate tetrahydrate produced the catalyst which achieved the highest activity. At an optimum

reaction temperature of 360 °C, 98 % conversion and 82 % formaldehyde selectivity were reported, compared to 99 % conversion and 60 % selectivity using an un-promoted $(VO)_2P_2O_7$ catalyst. X-ray diffraction analysis of molybdenum promoted $(VO)_2P_2O_7$ suggested that a solid solution of $(MoO_2)_2P_2O_7/(VO)_2P_2O_7$ had formed, possibly creating redox couples of $V^{4+} + Mo^{6+} \leftrightarrow V^{5+} + Mo^{4+}$ which could explain the enhanced activity of molybdenum promoted catalysts. When comparing to the activity of supported $V_2O_5/SiO_2/TiO_2$ catalysts reported by Niskala *et al.* a considerabe increase in activity is noticeable for the Mo promoted $(VO)_2P_2O_7$ catalysts.

### 6.1.2 – *CO oxidation using mono-metallic Au/TiO₂*

Since the pioneering discovery by Haruta in 1989 whereby supported gold nanoparticles were found to be highly active catalysts for CO oxidation at room temperature or below, further discoveries have been made, which links the gold nanoparticle size to catalytic activity, with smaller nanoparticles favouring high activity. The two common methods for producing supported Au catalysts involves co-precipitation and deposition precipitation, using a stabilising ligand such as PVA (to maintain small nanoparticle size) followed by a thermal treatment method (which removes the stabilising ligand and exposes the active sites). It has been shown that the standard high temperature heat treatment procedure of removing the stabilising ligand, leads to increased gold nanoparticle size,[15,16] however, the use of high heat treatment methods negates the use of the stabilising ligand in the first place, as it causes the Au particles to sinter and leads to growth in nanoparticle size,[15,16] (hence decreasing activity). The work revealed in chapter 5 introduces an approach to producing and maintaining very small gold nanoparticles during sol-immobilisation preparation of the supported mono-metallic catalysts, by using a solvent extraction treatment[17] (in place of the frequently used thermal treatment), which

involves suspending the catalyst in water and refluxing for a period of time at a certain temperature. Two series of catalysts were prepared; 1 wt% $Au/TiO_2$ with various solvent extraction conditions (reflux time and reflux temperature) and 1 wt% $Au/TiO_2$ with various heat treatment conditions (200, 300 and 400 °C), and these were tested for CO oxidation to study the effect of gold nanoparticle size on activity. As expected, the catalysts treated at 300 °C and 400 °C were mainly inactive with <10 % CO conversion, however, the solvent extraction treated catalyst (water reflux for 60 min at 90 °C) produced >40 % conversion. These results accompanied by high resolution microscopy, chemical analysis and Raman spectroscopy, providing evidence as to the advantage of using the solvent extraction treatment in place of thermal treatment, as both small gold nanoparticles and high activity were achieved.

### 6.1.3 – *Selective methanol oxidation to methyl formate*

As well as the selective oxidation of methanol to formaldehyde, this thesis also covers the selective oxidation of methanol to methyl formate. The commercial production of methyl formate is via the carbonylation of methanol and catalyzed by sodium methoxide, using temperatures around 100 °C and achieving 96 % selectivity. The main disadvantage of this process however, is that impurities in the carbon monoxide source (for carbonylation of methanol) are detrimental to the sodium methoxide catalyst, and so discovering alternative methods of producing high yields of methyl formate are necessary. Such is the need to discover alternative catalysts to sodium methoxide, many supported precious metal catalytic systems have been reported in the literature. Liu and Iglesia[18] investigated an alumina supported ruthenium oxide catalyst which produced moderate activity at low reaction temperatures, with 20 % conversion and 30 % methyl formate selectivity. Lichtenberger *et al.*[19] have reported the catalytic oxidation of methanol on

alumina supported palladium metal at near ambient temperatures (40 °C), achieving 6.6 % conversion and 90 % methyl formate selectivity. A recent article by Wittstock *et al.*[20] studied the use of a nanoporous gold monolith catalyst which reported the highest activity to date, where, at ambient temperature (~20 °C), 10 % methanol conversion and 100 % methyl formate selectivity is achieved.

Again, it is clear that a significant step forward has been achieved by the work carried out in this thesis (chapter 5), reporting the use of 1 wt% Au(Pd)/$TiO_2$ as a highly active catalyst for the production of methyl formate during methanol oxidation at remarkably low reaction temperatures. Although gold catalysts have been revealed as active and selective for methanol oxidation to methyl formate, the significance of the work investigated here relates to the use of the solvent extraction treatment (discussed earlier) in preparing supported bi-metallic Au(Pd), to produce very small nanoparticles. For the first time, the work carried out in this thesis compares how the Au(Pd) nanoparticle size effects catalytic activity towards the oxidation of methanol to methyl formate. Four series of catalysts were prepared; 1 wt% Au/$TiO_2$ with various solvent extraction conditions (reflux time and reflux temperature), 1 wt% Au/$TiO_2$ with various heat treatment conditions (200, 300 and 400 °C), 1 wt% Au(Pd)/$TiO_2$ with various solvent extraction treatments (reflux time and reflux temperature), and finally 1 wt% Au(Pd)/$TiO_2$ with various heat treatment conditions (200, 300 and 400 °C). High resolution microscopy, accompanied by chemical analysis and Raman spectroscopy confirmed that the heat treated catalysts removed virtually all of the stabilising ligand, with higher temperatures favouring greater removal, however, as expected, the growth of nanoparticles size increases dramatically with increasing treatment temperature. Characterization of the solvent extraction method revealed that there was minimal growth of nanoparticle size

and sufficient removal of the stabilising ligand when refluxing the catalysts at 90 °C for 60 minutes, with higher reflux temperatures favouring an increase in particle size.

Preliminary catalytic tests were carried out on mono-metallic Au/$TiO_2$ catalysts, revealing no correlation between particle size and activity was present, with the heat treated catalyst (300 °C) providing the highest activity at a reaction temperature of 150 °C, with 29 % methanol conversion and 21 % methyl formate selectivity (6 % per pass yield). Activity for 1 wt% Au/$TiO_2$ followed the trend: 300 °C (heat treated) > 200 °C > 400 °C > reflux treated (90 °C/60 min) > non-treated. Subsequent catalytic testing of the supported bi-metallic Au(Pd)/$TiO_2$ series provided extremely promising results for the water reflux treated catalyst however, as it produced the highest activity when compared with the heat treated series of catalysts. The activity trend for 1 wt% Au(Pd)/$TiO_2$ followed: reflux treated (90 °C/60 min) > 200 °C (heat treated) > 300 °C > 400 °C > non-treated, which showed a clear correlation between nanoparticle size and PVA removal, with catalytic activity. The interesting feature of the reflux treated bi-metallic catalyst, was its ability to activate the oxidation of methanol to methyl formate at temperatures well below 100 °C, with 100 % selectivity at low methanol conversion (2.5 % at a reaction temperature of 30 °C). Using the theory by Comotti *et al.*[21] that thermal activation is needed to remove further amounts of stabilising ligand before optimising catalytic activity, catalytic cycles were performed using the reflux-treated 1 wt% Au(Pd)/$TiO_2$ catalyst, (increasing reaction temperature under methanol oxidation conditions, and decreasing the reaction temperature whilst recording activity and selectivity). This lead to a remarkable discovery, whereby the activity of the supported bi-metallic catalyst increased further at low reactions temperatures, with 25 % conversion and 65 % methyl formate selectivity (15 % per pass yield) at 30 °C (after thermal activation). When comparing this result to Wittstock *et al*. who report a 10 % methyl

formate yield at this temperature under similar reaction conditions, it is clear that a promising catalyst for the oxidation of methanol to methyl formate has been discovered. However, for this catalyst to be used industrially to produce methyl formate, operating at ambient temperature is not viable, as this is an exothermic reaction, and so maintaining reactor temperature at 30 °C is inappropriate. To avoid this problem, the reaction can be performed at 70 °C, where 19 % conversion and 73 % methyl formate selectivity (14 % per pass yield) is recorded.

## 6.2 – Future work

Following the discoveries presented by the research conducted in this thesis, and accompanied by the need to understand them in more detail, several lines of further work are summarised which should be pursued;

- Due to the impressive catalytic activity of silica supported $(MoO_2)_2P_2O_7$ catalysts, it would be interesting to understand how the molybdenum phase is distributed over the surface of the support, and also determine the active sites involved in methanol oxidation to formaldehyde. Therefore, *in-situ* Raman spectroscopy studies using methanol as the absorbent could provide detailed information, as the molybdenum species (active site) when bonded to methanol, will cause a decrease in intensity of the Raman band.
- The high activity of the 1 mol% vanadium promoted $(MoO_2)_2P_2O_7/SiO_2$ catalyst, accompanied by the limited information on the role of vanadium in increasing the activity compared to the un-promoted catalyst, leads to requirement of further studies, in the hope to develop the catalyst further. With the use of high resolution transition electron microscopy (TEM), it could be possible to observe the

presence of vanadium on the surface and how it is distributed, as XRD and Raman spectroscopy studied here provide limited insight.

- Silver promoted molybdenum phosphate catalysts have been reported in the literature as active in the oxidation of propane to propene, and judging from the highly active nature of the 1 mol% vanadium promoted $(MoO_2)_2P_2O_7/SiO_2$ catalyst discovered for methanol oxidation to formaldehyde here, testing for propane oxidation to propene could provide an interesting project.
- Although the molybdenum promoted $(VO)_2P_2O_7$ catalysts studied here were active for methanol oxidation to formaldehyde, it is reasonable to suggest, (owing to the high activity of supported $V_2O_5$ catalysts) that by supporting the molybdenum promoted vanadium phosphate catalysts could increase the distribution of active sites and hence improve activity further.
- Following the trend associated with increasing activity with increasing molybdenum concentration in promoted $(VO)_2P_2O_7$ catalysts, it would be intriguing to study the catalytic activity of a catalyst with a 50:50 ratio of $(MoO_2)_2P_2O_7$:$(VO)_2P_2O_7$.
- The remarkably high activity of the bi-metallic 1 wt% Au(Pd)/$TiO_2$ during methanol oxidation to methyl formate leads to many unanswered questions. The increase in activity of the bi-metallic Au(Pd)/$TiO_2$ catalysts compared to the mono-metallic 1 wt% Au/$TiO_2$ catalysts suggests that there is a synergistic effect, and therefore, the preparation and testing of a 1 wt% Pd/$TiO_2$ catalysts is essential. It would then be beneficial to optimise the Au:Pd ratio in the catalysts to discover the optimum catalytic activity.
- Although the role of *in-situ* thermal activation is understood to be the removal of excess PVA from the catalyst, the reason behind the catalytic activity reverting

back to that of a fresh catalyst after testing the catalyst for a second time is still unknown. By heating the used (thermally activated) catalyst in an oxygen atmosphere, the Raman spectroscopy analysis showed an un-known species, thought to be condensed methanol, (due to low reaction temperatures) was covering the surface. However, TGA and XPS analysis provided mixed results with no definitive answer. High resolution (<5nm) HAADF microscopy is also needed to verify that there is no change in morphology of the Au(Pd) particles.

## 6.3 – References


1. H. R. Gerberich, A. L. Stautzenberger and W. C. Hopkins. *Formaldeyde. In Encyclopaedia of Chemical Technology, 3rd Edition*; D.F.A., Eds.; Standen Editores Jonh Wiley & Sons, Inc. **1983**, *Vol. 11*, 231.
2. M. Quain, M. A. Liaw, G. Emig. *Applied Catalysis A: General* **2003**, *238*, 211-222.
3. G. Waterhouse, G. Bowmaker and J. Metson. *Appl. Catal. A: General* **2004**, *265*, 85-101.
4. A. Andreasen, H. Lynggaard, C. Stegelmann and P. Stoltze. *Appl. Catal. A: General* **2005**, *289*, 267-273.
5. L. Lefferts and J. G. van Ommen, J. Ross. *Appl. Catal.* **1986**, *23*, 385-402.
6. M. Bowker, R. Holroyd, A. Elliott, P. Morrall, A. Alouche, C. Entwistle and A. Toerncrona, *Catalysis Letters* **2002**, *83* (3-4).
7. A. Andersson, M. Hernelind and O. Augustsson. *Catalysis Today* **2006**, *112*, 40.
8. A. P. V. Soares, M. F. Portela and A. Kiennemann. *Catalysis Reviews – Science and Engineering* **2004**, *47*, 125.
9. S. Ruf, A. May, G. Emig. *Applied Catalysis, A: General* **2001**, *213*, 203.
10. L. P. Ren. W. L. Dai. Y. Cao. K. N. Fan. *Catalysis Letters* **2003**, *85*, 81.
11. W-H. Cheng. *J. Catal.* **1996**, *158*, 477-485.
12. M. Seman, J. N. Kondo and K. Domen. *J. Phys. Chem. B* **2004,** *108,* 3231 3239
13. J. M. Tatibouet and J. E. Germain. *Bull. Soc. Chim.* **1980**, *1*, 343.

14. N. Niskala, T. Laitinen, S. Ojala, S. Pitkaaho, A. Kuverov, R. I. Keiski. *Proceeding of the Skypro Conference, University of Oulu, Finland*, **2010**, pp. 70-73.
15. L. Wen. *Appl. Catal. B*, **2008**, *79*, 402-409.
16. H. Yin, Z. Ma, M. Chi and S. Dai. *Catal. Lett.* **2010**, *136*, 209-221.
17. J. A. Lopez-Sanchez, N. Dimitratos, C. Hammond, G. L. Brett, L. Kesavan, S. White, P. Miedziak, R. Tiruvalam, R. L. Jenkins, A. F. Carley, D. Knight, C. J. Kiely and G. J. Hutchings. *Nature Chemistry* **2011**, *3*, 551-556.
18. H. Liu and E. Iglesia, *J. Phys. Chem. B*, **2005**, *109*, 2155–2163.
19. J. Lichtenberger, L. Doohwan and E. Iglesia. *Phys. Chem. Chem. Phys.* **2007**, *9*, 4902-4906.
20. A. Wittstock, V. Zielasek, J. Biener, C. M. Friend and M. Baumer. *Science* **2010**, *327 (5963)*, 319-322.
21. M. Comotti, Wen-Cui Li, B. Spliethoff, and F. Schuth. *J. Am. Chem. Soc.* **2006**, *128*, 917-924.

# 7

# *Chapter 7 - Appendix*

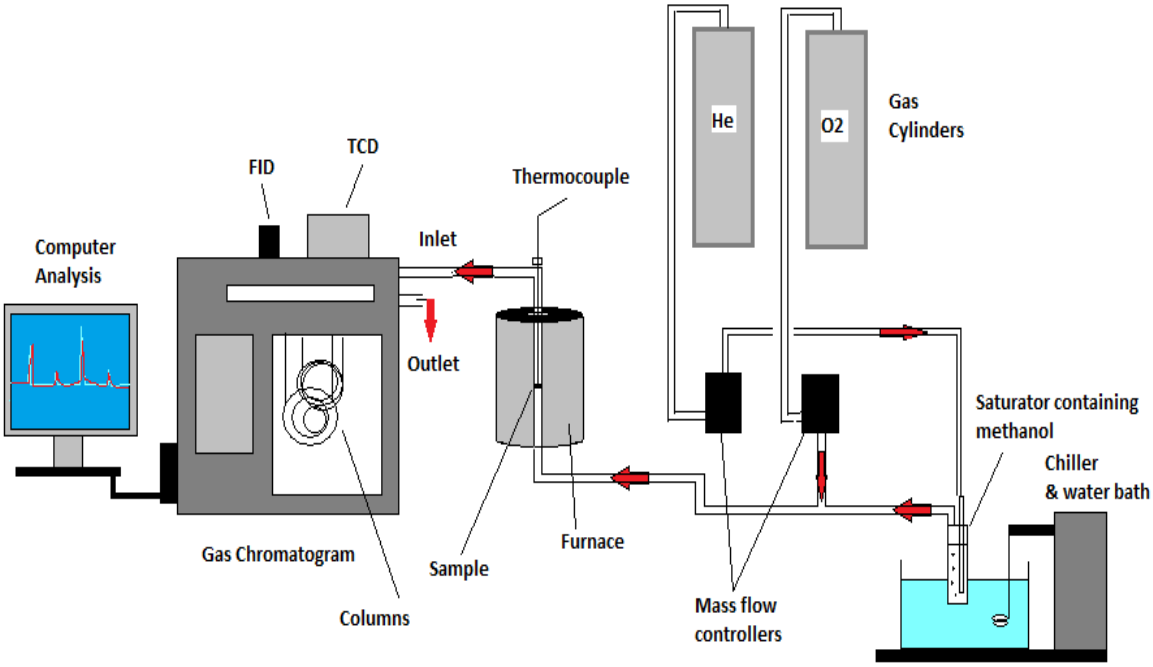


**Figure A.1:** Schematic of methanol oxidation reactor setup.

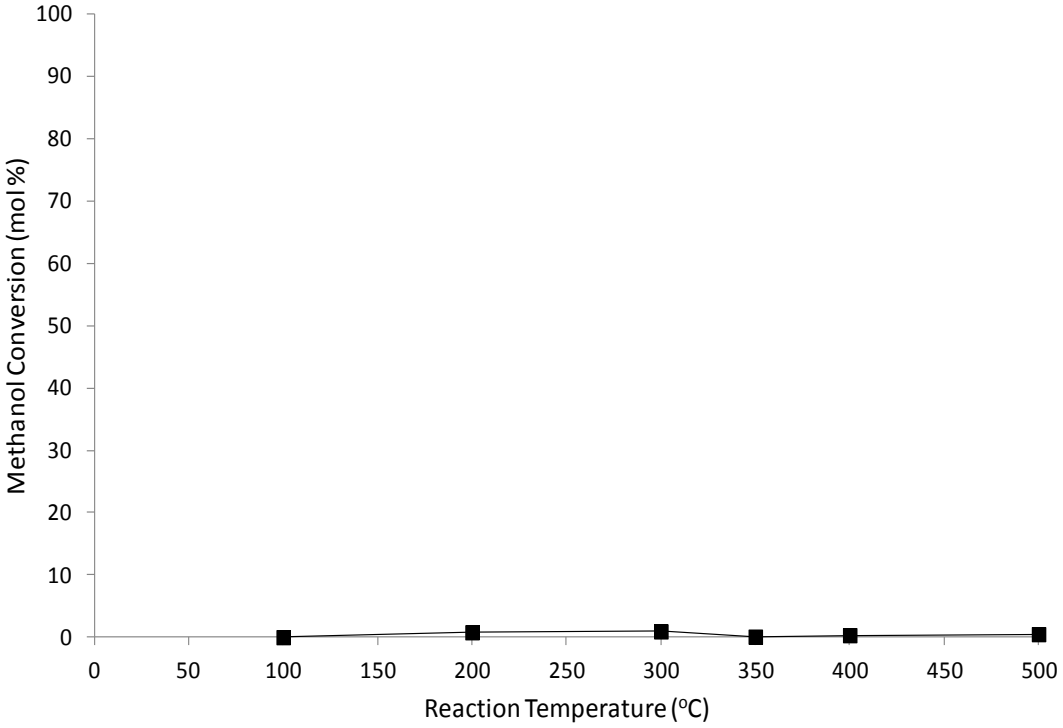


**Figure A.2:** Methanol oxidation using a blank quartz tube (no catalyst), showing no chemical reaction.

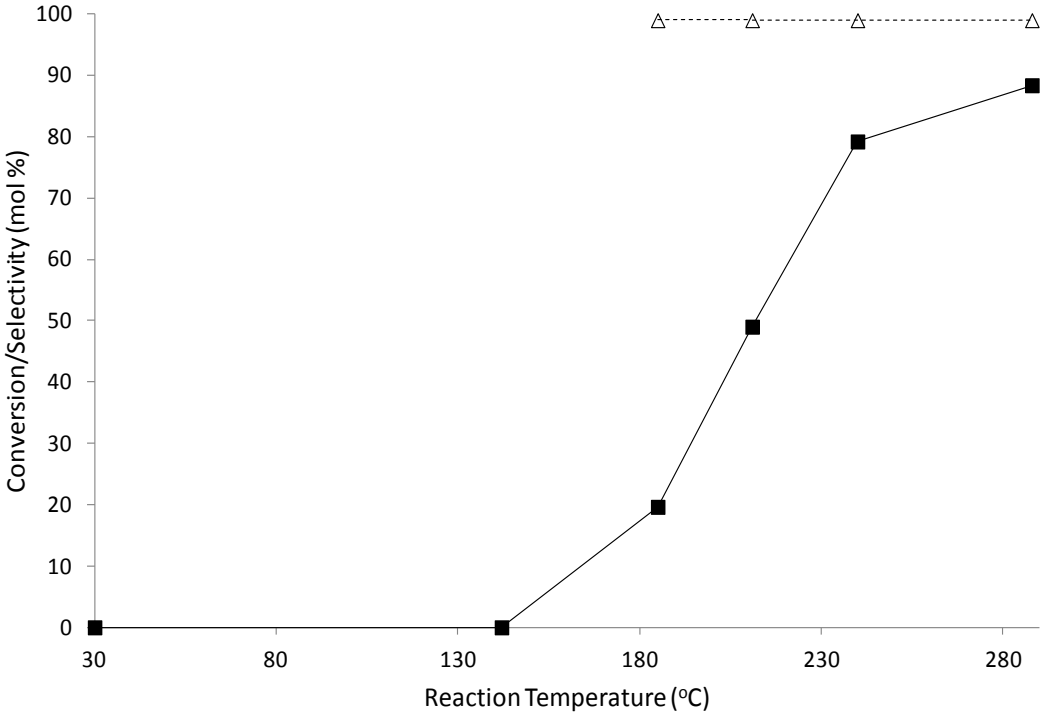


**Figure A.3:** Catalytic activity of γ-alumina during methanol oxidation towards dimethyl ether.

= Methanol conversion (mol %); = Dimethyl ether selectivity (mol %)

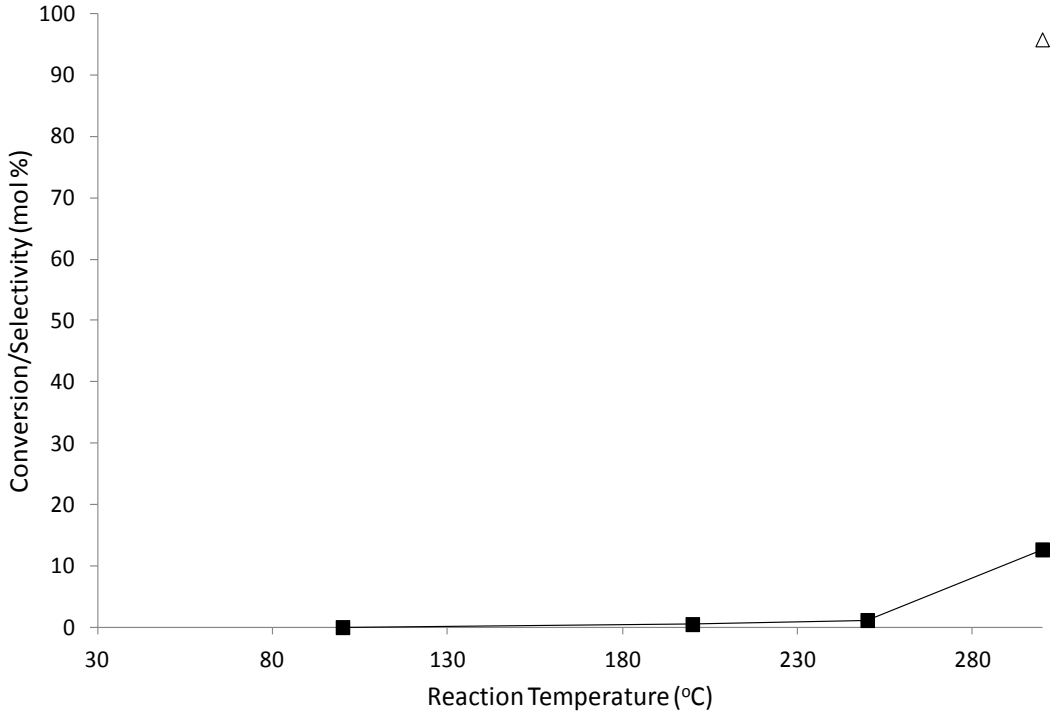


**Figure A.4:** Catalytic activity of $TiO_2$ during methanol oxidation towards formaldehyde.

■ = Methanol conversion (mol %); △ = Formaldehyde selectivity (mol %)

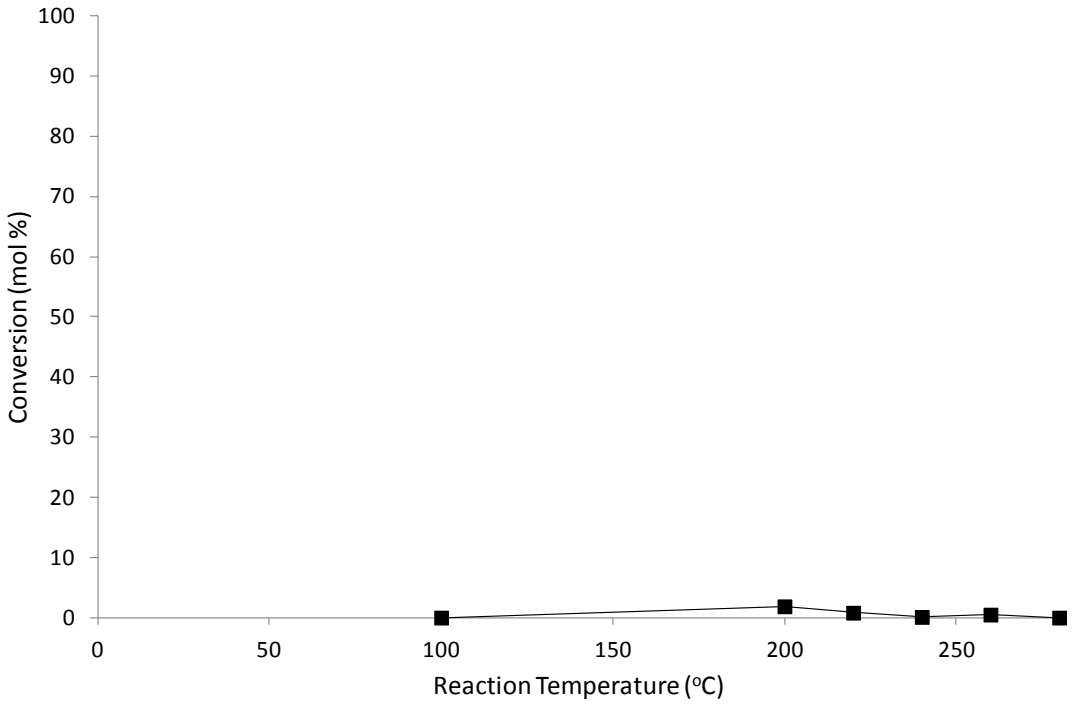


**Figure A.5:** Catalytic activity of $SiO_2$ during methanol oxidation, showing no activity in the reaction temperature range.

■ = Methanol conversion (mol %)

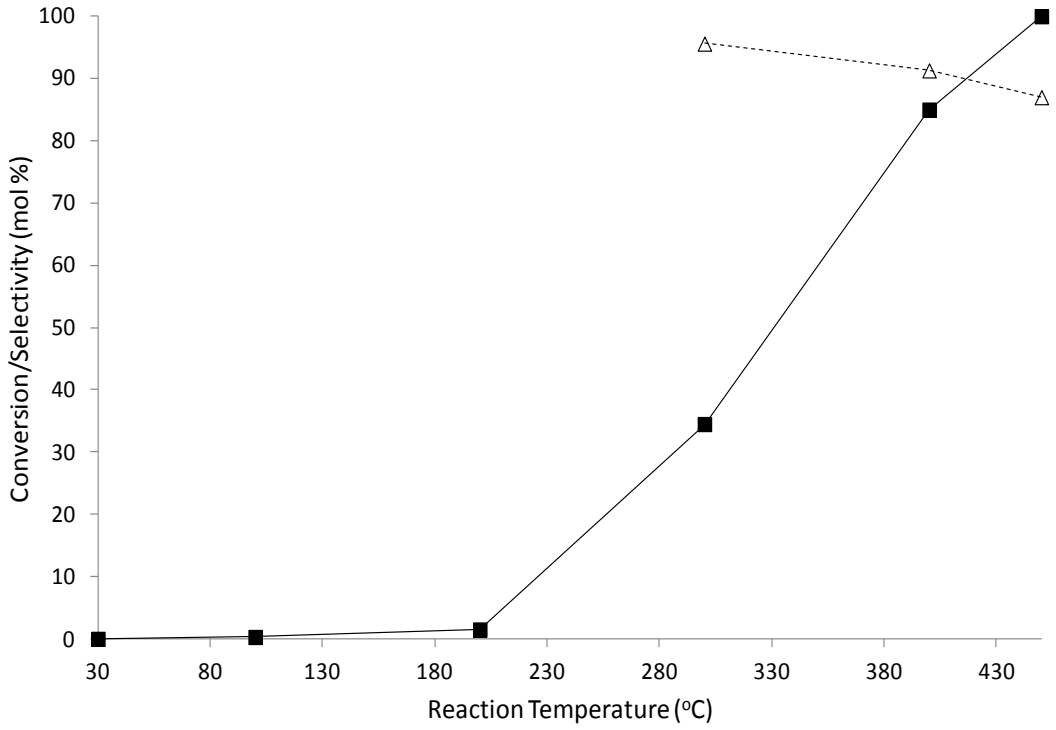


**Figure A.6:** Catalytic activity of $MoO_3$ catalyst during the selective oxidation of methanol to formaldehyde.

= Methanol conversion (mol %); = Formaldehyde selectivity (mol %)

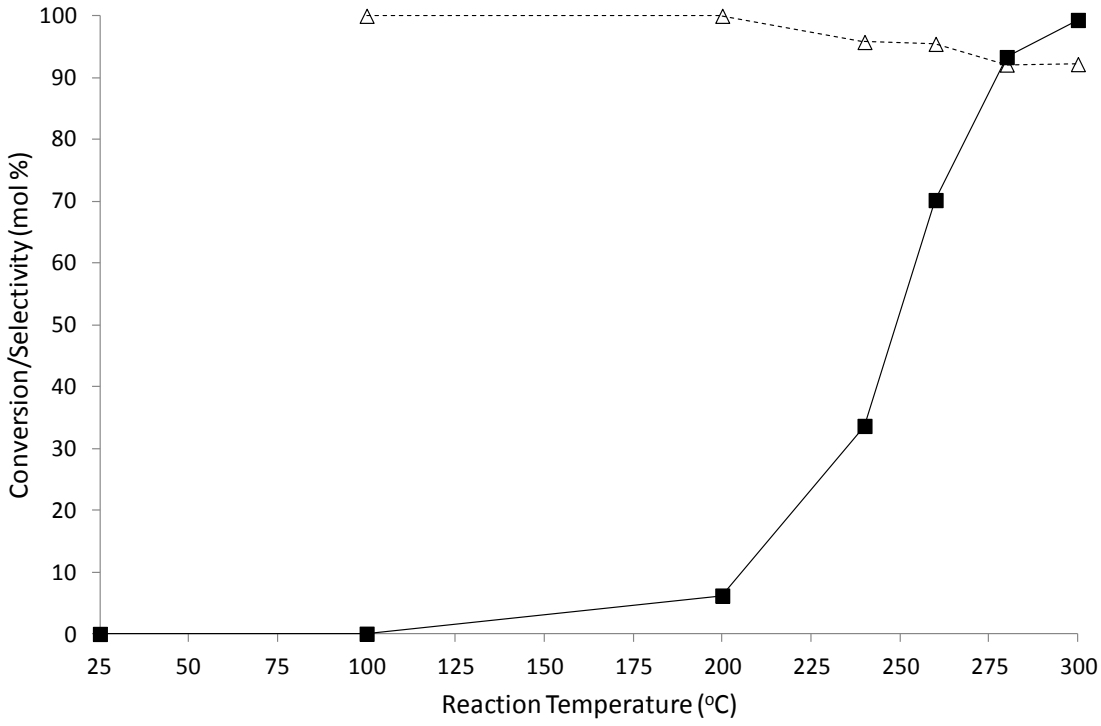


**Figure A.7:** Catalytic activity of an iron molybdate catalyst during selective oxidation of methanol towards formaldehyde.

= Methanol conversion (mol %); = Formaldehyde selectivity (mol %)

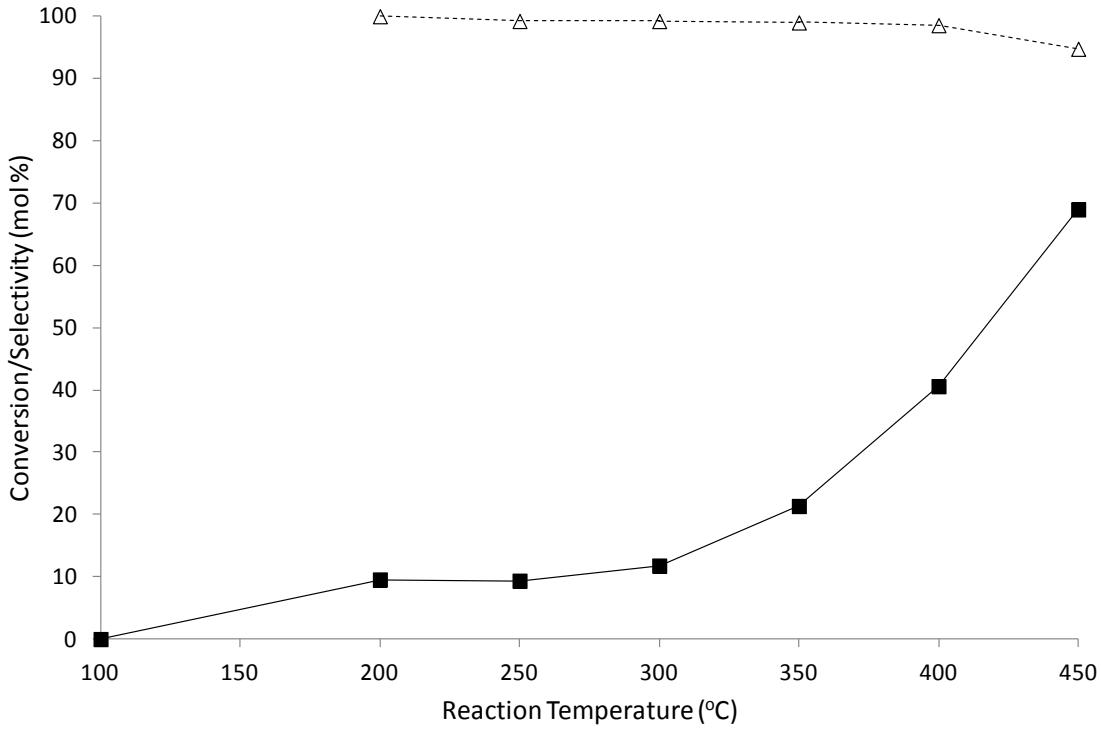


**Figure A.8:** Catalytic activity of a $VOPO_4.2H_2O$ catalyst during selective oxidation of methanol towards formaldehyde.

= Methanol conversion (mol %); = Formaldehyde selectivity (mol %)